

# **Modelling dryland vegetation patterns: nonlocal dispersal, temporal variability in precipitation and species coexistence**

Lukas Eigentler

SUBMITTED FOR THE DEGREE OF  
DOCTOR OF PHILOSOPHY

MAXWELL INSTITUTE GRADUATE SCHOOL IN ANALYSIS AND ITS  
APPLICATIONS,  
HERIOT-WATT UNIVERSITY & THE UNIVERSITY OF EDINBURGH.

June 2020

The copyright in this thesis is owned by the author. Any quotation from the thesis or use of any of the information contained in it must acknowledge this thesis as the source of the quotation or information.

## Abstract

Spatiotemporal patterns of vegetation are a characteristic feature of dryland ecosystems occurring on all continents except Antarctica. The development of an understanding of their ecosystem dynamics is an issue of considerable socio-economic importance as both the livestock and agricultural sectors in dryland economies heavily depend on ecosystem functioning. Mathematical modelling is a powerful tool to disentangle the complex ecosystem dynamics. In this thesis, I present theoretical models to explore the impact of nonlocal seed dispersal and temporal precipitation variability on dryland vegetation patterns and propose several mechanisms that enable species co-existence within vegetation patterns. To do so, I present extensions of the Klausmeier reaction-advection-diffusion model, a well-established model describing the ecohydrological dynamics of vegetation patterns. Model analyses focus on pattern onset at high precipitation values (i.e. on the transition from uniformly vegetated to spatially patterned states) to assess the impact of non-local seed dispersal and precipitation seasonality and intermittency, and on comprehensive bifurcation analyses, including results on pattern existence and stability to investigate coexistence of species in the mathematical framework. Results include the inhibition of pattern onset due to long-range seed dispersal and put emphasis on the functional response of plants to low soil moisture levels to understand effects of rainfall intermittency. Moreover, results suggest that coexistence is facilitated by resource heterogeneities induced by the plant's spatial self-organisation and highlight the importance of considering out-of-equilibrium solutions.

## Acknowledgements

The work presented in this thesis would not have been possible without the support of many people. First and foremost, I would like to thank my partner Nina Markl for her daily support and encouragement that made me feel at home in Edinburgh from the first day. I am also grateful to my parents Angelika and Karl Eigentler who have supported me throughout the PhD and indeed during my whole education over the last two decades.

Away from home, it has always been a pleasure to come to the office, thanks to all the amazing people in the department. I will dearly miss the daily coffee breaks with Gissell Estrada-Rodriguez, Jakub Stocek, Andres Barajaz-Paz and Heiko Gimperlein. All of you helped immensely to keep my sanity during difficult periods of the PhD. Despite she was never able to make our 8:00am coffee break, the same applies to Jeta Molla. Not only this, Jeta always ensured that good working conditions prevailed in the office, for which I am very grateful to her. A big shout-out also goes to the (not so) professional Heriot-Watt Maths Volleyball Team, including Stefania Lisai, Nikoletta Louca, Vincenzo Marotta, Albert Sola Vilalta, Xander O'Neill, Jeta Molla, Gissell Estrada-Rodriguez, Jakub Stocek, Andres Barajaz-Paz and Heiko Gimperlein.

Academically, I would like to express my gratitude to my supervisor Jonathan Sherratt, who has spent countless hours supporting my research. From our first meeting, his positive attitude created a research setting that enabled me to thrive. Without his helpful feedback, explanations of new concepts and general encouragement throughout the years, this thesis would not have been possible. A special thanks also goes to Jamie Bennett who introduced me to the numerical continuation software AUTO-07p, which I extensively used throughout my work.

It has been a pleasure to be part of the mathematical biology group at Heriot-Watt University. There is a real community spirit in the group and there were always many opportunities for fruitful discussions, which I enjoyed greatly.

I would also like to thank Dumitru Trucu for encouraging me to apply for PhD positions at a time when I was undecided about my future career.

Finally, I would also like to thank Arjen Doelman and Andy White for agreeing to read and examine this thesis.

## Funding information

Lukas Eigentler was supported by The Maxwell Institute Graduate School in Analysis and its Applications, a Centre for Doctoral Training funded by the UK Engineering and Physical Sciences Research Council (grant EP/L016508/01), the Scottish

Funding Council, Heriot-Watt University and the University of Edinburgh.

# Contents

<b>1</b>	<b>Introduction</b>	<b>1</b>
1.1	Ecological background . . . . .	1
1.2	Mathematical framework . . . . .	4
<b>2</b>	<b>Analysis of a model for banded vegetation patterns in semi-arid environments with nonlocal dispersal</b>	<b>7</b>
2.1	Author contribution . . . . .	7
2.2	Introduction . . . . .	8
2.2.1	Ecological Background . . . . .	8
2.2.2	The Models . . . . .	9
2.3	Linear Stability Analysis . . . . .	13
2.3.1	Wavelength . . . . .	15
2.4	Travelling Wave Solutions . . . . .	16
2.5	Asymptotic analysis of the integro-PDE model . . . . .	20
2.6	Numerical Simulations . . . . .	22
2.7	Discussion . . . . .	27
<b>3</b>	<b>An integrodifference model for vegetation patterns in semi-arid environments with seasonality</b>	<b>32</b>
3.1	Author contribution . . . . .	32
3.2	Introduction . . . . .	33
3.3	The Models . . . . .	35
3.3.1	Klausmeier Model . . . . .	36
3.3.2	Integrodifference Model . . . . .	38
3.4	Linear Stability Analysis . . . . .	45
3.5	Simulations . . . . .	51
3.6	Discussion . . . . .	56
<b>4</b>	<b>Effects of precipitation intermittency on vegetation patterns in semi-arid landscapes</b>	<b>62</b>
4.1	Author contribution . . . . .	62
4.2	Introduction . . . . .	63

## CONTENTS

4.3	Model description . . . . .	66
4.3.1	Klausmeier models . . . . .	66
4.3.2	Impulsive Model . . . . .	68
4.4	Onset of patterns . . . . .	72
4.4.1	Linear Stability Analysis . . . . .	72
4.5	Simulations of model extensions . . . . .	84
4.5.1	Method . . . . .	84
4.5.2	Nonlinear water uptake . . . . .	85
4.5.3	Nonlinear PDEs . . . . .	88
4.5.4	Kernel functions . . . . .	91
4.5.5	Slope . . . . .	92
4.6	Discussion . . . . .	93
<b>5</b>	<b>Metastability as a coexistence mechanism in a model for dryland vegetation patterns</b>	<b>99</b>
5.1	Author contribution . . . . .	99
5.2	Introduction . . . . .	100
5.3	Model . . . . .	102
5.4	Numerical Solutions of the Model . . . . .	108
5.5	Metastable coexistence patterns arising from stable one-species patterns	109
5.5.1	Turing-type patterns . . . . .	111
5.5.2	Metastable Patterns . . . . .	116
5.6	Metastable coexistence patterns originate from a coexistence equilibrium . . . . .	119
5.6.1	Stability to spatially uniform perturbations . . . . .	123
5.7	Discussion . . . . .	127
<b>6</b>	<b>Spatial self-organisation enables species coexistence in a model for savanna ecosystems</b>	<b>132</b>
6.1	Author contribution . . . . .	132
6.2	Introduction . . . . .	133
6.3	The model . . . . .	136
6.4	Existence and onset of patterns in which species coexistence occurs . . . . .	139
6.4.1	Stability of spatially uniform equilibria . . . . .	139
6.4.2	Single-species patterns . . . . .	140
6.4.3	Multispecies patterns . . . . .	141
6.5	Stability of coexistence pattern . . . . .	148
6.6	Phase difference . . . . .	153
6.7	Discussion . . . . .	155

6.8	Methods of calculating pattern existence and stability . . . . .	161
6.8.1	Single-species pattern existence . . . . .	161
6.8.2	Calculation of the essential spectrum . . . . .	162
6.8.3	Numerical continuation of stability boundaries . . . . .	165
<b>7</b>	<b>Species coexistence in vegetation patterns facilitated by the interplay of spatial self-organisation and intraspecific competition</b>	<b>168</b>
7.1	Author contribution . . . . .	168
7.2	Introduction . . . . .	169
7.3	Model & Methods . . . . .	172
7.3.1	Model details . . . . .	172
7.3.2	Model analysis . . . . .	175
7.4	Results . . . . .	175
7.4.1	Spatially uniform coexistence . . . . .	175
7.4.2	Patterned species coexistence . . . . .	176
7.4.3	Plant species' distribution . . . . .	181
7.5	Discussion . . . . .	181
7.6	Supplementary material . . . . .	184
7.6.1	Dimensional model and its nondimensionalisation . . . . .	184
7.6.2	Methods for model analysis . . . . .	186
7.6.3	Stability of spatially uniform single-species states . . . . .	187
7.6.4	Patterned model solutions . . . . .	188
7.6.5	Other model solutions . . . . .	191
<b>8</b>	<b>Intraspecific competition in models for vegetation patterns: decrease in resilience to aridity and facilitation of species coexistence</b>	<b>192</b>
8.1	Author contribution . . . . .	192
8.2	Introduction . . . . .	193
8.3	Single-species model . . . . .	195
8.3.1	Model . . . . .	195
8.3.2	Pattern onset, existence & stability . . . . .	198
8.4	Multispecies model . . . . .	200
8.4.1	Model . . . . .	200
8.4.2	Stability in spatially uniform model . . . . .	204
8.4.3	Single-species patterns . . . . .	207
8.4.4	Onset and existence of coexistence patterns . . . . .	208
8.4.5	The effects of plant dispersal . . . . .	214
8.5	Discussion . . . . .	218
<b>9</b>	<b>Conclusion</b>	<b>224</b>

# Chapter 1

## Introduction

The content of this thesis is centred around the general topic of *Modelling dryland vegetation patterns*, a research theme that has received significant attention from mathematical modellers and theoretical ecologists over the last three decades. In this introduction, I set the scene for the presentation of the research papers in Chapters 2 to 8 by providing an overview of ecological processes that characterise dryland ecosystems as well as by presenting the mathematical framework on which the content of this thesis is based.

### 1.1 Ecological background

More than 2.5 billion people live in drylands covering approximately 41% of the Earth's land mass [162]. A ubiquitous feature of many drylands is spatiotemporal patterns of vegetation, characterised by alternating patches of high biomass and patches of bare soil (Fig. 1.1) [222]. First documented through aerial photography in the 1940s [116], observations of vegetation patterns have been reported from all continents except Antarctica (see [71, 222] for reviews). This includes patterns in the African Sahel [48] and the Horn of Africa [79], Western Australia [72], Chile [68], Israel [182], the Chihuahuan Desert in the US and Mexico [48] and Spain [108]. The development of a understanding of ecosystem dynamics in drylands is therefore of crucial global socio-economic importance. In particular, many economies in drylands rely on the livestock and agriculture sectors [51, 219], whose developments are affected by future vegetation levels. For example, in Chad, the livestock sector contributes around 20% of the country's GPD and involves about 40% of its population.

Vegetation patterns are a classical example of a self-organisation principle in ecology. The separation of plants into patches of dense biomass and areas of bare soil is induced by a positive feedback between local vegetation growth and water redistribution towards areas of high biomass [166]. Depending on soil properties and plant species, a number of different mechanisms are involved in this pattern-inducing feedback loop. For example, overland water flow towards dense biomass

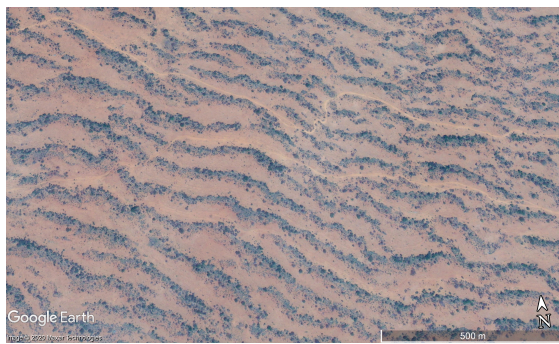


Figure 1.1: Vegetation bands in Somalia. A satellite image of a banded vegetation pattern in the Horn of Africa ( $7^{\circ}50' \text{ N}$ ,  $47^{\circ}4' \text{ E}$ ) is shown. It visualises the characteristic separation of plants into stripes of high biomass and bands of bare soil in between. The photograph, taken in 2013, has been obtained from Google Earth. Image © Maxar Technologies.



Figure 1.2: Uphill migration of vegetation stripes. Shortly after a precipitation event, the upslope region of the depicted vegetation band receives more water run-off from the upslope interband region than the downslope areas. Terrain elevation increases to the left of the figure. The photograph shows a vegetation pattern in New South Wales, Australia and is reproduced with permission from [54].

patches is induced by the formation of infiltration-inhibiting biogenic soil crusts on certain soil types; or laterally extended root systems as well as a combination of vertically extended roots and a soil type supporting fast water diffusion can cause water redistribution below ground [130]. As a consequence, vegetated patches act as resource sinks, which drives further plant growth and closes the feedback loop.

The self-organisation of plants can result in patterns of different shapes, including gap patterns, labyrinth patterns and spot patterns [129]. On gentle slopes (up to approximately 2% gradient), vegetation patterns occur as regular stripes parallel to the contours of the terrain [222]. A characteristic feature of regular vegetation bands is their uphill migration over a generational timescale (i.e. of the order of a few decimetres per year) [48, 222]. This property emerges from the positive feedback between local vegetation growth and water redistribution towards dense biomass patches. Due to the sloped terrain, the uphill edges of vegetation stripes profit most from this water redistribution, intercepting most of the water run-off from the upslope interband region (Fig. 1.2). The resulting hydrological distribution promotes upslope expansion and downslope contraction of the bands [48]. However, evidence of uphill migration is not unequivocal. Reports of stationary vegetation bands suggest that other processes, such as soil erosion, can counteract uphill migration [55].

Due to the long temporal and large spatial scales involved in the ecohydrological dynamics of vegetation patterns, the acquisition of high-quality empirical data is

notoriously difficult. While it is possible to obtain data on some properties, including pattern wavelength [48], terrain elevation [202] and historical rainfall data [193], I am not aware of methods that enable the collection of other relevant types of data, such as biomass densities or species composition, over long periods of time and wide areas of space. In isolation, datasets that are currently available can only provide limited information on the complex ecosystem dynamics. Nevertheless, empirical data can be used to complement and test hypotheses from mathematical models (e.g. [10, 72, 193]).

In this thesis, I focus on a number of different processes and phenomena affecting the ecosystem dynamics of dryland vegetation patterns: nonlocal dispersal of seeds (Chapter 2), temporal variability in precipitation (Chapters 3 and 4) and species coexistence (Chapters 5 to 8).

Dispersal behaviour has a key impact on ecosystem dynamics, including those in patterned vegetation [25]. Plant dispersal is considered to be a nonlocal process and is commonly quantified through dispersal kernels - probability density functions that describe the distribution of seed dispersal distances. Indeed, depending on plant species and dispersal agents, seeds may be dispersed over a couple of hundred metres [25]. Nevertheless, mathematical models generally describe plant dispersal through a local process (see Section 1.2). In Chapter 2, I address the impact of changes to plant dispersal kernels on dryland vegetation patterns.

Precipitation in drylands usually follows a seasonal or intermittent (or combination thereof) pattern [148]. Under intermittent rainfall regimes, only a small number of precipitation pulses each year are of sufficiently high intensities to activate plant growth and other processes [148]. Thus, drought periods are characterised by decay-type mechanisms, while key ecological processes, such as plant growth and seed dispersal are synchronised with rainfall pulses. Similarly, in latitudes featuring a seasonal climate (and thus seasonal precipitation regimes), seed dispersal either occurs during the dry season or is synchronised with the beginning of the wet season [146, 148, 181]. Chapters 3 and 4 present mathematical models that investigate the impact of both seasonal and intermittent rainfall regimes on dryland vegetation patterns.

A number of different plant types are commonly found within vegetation patterns. In particular, coexistence of herbaceous (*grasses*) and woody (*trees/shrubs*) species is widespread. In the context of striped patterns that gradually move upslope, grasses typically dominate the uphill edge of each stripe, with the tree species being confined to the central and downslope regions of the band [41, 179]. Verbal arguments exist that suggest that grasses act as *pioneer species* to colonise new ground, but cannot outcompete trees locally [179]. In Chapters 5 to 8 I use mathematical modelling to support this claim, as well as to suggest other mechan-

isms that enable species coexistence in vegetation patterns.

## 1.2 Mathematical framework

As a consequence of the challenges associated with the acquisition of high-quality data on vegetation patterns, mathematical modelling, in particular continuum approaches, play a crucial role in the development of a better understanding of dryland ecosystem dynamics [132]. A number of different modelling frameworks have been proposed over the last three decades (see [21, 124, 247] for reviews). Notable examples are the Gilad et al. model [74] and the HilleRisLambers and Rietkerk et al. model [86, 163]. One model that stands out due to its deliberate simplicity is the extended Klausmeier model [99], which, after a suitable nondimensionalisation [99, 185]<sup>1</sup> is

$$\frac{\partial u}{\partial t} = \underbrace{u^2 w}_{\text{plant growth}} - \underbrace{Bu}_{\text{plant loss}} + \underbrace{\frac{\partial^2 u}{\partial x^2}}_{\text{plant dispersal}}, \quad (1.1a)$$

$$\frac{\partial w}{\partial t} = \underbrace{A}_{\text{rainfall}} - \underbrace{w}_{\text{evaporation and drainage}} - \underbrace{u^2 w}_{\text{water uptake by plants}} + \underbrace{\nu \frac{\partial w}{\partial x}}_{\text{water flow downhill}} + \underbrace{d \frac{\partial^2 w}{\partial x^2}}_{\text{diffusion of water}}. \quad (1.1b)$$

The model describes the ecohydrological dynamics of the plant density  $u(x, t)$  and the water density  $w(x, t)$ , where time  $t \geq 0$  and the space coordinate  $x \in \mathbb{R}$  increases in the uphill direction of the one-dimensional sloped domain. A constant amount of water is added to the system per unit time, representing precipitation, while evaporation and drainage processes remove water at a constant rate. The third term in (1.1b) represents water consumption by plants. The nonlinearity in the term arises due to part of the positive feedback between local vegetation growth and water redistribution towards dense biomass patches. Water uptake depends on the consumer density ( $u$ ), the resource density ( $w$ ) and the enhancement of environmental conditions, for example due to increased soil permeability, in dense biomass patches ( $u$ ). As water is assumed to be the limiting resource in the ecosystem, plant growth is proportional to water consumption. Plant death is assumed to occur at a constant rate. Both densities undergo diffusion and water flow downhill is described through advection. The nondimensional parameters  $A$ ,  $B$ ,  $\nu$  and  $d$  are combinations of several dimensional parameters, but can be interpreted as rainfall volume, rate of plant death, speed of water flow downhill and the water's diffusion coefficient, respectively. The model is commonly referred to as the *extended Klausmeier model*,

---

<sup>1</sup>The diffusion parameter  $d = D_w/D_u$  is the ratio of the water diffusion coefficient  $D_w$  and the plant diffusion coefficient  $D_u$  (not given in the nondimensionalisations in [99, 185])

since the diffusion of water was not originally included in the system, but has become a well-established addition (e.g. [95, 199, 225, 247]).

Despite the model's simplicity, it exhibits a rich structure of spatially patterned solutions (periodic travelling waves), whose properties have been studied extensively in the past (e.g. [8, 9, 28, 99, 184–186, 190–192, 194, 199]). Moreover, the mathematical accessibility of the system selects it as an ideal candidate for model extensions. Among others, these include the inclusion of autotoxicity [120], grazing and browsing [68, 195, 197], secondary seed dispersal due to overland water flow [35] and spatial heterogeneities in the terrain [72]. In this thesis, I will add to these extensions by investigating the effects of nonlocal seed dispersal in Chapter 2 and temporal variability in precipitation in Chapters 3 and 4 (complementing previous work by Ursino and Contarini [221]), as well as exploring a model of two competing plant species in Chapters 5 to 8 (complementing previous work by Ursino and Callegaro [27, 220]).

Chapter 2 addresses the impact of nonlocal dispersal of seeds on the onset of vegetation patterns, i.e. on the phase transition from a spatially uniform vegetated state to a spatially patterned state as precipitation volume decreases. In Chapters 3 and 4, I discuss effects of temporal variability in precipitation (and other processes induced by temporal non-uniformity of rainfall) on vegetation pattern onset. An analysis of an integrodifference model capturing seasonality in precipitation regimes and synchronisation of (nonlocal) seed dispersal with the dry season or beginning of the wet season is presented in Chapter 3, while intermittency of precipitation is considered in Chapter 4 through an impulsive model (combination of PDEs and discrete maps). The remainder of the main text (Chapters 5 to 8) focusses on mechanisms to explain species coexistence under competition for a single limiting resource. To this end, a multispecies model is introduced in Chapter 5, followed by results that highlight the importance of considering nonequilibrium dynamics, as coexistence can occur as a metastable state. A different coexistence mechanism is presented in Chapter 6, in which I argue that the spatial self-organisation of plants is sufficient to explain species coexistence in savannas (continuous but not necessarily spatially uniform vegetation cover), but not in vegetation patterns (alternating patches of vegetation and bare soil). Finally, Chapters 7 and 8 show that intraspecific competition dynamics need to be considered to gain insights into species coexistence in vegetation patterns. Moreover, Chapter 8 discusses the impact of intraspecific competition dynamics on a single-species modelling framework. The final chapter (Chapter 9) includes an overarching discussion of results and a brief outlook into potential future work.

This thesis is a collection of seven research papers published in or submitted to peer-reviewed journals during my time at the *Maxwell Institute Graduate School*

*in Analysis and its Applications* [58–64]. The papers forming Chapters 2 to 8 of this thesis are mostly presented in the form they were published in or submitted to journals. Thus, each chapter is in principle self-contained, but references to other chapters have been added. As a consequence, chapters include repetitions, in particular in their introductions and presentations of mathematical models. Moreover, chapters slightly differ in style. Chapters 2 to 6 and 8 are aimed at a mathematical biology/applied mathematics-oriented readership, while Chapter 7 addresses a biological audience.

## Chapter 2

# Analysis of a model for banded vegetation patterns in semi-arid environments with nonlocal dispersal

The contents of this chapter are published in [61].

### 2.1 Author contribution

The authors of the published paper [61] are Lukas Eigentler and Jonathan A Sherratt. Lukas Eigentler performed both the analytical and numerical analyses of the model, wrote the paper draft and reviewed and edited the manuscript. Jonathan A Sherratt conceptualised the research, formulated the mathematical model, reviewed and edited the manuscript and provided supervision.

### Abstract

Vegetation patterns are a characteristic feature of semi-arid regions. On hillsides these patterns occur as stripes running parallel to the contours. The Klausmeier model, a coupled reaction-advection-diffusion system, is a deliberately simple model describing the phenomenon. In this chapter, we replace the diffusion term describing plant dispersal by a more realistic nonlocal convolution integral to account for the possibility of long-range dispersal of seeds. Our analysis focuses on the rainfall level at which there is a transition between uniform vegetation and pattern formation. We obtain results, valid to leading order in the large parameter comparing the rate of water flow downhill to the rate of plant dispersal, for a negative exponential dispersal kernel. Our results indicate that both a wider dispersal of seeds and an increase in dispersal rate inhibit the formation of patterns. Assuming an evolutionary trade-off between these two quantities, mathematically motivated by the limiting behaviour of the convolution term, allows us to make comparisons to existing results for the original reaction-advection-diffusion system. These comparisons show that the nonlocal model always predicts a larger parameter region supporting pattern formation. We then numerically extend the results to other dispersal kernels, showing that the tendency to form patterns depends on the type of decay of the kernel.

## 2.2 Introduction

### 2.2.1 Ecological Background

Semi-arid environments are regions in which the level of rainfall is below a certain threshold, dependent on the mean temperature and spread of rainfall across the year [101, 151], creating a hostile environment for vegetation as plants compete for water. A characteristic feature of many of these semi-arid environments is self-organised patterns of vegetation. These occur due to a scale-dependent feedback, which is caused by the modification of the soil by the existing plants, creating a more favourable environment on a short range and the competition for water on a longer spatial distance [166]. On gentle slopes of a few percent gradient (0.2% to 2% [222]) striped patterns occur along the contours of the hill. Being wide and with large distances between them, these stripes are extremely difficult to detect from the ground. They were therefore first discovered using aerial photography in the 1950s in British Somaliland (today Somalia) [83, 116]. Since then, striped patterns have been observed on slopes in the Chihuahuan Desert in Mexico and the US [38, 136, 137], New South Wales in Australia [55, 214], Niger and other countries in the African Sahel [208, 239, 241] and many other regions as reviewed by [222, Table 1 and Figure 3]. Many ecologists studying these patterns reported that the vegetation bands slowly move uphill [137, 222, 241] with a migration speed varying between 0.2m and 1.5m per year [222]. They argue that the reason for this is that the rainwater, which often falls in form of torrential rain at irregular intervals [23], runs off the bare ground to the uphill edge of the vegetation band below, where it can infiltrate the ground more easily, providing a more favourable environment for plant growth on the uphill edge than on the downhill edge [138, 239]. Other authors observed stationary patterns [55], which they attribute to changes in the soil on bare ground that inhibits plant growth [55] and a skewed distribution of plant dispersal caused by seeds travelling downhill in the flow of the water [169, 210]. A more recent survey confirms the occurrence of both upward migration and static vegetation bands, by comparing satellite data from spy satellites used during the Cold War to more recent data [46]. Studying these patterns is of crucial importance as changes in the width of and distance between vegetation stripes may be an indicator for an imminent and irreversible switch to desertification [96, 164].

The long timescale in the evolution of patterned vegetation and the inability to generate it in laboratory settings limit the availability of observed data. Instead various different theoretical models have been developed [21]. These can be classified into two main groups; models based on plant to plant interactions, among other things including individual plant's morphology such as its root network and shading [74, 75, 81, 106] and models focusing on water redistribution. The latter class of

models are based on the Klausmeier model [99], on which we will focus here.

### 2.2.2 The Models

The nondimensionalised form of the Klausmeier model (see [99, 185] for details on the nondimensionalisation) is the reaction-advection-diffusion system

$$\frac{\partial u}{\partial t} = \underbrace{u^2 w}_{\text{plant growth}} - \underbrace{B u}_{\text{plant loss}} + \underbrace{\frac{\partial^2 u}{\partial x^2}}_{\text{plant dispersal}}, \quad (2.1a)$$

$$\frac{\partial w}{\partial t} = \underbrace{A}_{\text{rainfall}} - \underbrace{w}_{\text{evaporation}} - \underbrace{u^2 w}_{\substack{\text{water uptake} \\ \text{by plants}}} + \underbrace{\nu \frac{\partial w}{\partial x}}_{\substack{\text{water flow} \\ \text{downhill}}} + \underbrace{d \frac{\partial^2 w}{\partial x^2}}_{\text{diffusion of water}}. \quad (2.1b)$$

Originally, this model did not include diffusion of water, but this term was added later and is now well established [95, 199, 225, 247]. This extended Klausmeier model will be referred to as the “local Klausmeier model” throughout the text. In the model,  $u(x, t)$  represents the plant density,  $w(x, t)$  the water density,  $t > 0$  the time and  $x \in \mathbb{R}$  the space, where the positive direction is in the uphill direction of a one-dimensional domain of constant gradient. The system assumes constant rainfall, proportionality of water density to evaporation [167, 171] and correlation of plant growth to water uptake. The latter is assumed to be proportional to the water density and the plant density squared, because the water infiltration capacity of the soil depends on the presence of plants [165, 222]. The ground where vegetation stripes are situated is estimated to receive around 1.5 to 2.5 times as much water as the annual precipitation due to water running off the bare ground towards the vegetation stripes [38]. The parameters  $A > 0$ ,  $B > 0$ ,  $\nu > 0$  and  $d > 0$  represent rainfall, plant loss, the rate of the water flow in the downhill direction and the rate of water diffusion, respectively. Due to the nondimensionalisation they are however a combination of different ecological quantities. Parameter estimates are  $A \in [0.1, 3]$ ,  $B \in [0.05, 2]$  [99, 163] and  $\nu = 182.5$  [99]. The large size of  $\nu$  compared to the other parameters reflects the slow speed of plant dispersal compared to water flow, and it allows an analysis of patterned solutions of (2.1) by obtaining results for the model to leading order in  $\nu$ , such as by [184–186, 190–192]. The model is deliberately kept simple. There are however a wide range of systems all based on the Klausmeier model (2.1) that take into account variable precipitation [100] and grazing [86, 224] and models that distinguish between the surface water density and the water density in the soil [75, 86, 163].

In (2.1), plant dispersal is modelled by a diffusion term. In reality, nonlocal

processes are often involved, such as seed dispersal by wind or separated stages for plant growth and seed dispersal [156]. This can be modelled by integrodifferential equations [4, 155]. To do this, the change of the plant density  $u(x, t)$  at a point  $x$  that was caused by diffusion is replaced by the convolution integral

$$\int_{-\infty}^{\infty} \phi(x - y) (u(y, t) - u(x, t)) dy.$$

The kernel function  $\phi(x, y)$  is a probability density function, describing the probability of seeds originating at the point  $y$  being dispersed to point  $x$  [156]. This approach is not only used in modelling plant dispersal but can, among others, be considered to model dispersal in general competition models [40, 89] showing an evolutionary advantage of nonlocal dispersal under certain boundary conditions [94], or models describing a single species subject to a unidirectional flow [114]. It is assumed that seed dispersal only depends on the distance  $x - y$  (i.e. assuming homogeneous and isotropic dispersion of seeds [135]). This kind of nonlocal seed dispersal is considered for example by [16, 156, 157] for modified versions of the Klausmeier model that consider soil water separately from surface water [86, 163]. Motivated by this, we will consider the “nonlocal Klausmeier model”

$$\frac{\partial u}{\partial t} = u^2 w - Bu + C \left( \int_{-\infty}^{\infty} \phi(x - y) u(y, t) dy - u(x, t) \right), \quad (2.2a)$$

$$\frac{\partial w}{\partial t} = A - w - u^2 w + \nu \frac{\partial w}{\partial x} + d \frac{\partial^2 w}{\partial x^2}. \quad (2.2b)$$

The dispersal coefficient  $C > 0$ , which scales the convolution term, describes the plant’s dispersal rate by taking into account the plant’s fecundity, seed mortality and germination rate and seed establishment ability [156].

If the kernel function  $\phi(x)$  is decaying exponentially as  $x \rightarrow \infty$ , the local model can be obtained from the nonlocal model by setting  $C = 2/\sigma(a)^2$ , where  $\sigma(a)$  denotes the standard deviation of the dispersal kernel with scaling parameter  $a$ , and taking the limit as  $a \rightarrow \infty$ . To show this, write  $\phi(x) = a\varphi(ax)$ . Then, the integral in the dispersal term can be transformed to

$$\int_{-\infty}^{\infty} \phi(x - y) u(y, t) dy = \int_{-\infty}^{\infty} \varphi(z) u\left(x - \frac{z}{a}, t\right) dz,$$

by using the change of variables  $y = x - z/a$ . Considering the Taylor expansion of  $u(x - z/a, t)$  in  $z/a$ , an application of Watson’s lemma (i.e. integrating term-wise)

gives

$$\begin{aligned} & \int_{-\infty}^{\infty} \phi(x-y)u(y,t)dy \\ &= u(x,t) - \frac{1}{a} \frac{\partial u}{\partial x}(x,t) \int_{-\infty}^{\infty} \varphi(z)zdz + \frac{1}{2a^2} \frac{\partial^2 u}{\partial x^2}(x,t) \int_{-\infty}^{\infty} \varphi(z)z^2dz + O\left(\frac{1}{a^3}\right). \end{aligned} \quad (2.3)$$

In this study we will assume that the kernel  $\phi$  is even with its mean located at  $x = 0$ . Therefore the coefficient of the first order derivative in (2.3) is zero and thus

$$\int_{-\infty}^{\infty} \phi(x-y)u(y,t)dy = u(x,t) + \frac{\sigma(a)^2}{2} \frac{\partial^2 u}{\partial x^2}(x,t) + O\left(\frac{1}{a^3}\right),$$

using  $\varphi(x) = \phi(x/a)/a$  and the definition of the second moment of a probability distribution. Therefore, setting  $C = 2/\sigma(a)^2$  gives

$$C \left( \int_{-\infty}^{\infty} \phi(x-y)u(y,t)dy - u(x,t) \right) = \frac{\partial^2 u}{\partial x^2}(x,t) + O\left(\frac{1}{a}\right) \rightarrow \frac{\partial^2 u}{\partial x^2}(x,t),$$

as  $a \rightarrow \infty$ . This limiting behaviour will allow us to make comparisons between the local and the nonlocal model. Two kernel functions for which the derivation above holds true are the Laplacian

$$\phi(x) = \frac{a}{2} e^{-a|x|}, \quad (2.4)$$

and the Gaussian distribution

$$\phi(x) = \frac{a_g}{\sqrt{\pi}} e^{-a_g^2 x^2}, \quad (2.5)$$

where  $x \in \mathbb{R}$ , and  $a, a_g > 0$  are the scale parameters of the distributions, respectively. The Laplacian kernel corresponds to plants (seeds) dispersing as a random walk with individual plants (seeds) settling at different random times [25, 147]. One main goal of this chapter is to investigate how a change in the width of the kernel affects the tendency to form patterns. Closely related to this, a second main aspect we will address in this chapter is a comparison between different dispersal kernels. In particular we will show that the type of decay (i.e. exponential or algebraic) has an influence on the tendency to form patterns. The Laplacian kernel is not only biologically relevant [25, 92, 147] but also allows us to obtain analytic results due to the form of its Fourier transform and will therefore be the main focus of this chapter. Note that this kernel further allows a transformation from a nonlocal to a

local model by introducing an additional variable [22, 77, 128], but in the interest of considering other dispersal kernels we will not use this approach. To investigate the effects of the kind of decay of the kernel, we will finally consider the power law distribution

$$\phi(x) = \frac{(b-1)a_p}{2(1+a_p|x|)^b}, \quad b > 3, \quad (2.6)$$

where  $x \in \mathbb{R}$ , and  $a_p > 0$ ,  $b > 0$  are the scale and shape parameters of the distribution, respectively. Note that for this kernel function the derivation of the local model above does not hold. For a review of other biologically relevant plant dispersal kernels see [25, Table 1].

The purpose of this study is to gain an understanding of how the shape of the dispersal kernel in the nonlocal model (2.2) affects the tendency to form patterns. In particular, we will mainly focus on the maximum rainfall parameter  $A_{\max}$  that supports the formation of patterns, or in other words, the lowest amount of precipitation that allows plants to form a homogeneous vegetation cover. This critical rainfall level will be determined using different approaches for the Laplacian kernel (2.4). While all those approaches provide the same information on  $A_{\max}$ , they all give different further insights into other properties of the model. In Section 2.3 we will investigate the model using linear stability analysis, obtaining information on the pattern wavelength alongside the upper bound on the rainfall. The constant uphill migration of the plants suggests studying the system in its travelling wave form. This will be done in Section 2.4, where the critical rainfall level can be deduced from the loci of a Hopf bifurcation. Finally, the asymptotic form of the model is studied in Section 2.5. All these approaches make use of the size of the parameter  $\nu$  by obtaining conditions to leading order in  $\nu$  as  $\nu \rightarrow \infty$ . A comparison to other dispersal kernels is shown in Section 2.6 using numerical simulations of the model. From these we will be able to deduce parametric trends on how the tendency to form patterns is affected by the width and the type of decay of the dispersal. Finally, we discuss our results from an ecological viewpoint in Section 2.7. Motivated by the discussion above, the analysis will be done in three different cases; the situation in which  $C = 2/\sigma(a)^2$ , which allows us to compare our results for the Laplacian kernel to the corresponding results for the local model obtained by [184–186, 190–192], and the cases in which one of  $C$  or  $a$  is kept constant, while the other parameter is varied.

### 2.3 Linear Stability Analysis

In this section we will use linear stability analysis to investigate the occurrence of spatial patterns in the nonlocal Klausmeier model (2.2) with the Laplacian kernel (2.4). We will show that the maximum rainfall parameter  $A_{\max}$  supporting pattern formation is  $O_s(\nu^{1/2})$  ( $f = O_s(\nu) \iff f = O(\nu)$  and  $f \neq o(\nu)$ ), and will obtain an explicit expression for it. This will show that both an increase in  $a$  for  $C$  being kept constant and an increase in  $C$  for  $a$  being kept constant yields an increase of  $A_{\max}$ , while under the assumption that  $C = a^2$  an increase in  $a$  (and thus  $C$ ) results in a decrease of the critical value  $A_{\max}$ . Further this analysis will allow us to investigate the wavelength of the patterned solutions of the model.

The steady states of (2.2) are

$$\begin{aligned} (\bar{u}_1, \bar{w}_1) &= (0, A), \quad (\bar{u}_2, \bar{w}_2) = \left( \frac{2B}{A - \sqrt{A^2 - 4B^2}}, \frac{A - \sqrt{A^2 - 4B^2}}{2} \right), \\ (\bar{u}_3, \bar{w}_3) &= \left( \frac{2B}{A + \sqrt{A^2 - 4B^2}}, \frac{A + \sqrt{A^2 - 4B^2}}{2} \right), \end{aligned}$$

where  $(\bar{u}_2, \bar{w}_2)$  and  $(\bar{u}_3, \bar{w}_3)$  only exist if  $A \geq 2B$ . The steady state  $(\bar{u}_1, \bar{w}_1)$  describing extinction of plants  $u$  is always stable, while  $(\bar{u}_3, \bar{w}_3)$  is unstable for all choices of parameters, provided it exists. The steady state  $(\bar{u}, \bar{w}) := (\bar{u}_2, \bar{w}_2)$  is stable to spatially homogeneous perturbations if  $B < 2$ . For  $B > 2$ , it is only stable for sufficiently large values of  $A$ . Estimates of the parameters, however, suggest that  $B < 2$ .

To investigate the possibility of spatial patterns, consider spatially heterogeneous perturbations  $u = \bar{u} + \tilde{u}(x, t)$ ,  $w = \bar{w} + \tilde{w}(x, t)$  proportional to  $e^{\lambda t + ikx}$  for growth rate  $\lambda \in \mathbb{C}$  and wavenumber  $k > 0$ . Linearising the resulting system gives that  $\lambda$  satisfies the dispersion relation

$$\lambda = \frac{1}{2} \left( C \left( \hat{\phi}(k) - 1 \right) - dk^2 + \alpha + \delta + i\nu k \pm \sqrt{R + iI} \right),$$

where  $\hat{\phi}(k)$  is the Fourier transform of  $\phi$ ,  $\alpha = B$ ,  $\beta = 4B^2/(A - \sqrt{A^2 - 4B^2})$ ,  $\gamma = -2B$ ,  $\delta = -2A/(A - \sqrt{A^2 - 4B^2})$ ,

$$\begin{aligned} R &= \left( C \left( \hat{\phi}(k) - 1 \right) + dk^2 \right)^2 + 2C \left( \hat{\phi}(k) - 1 \right) (\alpha - \delta) \\ &\quad + (2\alpha d - 2\delta d - \nu^2) k^2 + 4\gamma\beta + (\alpha - \delta)^2, \end{aligned}$$

and

$$I = -2\nu k \left( C \left( \widehat{\phi}(k) - 1 \right) + dk^2 + \alpha - \delta \right).$$

For a Turing-Hopf bifurcation to occur, at least one eigenvalue needs to have positive real part. Therefore, the condition for patterns to form is

$$\Re(\lambda) = \frac{1}{2} \left( \alpha + \delta - dk^2 + C \left( \widehat{\phi}(k) - 1 \right) + \frac{1}{\sqrt{2}} \left( \sqrt{R^2 + I^2} + R \right)^{\frac{1}{2}} \right) > 0. \quad (2.7)$$

To investigate this further for  $\phi$  being the Laplacian kernel (2.4), we will make use of  $\nu \gg 1$ , by expanding (2.7) in  $\nu$ . With all other parameters  $O_s(1)$  as  $\nu \rightarrow \infty$ , this gives

$$\Re(\lambda) = \alpha - \frac{Ck^2}{a^2 + k^2} + O\left(\frac{1}{\nu^2}\right), \quad (2.8)$$

provided that  $(a^2 + k^2)(\delta - \alpha - dk^2) + Ck^2 < 0$ . If this condition is not satisfied, the expansion is  $\Re(\lambda) = -dk^2 + \delta < 0$  for any  $k > 0$ . Substituting  $k = 0$  into (2.8), yields  $\Re(\lambda) = \alpha > 0$ , which contradicts the stability of  $(\bar{u}, \bar{w})$  to spatially homogeneous perturbations. The occurrence of patterns is captured by assuming that  $A$  is  $O_s(\nu^{1/2})$ . Expanding in  $\nu \gg 1$  then gives

$$\Re(\lambda) = -\frac{(-B^5\nu^2 + B^4C\nu^2)k^4 + (-B^5a^2\nu^2 + A^4B + A^4C)k^2 + A^4Ba^2}{(B^4\nu^2k^2 + A^4)(a^2 + k^2)} + O\left(\frac{1}{\nu}\right). \quad (2.9)$$

Therefore,  $\Re(\lambda) > 0$  if

$$q(k^2) := (-B^5\nu^2 + B^4C\nu^2)k^4 + (-B^5a^2\nu^2 + A^4B + A^4C)k^2 + A^4Ba^2 < 0.$$

This polynomial in  $k^2$  attains its minimum

$$q(k_{\min}^2) = \frac{-(B+C)^2 A^8 - 2 B^5 a^2 \nu^2 (B - 3C) A^4 - B^{10} a^4 \nu^4}{4 B^4 \nu^2 (B - C)}, \quad (2.10)$$

at

$$k_{\min}^2 = \frac{-B^5 a^2 \nu^2 + A^4 B + A^4 C}{2 B^4 \nu^2 (B - C)}.$$

Solving  $q(k_{\min}^2) < 0$  for  $A^4$  gives  $A_1^4 < A^4 < A_2^4$  provided  $C > B$ , where  $A_1^4 < A_2^4$  are the roots of (2.10). Substituting  $A_1^4$  into  $k_{\min}^2$  gives  $k_{\min}^2 < 0$ , which contradicts

$k_{\min} \in \mathbb{R}$ . Therefore, the sufficient condition for patterns to occur is

$$A < A_{\max} = \left( \frac{3C - B - 2\sqrt{2C}\sqrt{C-B}}{(B+C)^2} \right)^{\frac{1}{4}} a^{\frac{1}{2}} B^{\frac{5}{4}} \nu^{\frac{1}{2}}, \quad (2.11)$$

valid to leading order in  $\nu$  as  $\nu \rightarrow \infty$ . As expected, setting  $C = a^2$  and taking the limit  $a \rightarrow \infty$  yields the corresponding condition for the local model obtained by [191], which is

$$A < A_{\max} = \left( \sqrt{2} - 1 \right)^{\frac{1}{2}} B^{\frac{5}{4}} \nu^{\frac{1}{2}}. \quad (2.12)$$

### 2.3.1 Wavelength

It is of interest to investigate the wavelength of the patterns. While a rigorous analysis of this requires tools from nonlinear analysis, one can obtain some information about the wavelength from the results obtained in this section. For this we will assume that the patterns are dominated by the wavenumber giving the largest growth, that is the wavenumber  $k_{\max}$  giving the maximum of  $\Re(\lambda)$  given in (2.9). Differentiating  $\Re(\lambda)$  with respect to  $k^2$  shows that it obtains its maximum at

$$k_{\max}^2 = -\frac{A^2 a \left( 2A^2 B^2 a \nu \left( B - \frac{C}{2} \right) + \sqrt{2BC} (-B^4 a^2 \nu^2 + A^4) \right)}{-B^6 C a^2 \nu^3 + 2A^4 B^3 \nu}.$$

Therefore the wavelength  $L$  is given by

$$\begin{aligned} L &= \frac{2\pi}{k_{\max}} \\ &= 2\pi \left( \frac{-B^6 C a^2 \nu^3 + 2A^4 B^3 \nu}{A^2 a \left( A^2 B^2 a \nu (2B - C) + \sqrt{2} \sqrt{BC} (-B^2 a \nu + A^2)^2 (B^2 a \nu + A^2)^2 \right)} \right)^{\frac{1}{2}}. \end{aligned} \quad (2.13)$$

The wavelength  $L$  is decreasing in the rainfall parameter  $A$ , decreasing in the dispersal parameter  $a$  if the dispersal coefficient  $C$  is fixed, increasing in  $C$  when  $a$  is kept constant, and increasing in  $a$  if one sets  $C = a^2$ . Figure 2.1a shows the wavelength as it varies with the rainfall parameter  $A$  for some fixed  $B$ ,  $C$ ,  $a$  and  $\nu$ . Also note that when  $C = a^2$ , the wavelength (2.13) for the nonlocal model approaches the wavelength predicted by the local model as  $a \rightarrow \infty$ , as expected by the limiting behaviour of the nonlocal model. Combining these two results shows

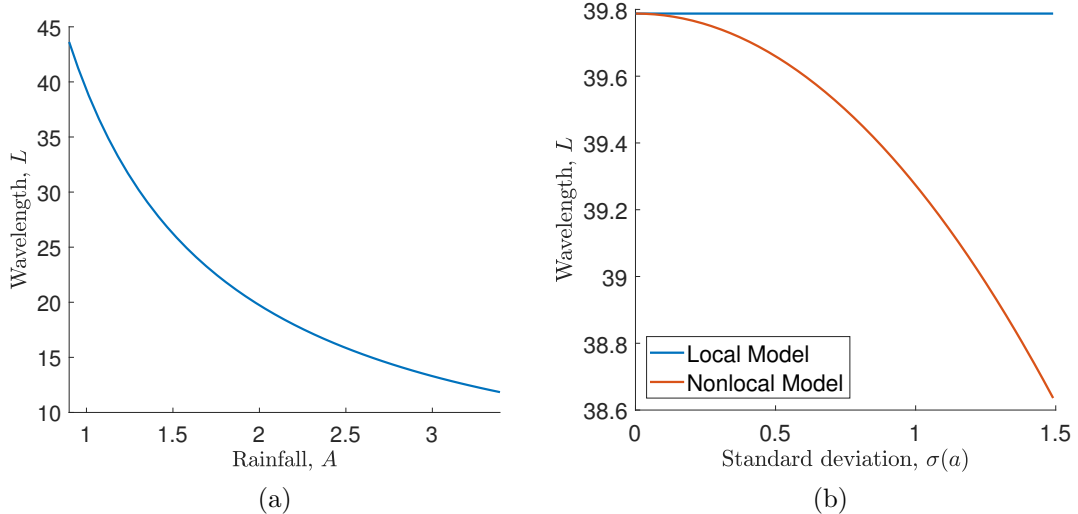


Figure 2.1: Variation in pattern wavelength with rainfall  $A$  and standard deviation  $\sigma(a)$ . Part (a) shows the wavelength (2.13) of the patterns as it decreases with the rainfall  $A$  for nonlocal model. The parameter values are  $B = 0.45$ ,  $\nu = 182.5$ ,  $C = 1$  and  $a = 1$ . Part (b) compares the wavelength predicted from the nonlocal model with the setting  $C = a^2$  as it varies with the dispersal parameter  $a$  and compares it to the wavelength obtained from the local model. It shows that the nonlocal model predicts a shorter distance between the vegetation stripes, especially if the shape of the dispersal kernel is wide. However, the difference is very small (see the  $y$ -axis of the plot). The parameter values used for this are  $A = 1$ ,  $B = 0.45$ ,  $\nu = 182.5$

that the nonlocal model predicts a shorter distance between vegetation stripes than the local model with this setting of  $C$ . This is visualised in Figure 2.1b.

## 2.4 Travelling Wave Solutions

The constant uphill migration of the vegetation patterns suggests considering travelling waves. In this section we will investigate the travelling wave form of the nonlocal Klausmeier model (2.2). Pattern solutions of the original PDE model then correspond to periodic solutions of the travelling wave ODEs. From the equations in their travelling wave form we will not only be able to confirm the results on the maximum rainfall supporting pattern formation obtained by performing linear stability analysis in Section 2.3, but also deduce more information about the migration speed of the patterns. The nature of the patterned solutions fundamentally depends on the scaling of the migration speed  $c$ . The highest rainfall level supporting pattern formation occurs for  $c = O_s(1)$ . For this situation we determine conditions for Hopf bifurcations to occur; for the local Klausmeier model (2.1) the parameter range in the  $A$ - $c$  plane that supports pattern formation is bounded above by the locus of a Hopf bifurcation [194], and we anticipate the same for the nonlocal model.

Applying the travelling wave ansatz  $u(x, t) = U(z)$ ,  $w(x, t) = W(z)$ ,  $z = x - ct$  to the nonlocal model (2.2), gives

$$\begin{aligned}\frac{dU}{dz} &= -\frac{1}{c} \left( U^2 W - BU + C \left( \int_{-\infty}^{\infty} \phi(z-z') U(z') dz' - U(z) \right) \right), \\ \frac{dW}{dz} &= -\frac{1}{c+\nu} \left( A - W - U^2 W + d \frac{d^2 W}{dz^2} \right).\end{aligned}$$

To investigate the occurrence of a Hopf bifurcation, consider perturbations  $\tilde{U}(z)$ ,  $\tilde{W}(z)$  proportional to  $e^{\lambda z}$  of the steady state  $(\bar{U}, \bar{W}) = (\bar{u}, \bar{w})$ . Setting  $\phi$  to be the Laplacian kernel (2.4) and linearising the resulting system gives that  $\lambda$  satisfies

$$\lambda^5 + \alpha \lambda^4 + \beta \lambda^3 + \gamma \lambda^2 + \delta \lambda + \varepsilon = 0, \quad (2.14)$$

where

$$\begin{aligned}\alpha &= \frac{d(B-C) + c(c+\nu)}{cd}, \\ \beta &= \frac{-2B^2(a^2cd - (B-C)(c+\nu)) - Ac(A + \sqrt{A^2 - 4B^2})}{2B^2cd}, \\ \gamma &= \frac{-2B^2a^2(d + c(c+\nu)) + A(B+C)(A + \sqrt{A^2 - 4B^2}) - 4B^3}{2B^2cd}, \\ \delta &= \frac{a^2(-2B^3(c+\nu) + Ac(A + \sqrt{A^2 - 4B^2}))}{2B^2cd}, \\ \varepsilon &= \frac{a^2(-A(A + \sqrt{A^2 - 4B^2}) + 4B^2)}{2B^2cd}.\end{aligned}$$

To find conditions for a Hopf bifurcation to occur, set  $\lambda = i\omega$ ,  $\omega \in \mathbb{R}$ . This splits (2.14) into its real and imaginary parts, which after solving for and eliminating  $\omega^2$  gives the condition

$$\frac{\gamma \pm \sqrt{\gamma^2 - 4\alpha\varepsilon}}{2\alpha} = \frac{\beta \pm \sqrt{\beta^2 - 4\delta}}{2}. \quad (2.15)$$

The assumption  $\omega \in \mathbb{R}$  requires that the left and right hand sides of this equation are both positive. This leads to an additional condition (2.18) that will be considered later. To further investigate (2.15), we expand it in  $1/\nu$ . This gives

$$\frac{((B-C)\text{sign}(c) + B+C)a^2}{B-C} + O\left(\frac{1}{\nu}\right) = 0.$$

For the first term of the expansion to be zero, one would require  $B > C$  with one of the parameters being equal to zero, depending on the sign of  $c$ . This is, however, not possible due to the positivity assumptions on the parameters. Investigating the next term of the expansion suggests using the scaling  $A = O_s(\nu^{1/2})$ . Applying this scaling to (2.15), expanding in  $\nu \gg 1$  and then solving for  $c$  shows that a Hopf bifurcation exists at

$$c_{\pm} = \left( \frac{B}{2A^2} + \frac{A^2(2B - C)}{2(-B^4a^2\nu^2 + A^4)} \right. \\ \left. \pm \left( \frac{B^2}{4A^4} + \frac{3BC}{2(-B^4a^2\nu^2 + A^4)} + \frac{4B^6a^2\nu^2 - 4A^4BC + A^4C^2}{4(-B^4a^2\nu^2 + A^4)^2} \right)^{\frac{1}{2}} \right) \nu B^2, \quad (2.16)$$

to leading order in  $\nu$  as  $\nu \rightarrow \infty$ . Since the migration speed  $c \in \mathbb{R}$ , this requires

$$A < A_{\max} = \left( \frac{3C - B - 2\sqrt{2C}\sqrt{C - B}}{(B + C)^2} \right)^{\frac{1}{4}} a^{\frac{1}{2}} B^{\frac{5}{4}} \nu^{\frac{1}{2}}, \quad (2.17)$$

and  $C > B$ . This is the same condition as (2.11) obtained in Section 2.3.

In deriving this condition we assumed that the terms in (2.15) were positive. By applying the scaling  $A = O_s(\nu^{1/2})$  and expanding in  $\nu \gg 1$ , this yields the bounds

$$\max \left\{ 0, \frac{B^2(B - C)\nu}{A^2} \right\} < c < \frac{B^3\nu}{A^2}, \quad (2.18)$$

to leading order in  $\nu$ . This condition is satisfied if  $C > B$ . In the case of  $C = a^2$  it holds if  $a > \sqrt{B}$ .

Setting  $C = a^2$  and taking the limit  $a \rightarrow \infty$  in both (2.16) and (2.17) gives, as expected by the considerations on the limiting behaviour of the model, the corresponding conditions obtained by [191] for the local model. Further the right hand side of (2.17) is decreasing for all  $a > \sqrt{B}$  in the setting  $C = a^2$ . Combined with the observation that it approaches the corresponding condition for the local model as  $a \rightarrow \infty$ , this shows that pattern formation is more likely in the nonlocal model with the tendency to form patterns increasing as the dispersal parameter  $a$  decreases, i.e. as the width of the kernel  $\phi$  increases. Figure 2.2a shows this for some fixed parameter values. Finally, Figure 2.2b combines these considerations by showing the loci (2.16) of the Hopf bifurcations of the nonlocal model for different values of the dispersal parameter  $a$  in the  $A$ - $c$  plane and compares it to the corresponding locus of the local model. As shown previously, this implies that in the nonlocal model a larger parameter region supports pattern formation, especially as the dispersal parameter  $a$  is decreased, i.e. as the width of the kernel is increased. This means

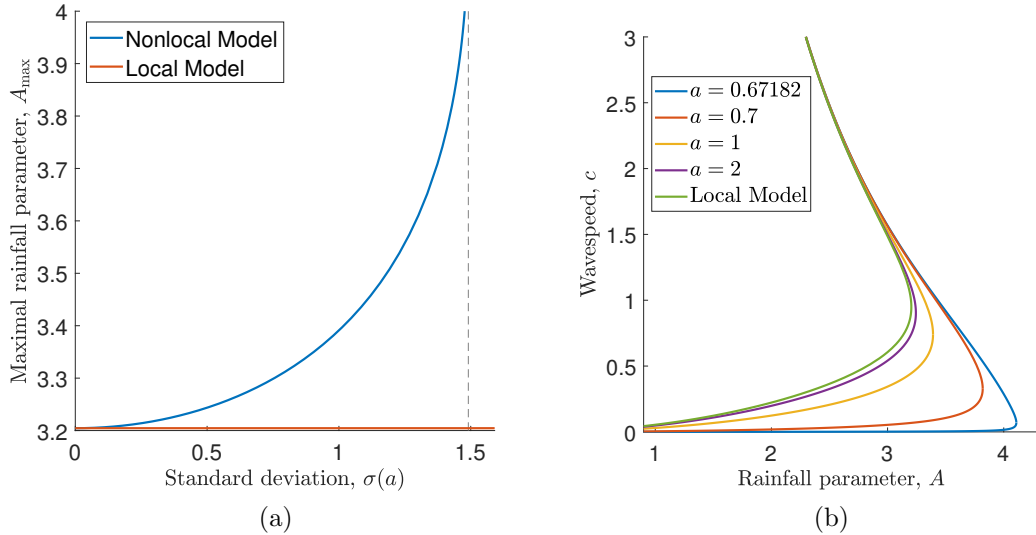


Figure 2.2: Variation in the loci of the Hopf bifurcation and maximum rainfall parameter  $A_{\max}$  with kernel width in the case  $C = a^2$ . The plot in (a) compares the upper bound (2.11) on the rainfall parameter  $A$  of the nonlocal model using the Laplacian kernel with  $C = a^2$  with condition (2.12) obtained for the local model. Note that one requires  $a > \sqrt{B}$  for  $A_{\max} \in \mathbb{R}$  in the case of the nonlocal model. Part (b) compares the loci (2.16) of the Hopf bifurcations of the nonlocal model for different values of the dispersal parameter  $a$  to the locus of the local model obtained by [191]. The parameter values used in both figures are  $B = 0.45$ ,  $\nu = 182.5$ .

that the nonlocal model predicts that plants which disperse their seeds over a larger distance will undergo a change from homogeneous vegetation to patterns at a higher level of rainfall than those plants with a narrower and diffusion-like dispersal, as the amount of rainfall is gradually decreased.

If  $C \neq a^2$ , it is not appropriate to compare the nonlocal model to the local model. However, one can still investigate how a change in the dispersal parameter  $a$  affects the tendency to form patterns in this situation. We will first consider the case in which  $C$  is constant. In this situation (2.17) yields that the highest rainfall parameter supporting pattern formation  $A_{\max}$  is proportional to  $a^{1/2}$ . This means that if the dispersal kernel gets narrower, a larger range of the rainfall parameter  $A$  supports pattern formation. This is visualised in Figure 2.3a, which shows the maximum rainfall parameter  $A_{\max}$  plotted against the dispersal parameter  $a$  and in Figure 2.3b, which visualises the location of the Hopf bifurcation (2.16), where  $C$  is constant. This is contrary to the behaviour observed in the case of  $C = a^2$ , where a narrower kernel gave less tendency to form patterns.

Investigating the final case, i.e. the one of fixed  $a$  and varying  $C$ , shows that the critical rainfall parameter  $A_{\max}$  is decreasing with increasing  $C$  for all  $C > B$ . This shows that the more the plants invest in their dispersal, the less likely is the formation of patterns. Similar to the previous two cases, the change in  $A_{\max}$  is

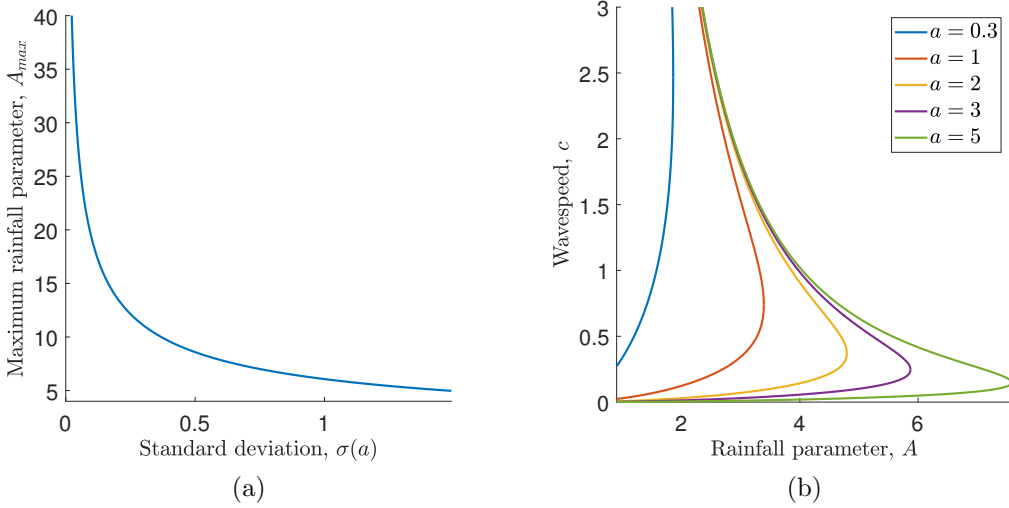


Figure 2.3: Variation in the loci of the Hopf bifurcation and maximum rainfall parameter  $A_{\max}$  with kernel width in the case of constant  $C$ . The plot in (a) shows how upper bound  $A_{\max}$  given in (2.17) of the rainfall parameter  $A$  that supports pattern formation in the nonlocal model using the Laplacian kernel varies as the dispersal parameter  $a$  is changed. Here  $C = 1$  is fixed. Part (b) shows the loci (2.16) of the Hopf bifurcations of the nonlocal model with the Laplacian kernel for different values of the dispersal parameter  $a$ , where the dispersal coefficient  $C$  is constant. The parameter values used here are  $B = 0.45$ ,  $C = 1$ ,  $\nu = 182.5$

visualised in Figure 2.4a and the loci of the Hopf bifurcations in the  $A$ - $c$  plane is shown in Figure 2.4b.

## 2.5 Asymptotic analysis of the integro-PDE model

In the previous sections we have applied different techniques to the model (2.2) to find conditions for pattern formation in their leading order form. In this section we will confirm these by first obtaining the leading order form of the Integro-PDE model and then deducing conditions for Hopf bifurcations from it.

Applying the rescalings  $u = AB^{-1}u^*$ ,  $w = A^{-1}B^2w^*$ ,  $t = B^{-1}t^*$ ,  $c = Bc^*$ ,  $\nu = A^2B^{-2}\Gamma^{-1}$ ,  $B^{-1}C = D$  to (2.2) gives

$$\frac{\partial u}{\partial t} = u^2 w - u + D \left( \int_{-\infty}^{\infty} \phi(x-y) u(y, t) dy - u(x, t) \right),$$

$$B\nu^{-1} \frac{\partial w}{\partial t} = \Gamma(1 - u^2 w) - \nu^{-1} w + \frac{\partial w}{\partial x} + d\nu^{-1} \frac{\partial^2 w}{\partial x^2},$$

where the  $^*$ 's were dropped for brevity. Again assuming that  $A = O_s(\nu^{1/2})$ , the

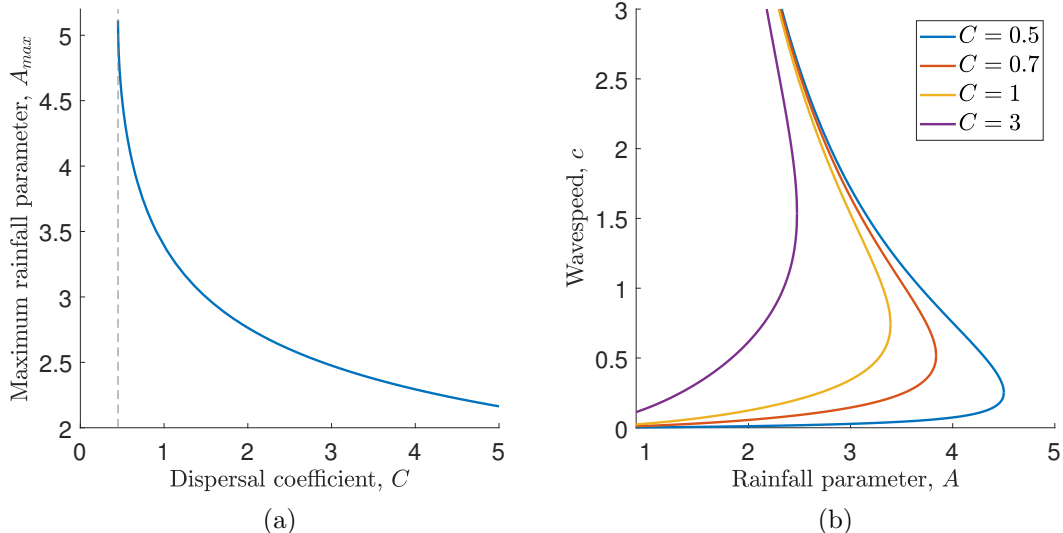


Figure 2.4: Variation in the loci of the Hopf bifurcation and maximum rainfall parameter  $A_{\max}$  with kernel width in the case of constant  $a$ . The plot in (a) shows how upper bound  $A_{\max}$  given in (2.17) of the rainfall parameter  $A$  that supports pattern formation in the nonlocal model with Laplacian kernel varies as the dispersal coefficient  $C$  is changed. Here  $a = 1$  is fixed. Note that  $C > B$  is required for  $A_{\max} \in \mathbb{R}$ . Part (b) shows the loci (2.16) of the Hopf bifurcations in the same situation. The parameter values used here are  $B = 0.45$ ,  $C = 1$ ,  $\nu = 182.5$

leading order form in  $\nu$  of this is

$$\frac{\partial u}{\partial t} = u^2 w - u + D \left( \int_{-\infty}^{\infty} \phi(x-y) u(y, t) dy - u(x, t) \right),$$

$$0 = \Gamma (1 - u^2 w) + \frac{\partial w}{\partial x}.$$

Applying the travelling wave ansatz  $u(x, t) = U(z)$ ,  $w(x, t) = W(z)$ ,  $z = x - ct$ , gives

$$-c \frac{dU}{dz} = U^2 W - U + D \left( \int_{-\infty}^{\infty} \phi(z-z') U(z') dz' - U(z) \right),$$

$$0 = \Gamma(1 - U^2 W) + \frac{dW}{dz}.$$

This system has a unique steady state given by  $(\bar{U}, \bar{W}) = (1, 1)$ . Consider small perturbations  $\tilde{U}, \tilde{W}$  of the steady state that are proportional to  $e^{\lambda z}$ . Letting  $\phi$  to be the Laplacian kernel (2.4) and linearising the resulting system yields that  $\lambda$  satisfies

$$\lambda^4 + \bar{\alpha}\lambda^3 + \bar{\beta}\lambda^2 + \bar{\gamma}\lambda + \bar{\delta} = 0, \quad (2.19)$$

where

$$\bar{\alpha} = \frac{1 - D - \Gamma c}{c}, \quad \bar{\beta} = \frac{\Gamma(1 - D) - a^2 c}{c}, \quad \bar{\gamma} = \frac{a^2(\Gamma c - 1)}{c}, \quad \bar{\delta} = -\frac{\Gamma a^2}{c}.$$

To find conditions for a Hopf bifurcation to occur, again set  $\lambda = i\omega$ ,  $\omega \in \mathbb{R}$ . Analogous to the preceding sections, this allows splitting (2.19) into its real and imaginary parts, which after solving for  $\omega^2$ , assuming that  $\omega \neq 0$ , gives

$$\frac{\bar{\beta} \pm \sqrt{\bar{\beta}^2 - 4\bar{\delta}}}{2} = \frac{\bar{\gamma}}{\bar{\alpha}}, \quad (2.20)$$

as the leading order condition for a Hopf bifurcation to occur. The restriction  $\omega \in \mathbb{R}$ , implies the additional requirement

$$\max \left\{ 0, \frac{1 - D}{\Gamma} \right\} < c < \frac{1}{\Gamma}. \quad (2.21)$$

Solving (2.20) for  $c$  gives

$$c_{\pm} = \frac{(D - 3)\Gamma^2 + a^2 \pm \sqrt{(D + 1)^2\Gamma^4 - 2a^2(3D - 1)\Gamma^2 + a^4}}{2\Gamma(a^2 - \Gamma^2)}. \quad (2.22)$$

To satisfy (2.21), one requires  $C > B$  and

$$\Gamma < \left( \frac{3D - 1 + 2\sqrt{2D(D - 1)}}{(D + 1)^2} \right)^{\frac{1}{2}} a. \quad (2.23)$$

Therefore, the steady state  $(\bar{U}, \bar{W}) = (1, 1)$  undergoes a Hopf bifurcation if (2.21), (2.22) and (2.23) are satisfied. Substituting the rescalings used at the beginning of this section into these three conditions gives the same conditions (2.18), (2.16) and (2.17) that were obtained from the travelling wave equations in Section 2.4.

## 2.6 Numerical Simulations

So far, we have only considered one particular form of dispersal kernel in the non-local Klausmeier model (2.2). In this section we will solve the model numerically for different kernel functions and use the solutions to estimate the maximum rainfall parameter giving patterns for each kernel. The simulations will show that the parametric trends that were obtained for the Laplacian kernel carry over to other kernel functions, i.e. a wider dispersal kernel and a higher dispersal rate decrease the tendency to form patterns, while under the assumption that  $C = 2/\sigma(a)^2$ , an increase in kernel width causes an increase in the size of the parameter region giving

patterns. Our numerical simulations will further show that the tendency to form patterns depends on the type of decay of the dispersal kernel.

In the analysis performed in previous sections, we considered the model on an infinite domain. To mimic this in the simulations, we will consider a subdomain centred in a larger domain with the following initial conditions; outside the smaller subdomain the system's initial state will be set to the steady state, while on the subdomain a random perturbation will be added. The idea of this is to choose the outer domain large enough so that any conditions imposed on the boundary of this domain (which are set to be periodic in our simulations) do no affect the solution on the inner subdomain in the finite time that is considered in the simulation. The solution is then only considered on the subdomain on which a perturbation was introduced. To solve the Integro-PDE system (2.2), it is first transformed into an ODE system by discretising its space domain and then solved by the built-in MATLAB ODE solver `ode15s`. A significant simplification is made by computing the convolution term using the fast Fourier transform, as it reduces the number of operations required to find the convolution from  $O(M^2)$  to  $O(M \log(M))$  in each step (e.g. [36]), where  $M$  is the number of points of the space domain. Figure 2.5 shows typical solutions obtained by this method; in Figure 2.5a the rainfall was chosen large enough for the solution to converge to the steady state, while for Figure 2.5b parameters that produce a patterned solution of the nonlocal Klausmeier model using the Laplacian kernel were used.

Using these simulations, we set up a scheme, based on the amplitude of the oscillation of the solution of the nonlocal Klausmeier model (2.2) relative to the steady state that approximates the critical rainfall parameter  $A_{\max}$ , that is the maximum rainfall parameter supporting pattern formation, for different kernel functions  $\phi(x)$ . Unlike in the simulation results shown in Figure 2.5, we run the simulations over a shorter amount of time (up to  $t = 30$ ), as we are only interested in the onset of spatial patterns rather than in any of their properties. The kernel functions used in our simulations are those introduced in Section 2.2, i.e. the Laplacian (2.4), the Gaussian (2.5) and the power law kernel (2.6). Note that the standard deviations  $\sigma(a)$  are given by  $\sigma(a) = \sqrt{2}/a$  for the Laplacian kernel,  $\sigma(a_g) = 1/(\sqrt{2} a_g)$  for the Gaussian kernel and  $\sigma(a_p) = \sqrt{2}/(\sqrt{b^2 - 5b + 6} a_p)$  for the power law kernel, provided  $b > 3$ . If the shape parameter of the power law kernel is  $b \leq 3$ , its standard deviation is infinite and a meaningful comparison to other kernel functions cannot be performed based on their standard deviations. In our simulations we consider both  $b = 3.1$  and  $b = 4$ . As in previous sections, we will consider the case in which  $C = 2/\sigma(a)^2$ , motivated by the limiting behaviour of the nonlocal model, and the cases in which either  $C$  or  $a$  is assumed to be constant and the other parameter is varied.

Figure 2.6a shows the results of our simulations in the case of  $C$  being con-

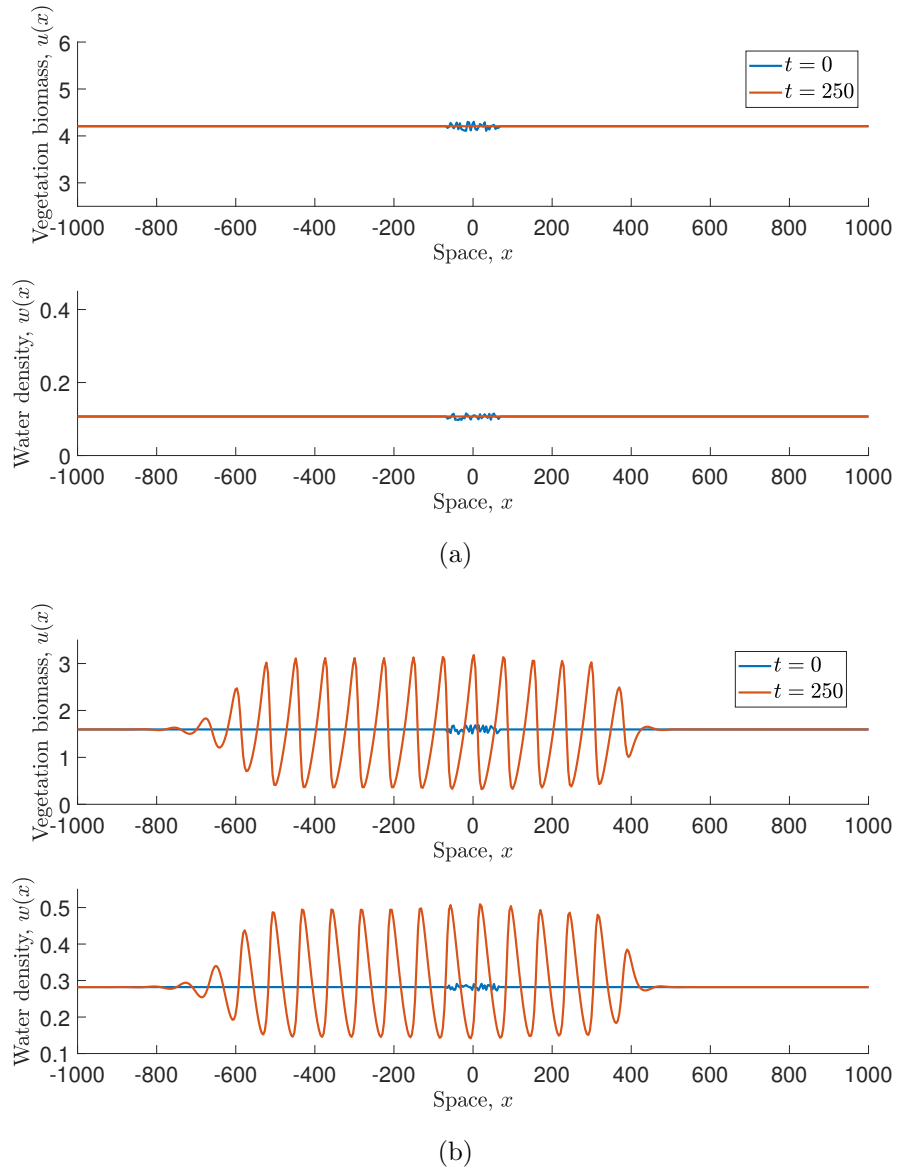


Figure 2.5: Numerical solution of the nonlocal Klausmeier model (2.2) using the Laplacian kernel (2.4) for different rainfall levels. In (a)  $A = 2$  yields convergence to the coexisting steady state from which the system is perturbed initially. Part (b) displays a patterned solution obtained by setting  $A = 1$ . The other parameter values used in both simulations are  $B = 0.45$ ,  $\nu = 50$ ,  $d = 100$ ,  $a = 2$ ,  $C = 4$  and the number of space points is  $M = 2^9$

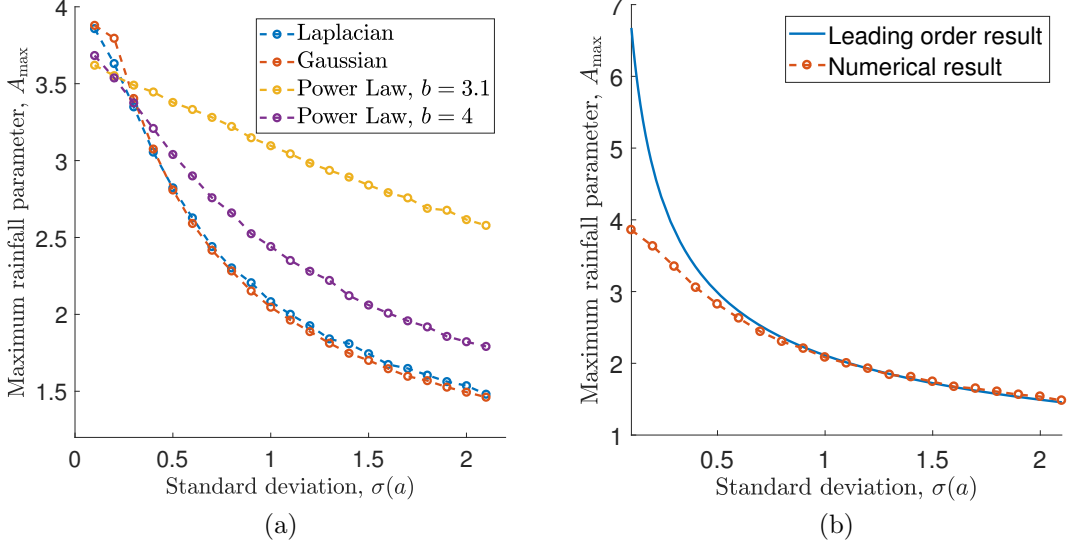


Figure 2.6: Illustration of the results of our numerical scheme to approximate the maximum rainfall parameter  $A_{\max}$  in the case of constant  $C$ . Part (a) shows the results of our simulations in the case of  $C$  being constant. We have determined the maximum rainfall parameter giving patterns for the Laplacian kernel (2.4), the Gaussian kernel (2.5) and the power law kernel (2.6) for both  $b = 3.1$  and  $b = 4$ , at  $\sigma(a) = \{0.1, 0.2, \dots, 2.1\}$ . The parameter values used in these simulations are  $B = 0.45$ ,  $C = 1$ ,  $\nu = 50$ ,  $d = 1$ . Part (b) compares the simulation results obtained for the Laplacian kernel to the corresponding condition (2.17) valid to leading order in  $\nu$

stant. The trend that a narrower dispersal kernel requires a higher level of rainfall to form homogeneous vegetation, which was predicted by the leading order form (2.17) of  $A_{\max}$  for the Laplacian kernel, carries over to the other kernels used in the simulations. Further one can observe that the power law distributions which have algebraic decay give a larger value of  $A_{\max}$  than those with exponential decay if the standard deviation is sufficiently large ( $\sigma(a) \gtrsim 0.3$ ), while for narrower kernels the opposite is true. While the results of our simulations for the Laplacian kernel and the corresponding leading order form of  $A_{\max}$  fit well for sufficiently large values of the standard deviation  $\sigma(a)$ , the fit is poorer for narrower kernel functions (see Figure 2.6b for a comparison). The reason for this is the relatively small choice of  $\nu = 50$ , which was taken to improve the speed of the simulations. Solutions for larger  $\nu$  indicate that the relative difference between  $A_{\max}$  in our simulations and in the analytical approximation decreases (slowly) with increasing  $\nu$ .

We repeat the same scheme in the setting of  $C = 2/\sigma(a)^2$  for the same kernel functions. The results of this are shown in Figure 2.7. Considering the type of decay of the kernel functions, the results of it are similar to the simulations of the case of  $C$  being constant. One can observe that the distributions with algebraic decay

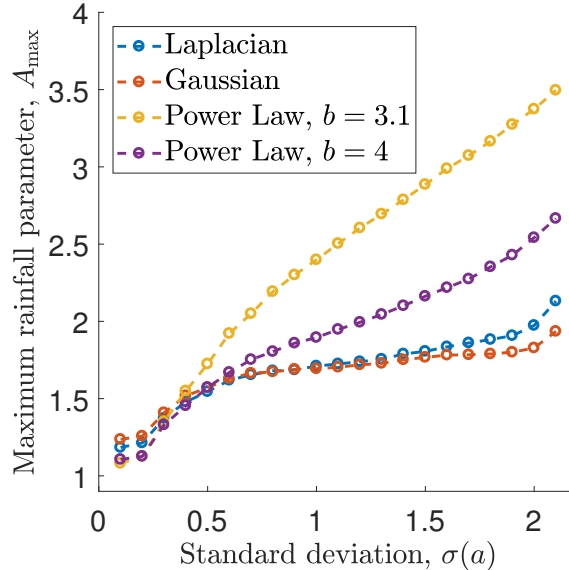


Figure 2.7: Illustration of the results of our numerical scheme to approximate the maximum rainfall parameter  $A_{\max}$  in the case of  $C = 2/\sigma(a)^2$ . We have considered the Laplacian kernel (2.4), the Gaussian kernel (2.5) and the power law kernel (2.6) for both  $b = 3.1$  and  $b = 4$  and determined the value of the maximum rainfall parameter giving patterns  $A_{\max}$  at  $\sigma(a) = \{0.1, 0.2, \dots, 2.1\}$  for each kernel function in the case of  $C = 2/\sigma(a)^2$ . The parameters used in this simulation are  $B = 0.45$ ,  $\nu = 50$ ,  $d = 1$ .

yield a larger value of  $A_{\max}$  than the distributions with exponential decay if the kernel is sufficiently wide, while for narrow kernels the opposite is true. Further, considering one specific kernel on its own, a narrower dispersal kernel now gives a lower value of the maximum rainfall parameter supporting pattern formation. This is in contrast to the case in which  $C$  was kept constant but in accord with the leading order form (2.17) of  $A_{\max}$ . As before, it can also be observed from the simulations of the model using the Laplacian kernel that for the choice of  $\nu = 50$ , the numerical simulations are a good approximation of the leading order result only for sufficiently wide kernels.

Finally, we apply the same scheme to the case of fixed dispersal parameter  $a$  and varying dispersal coefficient  $C$  (Figure 2.8). As in the previous cases, the trends of the simulations of other kernel functions are again in alignment with the leading order result (2.17) for the Laplacian kernel. An increase in dispersal rate  $C$  causes a decrease in  $A_{\max}$  for each of the dispersal kernels considered in our simulations. Further, the comparison of kernels with algebraic and exponential decay depends on the choice of standard deviation  $\sigma(a)$ , as indicated by the previous simulations in which the standard deviation was varied. Figure 2.8b shows that for a small standard deviation ( $\sigma(a) = 0.2$  in this case), the kernels with exponential decay predict that a higher level of rainfall is required to form a uniform vegetation cover than those with algebraic decay. If the standard deviation is sufficiently large, the

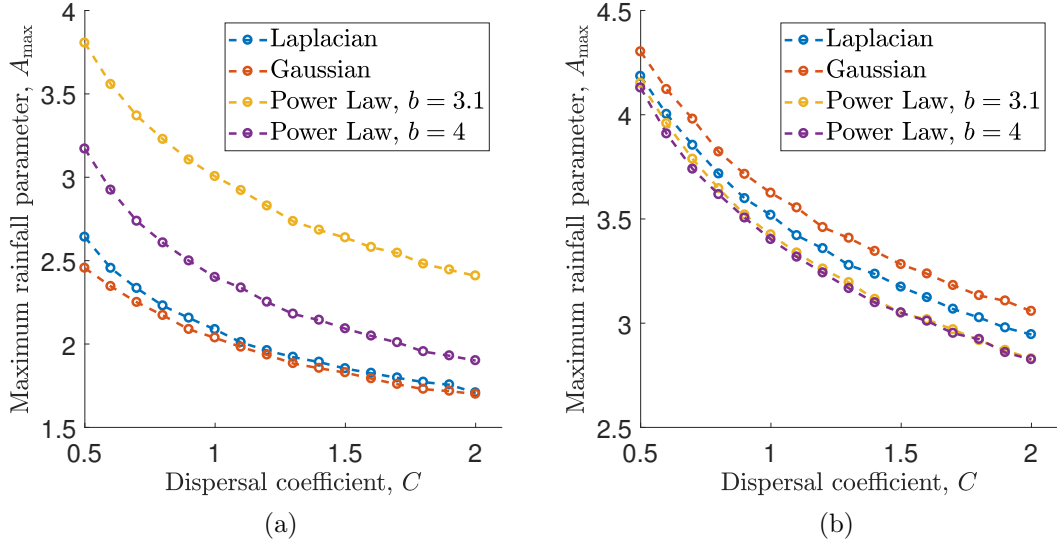


Figure 2.8: Illustration of the results of our numerical scheme to approximate the maximum rainfall parameter  $A_{\max}$  in the case of constant  $a$ . We have considered the Laplacian kernel (2.4), the Gaussian kernel (2.5) and the power law kernel (2.6) for both  $b = 3.1$  and  $b = 4$  and determined the value of the maximum rainfall parameter giving patterns  $A_{\max}$  at  $C = \{0.5, 0.6, \dots, 2\}$  for each kernel function, with  $a$  being fixed. In (a), the standard deviation was chosen as  $\sigma(a) = 1$ , in (b) as  $\sigma(a) = 0.2$ . The other parameters used in this simulation are  $B = 0.45$ ,  $\nu = 50$ ,  $d = 1$ .

opposite trend is observed. This is visualised in Figure 2.8a, where the standard deviation was set to  $\sigma(a) = 1$ .

## 2.7 Discussion

The main results of this chapter are given by (2.16) and (2.18), which give an upper bound for the parameter region in the  $A$ - $c$  plane supporting pattern formation, valid to leading order in  $\nu$ , for the nonlocal Klausmeier model (2.2) with the Laplacian kernel (2.4). In particular this gives the upper bound  $A_{\max}$ , defined in (2.17), on the rainfall parameter, again valid to leading order in  $\nu$ . In other words,  $A_{\max}$  represents the lowest level of rainfall that allows plants to form a homogeneous vegetation cover, while lower amounts of water only support banded vegetation. These results hold under the assumptions that the migration speed  $c$  is  $O_s(1)$  and that the parameter region supporting pattern formation is bounded above by the loci of Hopf bifurcations, which was shown by [194] for the local Klausmeier model (2.1). While the simple nature of the Klausmeier model makes it impossible to deduce any quantitative conclusions from these results, they do give a good insight into the parametric trends of the model. These trends fundamentally depend on the assumption made on the factor  $C$  scaling the convolution term in the nonlocal

model.

In this chapter we considered three different cases of the coefficient  $C$  in the nonlocal Klausmeier model; that of choosing it to be constant, the one of varying  $C$  for fixed dispersal parameter  $a$  and that of setting  $C = 2/\sigma(a)^2$ . In the case of  $C$  being fixed, a change in the dispersal parameter  $a$  only affects the width of the dispersal kernel, but leaves the term scaling the nonlocal plant dispersal term unchanged. It can be immediately concluded from (2.17) that the threshold  $A_{\max}$  increases as the kernel width decreases. This increase in the size of the parameter region supporting pattern formation is also visualised in Figure 2.3b. This means that the wider plants disperse their seeds, the less water they require to form a homogeneous vegetation cover. In particular, our results show that if plant dispersal is wide enough, the location of the Hopf bifurcation bounding the pattern forming parameter region completely lies in the region that only supports the trivial steady state describing complete desertification. In this case, the assumptions taken in this chapter predict that no striped vegetation can occur. Plants either form a homogeneous vegetation cover or disappear completely.

The expression given by (2.17) is only valid for the Laplacian kernel (2.4) and to leading order in  $\nu$ . The numerical simulations in Section 2.6 allow us to compare this condition to those for other kernel functions that have been suggested by studies on plant dispersal (see [25] for an overview). Our results suggest that the maximum rainfall level giving patterned vegetation depends on the width and therefore also on the type of decay of the dispersal kernel. It can be seen from Figures 2.6a and 2.7 that those probability distributions that decay algebraically predict a larger pattern-giving parameter region for some fixed standard deviation than those decaying exponentially under all the different assumptions taken on  $C$  in this chapter, if the dispersal kernel is sufficiently wide. If the kernel is narrow, the opposite behaviour is observed. Further, the simulations show that  $A_{\max}$  for each individual kernel is decreasing as the width of the kernel is increased if one assumes that  $C$  is constant. This is in accord with the behaviour of the leading order form (2.17) of the Laplacian kernel. Combining these observations, we can conclude that the narrower a plant's seed dispersal is, the more water is required to avoid the formation of patterns. Nevertheless, field data shows that plants in semi-arid ecosystems tend to establish narrow dispersal kernels [66, 227]. This is, however, only a side effect of other adaptations such as seed containers protecting seeds from flooding and predation [66]. Simulations show that short range dispersal yields a higher mean biomass in those ecosystems than a long distance spread of seeds [156]. Combining this with the results of this chapter shows that the shortening of dispersal ranges of plants in semi-arid environments increases their tendency to self-organise into patterns.

If one assumes that the width of the dispersal kernel is fixed and plant's dispersal rate is changed, (2.17) shows that, under the assumption that the dispersal of seeds fits the Laplacian kernel, the more the species invests in its dispersal rate, the less water it requires to form a homogeneous vegetation cover. For the other dispersal kernels we have considered, the same behaviour is shown in our simulations. Those simulations also show the same trend regarding the type of decay of the dispersal kernels as the simulations in the case of fixed  $C$  and varying range of dispersal. For wider dispersal kernels, those plants whose kernel functions decay algebraically have a higher tendency to form patterns than those plants dispersing their seeds according to an exponentially decaying kernel. For sufficiently narrow kernels, the opposite observation can be made.

The final choice of  $C$  assumes that it is correlated with the standard deviation of the dispersal kernel as  $C = 2/\sigma(a)^2$ . This choice is of particular significance because it leads to the local Klausmeier model being a limiting case of the nonlocal model using either the Laplacian or the Gaussian kernel. This allows us to compare our results to the corresponding results obtained for the local model by [191]. This choice is motivated purely mathematically and we are not aware of any evidence that the dispersal coefficient  $C$  is correlated with the seed distribution range in such a way. However, experiments have shown that plants' rate of dispersal increases in semi-arid environments [6], e.g. by the production of more but smaller seeds [230] as well as that plants develop short range dispersal of seeds [66, 227]. The analysis of the previous two cases has shown that an increase in the dispersal coefficient reduces the critical level of rainfall required to form a homogeneous vegetation cover, while the establishment of a narrow dispersal kernel increases this threshold. Therefore, this could be seen as an evolutionary trade-off.

The leading order results on quantities such as  $A_{\max}$  or the wavelength, obtained in Sections 2.3 and 2.4, resemble the limiting behaviour of this case. Apart from the limiting case, the results for the nonlocal model using the Laplacian kernel behave monotonically as the width of the dispersal kernel is changed. In particular, the results on the loci of the Hopf bifurcation and the maximum rainfall parameter giving patterns allow us to make the crucial observation that the nonlocal model predicts a larger range of parameters supporting pattern formation. Our results further show that the size of the parameter region giving patterns is larger for a wider dispersal kernel, which makes the dispersal term less influential, i.e. it decreases the plant's dispersal rate, due to the assumption  $C = a^2$ . This is most strikingly illustrated by Figure 2.2b, which shows the increase of this region as the scale parameter  $a$  of the kernel decreases. Under this assumption on the dispersal rate and the kernel width, our simulation results show that establishing short range dispersal increases plants' ability to form a homogeneous vegetation cover. This is

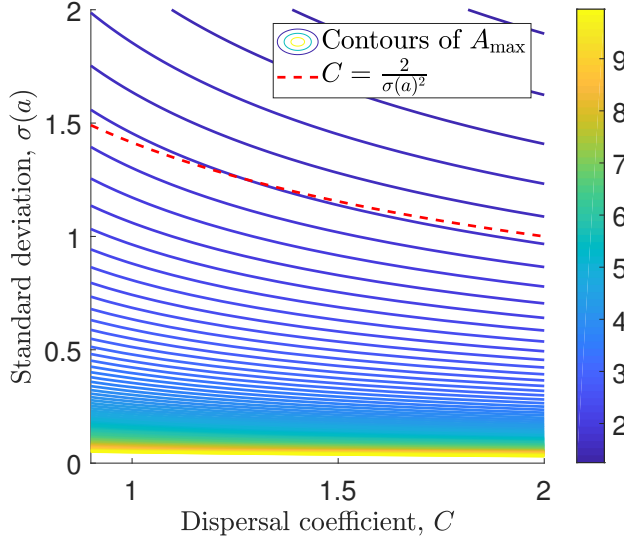


Figure 2.9: Contour plot of  $A_{\max}$ . This plot shows the contours of (2.17) as solid lines with the colours indicating the level of  $A_{\max}$ . The red dotted line is the suggested trade-off  $C = 2/\sigma(a)^2$ , which was mathematically motivated by the limiting behaviour of the convolution integral

further illustrated by Figure 2.9, which shows shows the contours of  $A_{\max}$  and the suggested evolutionary trade-off  $C = 2/\sigma(a)^2$ . The latter crosses the contours as the standard deviation is varied and thereby shows that an increase in kernel width yields an increase in the maximum rainfall parameter supporting pattern formation.

In this chapter we have also investigated the distance between the striped vegetation patches to leading order in  $\nu$ . It is of immense importance to have an understanding of the wavelength of the patterns as it might give an indication of whether the ecosystem is close to complete desertification. The results of this study show that the wavelength monotonically increases as the amount of rainfall decreases, before reaching a critical threshold, where patterns disappear and complete desertification takes over. While it is important to emphasise again that the simplifications assumed in deducing the Klausmeier model do not allow us to gain any quantitative information, we have shown how the wavelength is affected by changes in the width of the dispersal kernel or in the plant's dispersal rate. Interestingly, in the case of  $C = 2/\sigma(a)^2$ , the wavelength predicted by the nonlocal model using the Laplacian kernel does not differ much from the wavelength predicted by the local model, even for wide dispersal kernels (see the  $y$ -axis in Figure 2.1b). This suggests that one could make predictions on the possibility of desertification without having any information on the range of plant dispersal under the assumption that the dispersal coefficient  $C$  is correlated with the standard deviation of the dispersal kernel in such a way.

The pattern solutions of the Klausmeier model fundamentally depend on how the migration speed  $c$  scales with the parameter  $\nu$ , describing the rate of the water flow downhill. In this chapter we have only considered the case  $c = O_s(1)$  and the patterns forming in the vicinity of the Turing-Hopf bifurcation. For the local Klausmeier model results have been obtained for a wide range of migration speeds [184, 186, 190–192]. One natural extension of this work would be to do a similar comprehensive study of the whole parameter range for the nonlocal model. This would give insights into the existence and form of patterns away from the bifurcation point.

Another natural area for future work would be to consider other more realistic models for vegetation patterns. A number of such models and their underlying mechanisms and scale dependent feedbacks are reviewed by [129]. Some of these models already include nonlocal dispersal via convolution integrals [16, 156, 157], and in others [86, 163] such a term could be added in place of plant diffusion. While these as well as the model considered in this chapter assume an isotropic dispersal of plants, this simplification can be removed by including either advection of plants [169, 210] or an asymmetric dispersal kernel [210]. Similar to the relation between diffusion and the convolution with a symmetric kernel, both the advection and the diffusion terms arise from the convolution term with an asymmetric kernel. In this case the coefficient of the first order derivative in (2.3) is non-zero. Finally, some models use a nonlocal term for the water uptake and thus also for plant growth, reflecting the extensive root networks of plants in semi-arid regions [74, 75]. Investigation of these models using an approach similar to that in the current study would be of interest but would be particularly challenging because of the added complexity.

## Chapter 3

### An integrodifference model for vegetation patterns in semi-arid environments with seasonality

The contents of this chapter have been submitted to a journal and are currently under review. A preprint is available [62].

#### 3.1 Author contribution

The authors of the submitted paper [62] are Lukas Eigentler and Jonathan A Sherratt. Lukas Eigentler conceptualised the research, formulated the mathematical model, performed both the analytical and numerical analyses of the model, wrote the paper draft and reviewed and edited the manuscript. Jonathan A Sherratt conceptualised the research, reviewed and edited the manuscript and provided supervision.

#### Abstract

Vegetation patterns are a characteristic feature of semi-deserts occurring on all continents except Antarctica. In some semi-arid regions, the climate is characterised by seasonality, which yields a synchronisation of seed dispersal with the dry season or the beginning of the wet season. We reformulate the Klausmeier model, a reaction-advection-diffusion system that describes the plant-water dynamics in semi-arid environments, as an integrodifference model to account for the temporal separation of plant growth processes during the wet season and seed dispersal processes during the dry season. The model further accounts for nonlocal processes involved in the dispersal of seeds. Our analysis focusses on the onset of spatial patterns. The Klausmeier partial differential equations (PDE) model is linked to the integrodifference model in an appropriate limit, which yields a control parameter for the temporal separation of seed dispersal events. We find that the conditions for pattern onset in the integrodifference model are equivalent to those for the continuous PDE model and hence independent of the time between seed dispersal events. We thus conclude that in the context of seed dispersal, a PDE model provides a sufficiently accurate description, even if the environment is seasonal. This

emphasises the validity of results that have previously been obtained for the PDE model. Further, we numerically investigate the effects of changes to seed dispersal behaviour on the onset of patterns. We find that long-range seed dispersal inhibits the formation of spatial patterns and that the seed dispersal kernel's decay at infinity is a significant regulator of patterning.

### 3.2 Introduction

Vegetation patterns are a ubiquitous feature of ecosystems in semi-arid climate zones. Occurrences of such mosaics of plants and bare soil have been reported from all continents except Antarctica, including the African Sahel [48] and the Horn of Africa [79], Western Australia [72], northern Chile [68], Israel [182], the Chihuahuan Desert in North America [48] and Southeastern Spain [108]. A detailed understanding of the evolution of vegetation patterns is of considerable importance as they hold valuable information on the health of ecosystems. For example, changes to a pattern's properties such as its wavelength, its recovery time from perturbations, or the area fraction covered by biomass can act as early warning signals of desertification [39, 45, 78, 96, 164, 170, 246]. Desertification processes are a major threat to economies in semi-deserts as agriculture provides a significant contribution to GDP [218]. For example, the livestock sector, which depends in part on animals grazing on spatially patterned vegetation, accounts for 20% of GDP in Chad and involves 40% of its population [51, 219].

A number of feedback mechanisms may be involved in the pattern formation process (see [131] for a review), but it is widely agreed that a central mechanism is the vegetation-infiltration feedback loop, which results in a redistribution of water towards areas of high biomass. On bare soil, the formation of physical and biological soil crusts inhibits water infiltration into the soil [65]. Thus, water run-off towards existing vegetation patches occurs. The enhancement of environmental conditions in these sinks for the limiting resource drives further plant growth and thus closes the feedback loop [209].

Dryland plants have developed a range of seed production and dispersal strategies to cope with the environmental stress in their habitats [66, 227]. One such mechanism, commonly observed in water-controlled ecosystems, is ombrohydrochory, the dispersal of seeds caused by an opening of the seed container due to contact with water [146, 150, 227]. One particular form, exhibited by members of the Aizoaceae family in semi-arid regions of the Sahel, Australia and South America, is ballistic dispersal, which uses the kinetic energy of raindrops to expulse the plants' seeds [70, 150]. Some semi-arid environments such as those in the Mediterranean are characterised by seasonal fluctuations in their environmental conditions and in par-

ticular in their precipitation patterns [148]. In combination with processes that allow plants to store diaspores during periods of drought, ombrohydrochory yields a synchronisation of seed dispersal with the beginning of the wet season in such seasonal environments. This synchronisation has, for example, been reported in *Mesembryanthemum crystallinum* and *Mesembryanthemum nodiflorum* in Southeastern Spain [146]. If seed dispersal strategies different from ombrohydrochory are dominant, most species disperse their seeds during the dry season [146, 181].

The seasonal synchronisation of seed dispersal splits the annual life-cycle of a plant population into two distinct stages. During the wet season, seeds germinate, new seedlings emerge and adult plants increase their biomass, but no spatial movement takes place. Seed dispersal only occurs during, or at the end of the dry season, while growth processes are dormant [14]. By contrast, most mathematical models for dryland vegetation patterns consist of partial differential equations and thus assume that seed dispersal occurs continuously in time. A widely used approach to account for the temporal structure of the annual life cycle is the use of integrodifference equations. This splits the system into 2 distinct, non-overlapping phases, which are both described as discrete, instantaneous processes: a growth phase during which dispersal processes are either not present or negligible and a dispersal phase during which no growth occurs. The application of integrodifference equations to biological and ecological systems in which spatial dispersal plays a significant role was in part pioneered by Kot and Schaffer [102], and has become a well-established tool in the description of biological and ecological systems since then (e.g. [33, 143, 144, 147, 155]).

The spatial and temporal scales associated with the evolution of vegetation patterns do not allow their recreation in laboratory settings. Instead, a range of mathematical models have been proposed to address different aspects of the pattern dynamics [21, 247]. A significant amount of modelling work is based on systems of partial differential equations, most notably by Gilad et al. [74], HilleRisLambers and Rietkerk et al. [86, 163] and Klausmeier [99]. The reaction-advection-diffusion Klausmeier model [99] is a deliberately basic description of dryland ecosystems based on the vegetation-infiltration feedback loop. Its relative simplicity provides a rich framework for model analyses and extensions (e.g. [20, 34, 61, 63, 184, 186, 190–192, 199, 221]). The recent development of new remote sensing technology, using temporal sequences of satellite images, allows for comparisons between model predictions and field data [10, 72].

In the Klausmeier model, seed dispersal is modelled by a diffusion term. In reality, the dispersal of seeds is affected by nonlocal processes, such as ballistic dispersal or long range dispersal (e.g. via mammals or wind) [25, 156]. The Klausmeier model has been extended to account for such nonlocal processes in Chapter 2 and [20, 61]

and a similar approach has been applied to other models for dryland vegetation [16, 156, 157]. Integrodifference systems also provide a description of nonlocal dispersal effects through a convolution of the plant density with a kernel function. The kernel function is a probability density function describing the average distribution of seeds dispersed from a single plant. The dispersal kernel's properties (in particular its shape and standard deviation) depend on both plant species and environmental conditions [25].

In this chapter we address the significance of seed dispersal synchronisation and its temporal separation from growth processes in seasonal dryland environments. To do so, we introduce an integrodifference model describing the plant-water dynamics in semi-arid ecosystems in Section 3.3. We base our model on the Klausmeier model, to compare our results to previous model analyses of models with no temporal structure. To aid comparisons to the PDE model, we review the most relevant results for the Klausmeier model in Section 3.3. Even though an integrodifference model cannot explicitly take into account the length of the plant growth stage, a convergence result (Proposition 3.3.1) yields a control parameter for the temporal separation of seed dispersal events through an appropriate parameter setting. In Section 3.4 we focus on this special case and perform a linear stability analysis to determine a condition for pattern onset in the model and investigate this condition under variations in the growth season length. The analytical derivation of this condition relies on a specific (but nevertheless biologically relevant) choice of the dispersal kernels. To relax this assumption we perform numerical simulations in Section 3.5 to determine the parameter region in which pattern onset occurs for other biologically relevant dispersal kernels. Finally, we discuss our results in Section 3.6.

### 3.3 The Models

In this section we introduce the integrodifference model which we use to investigate the effects of seasonal synchronisation of seed dispersal on the onset of vegetation patterns in semi-arid environments. The model is based on the reaction-advection-diffusion model by Klausmeier [99] and to facilitate the comparison of our results on the discrete model to that of the time-continuous model, we start by reviewing relevant results for the Klausmeier model. We relate the models through a consistency result that shows that the Klausmeier PDE model can be obtained from the integrodifference model in an appropriate limit.

### 3.3.1 Klausmeier Model

One of the well-established models describing vegetation patterns in semi-arid environments is the Klausmeier model [99]. It reduces the plant-water dynamics to a small set of basic processes (rainfall, plant mortality, evaporation/drainage, vegetation-infiltration feedback and spatial dispersal). The relative simplicity of this modelling approach provides a framework for a rich mathematical analysis (e.g. [184–186, 190–192, 194, 199, 221]). Suitably nondimensionalised [99, 185], the model is

$$\frac{\partial u}{\partial t} = \underbrace{u^2 w}_{\text{plant growth}} - \underbrace{B u}_{\text{plant mortality}} + \underbrace{\frac{\partial^2 u}{\partial x^2}}_{\text{plant dispersal}}, \quad (3.1a)$$

$$\frac{\partial w}{\partial t} = \underbrace{A}_{\text{rainfall}} - \underbrace{w}_{\substack{\text{evaporation} \\ \text{and drainage}}} - \underbrace{u^2 w}_{\substack{\text{water consumption} \\ \text{by plants}}} + \underbrace{\nu \frac{\partial w}{\partial x}}_{\substack{\text{water flow} \\ \text{downhill}}} + \underbrace{d \frac{\partial^2 w}{\partial x^2}}_{\text{water diffusion}}. \quad (3.1b)$$

Here  $u(x, t)$  denotes the plant density,  $w(x, t)$  the water density,  $x \in \mathbb{R}$  the space domain where  $x$  is increasing in the uphill direction and  $t > 0$  the time. Originally, the model only focussed on a sloped spatial domain, but the addition of a water diffusion term to account for the possibility of a description on flat terrain is a well established addition [95, 199, 225, 247]. To emphasise on the description of seed dispersal as a local process, we refer to this model as the “local Klausmeier model” throughout the chapter. Water input to the system is assumed to occur at a constant rate, evaporation and drainage effects are proportional to the water density [167, 171] and the plant mortality rate is density-independent. The nonlinearity in the description of water uptake and plant growth processes arises due to a soil modification by plants. The term is the product of the density of the consumer  $u$  and of the available resource  $uw$ , the amount of water that is able to infiltrate into soil layers where plant roots consume water. The dependence on the plant density  $u$  in the latter term occurs due to a positive correlation between the plant density and the soil surface’s permeability [38, 165, 222]. Finally, plant growth is assumed to be proportional to the amount of consumed water [167, 171]. The parameters  $A$ ,  $B$ ,  $\nu$  and  $d$  are combinations of different dimensional parameters but can be interpreted as rainfall, plant loss, the slope and water diffusion, respectively.

In a previous chapter (Chapter 2) [61] we have introduced nonlocal seed dispersal effects to the model by replacing the plant diffusion term by a convolution of a dispersal kernel (a probability density function)  $\phi$  and the plant density  $u$ . The

resulting model is referred to as the “nonlocal Klausmeier model” and is

$$\frac{\partial u}{\partial t} = u^2 w - Bu + C (\phi(\cdot) * u(\cdot, t) - u(x, t)), \quad (3.2a)$$

$$\frac{\partial w}{\partial t} = A - w - u^2 w + \nu \frac{\partial w}{\partial x} + d \frac{\partial^2 w}{\partial x^2}. \quad (3.2b)$$

The additional parameters  $C$  and  $a$  represent the rate of plant dispersal and reciprocal width of the dispersal kernel, respectively. Note that the convolution  $(\phi * u)(x, t)$  accounts for all plant biomass dispersed to the space point  $x$ , including the fraction of biomass that is not dispersed. The final term in (3.2a) ensures that the total biomass over the whole domain remains unchanged by the seed dispersal term. The nonlocal model (3.2) and the local model (3.1) are related through a convergence result. If the dispersal kernel  $\phi$  is decaying exponentially as  $|x| \rightarrow \infty$ , then the local model (3.1) can be obtained from the nonlocal model (3.2) in the limit  $C \rightarrow \infty$  and  $\sigma \rightarrow 0$  with  $C = 2/\sigma^2$ , where  $\sigma$  denotes the standard deviation of  $\phi$  [61] (Chapter 2).

Linear stability analysis of both the local and the nonlocal Klausmeier model with the Laplace kernel

$$\phi(x) = \frac{a}{2} e^{-a|x|}, \quad a > 0, x \in \mathbb{R}. \quad (3.3)$$

provides analytically derived conditions for pattern onset to occur in the system. On flat ground, i.e.  $\nu = 0$ , Turing-type patterns form due to a diffusion-driven instability, i.e. there exists a threshold  $d_c > 0$  on the diffusion coefficient such that an instability occurs for all  $d > d_c$ . In the local model (3.1), the threshold is

$$d_c(A, B) = \frac{8B\sqrt{-A^2 + A\sqrt{A^2 - 4B^2} + 4B^2} - 2A^2 + 2A\sqrt{A^2 - 4B^2} + 16B^2}{B(A - \sqrt{A^2 - 4B^2})^2}. \quad (3.4)$$

A corresponding threshold  $\tilde{d}_c(A, B, C, a)$  for the nonlocal model (3.2) with the Laplace kernel (3.3) can be derived explicitly, but it omitted due to its algebraic complexity.

On sloped ground ( $\nu \neq 0$ ) pattern onset has been studied close to a Turing-Hopf bifurcation, which is characterised by an upper bound on the rainfall parameter  $A$  that has been derived analytically valid to leading order in  $\nu$  as  $\nu \rightarrow \infty$  for both models in Chapter 2 and [61, 191]. The calculation of this upper bound on the precipitation parameter for the nonlocal model with the Laplace kernel shows that long range dispersal of seeds inhibits the formation of patterns by decreasing the

size of the parameter region that supports the onset of patterns. On flat ground an increase of the dispersal kernel's standard deviation causes an increase in the threshold on the diffusion coefficient, while on sloped ground an increase in the dispersal kernel's width inhibits the formation of patterns by decreasing the upper bound on the rainfall parameter.

The analytical derivation of pattern onset conditions in the nonlocal model is facilitated by the simple algebraic form of the Laplace kernel's Fourier transform and the associated polynomial structure of the dispersion relation in the linear stability analysis. For other biologically relevant seed dispersal kernels, conditions for pattern onset are not analytically tractable. Numerical simulations, however, confirm the qualitative trends obtained for the model with the Laplace kernel. Simulations further suggest that the dispersal kernel's decay at infinity has an influence on the rainfall threshold. For narrow dispersal kernels, those that account for more rare long-range dispersal events (algebraic decay rather than exponential) have an inhibitory effect on the formation of patterns, while for sufficiently wide kernels those that decay algebraically at infinity promote pattern formation compared to exponentially decaying kernels.

### 3.3.2 Integrodifference Model

Integrodifference models are a common type of model widely used in the description of systems in which dispersal processes are temporally separated from other dynamics such as growth/birth and decay/death. To account for the separation of plant growth and seed dispersal stages in dryland ecosystems, we propose the integrodifference model

$$u_{n+1}(x) = C\phi * f(u_n, w_n), \quad (3.5a)$$

$$w_{n+1}(x) = D\phi_1 * g(u_n, w_n), \quad (3.5b)$$

where

$$f(u, w) = u^2 w - Bu + \frac{1}{C}u,$$

$$g(u, w) = A - u^2 w - w + \frac{1}{D}w.$$

Here  $u_n(x)$  denotes the plant density,  $w_n(x)$  the water density after  $2n, n \in \mathbb{N}$  seasons and location  $x \in \mathbb{R}$ , where  $x$  increases in the uphill direction. The formulation of the model splits the processes involved into two phases: a growth and evolution phase described by the functions  $f(u, w)$  and  $g(u, w)$  during which no dispersal occurs, and

a dispersal phase modelled as a convolution of the evolved densities with dispersal kernels. As in the nonlocal Klausmeier model (3.2), the plant dispersal kernel  $\phi$  is symmetric and represents isotropic dispersal of plants. To model the flow of water downhill, the water dispersal kernel  $\phi_1$  is in general asymmetric with mean  $\mu_{\phi_1} \leq 0$ . The special case of a symmetric kernel  $\phi_1$  corresponds to the model on flat ground, which is the main aspect of the study in this chapter. The model is based on the Klausmeier models (3.2) and (3.1) and thus the functions  $f(u, w)$  and  $g(u, w)$  consist of the terms describing the rate of change in the original model, appropriately scaled by the coefficients  $C$  and  $D$  to reflect the time between steps in the discrete model, added to the existing densities.

As the integrodifference model (3.5) arises directly from the local Klausmeier model (3.1), the two models can be linked through a consistency result in an appropriate limit which shows that *the integrodifference model (3.5) tends to the local Klausmeier model (3.1)* as  $T \rightarrow 0$ . To show this, we consider the parameter setting

$$C = T, \quad \sigma_\phi^2 = 2T, \quad D = T, \quad \mu_{\phi_1} = -\nu T, \quad \tilde{\sigma}_{\phi_1}^2 = 2dT, \quad (3.6)$$

where  $\mu$  and  $\sigma$  denote the mean and standard deviation of the respective kernels and  $\tilde{\sigma}_{\phi_1}^2 = \int_{-\infty}^{\infty} \phi_1(x)x^2dx$ , the second raw moment of the kernel function  $\phi_1$ . Further, we define operators  $P, P_T : C^\infty(\mathbb{R} \times [0, \infty), [0, \infty)^2) \rightarrow C^\infty(\mathbb{R} \times [0, \infty), [0, \infty)^2)$  by

$$P\mathbf{v}(x, t) = \frac{\partial \mathbf{v}}{\partial t}(x, t) - \Gamma\mathbf{v}(x, t) - h_1(\mathbf{v}(x, t)), \quad (3.7)$$

for any function  $\mathbf{v}(x, t) = (u(x, t), w(x, t)) \in C^\infty(\mathbb{R} \times [0, \infty), [0, \infty)^2)$ , where

$$\Gamma = \text{diag} \left( \frac{\partial^2}{\partial x^2}, \nu \frac{\partial}{\partial x} + d \frac{\partial^2}{\partial x^2} \right), \quad h_1(\mathbf{v}) = \begin{pmatrix} u^2 w - Bu \\ A - u^2 w - w \end{pmatrix},$$

and

$$P_T\mathbf{v}(x, t) = \frac{1}{T} (\mathbf{v}(x, t + T) - h_2(\mathbf{v}(x, t))), \quad (3.8)$$

where

$$h_2(\mathbf{v}(x, t)) = \begin{pmatrix} -C\phi(\cdot) * f(u(\cdot, t), w(\cdot, t)) \\ -D\phi_1(\cdot) * g(u(\cdot, t), w(\cdot, t)) \end{pmatrix}.$$

Note that the operator  $P$  arises from the local Klausmeier model (3.1), because  $P\mathbf{v} = 0$  for any  $\mathbf{v}$  that satisfies (3.1). Similarly,  $P_T$  represents the integrodifference model (3.5), because a sequence  $\mathbf{v}_n(x) = \mathbf{v}(x, nT)$  satisfies (3.5) if  $P_T\mathbf{v}_n = 0$  for all  $n \in \mathbb{N}$ . Utilising this reformulation of both models, it is possible to show the

following result.

**Proposition 3.3.1.** *Consider the parameter setting (3.6) and let the kernel functions  $\phi$  and  $\phi_1$  have finite moments of all orders and decay exponentially as  $|x| \rightarrow \infty$ . Then the integrodifference model (3.5) is consistent with the local Klausmeier model (3.1), i.e.*

$$P\mathbf{v} - P_T\mathbf{v} \rightarrow 0 \quad \text{as} \quad T \rightarrow 0^+,$$

for any  $\mathbf{v} \in C^\infty(\mathbb{R} \times [0, \infty), [0, \infty)^2)$ .

In other words, the model equations (3.5) converge to the model equations (3.1) as  $T \rightarrow 0^+$ . The notion of *consistency* is widely used in the field of numerical analysis, and crucially it does not imply convergence of model solutions. While we are unable to construct an argument to prove convergence, numerical simulations suggest that solutions of the integrodifference model (3.5) converge to solutions of the local Klausmeier model (3.1) in the parameter setting (3.6) as  $T \rightarrow 0^+$  (Fig. 3.2).

On sloped ground Prop. 3.3.1 requires that  $\nu = o(T^{-1})$ , so that  $T\nu \rightarrow 0$  as  $T \rightarrow 0^+$  and  $\nu \rightarrow \infty$ , to facilitate any asymptotic analysis in  $\nu$  similar to that of the local Klausmeier model [184–186, 190–192]. On flat ground,  $\phi_1$  is symmetric and thus  $\mu_{\phi_1} = 0$  and  $\tilde{\sigma}_{\phi_1}$  coincides with the kernel's standard deviation  $\sigma_{\phi_1}$ .

The parameter  $T$  can be interpreted as the time between separate dispersal events and the scalings (3.6) are thus the main focus of the model's analysis in Section 3.4. While the time between two seed dispersal events in a seasonal environment is usually fixed, we are interested in variations of  $T$  as this parameter establishes a connection between the local Klausmeier model (3.1) and the integrodifference model (3.5). In particular, as  $T \rightarrow 0^+$  in the model, the length of each season tends to zero. As a consequence, this limit corresponds to the disappearance of any seasonality in the model and all processes are assumed to occur continuously in time, as, for example, in the Klausmeier model (3.1).

One kernel function satisfying the conditions in Prop. 3.3.1 is the Laplacian kernel (3.3). We define the corresponding asymmetric Laplace kernel by  $\phi_1(x) = Ne^{-a_2|x|}$  for  $x \geq 0$  and  $\phi_1(x) = Ne^{(a_2-a_1)|x|}$  for  $x < 0$ , where  $N = (a_2-a_1)a_2/(2a_2-a_1)$  and  $a_2 > a_1 > 0$ . The parameter  $a_1$  controls the extent of the asymmetry of the kernel function and  $a_1 = 0$  yields the symmetric Laplace kernel (3.3). The model with this particular kernel function is studied in some detail in this chapter as the Fourier transform of the symmetric Laplacian kernel  $\hat{\phi}(k) = a^2/(a^2+k^2)$  provides a significant simplification in the analysis of pattern onset.

*Proof of Proposition 3.3.1.* Firstly, we show that

$$P_T \mathbf{v}(x, t) = \frac{\mathbf{v}(x, t+T) - \mathbf{v}(x, t)}{T} - \Gamma \mathbf{v}(x, t) - h_1(\mathbf{v}(x, t)) + O(T^2). \quad (3.9)$$

To this end, we define  $\phi(x) = \sigma_\phi^{-1}\varphi(\sigma_\phi^{-1}x)$  and  $\phi_1(x) = \tilde{\sigma}_{\phi_1}^{-1}\varphi_1(\tilde{\sigma}_{\phi_1}^{-1}x)$ . Under the changes of variables  $y = x - \sigma_\phi z$  and  $y = x - \tilde{\sigma}_{\phi_1} z$ , respectively,  $P_T \mathbf{v} = ((P_T \mathbf{v})_1, (P_T \mathbf{v})_2)$  satisfies

$$T(P_T \mathbf{v})_1 = u(x, t+T) - C \int_{-\infty}^{\infty} \varphi(z) f(u(x - \sigma_\phi z, t), w(x - \sigma_\phi z, t)) dz, \quad (3.10a)$$

$$T(P_T \mathbf{v})_2 = w(x, t+T) - D \int_{-\infty}^{\infty} \varphi_1(z) g(u(x - \tilde{\sigma}_{\phi_1} z, t), w(x - \tilde{\sigma}_{\phi_1} z, t)) dz. \quad (3.10b)$$

Due to the parameter setting (3.6), small values of  $T$  correspond to small values of  $\sigma_\phi$  and  $\tilde{\sigma}_{\phi_1}$ . Hence, to investigate the system's behaviour for  $T \ll 1$ , consider the Taylor expansions of  $u(x - \sigma_\phi z, t)$ ,  $w(x - \sigma_\phi z, t)$ ,  $u(x - \tilde{\sigma}_{\phi_1} z, t)$  and  $w(x - \tilde{\sigma}_{\phi_1} z, t)$  about  $x$ , which give

$$\begin{aligned} & f(u(x - \sigma_\phi z, t), w(x - \sigma_\phi z, t)) \\ &= u(x, t)^2 w(x, t) + \left( \frac{1}{C} - B \right) u(x, t) \\ &\quad - \sigma_\phi z \left( u(x, t)^2 w_x(x, t) + \left( \frac{1}{C} - B \right) u_x(x, t) + 2u(x, t)u_x(x, t)w(x, t) \right) \\ &\quad + \sigma_\phi^2 z^2 \left( \frac{1}{2} u(x, t)^2 w_{xx}(x, t) + u_x(x, t)^2 w(x, t) + \frac{1}{2} \left( \frac{1}{C} - B \right) u_{xx}(x, t) \right. \\ &\quad \left. + u(x, t)u_{xx}(x, t)w(x, t) + 2u(x, t)u_x(x, t)w_x(x, t) \right) + O(\sigma_\phi^3), \quad (3.11) \end{aligned}$$

and similarly

$$\begin{aligned}
 & g(u(x - \tilde{\sigma}_{\phi_1} z), w(x - \tilde{\sigma}_{\phi_1} z)) \\
 &= A - u(x, t)^2 w(x, t) + \left( \frac{1}{D} - 1 \right) w(x, t) \\
 &\quad - \tilde{\sigma}_{\phi_1} z \left( -u(x, t)^2 w_x(x, t) + \left( \frac{1}{D} - 1 \right) w_x(x, t) - 2u(x, t)u_x(x, t)w(x, t) \right) \\
 &\quad + \tilde{\sigma}_{\phi_1}^2 z^2 \left( -u_x(x, t)^2 w(x, t) - \frac{1}{2} u(x, t)^2 w_{xx}(x, t) + \frac{1}{2} \left( \frac{1}{D} - 1 \right) w_{xx}(x, t) \right. \\
 &\quad \left. - u(x, t)u_{xx}(x, t)w(x, t) - 2u(x, t)u_x(x, t)w_x(x, t) \right) + O(\tilde{\sigma}_{\phi_1}^3), \quad (3.12)
 \end{aligned}$$

where the subscripts of  $u$  and  $w$  denote partial differentiation. Substitution of this into (3.10) and term-wise integration using Watson's Lemma (e.g. [134]) gives

$$\begin{aligned}
 T(P_T \mathbf{v})_1 &= u(x, t + T) - C \left( u(x, t)^2 w(x, t) + \left( \frac{1}{C} - B \right) u(x, t) \right. \\
 &\quad \left. + \left( u(x, t)^2 w_{xx}(x, t) + 2(u_x(x, t))^2 w(x, t) + \left( \frac{1}{C} - B \right) u_{xx}(x, t) \right. \right. \\
 &\quad \left. \left. + 2u(x, t)u_{xx}(x, t)w(x, t) + 4u(x, t)u_x(x, t)w_x(x, t) \right) \sigma_{\phi}^2 \int_{-\infty}^{\infty} \varphi(z) z^2 dz + O(\sigma_{\phi}^3) \right),
 \end{aligned}$$

and

$$\begin{aligned}
 T(P_T \mathbf{v})_2 &= w(x, t + T) \\
 &\quad - D \left( 2 \left( A - u(x, t)^2 w(x, t) + \left( \frac{1}{D} - 1 \right) w(x, t) \right) \int_{-\infty}^{\infty} \varphi_1(z) dz \right. \\
 &\quad \left. + \left( u(x, t)^2 w_x(x, t) - \left( \frac{1}{D} - 1 \right) w_x(x, t) + 2u(x, t)u_x(x, t)w(x, t) \right) \right. \\
 &\quad \left. \tilde{\sigma}_{\phi_1} \int_{-\infty}^{\infty} \varphi_1(z) z dz \right. \\
 &\quad \left. + \left( -2(u_x(x, t))^2 w(x, t) - u(x, t)^2 w_{xx}(x, t) + \left( \frac{1}{D} - 1 \right) w_{xx}(x, t) \right. \right. \\
 &\quad \left. \left. - 2u(x, t)u_{xx}(x, t)w(x, t) - 4u(x, t)u_x(x, t)w_x(x, t) \right) \frac{\tilde{\sigma}_{\phi_1}^2}{2} \int_{-\infty}^{\infty} \varphi_1(z) z^2 dz \right. \\
 &\quad \left. + O(\tilde{\sigma}_{\phi_1}^3) \right).
 \end{aligned}$$

Using that  $\varphi(x) = \sigma_\phi \phi(\sigma_\phi x)$ ,  $\varphi_1(x) = \tilde{\sigma}_{\phi_1} \phi_1(\tilde{\sigma}_{\phi_1} x)$ , and the definition of the moments of a probability distribution give

$$\begin{aligned}
 T(P_T \mathbf{v})_1 &= u(x, t + T) - C \left( u(x, t)^2 w(x, t) + \left( \frac{1}{C} - B \right) u(x, t) + \frac{\sigma_\phi^2}{2C} u_{xx}(x, t) \right. \\
 &\quad \left. + \sigma_\phi^2 \left( \frac{1}{2} u(x, t)^2 w_{xx}(x, t) + (u_x(x, t))^2 w(x, t) - \frac{1}{2} B u_{xx}(x, t) \right. \right. \\
 &\quad \left. \left. + u(x, t)u_{xx}(x, t)w(x, t) + 2u(x, t)u_x(x, t)w_x(x, t) \right) + O(\sigma_\phi^3) \right),
 \end{aligned}$$

and

$$\begin{aligned}
 T(P_T \mathbf{v})_2 &= w(x, t + T) - D \left( A - u(x, t)^2 w(x, t) + \left( \frac{1}{D} - 1 \right) w(x, t) \right. \\
 &\quad - \frac{\mu_{\phi_1}}{D} w_x(x, t) + \frac{\tilde{\sigma}_{\phi_1}^2}{2D} w_{xx}(x, t) + \mu_{\phi_1} (u(x, t)^2 w_x(x, t) + w_x(x, t) \\
 &\quad + 2u(x, t) u_x(x, t) w(x, t)) + \tilde{\sigma}_{\phi_1}^2 \left( -(u_x(x, t))^2 w(x, t) - \frac{1}{2} u(x, t)^2 w_{xx}(x, t) \right. \\
 &\quad \left. \left. - \frac{1}{2} w_{xx}(x, t) - u(x, t) u_{xx}(x, t) w(x, t) - 2u(x, t) u_x(x, t) w_x(x, t) \right) + O(\tilde{\sigma}_{\phi_1}^3) \right).
 \end{aligned}$$

Applying (3.6) yields

$$\begin{aligned}
 T(P_T \mathbf{v})_1 &= u(x, t + T) \\
 &\quad - (u(x, t) + T(u(x, t)^2 w(x, t) - Bu(x, t) + u_{xx}(x, t))) + O(T^2),
 \end{aligned}$$

and

$$\begin{aligned}
 T(P_T \mathbf{v})_2 &= w(x, t + T) \\
 &\quad - (w(x, t) + T(A - u(x, t)^2 w(x, t) - w(x, t) + \nu w_x(x, t) + dw_{xx}(x, t))) + O(T^2),
 \end{aligned}$$

which shows (3.9).

The Taylor expansions  $u(x, t + T) = u(x, t) + Tu_t(x, t) + O(T^2)$  and  $w(x, t + T) = w(x, t) + Tw_t(x, t) + O(T^2)$  yield

$$P_T \mathbf{v}(x, t) = \frac{\partial \mathbf{v}}{\partial t}(x, t) - \Gamma \mathbf{v}(x, t) - h_1(\mathbf{v}(x, t)) + O(T^2),$$

and thus

$$P \mathbf{v} - P_T \mathbf{v} = O(T^2),$$

which tends to zero as  $T \rightarrow 0$ .

□

### 3.4 Linear Stability Analysis

A common approach to study the onset of spatial patterns in a model is linear stability analysis. Spatial patterns occur if a steady state that is stable to spatially homogeneous perturbations becomes unstable if a spatially heterogeneous perturbation is introduced. In this section we show that such a linear stability analysis of the integrodifference model (3.5) on flat ground with the Laplacian kernels in the parameter setting (3.6) yields a condition for pattern onset that is equivalent to the corresponding condition for the local Klausmeier model (3.1). This implies that pattern onset is independent of the parameter  $T$ , the temporal separation of seed dispersal events.

The steady states of (3.5) are identical with those of the Klausmeier models (3.1) and (3.2), i.e.

$$(\bar{u}_1, \bar{w}_1) = (0, A), \quad (\bar{u}_2, \bar{w}_2) = \left( \frac{2B}{A - \sqrt{A^2 - 4B^2}}, \frac{A - \sqrt{A^2 - 4B^2}}{2} \right),$$

$$(\bar{u}_3, \bar{w}_3) = \left( \frac{2B}{A + \sqrt{A^2 - 4B^2}}, \frac{A + \sqrt{A^2 - 4B^2}}{2} \right).$$

Existence of  $(\bar{u}_2, \bar{w}_2)$  and  $(\bar{u}_3, \bar{w}_3)$  requires  $A > A_{\min} := 2B$ . The steady states are independent of  $C$ ,  $D$  and the dispersal widths  $a$ ,  $a_1$  and  $a_2$  and are thus independent of frequency changes to the temporal intermittency when using the scalings (3.6). For the Klausmeier models  $(\bar{u}_1, \bar{w}_1)$  and  $(\bar{u}_2, \bar{w}_2)$  are stable to spatially homogeneous perturbations, while  $(\bar{u}_3, \bar{w}_3)$  is unstable to spatially homogeneous perturbations in the biologically relevant parameter region  $B < 2$  [61, 99, 185]. Preservation of this structure of the steady states in the integrodifference model (3.5) is only achieved in a certain parameter region.

**Proposition 3.4.1.** *If*

$$D = \ell \bar{D}, \quad \ell < 1, \quad C = \frac{\ell_1 \bar{D}}{B(m - \ell_1 \bar{D})}, \quad m > 2, \quad \ell_1 < 1, \quad (3.13)$$

where

$$\bar{D} = \frac{2(A^2 - A\sqrt{A^2 - 4B^2} - 2B^2)}{A^2 - A\sqrt{A^2 - 4B^2}}, \quad (3.14)$$

then  $(\bar{u}_1, \bar{w}_1)$  and  $(\bar{u}_2, \bar{w}_2)$  are stable to spatially homogeneous perturbations, and  $(\bar{u}_3, \bar{w}_3)$  is unstable to spatially homogeneous perturbations.

This condition is sufficient but not necessary. Outside this region further restrictions on the rainfall parameter  $A$  can be imposed to guarantee conservation of the

steady state structure. In the limiting case (3.6) such a restriction on the rainfall parameter cannot be avoided. The following condition ensures that (3.13) holds in the limiting case (3.6).

**Corollary 3.4.2.** *If*

$$A^2 < A_+^2 := \min \left\{ \frac{4B^2}{(2-T)T}, \frac{B(BT+1)^2}{T} \right\}, \quad T < \frac{1}{2}, \quad B < 2, \quad (3.15)$$

*in (3.5) with  $C = D = T$ , then  $(\bar{u}_1, \bar{w}_1)$  and  $(\bar{u}_2, \bar{w}_2)$  are stable to spatially homogeneous perturbations, and  $(\bar{u}_3, \bar{w}_3)$  is unstable to spatially homogeneous perturbations.*

In the limit  $T \rightarrow 0^+$  this becomes the whole  $A$ - $B$  parameter region considered for the continuous-time Klausmeier models, providing a reasonable framework for a comparison of the two models. The upper bounds on  $T$  and  $A$  do, however, introduce a significant restriction on the model as no arbitrarily large time between dispersal events or large precipitation volumes  $A$  can be considered. In this, as well as the parameter region given by (3.13), the plant density  $u_n(x)$  and the water density  $w_n(x)$  remain positive for initial conditions close to the steady states. This is sufficient for the linear stability analysis and simulations that follow. In the parameter region in which  $(\bar{u}_2, \bar{w}_2)$  is unstable, four different behaviours of the system's solution can be observed; (i) convergence to the desert steady state, (ii) divergence, (iii) a chaotic solution or (iv) a periodic solution for which period doubling occurs as  $T$  is increased. However, these different behaviours can yield negative densities of the system's quantities and are thus not considered further in this study.

Spatial patterns of (3.5) arise if the steady state  $(\bar{u}, \bar{w}) := (\bar{u}_2, \bar{w}_2)$ , which is stable to spatially homogeneous perturbations, becomes unstable if a spatially heterogeneous perturbation is introduced.

**Proposition 3.4.3.** *The steady state  $(\bar{u}, \bar{w})$  is stable to spatially heterogeneous perturbations if  $|\lambda(k)| < 1$  for both eigenvalues of the Jacobian*

$$J = \begin{pmatrix} C\hat{\phi}(k)\alpha & C\hat{\phi}(k)\beta \\ D\hat{\phi}_1(k)\gamma & D\hat{\phi}_1(k)\delta \end{pmatrix}, \quad (3.16)$$

for all  $k > 0$ , where

$$\begin{aligned}\alpha &= f_u(\bar{u}, \bar{w}) = \frac{BC + 1}{C}, \\ \beta &= f_w(\bar{u}, \bar{w}) = \frac{4B^2}{(A - \sqrt{A^2 - 4B^2})^2}, \quad \gamma = g_u(\bar{u}, \bar{w}) = -2B, \\ \delta &= g_w(\bar{u}, \bar{w}) = -\frac{2(A^2D - AD\sqrt{A^2 - 4B^2} - A^2 + A\sqrt{A^2 - 4B^2} + 2B^2)}{D(A - \sqrt{A^2 - 4B^2})^2}.\end{aligned}\tag{3.17}$$

Due to the asymmetry of  $\phi_1$  some of the entries of the Jacobian (3.16) are complex-valued. A significant simplification can therefore be achieved by considering the integrodifference model (3.5) on flat ground. This corresponds to  $a_1 = 0$  in  $\phi_1$ . As a consequence, the Jury conditions (see e.g. [142]) can be used to determine the steady state's stability to spatially heterogeneous perturbations. To study this in more detail, and in particular to show that the model does not provide information on effects the temporal separation of seed dispersal events, we focus on the limiting case (3.6) and the Laplacian kernel (3.3).

**Proposition 3.4.4.** *The steady state  $(\bar{u}, \bar{w})$  of the integrodifference model (3.5) under the scalings (3.6) on flat ground with the Laplacian kernels (3.3) is unstable to spatially heterogeneous perturbations if*

$$1 + \det(J) - |\text{tr}(J)| < 0, \quad \text{for some } k > 0,\tag{3.18}$$

where  $J$  is the Jacobian given in Proposition 3.4.3 with  $a_1 = 0$ .

In other words, Proposition 3.4.4 provides a sufficient condition for spatial patterns to occur. The following proposition shows that (3.18) is equivalent to the stability condition (3.4) of  $(\bar{u}, \bar{w})$  in the local Klausmeier model. In other words, a diffusion driven instability causes the occurrence of spatial patterns in the integrodifference model, i.e. given a level of rainfall  $A$ , an instability occurs for  $d > d_c(A, B)$ , where  $d_c(A, B)$  is given in (3.4).

**Proposition 3.4.5.** *The steady state  $(\bar{u}, \bar{w})$  of the integrodifference model (3.5) under the scalings (3.6) on flat ground with the Laplacian kernels (3.3) is unstable to spatially heterogeneous perturbations if  $d > d_c(A, B)$ , where the threshold  $d_c$  is identical with the corresponding threshold (3.4) for the local Klausmeier model.*

The condition's independence of  $T$  yields that the integrodifference model does not provide any information on the effects of the temporal separation of seed dispersal events on the onset of spatial patterns. The equivalence of the condition

to that of the local Klausmeier model follows directly from the condition's independence of  $T$  and Proposition 3.3.1, which shows that the integrodifference model converges to the local Klausmeier model as  $T \rightarrow 0^+$ . Thus for sufficiently small values of  $T$ , Proposition 3.4.5 does indeed provide the exact same information as the diffusion threshold obtained for the local Klausmeier model. For larger  $T$  the model does not provide any information on the transition between uniform and patterned vegetation as the decrease in the upper bound  $A_+$  on the rainfall parameter reduces the size of the rainfall interval for which the derivation of  $d_c$  is valid.

*Proof of Proposition 3.4.1.* Stability of a steady state  $(\bar{u}, \bar{w})$  is determined by the Jury conditions applied to the Jacobian

$$J = \begin{pmatrix} C(2\bar{u}\bar{w} - B) + 1 & C\bar{u}^2 \\ -2D\bar{u}\bar{w} & -D(\bar{u}^2 + 1) + 1 \end{pmatrix}.$$

The steady state  $(\bar{u}_3, \bar{w}_3)$  is unstable in the whole parameter region, because

$$1 + \det(J) - |\text{tr}(J)| = -\frac{2BCD(A^2 + A\sqrt{A^2 - 4B^2} - 4B^2)}{(A + \sqrt{A^2 - 4B^2})^2} < 0.$$

The desert steady state  $(\bar{u}_1, \bar{w}_1)$  is monotonically stable if  $C < B^{-1}$  and  $D < 1$ . If  $1 < D < 2$  or  $B^{-1} < C < 2B^{-1}$  it is still stable but solutions are oscillating about  $(0, A)$ , which is biologically impossible. Finally, the Jury conditions yield that  $(\bar{u}_2, \bar{w}_2)$  is stable to spatially homogeneous perturbations if  $\min\{\bar{C}_2, \bar{C}_3\} < C < \bar{C}_1$ , where

$$\begin{aligned} \bar{C}_1 &= \frac{AD(A - \sqrt{A^2 - 4B^2})}{B((D-1)A(\sqrt{A^2 - 4B^2} - A) + 2B^2(2D-1))}, \\ \bar{C}_2 &= \frac{2((D-2)(A\sqrt{A^2 - 4B^2} - A^2) - 4B^2)}{B((D-2)(A^2 - A\sqrt{A^2 - 4B^2}) - 4B^2(D-1))}, \\ \bar{C}_3 &= \frac{(D-2)(A^2 - A\sqrt{A^2 - 4B^2}) + 4B^2}{B(A^2 - A\sqrt{A^2 - 4B^2} - 2B^2)}. \end{aligned}$$

Combined, this gives that the steady state structure of the continuous time model is preserved if

$$D < 1 \quad \text{and} \quad \max \left\{ 0, \min \{ \bar{C}_2, \bar{C}_3 \} \right\} < C < \min \left\{ \frac{1}{B}, \bar{C}_1 \right\}. \quad (3.19)$$

If  $D > 1/2$ , then  $\min \{1/B, \overline{C}_1\} = 1/B$ , because

$$\overline{C}_1 - \frac{1}{B} = -\frac{2(D - \frac{1}{2})(A^2 - A\sqrt{A^2 - 4B^2} - 2B^2)}{B((D - \frac{1}{2})(A^2 - A\sqrt{A^2 - 4B^2} - 4B^2) - (A^2 - A\sqrt{A^2 - 4B^2}))} > 0,$$

since  $A^2 - A\sqrt{A^2 - 4B^2} - 2B^2 > 0$  and  $A^2 - A\sqrt{A^2 - 4B^2} - 4B^2 < 0$ . Similarly, if  $D < 1/2$ , then  $\min \{1/B, \overline{C}_1\} = \overline{C}_1$ . Further, if  $D < \overline{D}$  (defined in (3.14)), then  $\max\{0, \min\{\overline{C}_2, \overline{C}_3\}\} = 0$  and similarly, if  $D > \overline{D}$ , then  $\max\{0, \min\{\overline{C}_2, \overline{C}_3\}\} = \overline{C}_2$ .

Hence, (3.19) can be simplified by splitting it into different parameter regions. It becomes (i)  $C < \overline{C}_1$  if  $D < 1/2$  and  $D < \overline{D}$ , (ii)  $\overline{C}_2 < C < \overline{C}_1$  if  $D < 1/2$  and  $\overline{D} < D < 1$ , (iii)  $C < 1/B$  if  $1/2 < D < 1$  and  $D < \overline{D}$  and (iv)  $\overline{C}_2 < C < 1/B$  if  $1/2 < D < 1$  and  $\overline{D} < D < 1$ . This classification is used below to show that if  $C$  and  $D$  are defined as in (3.13), then (3.19) is satisfied in the whole parameter plane that is considered in the continuous-time PDE models ( $A > 2B$ ,  $B < 2$ ). To show this it is sufficient to show that (i) and (iii) are satisfied because  $\ell < 1$ . For case (iii) note that

$$C = \frac{\ell_1 D}{B(m - \ell_1 D)} < \frac{1}{B} \iff \ell_1 D < \frac{m}{2},$$

which is satisfied since  $\ell_1 D < 1$  and  $m > 2$ . For case (i) note that

$$C = \frac{\ell_1 D}{B(m - \ell_1 D)} < \overline{C}_1 \iff \ell_1 D < \frac{2B^2 + (m-1)(A^2 - A\sqrt{A^2 + 4B^2})}{4B^2} := \overline{\overline{D}}.$$

This is always satisfied because  $\ell_1 D < 1$  and

$$\overline{\overline{D}} > 1 \iff m > \frac{2B^2}{A^2 - A\sqrt{A^2 + 4B^2}} + 1 := \overline{m},$$

which holds true since  $m > 2$  and

$$\overline{m} < 2 \iff A^2 - A\sqrt{A^2 - 2B^2} - 2B^2 > 0,$$

which is clearly satisfied. □

*Proof of Proposition 3.4.3.* Linearisation of the model (3.5) about the steady state  $(\bar{u}, \bar{w})$  gives  $u_{n+1}(x) = C\phi(\cdot) * (\alpha u_n(\cdot) + \beta w_n(\cdot))$  and  $w_{n+1}(x) = D\phi_1(\cdot) * (\gamma u_n(\cdot) +$

$\delta w_n(\cdot)$ ). Taking the Fourier transform of both equations yields

$$\widehat{u}_{n+1}(k) = C\widehat{\phi}(k)(\alpha\widehat{u}_n(k) + \beta\widehat{w}_n(k)),$$

$$\widehat{w}_{n+1}(k) = D\widehat{\phi}_1(k)(\gamma\widehat{u}_n(k) + \delta\widehat{w}_n(k)),$$

where  $\widehat{\phi}$  and  $\widehat{\phi}_1$  denote the Fourier transforms of the kernels  $\phi$ , and  $\phi_1$ , respectively. Under the assumption that  $\widehat{u}_n(k)$  and  $\widehat{w}_n(k)$  are proportional to  $\lambda^n\tilde{u}(k)$  and  $\lambda^n\tilde{w}(k)$ , respectively, where  $\lambda \in \mathbb{C}$  denotes the growth rate, the system becomes  $\lambda\tilde{u}(k) = C\widehat{\phi}(k)(\alpha\tilde{u}(k) + \beta\tilde{w}(k))$  and  $\lambda\tilde{w}(k) = D\widehat{\phi}_1(k)(\gamma\tilde{u}(k) + \delta\tilde{w}(k))$ , i.e.  $\lambda$  is an eigenvalue of the Jacobian  $J$ .  $\square$

*Proof of Proposition 3.4.4.* For an instability to occur, at least one of the Jury conditions  $\det(J) < 1$  and  $1 + \det(J) - |\text{tr}(J)| > 0$  needs to be violated for some wavenumber  $k > 0$ . The former condition is satisfied for all  $k > 0$ . To show this, note that that  $\max\{\det(J) - 1\}$  is at  $k = 0$  because

$$\det(J) - 1 = \frac{\alpha_4 k^4 + \alpha_2 k^2 + \alpha_0}{(dT k^2 + 1) (A - \sqrt{A^2 - 4B^2})^2 (Tk^2 + 1)}, \quad (3.20)$$

where

$$\alpha_4 = 2dT^2 \left( -A^2 + A\sqrt{A^2 - 4B^2} + 2B^2 \right),$$

$$\alpha_2 = -2T \left( A^2 - A\sqrt{A^2 - 4B^2} - 2B^2 \right) (d + 1),$$

$$\begin{aligned} \alpha_0 = 2T & \left( \left( \frac{1}{2}B - 1 \right) \left( A^2 - A\sqrt{A^2 - 4B^2} \right) \right. \\ & \left. + \left( \frac{1}{2}B - TB \right) \left( A^2 - A\sqrt{A^2 - 4B^2} - 4B^2 \right) \right). \end{aligned}$$

The denominator of (3.20) is clearly positive and increasing for  $k > 0$ . Since further  $\alpha_4 < 0$  and  $\alpha_2 < 0$ , the numerator and thus the whole of (3.20) is decreasing for  $k > 0$  and it attains its maximum at  $k = 0$ . The negativity of (3.20) then follows from that of  $\alpha_0$  which follows from  $B < 2$  and  $T < 1/2$ .  $\square$

*Proof of Proposition 3.4.5.* Firstly, we note that  $\partial d_c / \partial A \geq 0$  for all  $A \geq 2B$ . Hence,  $d_c$  attains its minimum on  $A = 2B$ , on which it simplifies to  $d_c = 2/B$ . Since  $B < 2$ ,  $d_c > 1$ . Next, we show that  $\text{tr}(J) > 0$ . To do this, note that

$$\text{tr}(J) = \frac{\beta_2 k^2 + \beta_0}{(dT k^2 + 1) (A - \sqrt{A^2 - 4B^2})^2 (Tk^2 + 1)} > 0,$$

for all  $k > 0$ , where

$$\beta_2 = 2 \left( A^2 - A\sqrt{A^2 - 4B^2} - 2B^2 \right) (BT^2d + T + Td) - 2T^2 \left( A^2 - A\sqrt{A^2 - 4B^2} \right),$$

$$\beta_0 = 2(BT - T + 2) \left( A^2 - A\sqrt{A^2 - 4B^2} - 2B^2 \right).$$

The denominator is clearly positive and thus the condition for positivity of  $\text{tr}(J)$  is  $\beta_2 k^2 + \beta_0 > 0$ . The left hand side of this is decreasing in  $A$  since  $A^2 - A\sqrt{A^2 - 4B^2}$  is decreasing in  $A$  and the assumptions on  $B$  and  $d$ , and thus obtains its minimum at  $A = A^+$ , where  $A^+$  is given in (3.15). If  $B < 1/(2 - T)$ , then  $A^+ = 4B^2/((2 - T)T)$  and

$$\text{tr}(J) \left( \sqrt{A^+} \right) > 0 \iff k^2 > \frac{B}{1 - d - BTd},$$

since  $d > 1$ . The right hand side is negative and thus  $\min(\text{tr}(J)) > 0$  for  $B < 1/(2 - T)$ . If  $B > 1/(2 - T)$ , then  $A^+ = (BT + 1)^2 B/T$  and

$$\text{tr}(J) \left( \sqrt{A^+} \right) > 0 \iff k^2 > -\frac{TB^2 + (2 - T)B - 1}{B^2 T^2 d + ((d + 1)T - T^2) B - T},$$

since  $d > 1$ . Negativity of the right hand side follows from the lower bound on  $B$  and thus  $\min(\text{tr}(J)) > 0$  for all  $B < 2$ . This shows that  $\text{tr}(J) > 0$ . The stability condition (3.18) thus becomes  $1 + \det(J) - \text{tr}(J) < 0 \iff \gamma_4 k^4 + \gamma_2 k^2 + \gamma_0 < 0$ , where  $\gamma_4 = d(A^2 - A\sqrt{A^2 - 4B^2} - 2B^2)$ ,  $\gamma_2 = (A^2 - A\sqrt{A^2 - 4B^2})(1 - Bd) + 2B^3d$  and  $\gamma_0 = B(A^2 - 4B^2)$ . This condition and thus its minimum  $-\gamma_2^2/(4\gamma_4) + \gamma_0$  is independent of  $T$ . Determining the locus at which the minimum changes sign gives the threshold  $d_c(A, B)$ .  $\square$

### 3.5 Simulations

The preceding linear stability analysis relies on the use of the Laplace kernel. For other kernel functions whose Fourier transforms do not provide such a simplification numerical simulations of the model are considered to investigate the onset of patterns. In particular, this allows us to make comparisons between different dispersal kernels, similar to the analysis performed for the nonlocal model in Chapter 2 and [61]. These show that both wide plant dispersal kernels and narrow water dispersal kernels inhibit the formation of patterns. Finally in this section, we show that as for the nonlocal Klausmeier model, the kind of decay of the plant dispersal kernel at infinity is also important.

Simulations are performed on the space domain  $[-x_{\max}, x_{\max}]$  centred at  $x = 0$ . This domain is discretised into  $M$  equidistant points  $x_1, \dots, x_M$  with  $-x_{\max} = x_1 <$

$x_2 < \dots < x_M = x_{\max}$  such that  $\Delta x = x_2 - x_1 = \dots = x_M - x_{M-1}$ . On flat ground (3.5) then becomes

$$u_{n+1}(x_k) = C\Delta x (\phi * f_n)_k, \quad (3.21a)$$

$$w_{n+1}(x_k) = D\Delta x (\phi_1 * g_n)_k, \quad (3.21b)$$

where  $\phi, \phi_1$  denote the vectors consisting of the elements obtained by evaluating the corresponding function at each mesh point,  $f_n, g_n$  denote the vectors consisting of the elements obtained by evaluating the corresponding function at each  $(u_n(x_k), w_n(x_k))$  and  $z_1 * z_2$  denotes the discrete convolution of two vectors  $z_1$  and  $z_2$ . The convolution terms in (3.21a) and (3.21b) are obtained by using the convolution theorem and the fast Fourier transform, providing a significant simplification as this reduces the number of operations required to obtain the convolution from  $O(M^2)$  to  $O(M \log(M))$  (see e.g. [36]).

To mimic the infinite domain used for the linear stability analysis (Section 3.4), we define the initial condition of the system as follows; on a subdomain  $[-x_{\text{sub}}, x_{\text{sub}}]$  centred at  $x = 0$  of the domain  $[-x_{\max}, x_{\max}]$  considered in the simulation the initial condition is a random perturbation of the steady state  $(\bar{u}, \bar{w})$ , while on the rest of the domain the densities are initially set to equal the densities of the steady state  $(\bar{u}, \bar{w})$ . In other words,  $u_0(x_k) = \bar{u} + \delta(x_k)$  and  $w_0(x_k) = \bar{w} + \varepsilon(x_k)$  for  $x_k \in [-x_{\text{sub}}, x_{\text{sub}}]$ , where  $\|\delta\|_\infty < 0.1\bar{u}$  and  $\|\varepsilon\|_\infty < 0.1\bar{w}$  and  $u_0(x_k) = \bar{u}$  and  $w_0(x_k) = \bar{w}$  for  $x_k \notin [-x_{\text{sub}}, x_{\text{sub}}]$ . The size of the outer domain is chosen large enough so that any boundary conditions (which are set to be periodic) that are imposed on  $[-x_{\max}, x_{\max}]$  do not affect the solution in the subdomain in the finite time that is considered in the simulation. Figure 3.1 shows a typical patterned solution obtained by these simulations.

Based on the amplitude of the oscillation relative to the steady state of the solutions obtained by the simulations we set up a scheme to determine the critical rainfall level  $A_{\max}$  below which pattern onset occurs. Doing this allows us to investigate how certain changes of parameters and kernel functions affect the onset of patterns. Due to the random perturbation of the initial state of the system, all simulation results shown below are the averages taken over 100 simulations. For the symmetric dispersal kernels  $\phi$  and  $\phi_1$  we consider the Laplacian (3.3), the Gaussian

$$\phi_g(x) = \frac{a_g}{\sqrt{\pi}} e^{-a_g^2 x^2}, \quad a > 0, x \in \mathbb{R}, \quad (3.22)$$

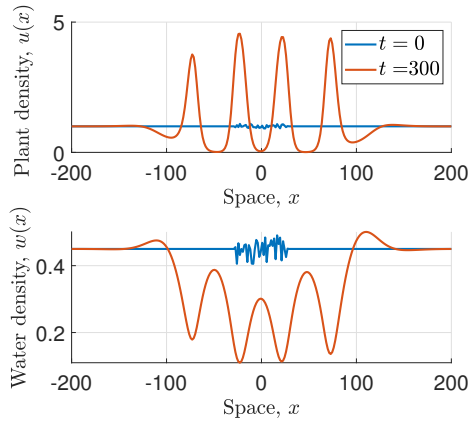


Figure 3.1: Simulation of the integrodifference model. This figure shows a patterned solution obtained by simulating the integrodifference model on flat ground. The kernels used in these simulations are the symmetric Laplacian kernels, respectively. The parameter setting (3.15) with  $T = 0.1$  is used in the simulation. The other parameters are  $A = 0.9$ ,  $B = 0.45$  and  $d = 500$ .

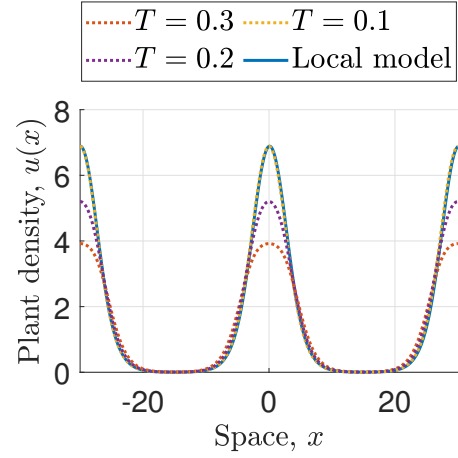


Figure 3.2: Convergence of solutions. This figure visualises the convergence of solutions to the local PDE model (3.1) as  $T \rightarrow 0^+$ , to complement the consistency result presented in Prop. 3.3.1. Solutions of the integrodifference model (3.5) are shown for  $T = 0.3$ ,  $T = 0.2$  and  $T = 0.1$  and are compared with the solution of the local Klausmeier PDE model (3.1). Note that unlike in Fig. 3.1, the spatial domain is chosen to be small to impose the same wavelength restrictions on both models to aid the visualisation of the convergence.

and the power law distribution

$$\phi_p(x) = \frac{(b-1)a_p}{2(1+a_p|x|)^b}, \quad a > 0, b > 3, x \in \mathbb{R}. \quad (3.23)$$

We base our comparison on the kernels' standard deviations, which are given by  $\sigma_\phi = \sqrt{2}/a$  for the Laplacian kernel (3.3),  $\sigma_{\phi_g} = 1/(\sqrt{2}a_g)$  for the Gaussian kernel (3.22) and  $\sigma_{\phi_p} = \sqrt{2}/(\sqrt{b^2 - 5b + 6}a_p)$  for the power law kernel (3.23) provided  $b > 3$ . It is perfectly reasonable to perform simulations with kernels of infinite standard deviation (e.g.  $b < 3$  in the power law kernel) but in the interest of comparing results for the kernels based on their standard deviation we consider only  $b = 3.1$  and  $b = 4$ .

To investigate the model's behaviour under changes to the dispersal kernels  $\phi$  and  $\phi_1$ , we start by considering simultaneous changes in the kernel functions  $\phi$ , and  $\phi_1$ . The comparison between the kernel functions is based on the standard deviation of the plant dispersal kernel  $\phi$  and the width of the water dispersal kernel  $\phi_1$  is set to  $a_2 = 0.1a$  to obtain a ratio similar to that of the standard deviations under the

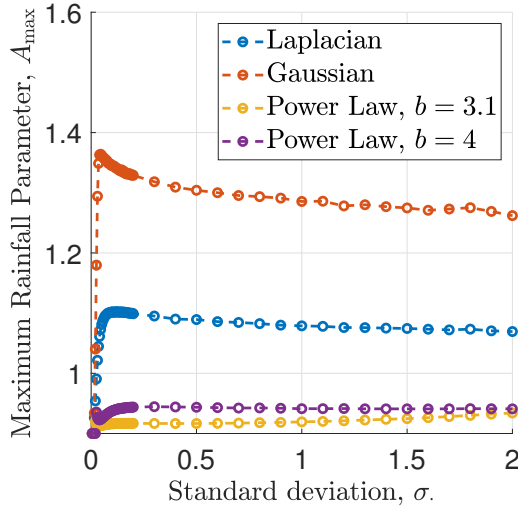


Figure 3.3: The maximum rainfall parameter  $A_{\max}$  under simultaneous changes of the dispersal kernels. This figure visualises variations of  $A_{\max}$  against simultaneous variations of both kernel functions. The standard deviation on the abscissa refers to the plant dispersal kernel  $\phi$ , the width of the water dispersal kernel  $\phi_1$  is set to  $a_2 = 0.1a$ . The rainfall threshold is determined up to an interval of length  $10^{-4}$  for  $\sigma_\phi = \{0.01, 0.02, \dots, 0.05, 0.1, 0.2, \dots, 2\}$ . The parameter values used for this simulation are  $B = 0.45$ ,  $\ell = \ell_1 = 0.5$ ,  $m = 5$

scalings (3.6), which corresponds to the large value of the diffusion parameter  $d$  in the PDE and integro-PDE models. Figure 3.3 visualises the simulation results, which show that for small standard deviations, the rainfall threshold  $A_{\max}$  is close to its lower bound, before an increase in the kernel width causes it to peak before slowly decreasing as the kernel widths are further increased. For very narrow dispersal kernels very little spatial interaction takes place. In particular, as  $\sigma \rightarrow 0$ , the kernel functions tend to the delta function  $\delta(x)$  centred at 0 and therefore the integrodifference system (3.5) becomes

$$u_{n+1}(x) = u_n(x) + C(u_n(x)^2 w_n(x) - Bu_n(x)),$$

$$w_{n+1}(x) = w_n(x) + D(A - u_n(x)^2 w_n(x) - w_n(x)).$$

For this system, the steady state  $(\bar{u}_2, \bar{w}_2)$ , which was randomly perturbed to set the initial condition of the system in the simulation, is always stable. Therefore, no patterns exist and  $A_{\max} = 2B$  is the minimum value of the rainfall parameter for which vegetation is growing uniformly, recalling that for  $A < 2B$ , the steady state  $(\bar{u}_2, \bar{w}_2)$  does not exist. Further, away from  $\sigma = 0$ , a change in kernel width only has very little effect on  $A_{\max}$ , an indication that an increase to the width of the plant dispersal kernel has the opposite effect on the tendency to form patterns as an increase to the width of the water dispersal kernel.

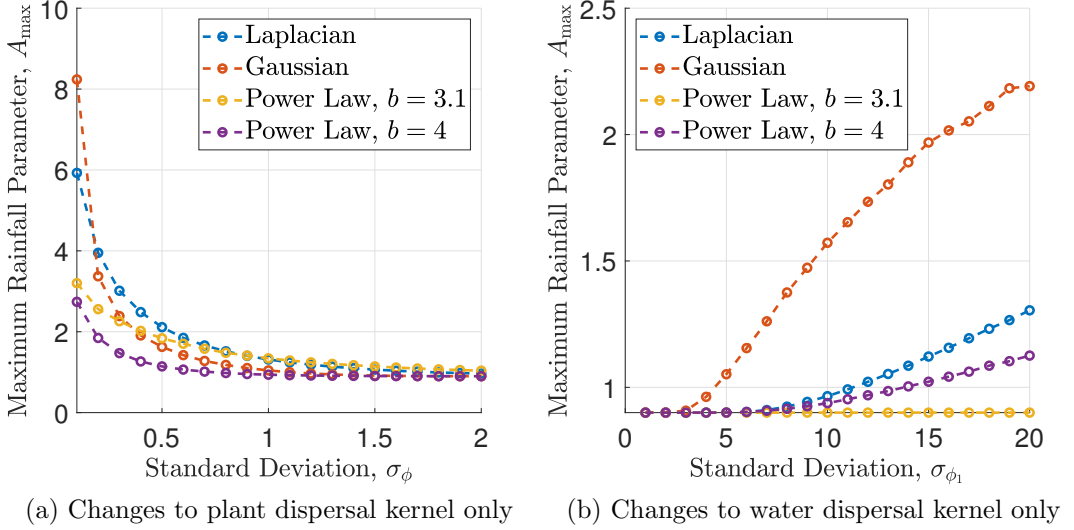


Figure 3.4: The maximum rainfall parameter  $A_{\max}$  under separate variations of the dispersal kernels.. Part (a) shows  $A_{\max}$  up to an interval of length  $10^{-4}$  with varying width ( $\sigma_\phi = \{0.05, 0.1, 0.2, \dots, 2\}$ ) and shape of the plant dispersal kernel  $\phi$ , while (b) visualises the effects of changes in the water dispersal kernel  $\phi_1$ . The latter was simulated for a larger range of the kernel's standard deviation  $\sigma_{\phi_1}$ , specifically  $\sigma_{\phi_1} = \{1, 2, \dots, 20\}$ , to account for the choice of  $a_2 = 0.1a$  in the previous simulation. Also in (b)  $A_{\max}$  is determined up to an interval of length  $10^{-4}$ . The widths of the fixed kernels are set to  $a_2 = 0.1$  (a) and  $a = 1$  (b), respectively. The other parameter values used both simulations are  $B = 0.45$ ,  $\ell = \ell_1 = 0.5$ ,  $m = 5$ .

To test this hypothesis, we investigate changes in the system's behaviour as individual kernel functions are changed. First, we consider how the critical rainfall parameter  $A_{\max}$  is affected by a change of the shape of the dispersal kernel  $\phi$  in the plant equation (3.21a). The result (see Figure 3.4a) is consistent with results of the integro-PDE model on sloped ground [61] (Chapter 2). Firstly, an increase in the width of the plant dispersal kernels reduces the size of the parameter region supporting pattern onset, where changes for larger values of the standard deviation  $\sigma_\phi$  are much smaller than close to  $\sigma_\phi = 0$ . Identical to the nonlocal Klausmeier model, a trend that for small standard deviations those kernel functions that decay algebraically at infinity predict a lower value of  $A_{\max}$  than those decaying exponentially, and vice versa for larger kernel widths, is also observed in these simulations.

Next, we perform a similar analysis for the symmetric water dispersal kernel  $\phi_1$ . To be consistent with the setting  $a_2 = 0.1a$  in the simulation for the simultaneous change of the kernel functions, we consider a larger range of  $\sigma_{\phi_1}$  for this simulation. The results (Figure 3.4b) show that for narrow kernels,  $A_{\max}$  is close to its minimum  $A = 2B$ , i.e. the rainfall interval supporting pattern formation is very small. In particular, as  $\sigma_{\phi_1} \rightarrow 0$ ,  $A_{\max} \rightarrow 2B$  and no patterns can occur. For the Laplace kernel, this can also be shown using linear stability analysis. If  $\sigma_{\phi_1} = 0$ , then  $\hat{\phi}_1 \equiv 1$

and thus the Jacobian (3.16) becomes

$$J = \begin{pmatrix} C\widehat{\phi}(k)\alpha & C\widehat{\phi}(k)\beta \\ D\gamma & D\delta \end{pmatrix}.$$

Further, the stability condition is

$$k^2 > \frac{BCa^2 (A^2 - A\sqrt{A^2 - 4B^2} - 4B^2)}{A^2 - A\sqrt{A^2 - 4B^2}}.$$

The right hand side is negative and thus the steady state is always stable to spatially heterogeneous perturbations. An increase of the kernel width then causes an increase in the rainfall threshold  $A_{\max}$ , where those kernels that decay exponentially at infinity, yield a larger increase than those decaying algebraically.

The results above confirm that the plant dispersal kernel  $\phi$  and the water dispersal kernel  $\phi_1$  have opposite effects on the rainfall threshold  $A_{\max}$ . While an increase in the width of the plant dispersal inhibits the onset of patterns, an increase in the standard deviation of the water dispersal kernel increases the tendency to form patterns. This explains the nearly constant value of  $A_{\max}$  in the simulations in which both kernel functions are varied simultaneously. Consequently, these results suggest that it is the ratio of plant dispersal to water dispersal, i.e. the ratio  $\sigma_\phi/\sigma_{\phi_1}$  that controls the tendency to form patterns. An increase in the ratio inhibits the onset of patterns, while a decrease has the opposite effect.

### 3.6 Discussion

The deliberately basic description of the plant-water dynamics in semi-arid environments by the Klausmeier model provides a rich framework for model extensions to address a range of different features of dryland ecosystems and their effects on vegetation patterns. Extensions include cross advection due to decreased surface water run-off resulting from an increase in infiltration in biomass patches [237]; terrain curvature [72]; nonlocal dispersal of seeds [20, 61]; secondary seed dispersal due to overland water flow [35]; nonlocal grazing effects [195, 197]; explicit modelling of a population of grazers [68]; local competition between plants [236]; the inclusion of autotoxicity [120]; multispecies plant communities [27, 63, 220] and seasonality and intermittency in precipitation [58, 221]. One aspect that has not yet been considered in this context is the seasonal separation of plant growth and seed dispersal. In this chapter we have considered the synchronised and seasonal occurrence of non-local seed dispersal through a system of integrodifference equations based on the Klausmeier reaction-advection-diffusion system.

While an integrodifference system cannot explicitly quantify the temporal sep-

aration of seed dispersal occurrences, the model's derivation and an associated consistency result (Proposition 3.3.1) yield a parameter setting in which the length of the growth phase between dispersal stages can be accounted for. However, the main result of the linear stability analysis of the integrodifference model in this chapter (Proposition 3.4.5) shows that conditions for pattern onset in the integrodifference model (3.5) are independent of the temporal separation of seed dispersal from plant growth. Moreover, due to the model's derivation from the Klausmeier model (3.1), the pattern onset conditions for both models are equivalent.

Some semi-arid environments in which vegetation patterning is a common phenomenon are characterised by large temporal and in particular seasonal fluctuations in their environmental conditions [31, 148]. For example, observed patterns in Spain, Israel and North America are all located in Mediterranean climate zones [151], in which precipitation mainly occurs during winter, while during the summer months little or no rainfall occurs. By contrast, most mathematical models describing these ecosystems employ partial differential equations. While PDE models provide a rich framework for mathematical model analysis, their use is based on the simplifying assumption that all processes occur continuously in time. The results presented in this chapter emphasise the importance and significance of results obtained from such models. In the context of seed dispersal, the biologically more realistic temporal separation of plant growth and seed dispersal has no effect on the conditions for pattern onset to occur. We thus conclude that the results obtained for the Klausmeier PDE model are robust to changes in the temporal properties of seed dispersal processes and that the assumption of continuous seed dispersal provides a sufficiently accurate description.

The parameter setting used to establish a connection between the Klausmeier model (3.1) and the integrodifference model (3.5) couples the scale parameter  $a$  of the seed dispersal kernel to other model parameters. If, however, a more general parameter setting is considered, then the effects of changes to the average seed dispersal distance and the shape of the seed dispersal kernel can be analysed numerically. Our results, which are in full agreement with an earlier investigation of the nonlocal Klausmeier model (3.2) [61] (Chapter 2), show that seed dispersal over longer distances inhibits the formation of patterns (Figure 3.4a). Indeed, the threshold  $A_{\max}$  on the rainfall parameter above which no pattern onset occurs, tends to  $A_{\min}$ , the minimum rainfall level required for the existence of a nontrivial spatially uniform equilibrium, as dispersal distances become sufficiently large. Nevertheless, many plant species in semi-arid ecosystems have developed antitelechoric mechanisms which inhibit long range seed dispersal [66, 227]. While in the context of this study this may appear as an evolutionary disadvantage, the development of narrow seed dispersal kernels is a side effect of other adaptations such as the development

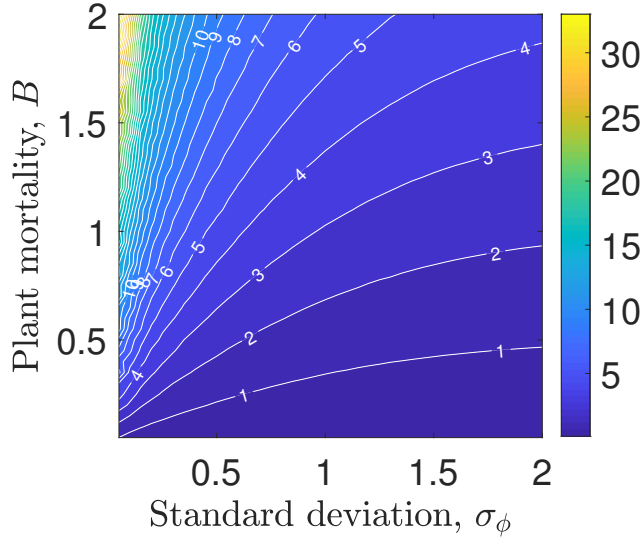


Figure 3.5: The threshold  $A_{\max}$  in the  $\sigma_\phi$ - $B$  parameter plane. The numerically obtained rainfall threshold  $A_{\max}$  is shown in the  $\sigma_\phi$ - $B$  parameter plane as a contour plot, where  $\sigma_\phi$  denotes the standard deviation of the plant dispersal kernel  $\phi$ . It was obtained on the spatial grid  $\{0.05, 0.1, \dots, 1.95, 2\} \times \{0.05, 0.1, \dots, 1.95, 2\}$  for the Laplace kernel (3.3) and  $a_2 = 0.1$ ,  $\ell = \ell_1 = 0.5$ ,  $m = 5$ . We speculate that there may be an evolutionary trade-off between dispersal distance and resistance to predation, which would restrict parameters to an increasing curve in the  $\sigma_\phi$ - $B$  plane.

of seed containers as a protection to predation [66]. This suggests the existence of an evolutionary trade-off between seed dispersal distance and plant mortality. A numerical study of the threshold  $A_{\max}$  in the  $\sigma_\phi$ - $B$  parameter plane (Figure 3.5) gives some useful insight into this. The trade-off would restrict parameters to some increasing curve in the  $\sigma_\phi$ - $B$  parameter plane. Depending on the exact functional form of such a trade-off, a decrease in the seed dispersal distance  $\sigma_\phi$  may cause a reduction in the precipitation threshold  $A_{\max}$ , if the trade-off implies a sufficiently large simultaneous decrease in the plant mortality rate  $B$ . A lower  $A_{\max}$  value corresponds to an inhibition of pattern onset. We thus conclude that our model can capture the evolutionary advantage associated with the development of protective antitelechoric mechanisms if the trade-off between seed dispersal distance  $\sigma_\phi$  and plant mortality  $B$  is chosen appropriately, but emphasise that we are not aware of any data that provides quantitative information on the exact form of this trade-off.

Our results further indicate that the shape of the seed dispersal kernel, and in particular its decay at infinity, has a significant effect on the onset of patterns. Fat-tailed kernels, for example, that account for a higher proportion of long-range dispersal events, yield a lower level of  $A_{\max}$  than kernel functions with exponential decay at infinity for a sufficiently small fixed standard deviation. This highlights the importance of obtaining knowledge of seed dispersal behaviour of plant species, a property that depends on both species and the environment (e.g. seed dispersal

agent) [25].

In our integrodifference model (3.5), we model the redistribution of water through a convolution similar to the modelling of the seed dispersal process. This nonlocal description can account for overland water flow from bare ground to biomass patches across larger distances during precipitation events. It does, however, rely on the assumption that the soil's properties enhance overland water flow in regions of low biomass. Some ecosystems in semi-arid environments are characterised by soil conditions and soil types (e.g. sand) for which this assumption is invalid [222]. The formation of vegetation patterns under such environmental conditions can, however, be explained by other mechanisms, such as laterally extended root networks [131]. The integrodifference model presented in this study is based on the assumption that little or no water infiltration occurs in regions of low biomass, and that the overland water flow towards regions of high biomass induced by this soil property is the main mechanism causing the self-organisation into patterns. In this context, our results show that water redistribution over longer distances yields the onset of patterns at higher precipitation levels (Figure 3.4b). This is due to the enhancement of the pattern-inducing vegetation-infiltration feedback. Existing biomass patches deplete the water density locally, while regions of bare soil retain a higher water levels. Hence, any redistribution of water has a homogenising effect on the water density which yields to a redistribution of the limiting resource from areas of low biomass to areas of high biomass. An increase in the spatial range of the water redistribution kernel thus strengthens the pattern-inducing feedback and causes pattern onset under larger precipitation volumes.

The work in this chapter shows that the description of seed dispersal as a synchronised event during a phase in which no plant growth occurs does not affect the condition for pattern onset compared to the continuous description of seed dispersal in the Klausmeier model (3.1). The stability of spatial patterns is equally important. A natural area of future work would therefore be an analysis of pattern stability in the integrodifference model (3.5) comparing results with stability results for the local Klausmeier model [194] and the nonlocal Klausmeier model [20]. For PDE models, the stability of spatial patterns can be determined through a calculation of their spectra. For this, a method based on numerical continuation has been developed by Rademacher et al. [160] (for details see [160, 187]). For integrodifference equations, however, we are not aware of any methods that allow the determination of the stability of a patterned solution.

The integrodifference model (3.5) not only splits the dynamics of the plant population into separate growth and dispersal stages, but also that of the water dynamics into a water consumption stage and a water redistribution stage. In the model, spatial redistribution of water is synchronised with seed dispersal. This can provide

an adequate description for species such as *Mesembryanthemum crystallinum* and *Mesembryanthemum nodiflorum*, which synchronise their seed dispersal with the beginning of the rain season [146], but cannot provide a description of seed dispersal during drought periods or of water flow at any other time during the rain season. While a description of the water flow dynamics during precipitation events in the context of a vegetation model has been proposed [198], the exact dynamics on flat ground are the subject of ongoing research (e.g. [168, 211, 235]) and could be utilised in a future extension of the integrodifference model (3.5). The description of the water density as one single variable would, however, be prohibitive for such an approach. Instead a distinction between surface water and soil moisture, such as in the Rietkerk et al. model [86, 163] or the Gilad et al. model [74], needs to be made to distinguish between surface water flow processes and water uptake processes that take place in the soil.

The integrodifference model (3.5) and its analysis presented in this chapter is restricted to a one-dimensional space domain, motivated by the original formulation of the Klaumeier model and its mathematical accessibility [99]. However, the consideration of a second space dimension is expected to give more insights into the ecohydrological dynamics, in particular on pattern existence and stability. For example, in related PDE models on two-dimensional space domains, different types of patterned solutions exist (gap patterns, labyrinth patterns, striped patterns and gap patterns) and phase transitions along the precipitation gradient can be investigated [129]. Moreover, even on sloped terrain, the impact of the consideration of a two-dimensional domain is significant, as the analysis on a one-dimensional domain may overestimate the size of the patterns' stability regions [196]. The analysis of the integrodifference model (3.5) on a two-dimensional domain presents a considerable challenge, in particular if one would want to obtain a wavenumber-independent results analogous to Prop. 3.4.5. Nevertheless, this would be a natural area of potential future work to further disentangle the complex ecosystem dynamics.

Finally, we remark that the integrodifference model (3.5) describes the discrete structure of plant growth mechanisms caused by the seasonality in precipitation. However, it does not capture the dynamics specific to drought periods between rainfall events and is thus only able to provide an insight into effects of accumulated rainfall volume rather than the temporal separation of precipitation seasons. In separate work, we account for a combination of rainfall, plant growth and seed dispersal pulses with the continuous nature of plant loss and water evaporation and drainage, using an impulsive model [58] (Chapter 4). Such models combine partial differential equations with integrodifference equations (see for example [238] for an impulsive model in the context of predator-prey dynamics with synchronised predator reproduction). The impulsive model has its own limitations as it can only

take into account a periodic separation of precipitation events, but not any seasonal patterns. A potential area of future work therefore consists of a combination of these approaches to describe both the seasonal and intermittent nature of rainfall in semi-arid climate zones.

## Chapter 4

### Effects of precipitation intermittency on vegetation patterns in semi-arid landscapes

The contents of this chapter are published in [58].

#### 4.1 Author contribution

The authors of the published paper [58] are Lukas Eigentler and Jonathan A Sherratt. Lukas Eigentler conceptualised the research, formulated the mathematical model, performed both the analytical and numerical analyses of the model, wrote the paper draft and reviewed and edited the manuscript. Jonathan A Sherratt conceptualised the research, reviewed and edited the manuscript and provided supervision.

#### Abstract

Patterns of vegetation are a characteristic feature of many semi-arid regions. The limiting resource in these ecosystems is water, which is added to the system through short and intense rainfall events that cause a pulse of biological processes such as plant growth and seed dispersal. We propose an impulsive model based on the Klausmeier reaction-advection-diffusion system, analytically investigate the effects of rainfall intermittency on the onset of patterns, and augment our results by numerical simulations of model extensions. Our investigation focuses on the parameter region in which a transition between uniform and patterned vegetation occurs. Results show that decay-type processes associated with a low frequency of precipitation pulses inhibit the onset of patterns and that under intermittent rainfall regimes, a spatially uniform solution is sustained at lower total precipitation volumes than under continuous rainfall, if plant species are unable to efficiently use low soil moisture levels. Unlike in the classical setting of a reaction-diffusion model, patterns are not caused by a diffusion-driven instability but by a combination of sufficiently long periods of droughts between precipitation pulses and water diffusion. Our results further indicate that the introduction of pulse-type seed dispersal weakens the effects of changes to width and shape of the plant dispersal kernel on the onset of patterns.

## 4.2 Introduction

Self-organised vegetation patterns are a characteristic feature of semi-arid regions around the world. The formation of patterns is caused by a positive feedback between plant growth and water redistribution towards areas of high biomass [166]. Mechanisms involved in the establishment of such a feedback loop include the formation of infiltration-inhibiting soil crusts in areas of bare ground that induce overland water flow, a combination of strong local water uptake (vertically extended root systems) and fast soil water diffusion, nonlocal water uptake (laterally extended root systems), or a combination thereof [130]. Redistribution of water towards dense biomass patches drives further plant growth in these regions and thus closes the feedback loop. First discovered through areal photography in the 1950s [116], vegetation patterns have been detected in various semi-arid regions of the world (see [71, 222] for reviews) such as in the African Sahel [48, 141], Somalia [79, 83], Australia [55, 84], Israel [24, 182], Mexico and the US [48, 152, 153] and northern Chile [68]. The understanding of the evolution and underlying dynamics of patterned vegetation is of crucial importance as changes to properties such as pattern wavelength, recovery time from perturbations or the area fraction colonised by plants may provide an early indication of an irreversible transition to full desert [39, 45, 78, 96, 131, 164, 170, 246].

The amount of empirical data on vegetation patterns is limited due to the inability to reproduce patterns in a laboratory setting and the long time scale involved in the formation and evolution of them. Thus, a range of different mathematical models describing the phenomenon have been proposed (in particular by Rietkerk et al. [163] and Gilad et al. [74]), which focus on various different processes that are involved in the formation of vegetation patterns. One model that stands out due to its deliberately basic description of the plant-water-dynamics in semi-arid environments is the Klausmeier model [99]. The excellent framework for mathematical analysis and model extensions provided by the Klausmeier reaction-advection-diffusion model has been utilised extensively in the past (e.g. [10, 20, 34, 35, 61–64, 120, 184–186, 190–192, 194, 199, 221, 236, 237]).

Rainfall in semi-arid regions occurs intermittently, seasonally or as a combination of both. Under intermittent rainfall regimes only a small number of short-lasting precipitation events per year provide a sufficiently large amount of water to affect vegetation growing in these regions [148]. If such rainfall events are sufficiently separated, they cause a pulse of biological processes before decay-type phenomena of dry spells take over [148]. Besides plant growth, seed dispersal is also commonly observed to be synchronised with precipitation events. One mechanism, widespread in dryland ecosystems, which causes such a behaviour is ombrohydrochory, the opening

of a seed container due to contact with water [146, 227]. Plants in semi-arid regions are sensitive to quantity, frequency and temporal spread of intermittent precipitation events [67, 69, 82, 111].

Experimental studies suggest that if the total precipitation volume is kept constant, then a lower frequency of rainfall events yields higher plant biomass [113], an increase in the aboveground net primary productivity [82] and an increase in the seedlings' survival rate [183]. The main factor for these beneficial effects is the temporal increase in soil moisture caused by larger rain events, while a higher number of smaller individual events keeps the moisture level below a threshold needed for the activation of biological processes in plants [82, 183]. Contradictory evidence regarding seedling survival exists, which suggests that the effects of rain intermittency depend on a range of factors [113]. In the future, changes to the temporal variability of precipitation (in particular the intensity of rainfall events) are expected to occur globally [57, 90].

Despite the fact that seasonality, intermittency and intensity of precipitation has an important influence on semi-desert ecosystems, most mathematical models assume that rainfall occurs continuously and uniformly in time. Some simulation-based studies, however, have addressed the phenomenon by introducing seasonality (i.e. a wet and dry season) and intermittency of rainfall to existing models for dryland vegetation dynamics. These include modifications of the Rietkerk model [80, 198], of the Klausmeier model [221] as well as of the Gilad model [100]. Baudena et al. [13, 14] couple a model describing the soil moisture proposed by Laio [104] for the upper soil layer, in which water is added during a wet season either at a constant rate or as an instantaneous event, to vegetation dynamics. The results of these studies show beneficial effects of rainfall intermittency, such as an increase in the area covered by vegetation [100] or plant biomass [13, 100] but also suggest that a lower frequency of rain pulses increases the minimum requirement on the total annual precipitation needed to avoid convergence to a bare soil state [221]. The latter result also suggests that the size of the parameter region in which pattern onset occurs reduces under intermittent rainfall regimes [221]. Seasonality of precipitation may have similar effects [80], but can also be detrimental to plants by reducing their biomass and area fraction covered [13, 100].

Effects due to changes in the frequency of rainfall events have received very little attention in the mathematical modelling of vegetation patterns, with the works of Ursino and Contarini [221] on the Klausmeier model, Kletter et al.[100] on the Gilad model, and Siteur et al. [198] on the Rietkerk model being notable exceptions. However, none of these papers consider both a wide range of biologically relevant interpulse times and the system dynamics in drought periods. For example, both Kletter et al. and Ursino and Contarini restrict their investigation to a small number

of different precipitation frequencies, while Siteur et al. neglect the ecohydrological dynamics between rainfall events. Moreover, most theoretical approaches to study temporal non-uniformity in precipitation are simulation-based. In this chapter, we introduce a model based on the Klausmeier model that captures both the impulsive nature of precipitation pulses and associated processes, and also the drought period dynamics. We keep our model sufficiently simple to allow for an analytical investigation of pattern onset in the system. This enables us to consider a wide range of different rainfall regimes and study the effects of precipitation intermittency on the ecohydrological dynamics.

One approach to modelling a system in which pulse-type phenomena occur is the use of integrodifference equations. In separate work [62] (Chapter 3), we show that such a framework is insufficient to capture effects of precipitation intermittency as it is unable to account for the dynamics specific to drought periods between rainfall pulses. To instead describe situations in which pulse-type phenomena occur alongside the continuous processes of dry spells, impulsive-type systems are used. Such models consist of a system of PDEs describing continuous processes on a finite time domain  $(n - 1)T < t < nT$ ,  $n \in \mathbb{N}$  and a set of discrete equations that update the densities at times  $nT$ . The use of impulsive models is a relatively new approach in mathematical modelling but such models are suitable for the description of a wide range of systems. Previous applications include descriptions of populations whose life cycle consists of two non-overlapping stages, such as organisms whose larvae are subjected to a water flow [87, 229]; predator-prey systems in which consumer reproduction occurs only once a year and is based on the amount of stored energy accumulated through consumption of prey during the year [238] or that are periodically subjected to external inputs [2]; and more general consumer-resource systems in which the consumer reproduction is synchronised [110, 149] or in which seasonal harvesting occurs [110]. Impulsive models can further provide a mechanistic interpretation of the underlying ecological processes involved in purely discrete systems [73].

The modelling of plant dispersal as an instantaneous event requires its description by a convolution integral instead of the widely used and mathematically more accessible diffusion term. Biologically, however, this provides a more realistic description of the spatial redistribution of plants as the dynamics of seed dispersal are often affected by nonlocal processes [25]. The use of a convolution term in the description of seed dispersal is thus not a novelty of this study but has been also been used in a number of previous models for dryland ecosystems [16, 61, 156, 157].

In this chapter, we introduce and analytically study an impulsive model based on the Klausmeier model to gain a better understanding of the effects of pulse-type processes on the onset of vegetation patterns. We motivate the presentation

of the model in Section 4.3 by a review of the Klausmeier model and its most relevant results. In Section 4.4 we derive conditions for the onset of patterns in the impulsive model based on a linear stability analysis. This allows us to investigate how changes in the rainfall regime affect pattern onset and provides an insight into the mechanism that is responsible for the formation of patterns in the model. The analysis presented in Section 4.4 is tractable due to some simplifications, such as the use of a specific plant dispersal kernel and the restriction to a flat domain. In Section 4.5 we augment our analytical results by numerical simulations of extensions of the basic model studied in Section 4.4 to analyse and discuss the effects of our simplifying assumptions. We present an interpretation of our results and address potential shortfalls in Section 4.6.

### 4.3 Model description

In this section we introduce the model which we use to investigate the effects of rainfall intermittency on the onset of patterns in semi-arid environments. We base our model on an extension of the Klausmeier model, whose most relevant results are reviewed.

#### 4.3.1 Klausmeier models

One of the earliest models describing the plant-water dynamics in semi-arid environments is due to Klausmeier [99]. The relative simplicity of the model provides a framework for a rich mathematical analysis (e.g. [184–186, 190–192, 194, 199, 221]). After a suitable nondimensionalisation [99, 185] the model is

$$\frac{\partial u}{\partial t} = \underbrace{u^2 w}_{\text{plant growth}} - \underbrace{B u}_{\text{plant mortality}} + \underbrace{\frac{\partial^2 u}{\partial x^2}}_{\text{plant dispersal}}, \quad (4.1a)$$

$$\frac{\partial w}{\partial t} = \underbrace{A}_{\text{rainfall}} - \underbrace{w}_{\text{evaporation}} - \underbrace{u^2 w}_{\substack{\text{water consumption} \\ \text{by plants}}} + \underbrace{\nu \frac{\partial w}{\partial x}}_{\substack{\text{water flow} \\ \text{downhill}}} + \underbrace{d \frac{\partial^2 w}{\partial x^2}}_{\text{water diffusion}}, \quad (4.1b)$$

where  $u(x, t)$  denotes the plant density,  $w(x, t)$  the water density,  $x \in \mathbb{R}$  the space domain where  $x$  is increasing in the uphill direction and  $t > 0$  denotes the time. The diffusion of water was not originally included in the model but is a well established addition [95, 199, 225, 247]. It is assumed that water is added to the system at a constant rate, evaporation effects are proportional to the water density [167, 171] and the plant mortality rate is density-independent. The nonlinearity in the water consumption and plant growth terms arises due to the positive feedback

between local vegetation growth and water redistribution. Water uptake by plants is the product of the consumer density ( $u$ ), the resource density ( $w$ ) and a term that accounts for the increased resource availability due to the positive feedback caused, for example, by an increase of soil permeability in vegetated areas ( $u$ ). This nonlinearity drives the formation of spatial patterns. The parameters  $A$ ,  $B$ ,  $\nu$  and  $d$  represent rainfall, plant loss, the slope and water diffusion, respectively.

The Klausmeier model (4.1) combines all hydrological dynamics into one single variable  $w$ . By contrast, some other modelling frameworks distinguish between surface water and soil moisture dynamics [74, 163]. In this chapter, we focus on the modelling framework presented by the Klausmeier model without such a distinction, but the application of our modelling approach to a system with both surface and soil water density is briefly discussed in Sec. 4.6.

In a previous chapter (Chapter 2) [61], we have studied the effects of replacing the plant diffusion term in the Klausmeier model by a convolution of a probability density  $\phi$  and the plant density  $u$ , i.e.

$$\frac{\partial u}{\partial t} = u^2 w - Bu + C(\phi(\cdot; a) * u(\cdot, t) - u(x, t)), \quad (4.2a)$$

$$\frac{\partial w}{\partial t} = A - w - u^2 w + \nu \frac{\partial w}{\partial x} + d \frac{\partial^2 w}{\partial x^2}. \quad (4.2b)$$

The additional parameters  $C$  and  $a$  represent the rate of plant dispersal and reciprocal width of the dispersal kernel, respectively.

A linear stability analysis of both the local model (4.1) and the nonlocal model (4.2), with the Laplace kernel

$$\phi(x) = \frac{a}{2} e^{-a|x|}, \quad a > 0, x \in \mathbb{R}, \quad (4.3)$$

used in the latter, gives an insight into the nature of patterned solutions of the system. On flat ground, i.e.  $\nu = 0$ , the onset of spatial patterns occurs due to a diffusion-driven instability. Thus for any level of rainfall  $A$ , there exists a threshold  $d_c \in \mathbb{R}$  on the diffusion coefficient such that an instability occurs for all  $d > d_c$ . The analysis for the nonlocal model with the Laplace kernel shows that an increase in the width of the dispersal kernel inhibits the formation of patterns by causing an increase in the diffusion threshold.

Unlike the Laplace kernel, other kernel functions do not provide a simplification sufficient to study the onset of patterns analytically. Numerical simulations, however, confirm that the trends observed from the linear stability analysis for the Laplace kernel also apply to other kernel functions [61] (Chapter 2).

### 4.3.2 Impulsive Model

The Klausmeier model assumes that all processes occur continuously in time. To account for the more realistic combination of pulse-type events associated with short, high intensity precipitation events with the continuous nature of plant loss, water evaporation and water dispersal, we propose an impulsive model to describe the plant and water dynamics in semi-arid environments. Under the assumption that water transport and the decay-type processes of plant mortality and water evaporation are the only processes occurring in drought periods between rainfall pulses [148], the model is

$$\frac{\partial u_n}{\partial t} = \underbrace{-k_1 u_n}_{\text{plant loss}}, \quad (4.4a)$$

$$\frac{\partial w_n}{\partial t} = \underbrace{-k_2 w_n}_{\text{evaporation}} + \underbrace{k_3 \frac{\partial w_n}{\partial x}}_{\text{water flow downhill}} + \underbrace{k_4 \frac{\partial^2 w_n}{\partial x^2}}_{\text{water diffusion}}, \quad (4.4b)$$

$$u_{n+1}(x, 0) = \tilde{f}(u_n(x, \tau), w_n(x, \tau)), \quad (4.4c)$$

$$w_{n+1}(x, 0) = \tilde{g}(u_n(x, \tau), w_n(x, \tau)), \quad (4.4d)$$

where  $u_n = u_n(x, t)$ ,  $w_n = w_n(x, t)$ ,  $x \in \mathbb{R}$ ,  $0 < t < \tau$  and  $n \in \mathbb{N}$ . The spatial domain is considered to be infinite with  $x$  increasing in the uphill direction. Between the  $(n - 1)$ -th and  $n$ -th precipitation pulse, the interpulse PDEs (4.4a) and (4.4b) are considered on the finite time domain  $0 < t < \tau$ , where  $\tau$  is the time (in years) between the occurrence of the pulse events described by the update equations (4.4c) and (4.4d). The interpulse PDEs (4.4a) and (4.4b) describe the continuous loss of plants at rate  $k_1$ , and evaporation at rate  $k_2$ . While no plant dispersal is assumed to occur during this phase, water diffuses with diffusion coefficient  $k_4$  and flows downhill at velocity  $k_3$ . The simplistic nature of the PDE system allows for an analytical study of conditions for pattern onset to occur (Section 4.4.1), but an extension which also includes plant growth during drought periods is considered using numerical simulations in Section 4.5.

The functions  $\tilde{f}(u_n(x, \tau), w_n(x, \tau))$  and  $\tilde{g}(u_n(x, \tau), w_n(x, \tau))$  in the update equations (4.4c) and (4.4d) describe the system's dynamics during short rainfall pulses, which are assumed to occur periodically in time. To account for plant growth and the associated consumption of water as well as seed dispersal synchronised with a

precipitation event, we choose

$$\begin{aligned}\tilde{f}(u_n(x, \tau), w_n(x, \tau)) &= \underbrace{u_n(x, \tau)}_{\text{existing plants}} \\ &\quad + \overbrace{\phi(\cdot; a) * \left( k_5 \left( \frac{u_n(\cdot, \tau)}{k_6 + u_n(\cdot, \tau)} \right)^2 (w_n(\cdot, \tau) + \tau k_7) \right)}^{\text{dispersal of newly added biomass}}, \\ \tilde{g}(u_n(x, \tau), w_n(x, \tau)) &= \underbrace{w_n(x, \tau)}_{\text{existing water}} + \underbrace{\tau k_7}_{\text{rainfall}} - \underbrace{\left( \frac{u_n(x, \tau)}{k_6 + u_n(x, \tau)} \right)^2 (w_n(x, \tau) + \tau k_7)}_{\text{water uptake}}.\end{aligned}$$

In the update equation (4.4d) a constant amount water  $\tau k_7$  is added to the existing water density. The parameter  $k_7$  denotes the total amount of rainfall that occurs over one year and  $\tau$  (in years) is the time between two rainfall events. The water volume added to the system during one precipitation event thus is  $\tau k_7$ . At the same time, water is converted into biomass.

Similar to the Klausmeier model (4.1), the term describing water consumption by plants consists of the total resource density ( $w + \tau k_7$ ), a term describing the water uptake by the plants' roots ( $u/(k_6 + u)$ ), and a term accounting for the increased ability of plants to consume water in dense patches ( $u/(k_6 + u)$ ). As in the Klausmeier model, the functional responses of the latter two to the plant density are chosen to be identical for mathematical convenience. However, the functional response is different to that used in the Klausmeier model. In the impulsive model  $H_{\text{up}}(u) = u/(k_6 + u)$ , motivated by the saturating behaviour of water infiltration into the soil based on empirical evidence [228] and previous applications in mathematical models [74, 86], while in the Klausmeier model  $H_{\text{up}}(u) = u$ . The pulse-type occurrence of precipitation and water uptake in (4.5) necessitates a saturating behaviour ( $H_{\text{up}}^2(u) < 1$  for all  $u \geq 0$ ) of the functional response to ensure positivity of (4.5d). The parameter  $k_6$  is the half saturation constant of the water infiltration and corresponds to the level of plant biomass at which the water infiltration into the soil is at half of its maximum. This water uptake term directly corresponds to the term in (4.4c), describing plant growth, where  $k_5$  quantifies the plant species' water to biomass conversion rate. We have numerically tested the model for other nonlinearities in this term with such a saturating behaviour without observing any qualitative differences in the results on pattern onset.

Finally, dispersal of the newly added biomass is described by the convolution term of that biomass with a probability density function  $\phi$ . This introduces an additional parameter  $a$ , describing the width of the dispersal kernel in a reciprocal

way. This constitutes a second main difference to the models discussed above. While in the Klausmeier models the whole plant density undergoes diffusion/nonlocal dispersal, in the impulsive model only newly added biomass is dispersed, weakening the role of dispersal in the model.

No water redistribution is assumed to occur in this stage. While overland water flow during intense rainfall events is an area of active research [168, 211, 235], some hydrological modelling approaches suggest that if the contrast in water infiltration rates between bare and vegetated soil is small (e.g. in non crust-forming soil types such as sandy soil), then no water run-on occurs at plant patches during precipitation pulses [168]. An overview of all parameters, including estimates, is given in Table 4.1.

The formulation of (4.4) is based on a number of simplifying assumptions (e.g. flat terrain, no plant growth during drought periods, linear functional response to the water density in the water consumption term) to make the model analytically tractable (Sec 4.4.1). In Sec. 4.5, we relax these assumptions and analyse their effects using numerical methods.

The model can be nondimensionalised by  $u = k_6 \tilde{u}$ ,  $w = k_5^{-1} k_6 \tilde{w}$ ,  $x = a^{-1} \tilde{x}$ ,  $t = k_2^{-1} \tilde{t}$ ,  $A = k_2^{-1} k_5 k_6^{-1} k_7$ ,  $B = k_1 k_2^{-1}$ ,  $T = k_2 \tau$ ,  $\nu = k_2^{-1} k_3 a$  and  $d = k_2^{-1} k_4 a^2$ , to give

$$\frac{\partial u_n}{\partial t} = -B u_n, \quad (4.5a)$$

$$\frac{\partial w_n}{\partial t} = -w_n + \nu \frac{\partial w_n}{\partial x} + d \frac{\partial^2 w_n}{\partial x^2}, \quad (4.5b)$$

$$u_{n+1}(x, 0) = u_n(x, T) + \phi(\cdot; 1) * \left( \left( \frac{u_n(\cdot, T)}{1 + u_n(\cdot, T)} \right)^2 (w_n(\cdot, T) + TA) \right), \quad (4.5c)$$

$$w_{n+1}(x, 0) = (w_n(x, T) + TA) \left( 1 - \left( \frac{u_n(x, T)}{1 + u_n(x, T)} \right)^2 \right), \quad (4.5d)$$

after dropping the tildes for brevity, where  $u_n = u_n(x, t)$ ,  $w_n = w_n(x, t)$ ,  $x \in \mathbb{R}$ ,  $0 < t < T$  and  $n \in \mathbb{N}$ . While the dimensionless parameters  $A$ ,  $B$  and  $T$  are combinations of several of the original parameters, they can be interpreted as the total amount of rainfall per year, rate of plant loss and time between separate rain and dispersal events, respectively. The water redistribution parameters  $\nu$  and  $d$  describe the ratio of the water flow coefficients (advection and diffusion, respectively) to the plant dispersal kernel width  $1/a$ . Their estimates are also included in Table 4.1.

In this form,  $T = 4$  corresponds to rain/dispersal events occurring once per

**Dimensional parameters of (4.4)**

Parameter	Units	Estimates	Description
$k_1$	$\text{year}^{-1}$	1.8 [99], 0.18 [99], 1.2[75]	Rate of plant loss
$k_2$	$\text{year}^{-1}$	4 [75, 99, 199], 0.2[163]	Rate of evaporation
$k_3$	$\text{m year}^{-1}$	0-365 [99]	Velocity of water flow downhill
$k_4$	$\text{m}^2 \text{year}^{-1}$	500 [199],	Water diffusion coefficient
$k_5$	(kg biomass) (kg H <sub>2</sub> O) <sup>-1</sup>	0.01[163], 0.003 [99], 0.002 [99]	Yield of plant biomass per kg water
$k_6$	(kg biomass) $\text{m}^{-2}$	0.05 [75]	Half saturation constant of wa- ter uptake
$k_7$	(kg H <sub>2</sub> O) $\text{m}^{-2} \text{year}^{-1}$	250-750 [99], 0-1000 [75]	Total amount of rainfall in one year
$\tau$	year	0-1	Interpulse time
$a$	$\text{m}^{-1}$	0.03-100 [25]	Scale parameter of dispersal kernel, reciprocal of the width

**Nondimensional parameters of (4.5)**

Parameter	Scaling	Estimates	Description
$A$	$k_2^{-1}k_5k_6^{-1}k_7$	0-15 [75, 99, 199]	Precipitation per year
$B$	$k_1k_2^{-1}$	0.45 [99], 0.3[75] 0.045 [99]	Plant mortality rate
$T$	$k_2\tau$	0-4	Interpulse time
$\nu$	$k_2^{-1}k_3a$	0-10 <sup>3</sup> [25, 99]	Slope (water flow downhill)
$d$	$k_2^{-1}k_4a^2$	0.1-10 <sup>6</sup> [25, 199]	Water diffusion coefficient

Table 4.1: Overview of parameters in (4.4) and (4.5). This table gives an overview of both the dimensional parameters of model (4.4) and the nondimensional parameters of (4.5), including their units (dimensional parameters) or scalings (nondimensional parameters), and their estimated values as well as an interpretation/description. Note that parameter  $k_5$  is dimensionless. However, for ease of interpretation, we distinguish between (kg biomass) and (kg H<sub>2</sub>O). The wide ranges for the water dispersal rates  $\nu$  and  $d$  arise from their dependence on the variations in the width  $a$  of the plant dispersal kernel.

year. Even though we present results for  $0 < T < 4$  in this study, it is important to emphasise that ecologically it is meaningless to consider the limit  $T \rightarrow 0$ . As the interpulse time  $T$  becomes small, the interpulse PDEs (4.5a) and (4.5b), and in particular the decay-type processes that are described by those equations, become less significant, while the update equations (4.5c) and (4.5d) remain unaffected by changes in  $T$ . Moreover, substitution of  $T = 0$  into (4.5) reduces the impulsive system to an integrodifference system given by (4.5c) and (4.5d) in which no plant death and water evaporation occur. In this setting, due to the lack of water evaporation in the system, resources would be added to the system without being removed, yielding biomass growth without bound.

## 4.4 Onset of patterns

A common method to study the onset of patterns is linear stability analysis. Spatial patterns occur if a steady state that is stable to spatially homogeneous perturbations becomes unstable if a spatially heterogeneous perturbation is introduced. In this section we apply such an approach to the impulsive model (4.5) on flat ground for the Laplace kernel. Our analysis shows that while a smaller number of strong precipitation events inhibits their onset by decreasing the size of the parameter region supporting the onset of patterns, it also increases the requirements on the total amount of rainfall for plants to persist in a spatially uniform equilibrium. We further show that the introduction of temporal rainfall intermittency replaces water diffusion as the main cause of spatial patterns.

### 4.4.1 Linear Stability Analysis

The use of linear stability analysis to determine conditions for the onset of patterns in a system concentrates on the calculation of growth/decay rates of perturbations to a spatially uniform equilibrium. In PDE systems and integrodifference systems, spatially uniform steady states are constant in both space and time, and can be calculated by setting all derivatives to zero (PDE systems) or imposing  $u_{n+1} = u_n$  (integrodifference systems). By contrast, spatially uniform equilibria of impulsive systems are not constant in time. Instead, they are periodic in time with period  $T$ , the time between the occurrences of pulse-type events, and undergo the same cycle during each interpulse period. Consequently, time derivatives in the interpulse PDEs cannot be neglected in the calculation of spatially uniform equilibria. For the

given impulsive model

$$\frac{\partial u_n}{\partial t} = -Bu_n, \quad (4.6a)$$

$$\frac{\partial w_n}{\partial t} = -w_n + \nu \frac{\partial w_n}{\partial x} + d \frac{\partial^2 w_n}{\partial x^2}, \quad (4.6b)$$

$$u_{n+1}(x, 0) = \tilde{f}(u_n(x, T), w_n(x, T)), \quad (4.6c)$$

$$w_{n+1}(x, 0) = \tilde{g}(u_n(x, T), w_n(x, T)), \quad (4.6d)$$

where  $u_n = u_n(x, t)$ ,  $w_n = w_n(x, t)$ ,  $x \in \mathbb{R}$ ,  $0 < t < T$  and  $n \in \mathbb{N}$ , the assumption of spatial uniformity reduces the impulsive system to the difference system

$$u_{n+1}(0) = \tilde{f}(u_n(0)e^{-BT}, w_n(0)e^{-T}), \quad (4.7a)$$

$$w_{n+1}(0) = \tilde{g}(u_n(0)e^{-BT}, w_n(0)e^{-T}), \quad (4.7b)$$

after solving (4.6a) and (4.6b), where the densities during any interpulse period are given by  $u_n(t) = u_n(0)e^{-Bt}$  and  $w_n(t) = w_n(0)e^{-t}$  for  $0 \leq t \leq T$ . Even though a non-trivial equilibrium  $(\bar{u}(t), \bar{w}(t))$  of (4.6) is a periodic function of time, we introduce the notation  $\bar{u}^0$  and  $\bar{w}^0$  to denote the equilibrium densities at the start of the interpulse period, i.e.  $\bar{u}^0 := \bar{u}(0)$  and  $\bar{w}^0 := \bar{w}(0)$ . This yields that the general, time-dependent equilibrium densities can be written as  $\bar{u}(t) = \bar{u}^0 e^{-Bt}$  and  $\bar{w} = \bar{w}^0 e^{-t}$  for  $0 \leq t \leq T$ . For brevity, we use the notation  $(\bar{u}^0, \bar{w}^0)$  to refer to the equilibrium in the analysis that follows. Thus, from the reduced difference model (4.7) it follows that the equilibria of (4.6) can be found by solving

$$\bar{u}^0 = \tilde{f}(\bar{u}^0 e^{-BT}, \bar{w}^0 e^{-T}),$$

$$\bar{w}^0 = \tilde{g}(\bar{u}^0 e^{-BT}, \bar{w}^0 e^{-T}).$$

Application of this procedure to (4.5) gives the spatially uniform equilibria of the impulsive system as

$$\begin{aligned} (\bar{u}_d^0, \bar{w}_d^0) &= \left( 0, \frac{ATe^T}{e^T - 1} \right), (\bar{u}_\pm^0, \bar{w}_\pm^0) = \left( \frac{(AT - 2e^{-T} + 2)e^{-BT} \pm \sqrt{\eta} + 2e^{-T} - 2}{2e^{-BT}(1 - e^{-BT})}, \right. \\ &\quad \left. \frac{2((AT - 2e^{-T} + 1)e^{-BT} \pm \sqrt{\eta} + 2e^{-T} - 1)(1 - e^{-BT})}{((AT - 2e^{-T} + 2)e^{-BT} \pm \sqrt{\eta} + 2e^{-T} - 2)e^{-BT}} \right), \end{aligned}$$

where

$$\begin{aligned}\eta = & \left( 4(e^{-T})^2 + (-4AT - 4)e^{-T} + A^2T^2 + 4AT \right) (e^{-BT})^2 \\ & + 4(e^{-T} - 1)(AT - 2e^{-T}) e^{-BT} + 4(e^{-T})^2 - 4e^{-T}.\end{aligned}$$

The steady states  $(\bar{u}_\pm^0, \bar{w}_\pm^0)$  only exist provided that

$$A > A_{\min} := \frac{2(1 - e^{-T} + \sqrt{1 - e^{-T}})(1 - e^{-BT})}{Te^{-BT}}, \quad (4.8)$$

to ensure positivity of  $\eta$ . In principle, this structure is very similar to that of the Klausmeier models (4.1) and (4.2). For rainfall levels below  $A_{\min}$  only the desert steady state  $(\bar{u}_d^0, \bar{w}_d^0)$  exists and plants die out, while for sufficiently large amounts of precipitation two further spatially uniform equilibria with non-zero vegetation density exist. An initial conclusion therefore is the existence of an inhibitory effect of long drought periods. The existence threshold  $A_{\min}$  of  $(\bar{u}_+^0, \bar{w}_+^0)$  increases with the interpulse time  $T$  and thus enlarges the parameter region in which the desert equilibrium  $(\bar{u}_d^0, \bar{w}_d^0)$  is the only spatially uniform steady state. Even though  $A_{\min}$  does not yield any information on the existence of spatially non-uniform solutions for low precipitation levels, we use this threshold as a proxy for the minimum water requirements of the ecosystem. This crucial property is revisited in our discussion on model extensions in Sec. 4.5.

Similar to the Klausmeier models, spatial patterns arise from the steady state  $(\bar{u}_+^0, \bar{w}_+^0)$  which is stable to spatially homogeneous perturbations (Proposition 4.4.1). The stability structure of the steady states of the Klausmeier models is preserved in the impulsive model, i.e. the desert steady state  $(\bar{u}_d^0, \bar{w}_d^0)$  and the vegetation steady state  $(\bar{u}_+^0, \bar{w}_+^0)$  are stable to spatially homogeneous perturbations, while the other vegetation steady state  $(\bar{u}_-^0, \bar{w}_-^0)$  is unstable for all biologically realistic parameter choices.

**Proposition 4.4.1.** *Let  $A > A_{\min}$ ,*

$$\overline{B_2} = \frac{1}{T} \ln \left( 1 + \frac{ATe^T \sqrt{e^T - 1} (\sqrt{e^T} - \sqrt{e^T - 1})}{2(e^T - 1)} \right),$$

and  $J_1(B) := e^{-T(B+1)}(\bar{\alpha}\bar{\delta} - \bar{\gamma}\bar{\beta}) - 1$ , where

$$\begin{aligned}\bar{\alpha} &= \tilde{f}_u(\bar{u}^0 e^{-BT}, \bar{w}^0 e^{-T}), & \bar{\beta} &= \tilde{f}_w(\bar{u}^0 e^{-BT}, \bar{w}^0 e^{-T}), \\ \bar{\gamma} &= \tilde{g}_u(\bar{u}^0 e^{-BT}, \bar{w}^0 e^{-T}), & \bar{\delta} &= \tilde{g}_w(\bar{u}^0 e^{-BT}, \bar{w}^0 e^{-T}).\end{aligned}\tag{4.9}$$

If  $J_1(B)$  admits a positive real root  $\overline{B_1}$ , the steady state  $(\bar{u}_+^0, \bar{w}_+^0)$  is stable to spatially homogeneous perturbations if  $B < \min\{\overline{B_1}, \overline{B_2}\}$  provided that  $\overline{B_2} \in \mathbb{R}$  or  $B < \overline{B_1}$  provided that  $\overline{B_2} \notin \mathbb{R}$ . If no positive real solution of  $J_1(B) = 0$  exists, then  $(\bar{u}_+^0, \bar{w}_+^0)$  is stable if  $B < \overline{B_2}$  provided that  $\overline{B_2} \in \mathbb{R}$ .

The proof of Proposition 4.4.1, as well as all those of all other propositions, is deferred until the end of the section.

From Proposition 4.4.1 it follows that the steady state  $(\bar{u}_+^0, \bar{w}_+^0)$  is stable to spatially homogeneous perturbations close to  $B = 0$  for biologically relevant parameters (i.e.  $A, T > 0$ ). Similar calculations yield that  $(\bar{u}_-^0, \bar{w}_-^0)$  is unstable close to  $B = 0$ . In particular, for  $B = 0.45$ , the highest estimate of the plant mortality parameter (see Table 4.1), the steady state  $(\bar{u}_+^0, \bar{w}_+^0)$  is stable for all  $(A, T)$  pairs with  $A > A_{\min}$ , while similarly  $(\bar{u}_-^0, \bar{w}_-^0)$  is unstable.

We investigate the existence of spatial patterns by introducing spatially heterogeneous perturbations to the steady state  $(\bar{u}^0, \bar{w}^0) := (\bar{u}_+^0, \bar{w}_+^0)$ . The following propositions provide conditions for a steady state to be stable to such spatially heterogeneous perturbations and yield results on the effects of rainfall intermittency on the onset of spatial patterns.

**Proposition 4.4.2.** *Let  $\tilde{f}$  be of the form  $\tilde{f}(u, w) = u + \phi * \tilde{f}_1(u, w)$ . A steady state  $(\bar{u}^0, \bar{w}^0)$  of the impulsive model (4.6) is stable to spatially heterogeneous perturbations if  $|\lambda(k)| < 1$  for both eigenvalues  $\lambda \in \mathbb{C}$  of*

$$J = \begin{pmatrix} (1 + \hat{\phi}(k)\tilde{\alpha})e^{-BT} & \hat{\phi}(k)\tilde{\beta}e^{-(1-i\nu k+dk^2)T} \\ \tilde{\gamma}e^{-BT} & \tilde{\delta}e^{-(1-i\nu k+dk^2)T} \end{pmatrix},\tag{4.10}$$

for  $k > 0$ , where

$$\begin{aligned}\tilde{\alpha} &= \frac{\partial \tilde{f}_1}{\partial u}(\bar{u}^0 e^{-BT}, \bar{w}^0 e^{-T}), & \tilde{\beta} &= \frac{\partial \tilde{f}_1}{\partial w}(\bar{u}^0 e^{-BT}, \bar{w}^0 e^{-T}), \\ \tilde{\gamma} &= \frac{\partial \tilde{g}}{\partial u}(\bar{u}^0 e^{-BT}, \bar{w}^0 e^{-T}), & \tilde{\delta} &= \frac{\partial \tilde{g}}{\partial w}(\bar{u}^0 e^{-BT}, \bar{w}^0 e^{-T}).\end{aligned}\tag{4.11}$$

The entries of the Jacobian (4.10) are complex-valued. However, a significant simplification is achieved by considering the model on flat ground, i.e. the case of  $\nu = 0$ , thus allowing an application of the Jury criterion (see e.g. [142]) to determine

conditions such that  $|\lambda(k)| < 1$  for both eigenvalues of the Jacobian.

**Proposition 4.4.3.** *The steady state  $(\bar{u}^0, \bar{w}^0)$  of the impulsive model (4.6) on flat ground is stable to spatially heterogeneous perturbations if*

$$1 + \det(J(k)) - \text{tr}(J(k)) > 0, \quad (4.12)$$

for all  $k > 0$ , where  $J$  is the Jacobian defined in (4.10) with  $\nu = 0$ .

This provides a sufficient condition for the occurrence of spatial patterns. Both the local and the nonlocal Klausmeier models undergo a diffusion-driven instability on flat ground for any level of rainfall, meaning that a sufficiently large ratio of water diffusion rate to plant diffusion rate yields a pattern-inducing instability (see Figure 4.1b). This is not the case for the impulsive model. For sufficiently high levels of rainfall, patterns cannot occur for any level of the diffusion coefficient  $d$ , the ratio of the water diffusion rate to the plant dispersal kernel width. It is indeed the time  $T$  between rainfall pulses that determines for which levels of precipitation patterns can form. Only for smaller values of  $A$  an increase of diffusion through the critical value  $d_c(A)$  causes an instability and thus the onset of patterns. Reverting back to parameters in dimensional form, this also shows that for sufficiently low precipitation levels, wider plant dispersal kernels inhibit the onset of patterns, which is in agreement with results from the nonlocal Klausmeier model (4.2) [61] (Chapter 2). Similar to the Klausmeier models, diffusion levels close to  $d = 0$  do not yield an instability for any rainfall parameters and there is a direct transition from the stable plant steady state to the desert steady state as  $A$  is decreased through the lower bound  $A_{\min}$ . This is a conclusion of a numerical investigation (Figure 4.1) of the stability condition (4.12) using the Laplace kernel (4.3) in the  $A$ - $d$  parameter plane. This analysis was performed for various different choices of the parameters  $B$  and  $T$  without showing any qualitative differences.

The evaluation of (4.12) in the  $A$ - $d$  parameter plane suggests a closer investigation of the stability condition (4.12) for  $d \rightarrow \infty$  (Proposition 4.4.4) and  $A = A_{\min}$  (Proposition 4.4.6). The former provides information on the level of rainfall  $A_{\max}$  above which no instability can occur, while the latter yields the locus of  $d_{A_{\min}}$ , the minimum value of diffusion required for an instability to occur.

**Proposition 4.4.4.** *If  $d \rightarrow \infty$  in the impulsive model (4.6) on flat ground with the Laplace kernel (4.3), then  $(\bar{u}^0, \bar{w}^0)$  is unstable to spatially heterogeneous perturbations if  $A < A_{\max}$ , where  $A_{\max}$  satisfies*

$$(1 + \tilde{\alpha}(A_{\max})) e^{-BT} - 1 = 0. \quad (4.13)$$

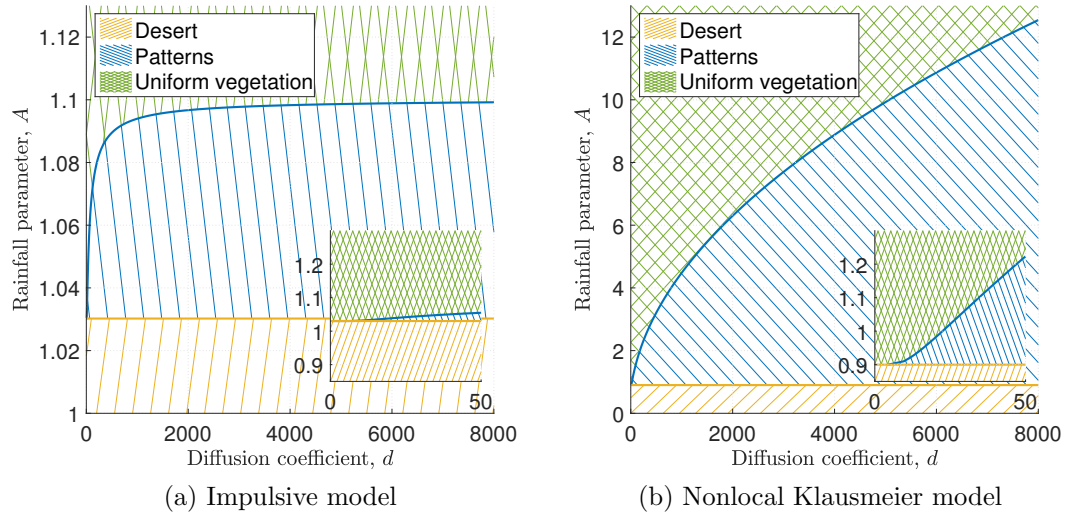


Figure 4.1: The stability criterion (4.12) in the  $A$ - $d$  parameter plane. Part (a) visualises where the second Jury condition (4.12) changes sign and thus yields an instability, which causes the onset of spatial patterns (blue line). Given some value of  $d$ , the value of  $A$  at which a transition between positivity and negativity of the condition occurs, is determined up to an interval of length  $10^{-10}$ . The level of  $d$  is increased in variable increments. For  $d$  close to 0, the increment is chosen to be  $\Delta d = 0.1$ , which then increases up to  $\Delta d = 100$  as the value of  $d$  increases. For any given  $(A, d)$  pair, (4.12) is evaluated for  $k > 0$  at increments of  $\Delta k = 0.01$  until a value of  $k_c$  is found for which the Jury condition is either negative or positive and increasing. In the former case, the  $(A, d)$  pair supports the onset of spatial patterns, in the latter the interval  $[k_c - \Delta k, k_c]$  is investigated further with smaller increments in  $k$ . If still no  $k$  is found for which the Jury condition is negative it is assumed that (4.12) is not satisfied. The other parameter values used in this analysis were  $T = 0.5$  and  $B = 0.45$ , with  $\phi$  being the Laplacian kernel (4.3). This yields  $A_{\min} = 1.03$ , and  $A_{\max} = 1.099$ . A comparison to the nonlocal Klausmeier model, which undergoes a diffusion-driven instability, is shown in (b). Here  $A_{\min} = 2B = 0.9$ . The insets show the behaviour close to  $d = 0$ .

**Corollary 4.4.5.** *The relative size  $(A_{\max} - A_{\min})/A_{\min}$  of the interval  $[A_{\min}, A_{\max}]$  is proportional to  $e^{-2T}$  as  $T \rightarrow \infty$ .*

Given a set of parameters  $(B, T)$ , (4.13) can be solved numerically to provide the level of rainfall  $A$  at which a transition between uniform and patterned vegetation occurs in the limit  $d \rightarrow \infty$ . In combination with the preceding results, this is the threshold  $A_{\max}$  beyond which no pattern onset can occur. This is in stark contrast to the classical case of a diffusion-driven instability which occurs in the Klausmeier models (4.1) and (4.2) for which  $A_{\max} \rightarrow \infty$  as  $d \rightarrow \infty$ . Together with the lower bound on the rainfall parameter  $A_{\min}$  this allows a classification of the  $T$ - $A$  parameter plane into three regions (Figure 4.2a); one in which the desert steady state is the only spatially uniform equilibrium to exist, one in which instability of the uniform plant steady state to spatially heterogeneous perturbations causes the onset of spatial patterns, and one in which any perturbations of the equilibrium  $(\bar{u}^0, \bar{w}^0)$  decay and no pattern onset occurs. This classification of the  $T$ - $A$  parameter plane is based on the preceding linear stability analysis and the perturbation of the spatially uniform equilibrium  $(\bar{u}^0, \bar{w}^0)$ . This results in a classification that provides information regarding the onset of patterns but does not yield any knowledge of the existence of patterns away from their onset. While no systematic study of the whole parameter space using numerical continuation was performed, patterns for parameters outside the interval given by the linear stability analysis can be observed by slowly increasing/decreasing the rainfall parameter  $A$  beyond/below the pattern onset-supporting interval when the system is already in a patterned state.

Proposition 4.4.4 indicates that a decrease in the frequency of precipitation events requires a higher amount of rainfall to avoid an instability. This does not mean that pattern onset occurs for a larger parameter range as periods of droughts become longer, as an increase in  $T$  also increases the lower bound on the rainfall for the vegetation steady state to exist. Indeed, Corollary 4.4.5 provides information on the size of the interval for the rainfall parameter  $A$  that supports the onset of patterns relative to the lower bound (4.8) on the rainfall (Figure 4.2b). For small values of  $T$  the size of this interval is larger than the lower bound on the rainfall, for larger  $T$  the size of the pattern onset-supporting interval of rainfall levels decreases at a rate proportional to  $e^{-2T}$ .

For  $A = A_{\min}$ , the previous analysis (Figure 4.1a) suggests the existence of a threshold  $d_{A_{\min}}$  on the diffusion coefficient  $d$  below which no instability occurs. Similar to the Klausmeier models (4.1) and (4.2) this corresponds to a direct transition between the spatially uniform vegetation state and the desert state as the rainfall parameter  $A$  decreases through  $A_{\min}$ .

**Proposition 4.4.6.** *If  $A = A_{\min}$ , there exists a threshold  $d_{A_{\min}} > 0$  such that*

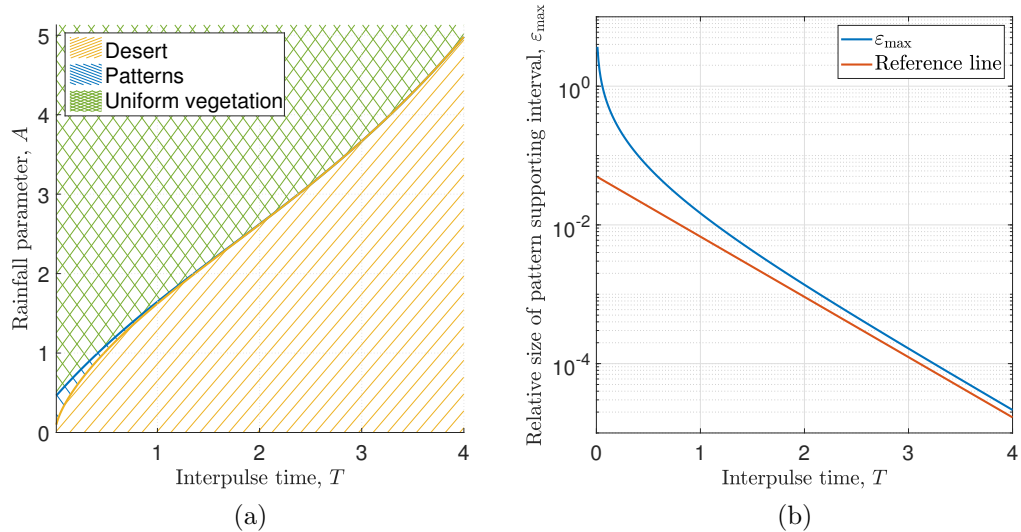


Figure 4.2: Classification of the  $A$ - $T$  parameter plane and the relative size of the rainfall interval supporting pattern onset as  $d \rightarrow \infty$ . Part (a) shows a classification of the  $A$ - $T$  parameter plane in the limit  $d \rightarrow \infty$  into regions in which uniform vegetation is stable, in which pattern onset occurs, and in which the desert state is the only spatially uniform equilibrium of the system. The transition  $A = A_{\max}$  between uniform and patterned vegetation (blue line) is obtained by numerically solving (4.13), while the lower bound  $A = A_{\min}$  on the parameter region supporting pattern onset (yellow line) is obtained from the analytic condition (4.8). The relative size  $\varepsilon_{\max} := A_{\max} - A_{\min}$  of the parameter region supporting pattern onset is visualised in (b) and is compared to a reference line of slope  $\exp(-2T)$ . The plant loss parameter is  $B = 0.45$ . Note the logarithmic scale in (b).

$(\bar{u}^0, \bar{w}^0)$  is unstable to spatially heterogeneous perturbations for  $d > d_{A_{\min}}$ .

The threshold given by Proposition 4.4.6 is independent of the plant loss parameter  $B$ . Plant mortality does, however, affect  $A_{\min}$ , the level of rainfall required for the plant steady state to exist. The simplification provided by setting  $A = A_{\min}$  is not sufficient to determine the threshold  $d_{A_{\min}}$  on the diffusion coefficient explicitly, but similar to the analysis in the  $d \rightarrow \infty$  case, it can be determined numerically for a given set of parameters. The results of this show that an increase in the time interpulse  $T$  causes an increase in the threshold  $d_{A_{\min}}$  on the diffusion coefficient, i.e. a higher ratio of water diffusion to plant dispersal kernel width is required to cause an instability leading to the onset of patterns.

*Proof of Proposition 4.4.1.* Linear stability analysis of a steady state  $(\bar{u}^0, \bar{w}^0)$  of the impulsive model (4.6) in a spatially uniform setting is equivalent to linear stability analysis of the difference system (4.7) with  $\tilde{f}(u, w) = u + (u/(1+u))^2(w + TA)$  and  $\tilde{g}(u, w) = (w + TA)(1 - (u/(1+u))^2)$ . Linearisation about the steady state and introduction of a perturbation proportional to  $\lambda^n$  yields that the growth factor  $\lambda \in \mathbb{C}$  is an eigenvalue of the Jacobian

$$J(\bar{u}^0, \bar{w}^0) = \begin{pmatrix} e^{-BT}\bar{\alpha} & e^{-T}\bar{\beta} \\ e^{-BT}\bar{\gamma} & e^{-T}\bar{\delta} \end{pmatrix}.$$

The Jury conditions then yield stability of a steady state  $(\bar{u}^0, \bar{w}^0)$  if

$$e^{-T(B+1)} (\bar{\alpha}\bar{\delta} - \bar{\gamma}\bar{\beta}) < 1, \quad (4.14a)$$

$$1 + e^{-T(B+1)} (\bar{\alpha}\bar{\delta} - \bar{\gamma}\bar{\beta}) > |e^{-BT}\bar{\alpha} + e^{-T}\bar{\delta}|, \quad (4.14b)$$

are both satisfied.

The first Jury condition (4.14a) yields  $J_1(B) < 0$ . For  $(\bar{u}^0, \bar{w}^0) = (\bar{u}_+, \bar{w}_+)$ ,  $J_1(0) = -1$  and thus the condition is satisfied for  $B < \bar{B}_1$ , where  $\bar{B}_1$  is the smallest real positive root of  $J_1(B)$  provided it exists. The second Jury condition (4.14b) is  $J_2(B) := 1 + e^{-T(B+1)}(\bar{\alpha}\bar{\delta} - \bar{\gamma}\bar{\beta}) - e^{-BT}\bar{\alpha} - e^{-T}\bar{\delta} > 0$ . For  $(\bar{u}^0, \bar{w}^0) = (\bar{u}_+, \bar{w}_+)$ ,  $J_2(0) = 0$  and  $dJ_2/dB(0) = T > 0$  and thus the condition is satisfied for  $B < \bar{B}_2$ , which is the smallest real positive root of  $J_2(B)$  provided it exists.  $\square$

*Proof of Proposition 4.4.2.* Similar to the Proposition 4.4.1, this proof is based on a linear stability analysis. Unlike in the proof of Proposition 4.4.1, the system cannot be immediately reduced to a difference system. Additionally, the convolution in (4.6c) adds a complication. However, both these issues can be addressed by performing the analysis in Fourier space.

As is standard with linear stability analysis, we set

$$u_n(x, t) = \bar{u}^0 e^{-Bt} + \tilde{u}(x, t) \quad \text{and} \quad w_n(x, t) = \bar{w}^0 e^{-t} + \tilde{w}(x, t). \quad (4.15)$$

to investigate the behaviour of perturbations  $(\tilde{u}(x, t), \tilde{w}(x, t))$  to a spatially uniform equilibrium  $(\bar{u}(t), \bar{w}(t)) = (\bar{u}^0 e^{-Bt}, \bar{w}^0 e^{-t})$ . Substitution into the update equations (4.6c) and (4.6d) and linearisation yields

$$\tilde{u}_{n+1}(x, 0) = \tilde{u}_n(x, T) + \phi * \left( \tilde{\alpha} \tilde{u}_n(\cdot, T) + \tilde{\beta} \tilde{w}_n(\cdot, T) \right), \quad (4.16a)$$

$$\tilde{w}_{n+1}(x, 0) = \tilde{\gamma} \tilde{u}_n(x, T) + \tilde{\delta} \tilde{w}_n(x, T), \quad (4.16b)$$

noting that  $\tilde{g}(\bar{u}^0 e^{-BT}, \bar{w}^0 e^{-T}) = \bar{w}^0$  and  $\tilde{f}_1(\bar{u}^0 e^{-BT}, \bar{w}^0 e^{-T}) = \bar{u}^0(1 - e^{-BT})$  by the definition of the spatially uniform equilibria. The Fourier transform applied to (4.16) gives

$$\widehat{\tilde{u}_{n+1}}(k, 0) = \left( 1 + \widehat{\phi}(k) \tilde{\alpha} \right) \widehat{\tilde{u}_n}(k, T) + \widehat{\phi}(k) \tilde{\beta} \widehat{\tilde{w}_n}(k, T), \quad (4.17a)$$

$$\widehat{\tilde{w}_{n+1}}(k, 0) = \tilde{\gamma} \widehat{\tilde{u}_n}(k, T) + \tilde{\delta} \widehat{\tilde{w}_n}(k, T), \quad (4.17b)$$

making use of the convolution theorem. The functions  $\widehat{\tilde{u}_n}$  and  $\widehat{\tilde{w}_n}$  satisfy the interpulse PDEs (4.6a) and (4.6b). Taking the Fourier transform of the interpulse PDEs (4.6a) and (4.6b) gives

$$\frac{\partial \widehat{\tilde{u}_n}(k, t)}{\partial t} = -B \widehat{\tilde{u}_n}(k, t), \quad \frac{\partial \widehat{\tilde{w}_n}(k, t)}{\partial t} = -(1 - i\nu k + dk^2) \widehat{\tilde{w}_n}(k, t),$$

which can be solved to

$$\widehat{\tilde{u}_n}(k, t) = \widehat{\tilde{u}_n}(k, 0) e^{-Bt}, \quad \widehat{\tilde{w}_n}(k, t) = \widehat{\tilde{w}_n}(k, 0) e^{-(1-i\nu k + dk^2)t}. \quad (4.18)$$

Substitution into (4.17) yields

$$\widehat{\tilde{u}_{n+1}}(k, 0) = \left( 1 + \widehat{\phi}(k) \tilde{\alpha} \right) e^{-BT} \widehat{\tilde{u}_n}(k, 0) + \widehat{\phi}(k) \tilde{\beta} e^{-(1-i\nu k + dk^2)T} \widehat{\tilde{w}_n}(k, 0),$$

$$\widehat{\tilde{w}_{n+1}}(k, 0) = \tilde{\gamma} e^{-BT} \widehat{\tilde{u}_n}(k, 0) + \tilde{\delta} e^{-(1-i\nu k + dk^2)T} \widehat{\tilde{w}_n}(k, 0).$$

from (4.17). This is a linear difference system to which standard tools of stability analysis can be applied. In other words, the assumption that the perturbations  $\widehat{\tilde{u}_n}$  and  $\widehat{\tilde{w}_n}$  are proportional to  $\lambda^n$  yields that the growth factor  $\lambda \in \mathbb{C}$  is an eigenvalue of the Jacobian  $J$ .  $\square$

*Proof of Proposition 4.4.3.* To investigate a steady state's stability on flat ground, the Jury conditions can be used. An instability occurs, if at least one of

$$\det(J) - 1 < 0, \quad (4.19a)$$

$$1 + \det(J) - |\text{tr}(J)| > 0, \quad (4.19b)$$

is not satisfied for some  $k > 0$ . The first Jury condition (4.19a) is automatically satisfied due to stability to spatially homogeneous perturbations, because

$$\begin{aligned} \det(J) &= e^{-T(B+1+dk^2)} \left( \left( 1 + \widehat{\phi}(k)\tilde{\alpha} \right) \tilde{\delta} - \widehat{\phi}(k)\tilde{\beta}\tilde{\gamma} \right) \\ &= e^{-T(B+1+dk^2)} \left( \tilde{\delta} + \widehat{\phi}(k) \left( \tilde{\alpha}\tilde{\delta} - \tilde{\beta}\tilde{\gamma} \right) \right) \\ &< e^{-T(B+1)} \left( \tilde{\delta} + \tilde{\alpha}\tilde{\delta} - \tilde{\beta}\tilde{\gamma} \right) = e^{-T(B+1)} (\bar{\alpha}\bar{\delta} - \bar{\beta}\bar{\gamma}) < 1, \end{aligned}$$

for all  $k > 0$ , noting that  $1 + \tilde{\alpha} = \bar{\alpha}$ ,  $\tilde{\beta} = \bar{\beta}$ ,  $\tilde{\gamma} = \bar{\gamma}$  and  $\tilde{\delta} = \bar{\delta}$ , where  $\bar{\alpha}$ ,  $\bar{\beta}$ ,  $\bar{\gamma}$  and  $\bar{\delta}$  are defined in (4.9). The last inequality makes use of the steady state's stability to spatially homogeneous perturbations, which in particular guarantees that (4.14a) holds. Therefore, assuming a steady state's stability to spatially homogeneous perturbations, a sufficient condition for spatial patterns to occur is the existence of some wavenumber  $k > 0$  such that the second Jury condition (4.12) does not hold. In the case of model (4.5) this condition can be slightly simplified by noting that  $\tilde{\alpha} > 0$  and  $\tilde{\delta} > 0$  and therefore  $\text{tr}(J) > 0$  for all  $k > 0$ . The condition thus becomes  $1 + \det(J) - \text{tr}(J) > 0$ .  $\square$

*Proof of Proposition 4.4.4.* If  $d \rightarrow \infty$  and  $\nu = 0$ , then the Jacobian (4.10) becomes

$$J = \begin{pmatrix} \left( 1 + \widehat{\phi}(k)\tilde{\alpha} \right) e^{-BT} & 0 \\ \tilde{\gamma}e^{-BT} & 0 \end{pmatrix}.$$

Its determinant is clearly zero and therefore the stability condition simplifies to  $1 - (1 + \widehat{\phi}(k)\tilde{\alpha})e^{-BT} > 0$ , for all  $k > 0$ . For the Laplacian kernel (4.3) this is a polynomial in  $k^2$ , which after rearranging becomes

$$k^2 > \frac{(1 + \tilde{\alpha})e^{-BT} - 1}{1 - e^{-BT}}. \quad (4.20)$$

Stability of the steady state requires (4.20) to hold for all  $k > 0$ . This is only possible if the right hand side of (4.20) is negative. Thus, an instability causing the onset of

spatial patterns occurs if

$$(1 + \tilde{\alpha}) e^{-BT} - 1 > 0. \quad (4.21)$$

The coefficient  $\tilde{\alpha}$  is decreasing in  $A$  and thus there exists a threshold  $A = A_{\max}$  such that an instability occurs for all  $A < A_{\max}$ .  $\square$

*Proof of Corollary 4.4.5.* Substitution of  $A = A_{\min}(1 + \varepsilon)$  into (4.21) gives

$$\varepsilon < \varepsilon_{\max} := \frac{1}{8 \left( e^{\frac{3T}{2}} \sqrt{e^T - 1} + e^{2T} - e^{\frac{T}{2}} \sqrt{e^T - 1} - e^T \right)},$$

after linearisation in  $\varepsilon$ . The right hand side  $\varepsilon_{\max}$  denotes the relative size of the rainfall interval supporting pattern onset. Its logarithm decreases at rate

$$(\ln(\varepsilon_{\max}))' = -\frac{4e^{\frac{3T}{2}} \sqrt{e^T - 1} + 4e^{2T} - 2e^{\frac{T}{2}} \sqrt{e^T - 1} - 5e^T + 1}{2\sqrt{e^T - 1} \left( e^T \sqrt{e^T - 1} + e^{\frac{3T}{2}} - \sqrt{e^T - 1} - e^{\frac{T}{2}} \right)} \rightarrow -2,$$

as  $T \rightarrow \infty$ . This shows the exponential decay of the relative interval size  $\varepsilon_{\max}$ .  $\square$

*Proof of Proposition 4.4.6.* Setting  $A = A_{\min}$  provides a significant simplification as the equilibrium becomes

$$(\bar{u}^0, \bar{w}^0) = \left( \sqrt{1 - e^{-T}} e^{BT}, \frac{(e^{BT} - 1)(1 + 2\sqrt{1 - e^{-T}})}{\sqrt{1 - e^{-T}}} \right).$$

Thus the coefficients  $\tilde{\alpha}$ ,  $\tilde{\beta}$ ,  $\tilde{\gamma}$  and  $\tilde{\delta}$  given by (4.11) become

$$\begin{aligned} \tilde{\alpha}_{A_{\min}} &= \frac{2(e^{BT} - 1)(2 - e^{-T} + 2\sqrt{1 - e^{-T}})}{(1 + \sqrt{1 - e^{-T}})^3}, & \tilde{\beta}_{A_{\min}} &= \frac{1 - e^{-T}}{(1 + \sqrt{1 - e^{-T}})^2}, \\ \tilde{\gamma}_{A_{\min}} &= -\tilde{\alpha}_{A_{\min}}, & \tilde{\delta}_{A_{\min}} &= \frac{2\sqrt{1 - e^{-T}} + 1}{(1 + \sqrt{1 - e^{-T}})^2}, \end{aligned}$$

respectively. The Jacobian (4.10) then is

$$J_{A_{\min}} = \begin{pmatrix} (1 + \hat{\phi}(k)\tilde{\alpha}_{A_{\min}}) e^{-BT} & \hat{\phi}(k)\tilde{\beta}_{A_{\min}} e^{-(1+dk^2)T} \\ \tilde{\gamma}_{A_{\min}} e^{-BT} & \tilde{\delta}_{A_{\min}} e^{-(1+dk^2)T} \end{pmatrix},$$

and hence the steady state  $(\bar{u}^0, \bar{w}^0)$  is stable to spatially heterogeneous perturbations if

$$1 + \det(J_{A_{\min}}) - \text{tr}(J_{A_{\min}}) = \zeta(1 - e^{-BT}) > 0 \iff \zeta > 0, \quad \text{for all } k > 0 \quad (4.22)$$

where

$$\begin{aligned}
 \zeta = & \frac{1}{(e^{T/2} + \sqrt{e^T - 1})^3} \left( \left( (-2\tilde{\beta}_{A_{\min}} - 2\tilde{\delta}_{A_{\min}}) \hat{\phi}(k) + 3\tilde{\delta}_{A_{\min}} \right) e^{-Tdk^2 - T/2} \right. \\
 & + \left( (4\tilde{\beta}_{A_{\min}} + 4\tilde{\delta}_{A_{\min}}) \hat{\phi}(k) - 4\tilde{\delta}_{A_{\min}} \right) e^{-Tdk^2 + T/2} + \sqrt{e^T - 1} e^{-(dk^2 + 1)T} \tilde{\delta}_{A_{\min}} \\
 & + 4\sqrt{e^T - 1} \left( (\tilde{\beta}_{A_{\min}} + \tilde{\delta}_{A_{\min}}) \hat{\phi}(k) - \tilde{\delta}_{A_{\min}} \right) e^{-Tdk^2} \\
 & \left. + \left( -1 + (4 - 4\hat{\phi}(k)) e^T \right) \sqrt{e^T - 1} + \left( -3 + 2\hat{\phi}(k) \right) e^{T/2} - 4e^{3/2T} (\hat{\phi}(k) - 1) \right).
 \end{aligned}$$

The minimum of the function  $\zeta$  is decreasing in  $d$  and thus there exists a threshold  $d_{A_{\min}}$  such that (4.22) does not hold for any  $d > d_{A_{\min}}$ .  $\square$

## 4.5 Simulations of model extensions

In the preceding linear stability analysis we have made a number of simplifying assumptions to make the derivation of the criteria for pattern onset analytically tractable. To investigate the impact of these simplifications on our results, we numerically investigate extensions of (4.5) in which some previous assumptions are relaxed.

The analysis in this section yields that the exponential decay (with increasing  $T$ ) of the size of the parameter region supporting pattern onset is due to the temporal separation of the components of the pattern-inducing feedback loop and does not occur if plant growth processes extend into drought periods. Results obtained in this section also highlight the importance of understanding a plant species' response to low soil moisture levels. This functional response is established to have an important influence on the ecosystem dynamics under precipitation regimes with intermediate interpulse times. Finally, the effects of sloped terrain and changes to the plant dispersal kernel are investigated.

### 4.5.1 Method

Simulations to determine the parameter region in which pattern onset occurs are performed in two stages. Unless the non-trivial spatially uniform equilibria of the system can be calculated analytically, we initially integrate the corresponding space-independent model to determine the threshold  $A_{\min}$  below which the desert equilibrium is the system's only spatially uniform steady state. The calculation of  $A_{\min}$  further provides the equilibrium plant and water densities  $(\bar{u}^0, \bar{w}^0)$  close to the threshold.

Numerical simulations of the full model are then performed on the space domain  $[-x_{\max}, x_{\max}]$  centred at  $x = 0$ . This domain is discretised into  $M$  equidistant points  $x_1, \dots, x_M$  with  $-x_{\max} = x_1 < x_2 < \dots < x_M = x_{\max}$  such that  $\Delta x = x_2 - x_1 = \dots = x_M - x_{M-1}$ . The ODE system resulting from the discretisation of the interpulse PDE system (4.5a) and (4.5b) is integrated, and the densities at every space point are updated at the end of each interpulse period of length  $T$ . The discrete convolution term arising from the discretisation of (4.5c) is obtained by using the convolution theorem and the fast Fourier transform, providing a significant simplification through a reduction of the number of operations from  $O(M^2)$  to  $O(M \log(M))$  required to obtain the convolution (see e.g. [36]).

To mimic the infinite domain used for the linear stability analysis (Section 4.4.1), we define the initial condition of the system as follows; on a subdomain  $[-x_{\text{sub}}, x_{\text{sub}}]$  centred at  $x = 0$  of the domain  $[-x_{\max}, x_{\max}]$  the steady state  $(\bar{u}^0, \bar{w}^0)$  near its existence threshold  $A_{\min}$  is perturbed by a function containing a collection of applicable spatial modes, while on the rest of the domain the densities are initially set to equal the densities of the steady state  $(\bar{u}^0, \bar{w}^0)$ . The restriction of the perturbations to a small subdomain is used to avoid difficulties posed by the boundaries. The size of the outer domain is therefore chosen large enough so that any boundary conditions (which are set to be periodic) that are imposed on  $[-x_{\max}, x_{\max}]$  do not affect the solution in the subdomain during the time that is considered in the simulation. Figure 4.3 shows a typical patterned solution obtained by these simulations.

We use model realisations obtained through this method to determine the critical rainfall level  $A_{\max}$  below which pattern onset occurs in the different model extensions.

#### 4.5.2 Nonlinear water uptake

In the original model (4.5), water consumption by plants (and the plant growth associated with it) is described by

$$\text{Up}(u, w) = G_{\text{up}}(w)H_{\text{up}}^2(u) = (w + TA) \left( \frac{u}{1+u} \right)^2.$$

The linearity in  $w$  is inherited from the Klausmeier model on which our impulsive model is based. Field observations indicate that dryland ecosystems remain dormant under low soil moisture levels and are only activated if the water density is sufficiently high [82, 183]. Mathematically, such a property can be described by a Holling type III functional response [31]. To incorporate such a nonlinear response into the

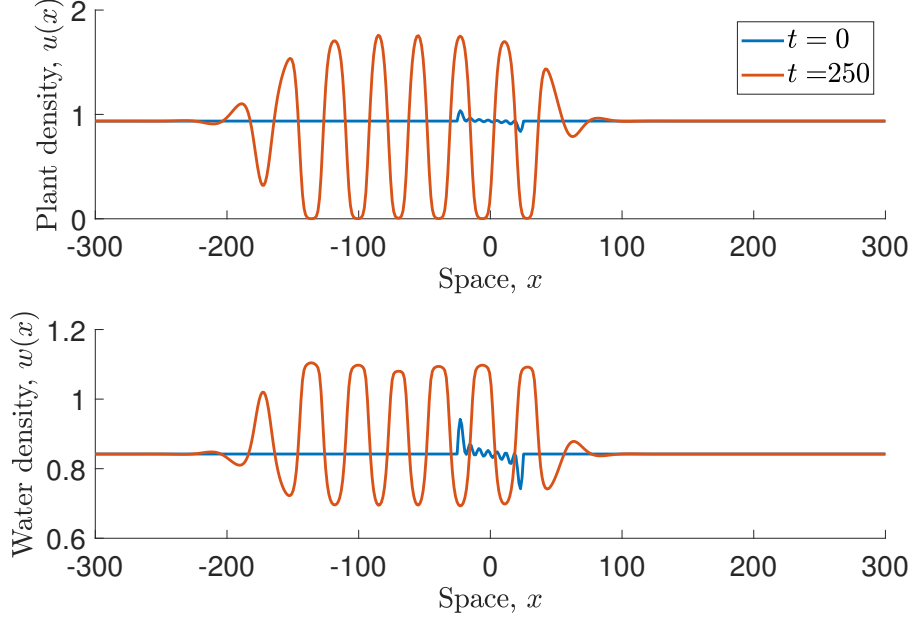


Figure 4.3: Solution of the impulsive model. This visualises a numerically obtained realisation of the impulsive model (4.5) on flat ground. The plant dispersal kernel  $\phi$  is set to the Laplacian kernel (4.3) and the parameter values are  $B = 0.45$ ,  $A = 1.623$ ,  $d = 100$  and  $T = 1$ . The number of space points is  $M = 10^9$ .

impulsive model, we consider an amended uptake function with

$$\widetilde{G}_{\text{up}}(w) = \frac{C_m (w + TA)^p}{C_h^p + (w + TA)^p}, \quad p > 1,$$

where  $C_m$  is the maximum water uptake per unit biomass,  $C_h$  is the half saturation constant of the water consumption and  $p$  accounts for the strength of the nonlinearity. Typical parameter values are  $C_m = 20$ ,  $C_h = \sqrt{2}$  and  $p = 4$  [31]. The introduction of this nonlinearity causes complications as positivity of the water density  $w$  is no longer guaranteed by the update equation (4.5d). To avoid the occurrence of negative densities, we cap the new water uptake function  $\widetilde{\text{Up}}(u, w)$  by  $w + TA$ , i.e. set

$$\widetilde{\text{Up}}(u, w) = \max\{w + TA, \widetilde{G}_{\text{up}}(w)\} H_{\text{up}}^2(u).$$

The most significant result of our numerical investigation of (4.5) with a Holling type III functional response in the water uptake and plant growth terms is that the minimum of the existence threshold  $A_{\min}$  of a non-trivial equilibrium (Figure 4.4a) occurs for intermediate interpulse times. Under the assumption that total annual rainfall  $A$  is fixed, longer drought periods between precipitation pulses correspond to higher intensity rainfall events. Resource availability at the time of water uptake

and plant growth is thus higher and exceeds the threshold required for plant growth processes to be activated, which is accounted for in the Holling type III functional response. Conversely, high frequency - low intensity precipitation pulses accumulating to the same amount of total annual rainfall volume are not sufficient to push the water density above this critical value. It is worth emphasising that further increases in the separation of precipitation events (and associated increases in rainfall intensity) to a low frequency - high intensity regime reverses the decrease in  $A_{\min}$  due to the saturating behaviour of the water uptake function.

Further, the property that an increase in the interpulse time  $T$  reduces the size of the parameter region in which onset of patterns occurs is unaffected by the introduction of a nonlinear water uptake term. Similar to the analytically derived exponential decay of the relative size of  $[A_{\min}, A_{\max}]$  for (4.5) with a linear functional response (Corollary 4.4.5), results of our numerical scheme for a Holling type III functional response also indicate an exponential decay of the interval's relative size with increasing interpulse times (Figure 4.4b).

Numerical solutions of the model do, however, become unreliable as the interpulse time  $T$  is increased. For larger  $T$ , the decay-type processes in the interpulse PDEs yield very low plant levels in the troughs of the pattern at the end of the interpulse period. This is a natural source of potential errors. Indeed, Figure 4.4c depicts that numerical solutions of the system for large  $T$  can yield negative plant densities at the end of the interpulse period, highlighting the difficulties encountered in a numerical approach.

To investigate the effects of the strength of the nonlinearity in more detail, we compare results on pattern onset as the strength of the nonlinearity gradually increases away from the linear behaviour considered in (4.5). While it is impossible to revert back to the linear term by parameter changes only, the behaviour for small values of the water density  $w$  can be mimicked by choosing  $p = 1$  and  $C_m = C_h$  sufficiently large. We use this as the reference point to the analytical results obtained in Section 4.4.1 and vary the extent of the nonlinearity in the functional response by fixing  $C_m = 20$  and setting  $C_h = 20 - (20 - \sqrt{2})\xi$  and  $p = 1 + 3\xi$  for  $0 \leq \xi \leq 1$ . For sufficiently low fixed interpulse times  $T$ , an initial increase of  $\xi$  causes an increase of the rainfall level  $A_{\min}$  that is required for a spatially uniform non-trivial equilibrium to exist (Figure 4.4d). As the strength of the nonlinearity increases further,  $A_{\min}$  attains a maximum and then decreases below its level for the model with linear functional water uptake response analysed in Section 4.4.1.

The reasoning for this behaviour stems from the variation in the functional response  $G_{\text{up}}$  under changes of  $\xi$ , which is visualised in Figure 4.4e. For sufficiently low  $T$ , the resource availability at the time of water uptake is also low. Thus a linear functional response yields a higher water consumption than a nonlinear response

with moderate  $\xi$ , but a lower consumption than a nonlinear response with larger  $\xi$ . More precisely, the increase in the exponent  $p$  and the associated concave-up shape of  $G_{\text{up}}$  causes the initial increase in  $A_{\min}$ . A further increase in  $\xi$  decreases the half-saturation parameter  $C_h$  and the range of resource densities affected by the concave-up behaviour decreases in size. This causes the eventual decrease in  $A_{\min}$  as the strength of the nonlinearity is increased further.

For sufficiently large drought lengths  $T$ , the maximum in  $A_{\min}$  occurs at  $\xi = 0$  and thus any  $\xi > 0$  reduces the minimum water requirements of the system. The upper bound  $A_{\max}$  of the parameter region supporting pattern onset mimics the behaviour of  $A_{\min}$ . The size of the parameter region in which pattern onset occurs increases slightly with increasing  $\xi$ , but changes to its size are insignificant compared to changes caused by variations in the interpulse time  $T$ .

#### 4.5.3 Nonlinear PDEs

The original impulsive model (4.5) is based on the assumption that no plant-water interactions take place during drought periods. The interpulse equations thus form a system of linear and decoupled PDEs that describe exponential decay of both plant and water densities between precipitation pulses. We relax this assumption by extending the occurrence of biomass growth into the interpulse phase. This changes the PDE system to

$$\begin{aligned}\frac{\partial u_n}{\partial t} &= -Bu_n + C \left( \frac{u_n}{1+u_n} \right)^2 w_n, \\ \frac{\partial w_n}{\partial t} &= -w_n - C \left( \frac{u_n}{1+u_n} \right)^2 w_n + d \frac{\partial^2 w_n}{\partial x^2},\end{aligned}$$

where the nondimensional constant  $C$  accounts for the rate of water uptake. The pulse equations (4.5c) and (4.5d) remain unchanged, i.e. there is still a pulse of plant growth synchronised with a precipitation event.

While a typical estimate is  $C = 10$  [75], we use our numerical scheme to investigate how a gradual increase from  $C = 0$  (which corresponds to the model studied analytically in Section 4.4) affects the pattern onset observed in the system. An increase in the plants' growth rate during drought periods causes a decrease in the existence threshold  $A_{\min}$  of a spatially uniform non-desert equilibrium and the precipitation level  $A_{\max}$  at which pattern onset occurs (Figure 4.5b). This decrease is caused by a reduction in total resource loss through evaporation and the associated increase in water availability to plants. In the original model (4.5) ( $C = 0$ ), water that is not consumed by plants during the rainfall pulse undergoes exponential decay due to evaporation during the interpulse period and is lost from the system. If

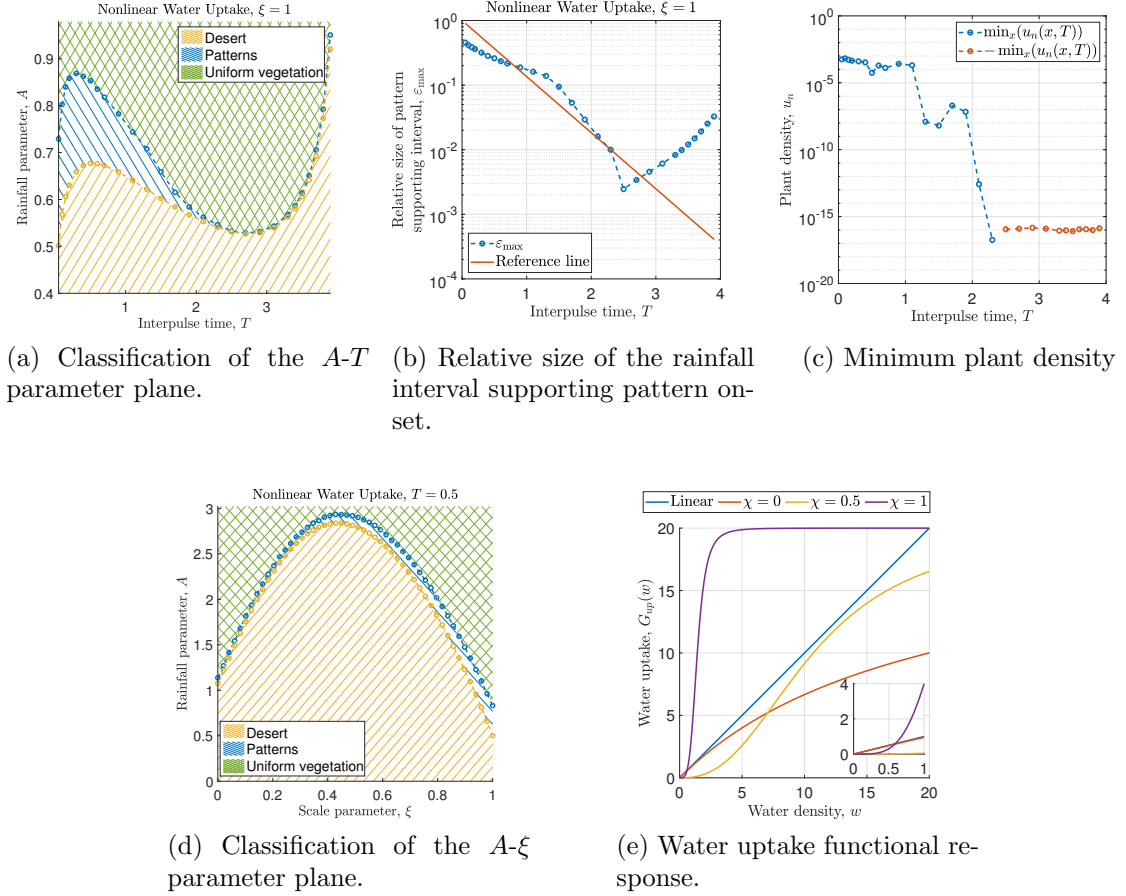
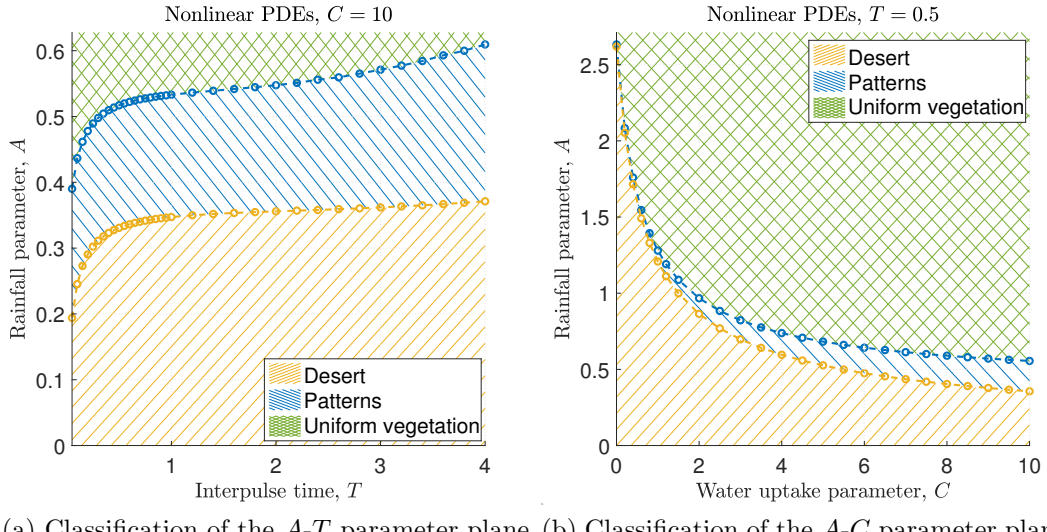


Figure 4.4: Classification plots for a nonlinear functional response in the water uptake function. The classifications (a) and (d) into states of desert, onset of spatial patterns and uniform vegetation are based on the numerical scheme described in Section 4.5.1. The transition threshold  $A_{\max}$  is determined up to an interval of size  $10^{-5}$ , the level of  $A_{\min}$  up to an interval of size  $10^{-8}$ . The relative size of  $[A_{\min}, A_{\max}]$  corresponding to the classification in (a) is shown in (b), where the reference line is of slope  $\exp(-2T)$ . The parameter values used in both simulations are  $B = 0.45$  and  $d = 500$ . The water uptake function  $G_{up}(w)$  is shown in (e) for several values of  $\xi$ , with its behaviour close to the origin shown in the inset. The minimum plant density before a rainfall pulse  $\min_{x \in [-x_{\max}, x_{\max}]} \{u_n(x, T)\}$  of a stable pattern is shown in (c), where the blue and red markers indicate positive and negative values of  $u_n$ , respectively. This visualises the numerical issues encountered in simulations for longer interpulse times  $T$ .



(a) Classification of the  $A$ - $T$  parameter plane. (b) Classification of the  $A$ - $C$  parameter plane.

Figure 4.5: Classification plots for the inclusion of plant growth in the interpulse PDEs. The classifications into states of desert, onset of spatial patterns and uniform vegetation is based on the numerical scheme described in Section 4.5.1. The transition threshold  $A_{\max}$  is determined up to an interval of size  $10^{-5}$ , the level of  $A_{\min}$  up to an interval of size  $10^{-8}$ . The parameter values used in both simulations are  $B = 0.45$  and  $d = 500$ .

$C \neq 0$ , however, water that enters the drought phase not only evaporates but also continues to be converted into plant biomass, which causes a reduction in evaporation losses.

The second main conclusion arising from the inclusion of a nonlinear coupling of the interpulse PDEs is the conservation of a large parameter region in which pattern onset occurs for large  $T$  (Figure 4.5a), instead of an exponential decay of its size with increasing  $T$ . The existence of such a region is due to the inclusion of a pattern-inducing feedback in the interpulse PDEs. More water is consumed in regions of high biomass density, which causes the homogenising effect of water diffusion to redistribute more water towards these regions yielding further plant growth. If water uptake between pulses is weak (small  $C$ ), or as in the original model nonexistent ( $C = 0$ ), the system's only pattern-forming feedback loop consists of the nonlinearity in the plant growth term in the update equations in combination with the homogenising property of water diffusion in the interpulse PDEs. The latter loses its impact as  $T$  is increased, as evaporation effects become dominant and cause a decrease in water availability at the end of the interpulse phase. The water density at the growth pulse therefore only depends on the intensity of the rain event, but is independent of the diffusion process that occurs before the rainfall pulse. This weakens the strength of the pattern-inducing feedback loop and causes the decrease in the size of the parameter region in which pattern onset occurs.

#### 4.5.4 Kernel functions

In the linear stability analysis in Section 4.4.1, we set the plant dispersal kernel to the Laplace kernel (4.3). Seed dispersal behaviour, however, depends both on species and environmental conditions [25]. Similar to the work on a previous model [61] (Chapter 2), we use our numerical scheme to investigate effects caused by setting the dispersal kernel to the Gaussian

$$\phi(x) = \frac{a_g}{\sqrt{\pi}} e^{-a_g^2 x^2}, \quad a > 0, x \in \mathbb{R}, \quad (4.23)$$

and the power law distribution

$$\phi(x) = \frac{(b-1)a_p}{2(1+a_p|x|)^b}, \quad a > 0, b > 3, x \in \mathbb{R}. \quad (4.24)$$

We base our comparison on the kernels' standard deviations, which are given by  $\sigma(a) = \sqrt{2}/a$  for the Laplacian kernel (4.3),  $\sigma(a_g) = 1/(\sqrt{2}a_g)$  for the Gaussian kernel (4.23) and  $\sigma(a_p) = \sqrt{2}/(\sqrt{b^2 - 5b + 6}a_p)$  for the power law kernel (4.24) provided  $b > 3$ . It is perfectly reasonable to perform simulations with kernels of infinite standard deviation (e.g.  $b < 3$  in the power law kernel) but in the interest of comparing results for the kernels based on their standard deviation we consider only  $b = 3.1$  and  $b = 4$ .

In the simulations we are interested in both the effects of changes to the shape of the dispersal kernel and the effects caused by a variation in the temporal intermittency of precipitation. As shown in Figure 4.6b, the latter bears much more influence on the rainfall threshold  $A_{\max}$  than the choice of plant dispersal kernel. Indeed, the results obtained for all kernel functions follow the narrow band of exponentially decaying size in the  $T$ - $A$  parameter region in which pattern existence has been shown for the Laplace kernel in Section 4.4.1 and in particular in Figure 4.2a.

While the effects of the kernel shape are negligible compared to changes of the interpulse time  $T$ , their influence on the system can still be studied if  $T$  is fixed. Instead of varying  $T$ , we opt to investigate how the threshold  $A_{\max}$ , at which pattern onset occurs, changes under variations of the water diffusion coefficient  $d$ . This allows us to draw a connection to the results of the linear stability analysis visualised in Figure 4.1. Our numerical scheme shows that all kernel functions considered in the simulations qualitatively follow the same behaviour, which agrees with the analytically deduced result for the Laplace kernel in Section 4.4.1. For sufficiently low levels of rainfall, the diffusion coefficient needs to exceed a threshold to give rise to an instability resulting in the onset of spatial patterns. There does, however, exist an upper bound (not shown in Figure 4.6a) on the rainfall parameter for each kernel function above which pattern onset from a perturbation of the steady state

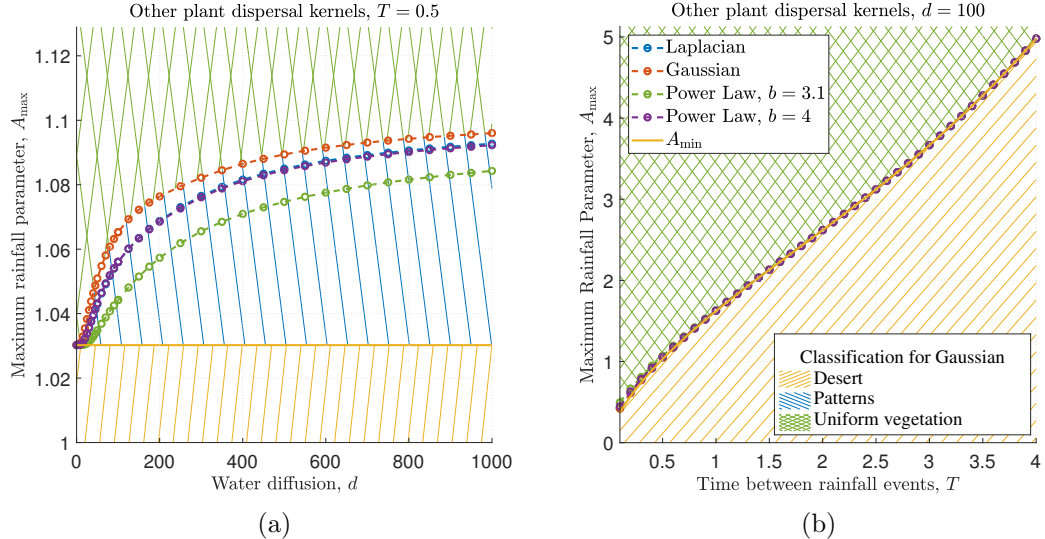


Figure 4.6: Changes to  $A_{\max}$  under variation of water diffusion and the time between rain pulses. This figure visualises changes to the critical rainfall parameter  $A_{\max}$  under changes of the water diffusion rate  $d$  ((a)) and the interpulse time  $T$  ((b)). The rainfall threshold  $A_{\max}$  is determined up to an interval of length  $10^{-4}$  for  $d = \{0, 5, \dots, 50, 60 \dots 100, 125, \dots, 200, 250, \dots, 1000\}$  and  $T = \{0.1, 0.2, \dots, 4\}$ , respectively. Plant mortality is set to  $B = 0.45$ . The legend applies to both parts of the figure.

is impossible. Due to the nondimensionalisation of the model an increase in the diffusion coefficient  $d$  corresponds to a decrease in the width of the dispersal kernels. Thus, for a fixed kernel function an increase in kernel width inhibits the onset of patterns. Note, however, that information on the kernels' standard deviation, which we use as a measurement of kernel width, is insufficient to make comparisons between results for different kernel functions. Conditions for pattern onset also depend on the dispersal kernel's type of decay at infinity; for example  $A_{\max}$  for the Laplace kernel and the power law kernel with  $b = 4$  coincide in Figure 4.6a, even though their standard deviations are  $\sigma_L = \sqrt{2}$  and  $\sigma_P = 1$ , respectively.

#### 4.5.5 Slope

Finally, we lift the restriction of the flat spatial domain for which the linear stability analysis of (4.5) was performed in Section 4.4. Originally, the Klausmeier model was proposed to describe vegetation bands on sloped terrain and a lot of previous work has focussed on this scenario (e.g. [61, 99, 191]). A numerical investigation into the existence of spatial patterns of (4.5) on a sloped spatial domain shows that the threshold  $A_{\max}$  at which a transition between uniform and patterned vegetation occurs, increases with increasing slope  $\nu$  (Figure 4.7c). The lower bound  $A_{\min}$  of the parameter region supporting the onset of spatial patterns from spatially nonuniform

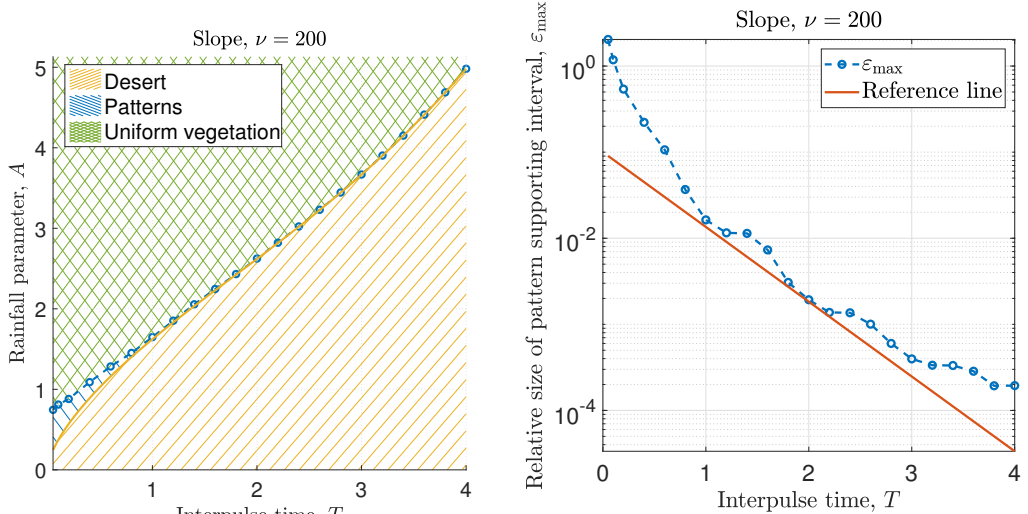
perturbations of the equilibrium, is a non-spatial property and thus independent of the slope parameter  $\nu$ . Thus the size of  $[A_{\min}, A_{\max}]$  increases with increasing  $\nu$ . Ecologically, this stems from an increase in the strength of the pattern-forming mechanism. On steeper slopes water flows downhill faster and thus increases the competitive advantage of existing biomass patches.

This increase in the size of  $[A_{\min}, A_{\max}]$  is, however, negligible compared to the decay of the interval's size for increasing interpulse time  $T$  (Figures 4.7a and 4.7b). Our results indicate that the interval's size decays exponentially, similar to the analytically obtained result (Corollary 4.4.5) for the model on flat ground in the limit  $d \rightarrow \infty$ . We thus conclude that the simplified model ( $\nu = 0$ ) qualitatively yields the same results on the onset of patterns under variations in the length of the drought period  $T$ .

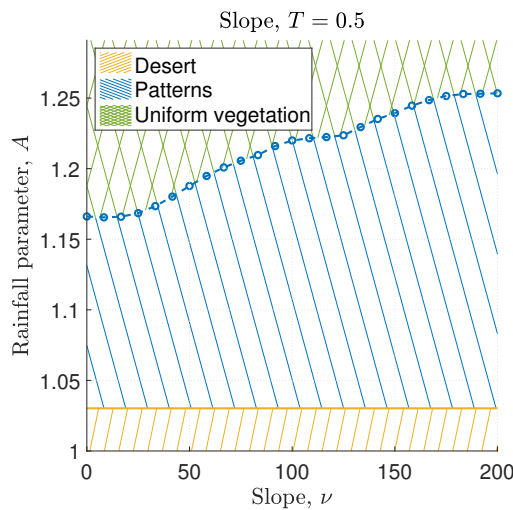
## 4.6 Discussion

In this chapter, we consider a new impulsive-type model to investigate the effects of rainfall intermittency on the onset of vegetation patterns in semi-arid environments. Most significantly, our results suggest that the decay-type behaviour which dominates during long drought periods inhibits the onset of spatial patterns and that ecosystems benefit from precipitation intermittency if plant species are unable to efficiently use low soil moisture levels.

The inhibition of patterns by low frequency rain events is quantified by the small size of the interval of rainfall levels in which pattern onset occurs. Therefore, plants are able to form a uniform vegetation cover for rainfall levels very close to the minimum required for the corresponding spatially uniform equilibrium to exist. This pattern-inhibitory effect in the impulsive model (see Proposition 4.4.5 and Figures 4.2 and 4.6b) can be explained by the weakening effect of the temporal separation of rainfall pulses on the plant growth-water redistribution feedback which is the main contributor in the formation of patterns [107, 166]. This positive feedback loop consists of two processes; the increased water utilisation in regions of high biomass and the redistribution of water. In (4.5) these processes occur in different stages. The soil modification by plants affects water consumption and plant growth which only occur in the update equations associated with a rainfall pulse, while water diffusion is accounted for in the interpulse PDE system. Therefore, if plants are in a patterned state, the water density immediately after a rainfall pulse is in antiphase to the plant density (i.e. high water density in regions of low biomass and vice versa). The homogenising property of diffusion thus redistributes water from patches of low biomass to regions where plant density is high. If, however, the separation of precipitation pulses is too long, this homogenising effect loses its



(a) Classification of the  $A$ - $T$  parameter plane. (b) Relative size of the rainfall interval supporting pattern onset.



(c) Classification of the  $A$ - $\nu$  parameter plane.

Figure 4.7: Classification plots for the model on a slope. The classifications into states of desert, onset of spatial patterns and uniform vegetation are based on the numerical scheme described in Section 4.5.1. The transition threshold  $A_{\max}$  is determined up to an interval of size  $10^{-8}$ , the level of  $A_{\min}$  is given by (4.8). The relative size of  $[A_{\min}, A_{\max}]$  is shown in (b), where the reference line has slope  $\exp(-2T)$ . The parameter values used in both simulations are  $B = 0.45$  and  $d = 500$ .

impact as water evaporation becomes the dominant process. In the model extension which assumes that plant growth occurs in both the pulse stage and during the interpulse period (Section 4.5.3), the temporal separation of rainfall events does not weaken the pattern-inducing feedback. The closure of the feedback loop in the interpulse PDEs allows for more water transported to regions of high biomass during drought periods to be utilised and thus supports the pattern-forming mechanism.

For a fixed interpulse time  $T$ , the reduction in water evaporation associated with this increase in water to biomass conversion causes a reduction in the minimum amount of precipitation required for a spatially uniform equilibrium to exist. We use this minimum on the rainfall parameter ( $A_{\min}$ ) as a proxy for the minimum water requirements of the ecosystem, but emphasise the fact that spatially non-uniform stable states with non-zero plant densities are likely to exist for lower precipitation levels and no information on the resilience of the ecosystem can be extracted from the analysis presented in this chapter. For both the extension with nonlinear interpulse PDEs and the original model (4.5), the threshold  $A_{\min}$  increases with the drought period length  $T$ , which indicates that an increase in the time between rainfall events has a detrimental effect on the ecosystem. Even though this does not agree with the majority of reported field observations [82, 183], there exists evidence of this inhibitory effect for some dryland species, with an increase in seeds germination rates, a decrease in emergence rates and an increase in seedling mortalities under longer periods of droughts [109, 113]. This suggests that an ecosystem's response to temporal variability in precipitation is highly species-dependent and it is important to understand a species' response to oscillations in soil moisture to model its dynamics. Indeed, we have established that changes to the plants' water uptake functional response to the water density (Section 4.5.2) can reverse the increasing behaviour of the minimum water requirement proxy  $A_{\min}$  observed in the original model in which the functional response is linear (Figure 4.2a). If species in an ecosystem remain dormant under low soil moisture levels caused by a high frequency - low intensity rainfall regime, then rainfall intermittency and the associated temporal increases in soil moisture can have a positive impact on the ecosystem [82, 183]. Mathematically, we used a Holling type III functional response to model this dormant behaviour under low soil moisture levels. If the concave-up shape of this species-dependent functional response is sufficiently strong for low water densities, then  $A_{\min}$  attains a minimum for an intermediate interpulse time  $T$  because water uptake is maximised under such conditions. This is in agreement with results obtained for the Gilad [74] model [100].

The dominant role of precipitation intermittency on the onset of patterns also manifests itself in the fact that, unlike in the Klausmeier models, diffusion alone is insufficient to cause pattern onset in the impulsive model. The onset of spatial pat-

terns still requires the diffusion coefficient to exceed a threshold (Proposition 4.4.6) but in stark contrast to the Klausmeier models in which a sufficiently large level of diffusion can cause an instability for an arbitrarily large level of rainfall, the effects of diffusion are limited to a small interval of the rainfall parameter (Proposition 4.4.4), whose size decreases exponentially as precipitation pulses become more infrequent (Corollary 4.4.5). This deviation from the classical case of a diffusion-driven instability is due to the previously discussed temporal separation of the components of the pattern-inducing feedback that renders diffusion effects insignificant under long drought spells. This property is specific to the system considered in this study and no generalisations can be made. Indeed, diffusion-driven instabilities have been shown to occur in other impulsive models [238].

A second key aspect of this study is the effects caused by changes to the width and shape of the plant dispersal kernel. Contrary to the beneficial effect associated with the inhibition of pattern onset due to wide plant dispersal kernels shown by the model in this chapter (Figure 4.6a), plants in semi-arid regions are observed to establish narrow dispersal kernels [66]. This is, however, only a secondary effect caused by other adaptations such as protection from seed predators, that are not accounted for in these models but nevertheless affect the vegetation's evolution in arid regions [66]. The quantitatively small changes to the rainfall threshold  $A_{\max}$  in the impulsive model are caused by the fact that in the impulsive model only the newly added biomass is dispersed, while in the other models the whole plant density undergoes dispersal. Combined with the claim that plants compensate for the negative effect of a narrow seed dispersal kernel by changes of traits not included in this model, this suggests the combination of the weak response of the impulsive model to changes in the width of the dispersal kernel and the stronger effect of rainfall intermittency provides a more realistic framework than a previous model in which the seed dispersal distance played an important role in the absence of any pulse-type events [61] (Chapter 2).

To facilitate the mathematical analysis presented in this chapter we have opted for a fully deterministic modelling of precipitation. The assumption that rainfall events occur periodically in time and are all of the same intensity is, however, an inaccurate description of the inherently stochastic nature of this key process. A more realistic description of such precipitation events can be achieved through a Poisson process with exponentially distributed rainfall intensities [167]. The model framework presented in this model is, however, insufficient to consider any stochasticity in the rainfall regime. Neither the original model (4.5) nor any of its extensions presented in Section 4.5 include mechanisms that allow plants to recover from a very low density. Thus, the eventual occurrence of a long drought period (possibly combined with low intensity pulses) under a stochastic precipitation regime inevitably

causes the extinction of plants in the long term. In reality, plants have developed mechanisms such as seed dormancy that allow recovery from low biomass densities [109]. Their inclusion in a mathematical model is required to better understand an ecosystem's response to stochasticity in environmental conditions. Nevertheless, it is possible to relate the results of the deterministic model presented in this study to a stochastic setting. Similar to a previous study of effects of temporal variations of rainfall pulses on dryland ecosystems, the constants involved in the deterministic modelling of precipitation can be seen as the expected values that arise from the underlying stochastic processes [198]. If this assumption is applied then our results on thresholds such as  $A_{\max}$  present an approximation to the expectations of the respective quantities when any higher order moments (variance, etc.) of the random variables associated with the description of precipitation are neglected [198].

While the model extensions (and possibly combinations thereof) presented in Section 4.5 provide a more realistic description of the ecosystem dynamics under a pulse type precipitation regime, the analytical study of the simpler model (4.5) in Section 4.4 is an important tool to gain a better understanding of vegetation patterns in semi-arid environments. Numerical approaches tend to become unreliable as the length of the drought periods increases because decay-type processes of long dry spells reduce the plant density in troughs of the spatial pattern to very small values. This makes numerical integration techniques error-prone and emphasises the importance of analytical pathways into the problem (Figure 4.4c).

The results presented in this chapter are based on our analysis of a theoretical model and a comparison with empirical data would be desirable to test these hypotheses. Daily rainfall data is available from the 1980s to the present (see e.g. [118] for data from Africa), and data with a coarser temporal scale dates back to the 1940s [52]. However, obtaining high-quality data for vegetation in dryland ecosystems is notoriously difficult due to the large spatial and temporal scales of the ecosystem dynamics. Some limited data obtained from satellite images exists (e.g. [48]), for example on wavelength which can be used as a proxy for biomass, but a comparison with any model predictions would require a better measure of key ecological properties, as well as a long time series of data points.

In this study, we have analysed the effects of rainfall intermittency on pattern onset in dryland vegetation in one space dimension only. On flat ground in particular, the consideration of a two-dimensional domain would be a natural extension. This could provide more insight into the patterns' properties such as its type (gap pattern, labyrinth pattern, stripes or spots) under changes to the precipitation regime [129]. The analysis of the impulsive model on a two-dimensional domain would be significantly more challenging, but methods for studying pattern formation in PDEs on such domains exist (see, for example, [196] for an analysis of the Klausmeier

model), which hold the potential to be adapted to the framework of an impulsive model.

A further natural area of potential future work could involve an accurate description of overland water flow during a rainfall event. For sloped terrain such a description has been provided and applied to a mathematical model describing the evolution of vegetation patterns by Siteur et al [198]. Their argument is based on water instantaneously flowing downhill and infiltrating the soil in areas of high biomass and can thus not be applied to a flat spatial domain. Indeed, overland flow of water during intense rainfall events on semi-arid flat plains is the subject of ongoing research (e.g. [168, 211, 235]). A detailed description of the overland water flow and infiltration into the soil that occurs before water is consumed by plants relies on a clear distinction between the surface water density and the soil moisture. Such a separation is used in alternative model frameworks [74, 86, 163], which could be utilised to include the description of water redistribution during rainfall events under a pulse-type precipitation regime.

The model introduced in this chapter is based on the Klausmeier model, which is a model that is deliberately kept simple to facilitate a mathematical analysis of it. A number of more complex models exist (see [21, 124, 247] for reviews) that study different aspects of patterned vegetation in more detail by, for example, including two coexisting plant species [16, 63, 76, 157], describing water uptake as a nonlocal process [74, 75] or considering effects of nonlocal grazing [195, 197]. For some of these models numerical studies have investigated the effects of temporal rainfall variability [80, 100, 198] and an analytical analysis of those models similar to the work done in this study could provide further insight how pulse-type phenomena affect patterns in semi-arid environments.

## Chapter 5

# Metastability as a coexistence mechanism in a model for dryland vegetation patterns

The contents of this chapter are published in [63].

### 5.1 Author contribution

The authors of the published paper [63] are Lukas Eigentler and Jonathan A Sherratt. Lukas Eigentler conceptualised the research, formulated the mathematical model, performed both the analytical and numerical analyses of the model, wrote the paper draft and reviewed and edited the manuscript. Jonathan A Sherratt conceptualised the research, reviewed and edited the manuscript and provided supervision.

### Abstract

Vegetation patterns are a ubiquitous feature of water-deprived ecosystems. Despite the competition for the same limiting resource, coexistence of several plant species is commonly observed. We propose a two-species reaction-diffusion model based on the single-species Klausmeier model, to analytically investigate the existence of states in which both species coexist. Ecologically, the study finds that coexistence is supported if there is a small difference in the plant species' average fitness, measured by the ratio of a species' capabilities to convert water into new biomass to its mortality rate. Mathematically, coexistence is not a stable solution of the system, but both spatially uniform and patterned coexistence states occur as metastable states. In this context, a metastable solution in which both species coexist corresponds to a long transient (exceeding  $10^3$  years in dimensional parameters) to a stable one-species state. This behaviour is characterised by the small size of a positive eigenvalue which has the same order of magnitude as the average fitness difference between the two species. Two mechanisms causing the occurrence of metastable solutions are established: a spatially uniform unstable equilibrium and a stable one-species pattern which is unstable to the introduction of a competitor. We further discuss effects of asymmetric interspecific competition (e.g. shading) on the metastability property.

## 5.2 Introduction

Patterns of vegetation in semi-arid climate zones are a prime example of a self-organisation principle in ecology [47, 222]. One of the main mechanisms that creates such a mosaic of biomass and bare soil is a modification of soil properties by plants that induces a water redistribution feedback loop [129–131, 166]. On bare ground only small amounts of water are able to infiltrate into the soil and water run-off occurs, while in regions covered by biomass the soil’s water infiltration capacity is increased. Dense plant patches therefore act as sinks and deplete soil water in regions of bare ground [65, 209]. This redistribution of the limiting resource drives further growth in vegetation patches and thus closes the feedback loop.

Drylands account for approximately 41% of the Earth’s land mass and are home to a similar proportion (38%) of the world’s human population. The sizes of arid and semi-arid regions that suffer from land degradation are expected to increase over the coming decades due to climate change [162]. Vegetation patterns are a characteristic feature of such fragile ecosystems. Patterns have been detected in semi-desert regions in the African Sahel [48, 141, 208, 239, 241], Somalia [79, 83], Australia [55, 84, 214], Israel [24, 182] and Mexico and the US [38, 48, 136, 137, 152, 153]. Changes to characteristic features of vegetation patterns in these regions such as the pattern wavelength, the area fraction covered by biomass, or the recovery time from perturbations can act as early indicators of desertification as they provide a useful tool in predicting further changes to ecosystems [39, 45, 78, 96, 164, 170, 246]. This is an issue of considerable socio-economic importance since agriculture is a major contributor to the economy in many drylands [218]. For example, in sub-Saharan Africa livestock frequently graze on spatially patterned vegetation. Thus changes in vegetation levels have a major effect on the livestock sector, which makes a very significant contribution to GDP, e.g. 20% in Chad, 15% in Mali, 12% in Niger and 7.5% in Burkina Faso [51, 219], with involvement of high proportions of the population (e.g. 40% in Chad [51]).

Due to the temporal and spatial scales involved in the evolution of vegetation patterns, these ecosystems cannot be recreated in a laboratory setting. To gain a better understanding of the pattern dynamics a number of mathematical models have been proposed (see [21, 247] for reviews). In particular, modelling efforts based on partial differential equations, most notably by Gilad et al. [74, 75] and HilleRisLambers et al. [86, 163], provide a rich framework for mathematical analysis. One model that stands out due to its simplicity is the Klausmeier model [99], which provides a deliberately basic description of the plant-water dynamics in semi-arid environments. The highly accessible nature of the model enables a detailed model analysis (e.g. [20, 34, 61, 184–186, 190–192, 194, 199, 221]). Recent advances in

remote sensing technology using satellite data provide a promising tool to test model predictions on pattern resilience [10, 72].

Most models in this context only consider a single plant species or combine several species into one single variable. However, vegetation patches often consist of a mix of herbaceous and woody species, where the latter can usually be found in the centre of a patch, surrounded by the former [41, 179]. Previous simulation-based studies of dryland ecosystem models have indeed been able to reproduce patterns in which two species coexist by considering a variety of different mechanisms and feedbacks that enable diversity in ecosystems [16, 27, 76, 145, 220]. One such facilitative mechanism occurs in a system of two species in which only one plant type induces a pattern forming feedback. If, additionally, the non-pattern forming species is superior in its water uptake and dispersal capabilities, then the pattern-forming species can act as an ecosystem engineer to facilitate coexistence of both species in patterned form [16, 145]. Even if patterns in which two species coexist are not observed as long-term solutions of a system, they can feature in a transition between two stable states. Gilad et al. [76] briefly report on the observation of coexistence patterns as a slow (several hundred years) transient during which patterns form due to facilitation between two species before eventually one of the species becomes extinct as competitive feedbacks take over. A different mechanism that enables coexistence of two species in both uniform and spatially patterned settings is adaptation to different ecological niches, such as soil moisture [27, 221].

In-phase spatial patterns are not the only phenomenon that is studied in the context of species coexistence. The existence of a multitude of localised patterns of one species in an otherwise uniform cover of a second species (homoclinic snaking) has also been observed as a possible form of coexistence in a mathematical model [103]. The solution arises from a model that assumes a trade-off between root and shoot growth causing a balance between the competition for water and for light that supports coexistence. Other models are not able to make any statement on the coexistence of species, but yield valuable information on facilitation and competition between the plant types based on differences in traits such as their dispersal behaviour [157].

The savanna biome has also been studied by various non-spatial models that describe the dynamics of the relative abundances of grass, trees and water. While such models are unable to make any statements on the formation of spatial patterns, they still provide valuable insights into coexistence-preserving effects of processes such as precipitation intermittency [43], facilitation by grasses towards trees [204] or fire disturbances [15, 175].

Previous model analyses on species coexistence in semi-arid landscapes have mainly focussed on feedback loops induced through differences in the plant species'

traits and their effects on multi-species plant communities. We are not aware of any studies that investigate effects of the differences in basic properties such as plant mortality or plant growth rate on semi-arid vegetation patterns. In this chapter we aim to analytically address the question how the difference between two plant types can give rise to a multispecies metastable vegetation pattern (a unstable pattern whose instability is caused by a very small unstable eigenvalue [154]) and how the pattern's properties are affected by changes to the difference between the species.

To do this we introduce a multi-species model based on the Klausmeier model in Section 5.3. Numerical simulations of the model presented in Section 5.4 suggest two different origins of metastable coexistence patterns. These two pathways into the problem are closely examined through a linear stability analysis in Sections 5.5 and 5.6. Finally, we discuss our results in Section 5.7.

### 5.3 Model

In this section we lay out the framework used in this chapter to analyse the coexistence of grass and trees in dryland ecosystems. We propose a model based on the extended Klausmeier model [99], which in dimensional form is

$$\frac{\partial u}{\partial t} = \underbrace{c_1 c_2 u^2 w}_{\text{plant growth}} - \underbrace{c_3 u}_{\text{plant mortality}} + \underbrace{c_4 \frac{\partial^2 u}{\partial x^2}}_{\text{plant dispersal}}, \quad (5.1a)$$

$$\frac{\partial w}{\partial t} = \underbrace{c_5}_{\text{rainfall}} - \underbrace{c_6 w}_{\text{evaporation}} - \underbrace{c_2 u^2 w}_{\text{water uptake by plants}} + \underbrace{c_7 \frac{\partial w}{\partial x}}_{\text{water advection}} + \underbrace{c_8 \frac{\partial^2 w}{\partial x^2}}_{\text{water diffusion}}, \quad (5.1b)$$

where  $u(x, t)$  is the weight of plants per unit area and  $w(x, t)$  is the mass of water per unit area in the one-dimensional space domain  $x \in \mathbb{R}$  at time  $t > 0$ . The water supply (precipitation) of the system is assumed to be constant at rate  $c_5$ , while evaporation and plant loss effects are assumed to be proportional to the respective densities at rates  $c_6$  and  $c_3$ , respectively. The nonlinearity in the terms describing water uptake and biomass growth arises due to a soil modification by plants. The term is the product of the density of the consumer  $u$  and of the available resource  $c_2 uw$ , which corresponds to water being able to infiltrate into the soil. The dependence on the plant density  $u$  in the latter term occurs due to a positive correlation between the plant density and the soil surface's permeability [38, 165, 222]. Plant growth is assumed to be proportional to water uptake [167, 171] and water to biomass conversion takes place at rate  $c_1$ . In its original setting, the Klausmeier model is formulated to describe the dynamics on sloped terrain on which water flow downhill is modelled by advection at rate  $c_7$ . An extension includes diffusion of water

at rate  $c_8$  to account for water redistribution on flat ground and is well established now (e.g. [95, 199, 225, 247]). Plant dispersal is also modelled by a diffusion term (with diffusion rate  $c_4$ ).

Both on flat ground and on sloped terrain (5.1) captures the formation of patterns for sufficiently low levels of precipitation and their properties have been studied extensively [99, 184–186, 190–192, 194, 199]. In (5.1) the plant density  $u$  either describes one single species or accounts for the totality of all plant types in the ecosystem. While an ecosystem rarely consists of only one single species, estimation of species-dependent parameters such as the plant mortality rate  $c_3$  may be impractical if  $u$  is comprised of many different species for which parameter estimates differ significantly (see for example estimates for tree and grass species by Klausmeier [99]).

An extension of (5.1) that accounts for the differences between plant species in the same ecosystem can be obtained by separating the plant density  $u$  into  $n \in \mathbb{N}$  different species  $u_i$ ,  $i = 1, \dots, n$  that satisfy (5.1) with an appropriate set of parameters in the absence of all other species. The model arising from this assumption is

$$\frac{\partial u_i}{\partial t} = \underbrace{k_1^{(i)} w u_i}_{\text{plant growth}} \left( \sum_{j=1}^n k_2^{(j)} u_j \right) - \underbrace{k_3^{(i)} u_i}_{\text{plant mortality}} + \underbrace{k_5^{(i)} \frac{\partial^2 u_i}{\partial x^2}}_{\text{plant dispersal}}, \quad (5.2a)$$

$$\frac{\partial w}{\partial t} = \underbrace{k_6}_{\text{rainfall}} - \underbrace{k_7 w}_{\text{evaporation}} - w \underbrace{\left( \sum_{j=1}^n u_j \right) \left( \sum_{j=1}^n k_2^{(j)} u_j \right)}_{\text{water uptake by plants}} + \underbrace{k_8 \frac{\partial w}{\partial x}}_{\text{water advection}} + \underbrace{k_9 \frac{\partial^2 w}{\partial x^2}}_{\text{water diffusion}}. \quad (5.2b)$$

for  $i = 1, \dots, n$ . In this multi-species model, the term describing water uptake by plants is, as in (5.1), the product of the water density  $w$ , the total plant density  $\sum_{j=1}^n u_j$  and the soil's infiltration capacity  $\sum_{j=1}^n k_2^{(j)} u_j$ . The species-dependent constants  $k_2^{(i)}$  account for the plant types' different contributions to the soil's properties. The summands in  $\sum_{j=1}^n u_j$  correspond to the consumption of water by each single species and are therefore not replicated in the term describing plant growth. Thus, the addition of new biomass of species  $u_i$  with water to biomass conversion rate  $k_1^{(i)}$  only depends on the water density, the soil's infiltration capacity and the density of species  $u_i$  itself. The remaining assumptions are identical to those taken in the formulation of (5.1), i.e.  $k_3^{(i)}$  and  $k_5^{(i)}$  denote the mortality and diffusion rates of species  $u_i$ , respectively;  $k_6$  is the constant amount of rainfall which adds water to the system; and  $k_7$ ,  $k_8$ , and  $k_9$  are the evaporation, advection and diffusion rates of water, respectively.

In (5.2) no direct interspecific interaction takes place. Instead plant species only compete indirectly through depletion of the limiting resource - water. Models of this type, in which species compete for the same limiting resource without any direct competition between the different types do not provide a framework able to describe coexistence as the species that can tolerate the lowest level of the limiting resource outcompetes all competitors [212]. Thus, a description of an ecosystem in which plant species coexist needs to take interspecific dynamics, such as shading, into account.

For simplicity we restrict the model to a system on flat ground of two plant species  $u_1$  and  $u_2$  only, in which one species inhibits the other by increasing its competitor's mortality rate but its own mortality rate remains unaffected by the presence of the other species. An alternative approach to model direct interspecific competition would be a reduction of a species' biomass growth rate [103]. A classic example of such an one-sided inhibitory direct interaction are two species, such as a herbaceous and a woody species, where the latter grows much taller than the former and thus imposes a shading effect on its competitor. Shading may also have a facilitative effect on plants and induce a positive feedback loop due to a reduction in evaporation [16, 76]. In contrast to a one-sided inhibitory shading effect, shading-induced evaporation reduction affects both species as beneficial effects occur indirectly through a variation in resource availability. Thus, the nonlinearity in the plant densities of the water consumption and plant growth terms can account for such a beneficial effect as it collectively describes all positive feedback loops increasing the growth of biomass.

Adding an inhibitory shading term to (5.2) with  $n = 2$ , we propose the model studied in this chapter, which is

$$\frac{\partial u_1}{\partial t} = \underbrace{k_1^{(1)} w u_1}_{\text{plant growth}} \left( k_2^{(1)} u_1 + k_2^{(2)} u_2 \right) - \underbrace{k_3^{(1)} u_1}_{\text{plant mortality}} - \underbrace{k_4 u_1 u_2}_{\text{interspecific competition}} + \underbrace{k_5^{(1)} \frac{\partial^2 u_1}{\partial x^2}}_{\text{plant dispersal}}, \quad (5.3a)$$

$$\frac{\partial u_2}{\partial t} = \underbrace{k_1^{(2)} w u_2}_{\text{plant growth}} \left( k_2^{(1)} u_1 + k_2^{(2)} u_2 \right) - \underbrace{k_3^{(2)} u_2}_{\text{plant mortality}} + \underbrace{k_5^{(2)} \frac{\partial^2 u_2}{\partial x^2}}_{\text{plant dispersal}}, \quad (5.3b)$$

$$\frac{\partial w}{\partial t} = \underbrace{k_6}_{\text{rainfall}} - \underbrace{k_7 w}_{\text{evaporation}} - \underbrace{w (u_1 + u_2) \left( k_2^{(1)} u_1 + k_2^{(2)} u_2 \right)}_{\text{water uptake by plants}} + \underbrace{k_9 \frac{\partial^2 w}{\partial x^2}}_{\text{water diffusion}}. \quad (5.3c)$$

The shading effect causes species  $u_2$  to impose an additional mortality effect on  $u_1$  that is dependent on the density  $u_2$ , while  $u_1$  does not have such an effect on  $u_2$ . The results presented in this chapter are robust to changes in the functional

response of this shading effect. Results for shading effects with a Holling type II and Holling type III functional response show no qualitative difference to the algebraically simpler term in (5.3). Table 5.1 provides an overview of parameter estimates used in the model. As indicated in the table, we were able to obtain estimates for parameters from previous models on dryland vegetation, except for the rate of the direct interspecific interaction  $k_4$ . However, our model analysis in Sections 5.5 and 5.6 suggests a suitable range for the shading parameter that yields biologically relevant results and we briefly discuss effects caused by deviations from this range.

A suitable nondimensionalisation for the model is

$$u_1 = \left( \frac{k_7}{k_2^{(1)}} \right)^{\frac{1}{2}} \tilde{u}_1, \quad u_2 = \left( \frac{k_7}{k_2^{(1)}} \right)^{\frac{1}{2}} \tilde{u}_2, \quad w = \frac{k_7^{\frac{1}{2}}}{k_1^{(1)} \left( k_2^{(1)} \right)^{\frac{1}{2}}} \tilde{w},$$

$$x = \left( \frac{k_5^{(1)}}{k_7} \right)^{\frac{1}{2}} \tilde{x}, \quad t = \frac{1}{k_7} \tilde{t}.$$

The model thus becomes

$$\frac{\partial u_1}{\partial t} = wu_1(u_1 + Hu_2) - B_1u_1 - Su_1u_2 + \frac{\partial^2 u_1}{\partial x^2}, \quad (5.4a)$$

$$\frac{\partial u_2}{\partial t} = Fwu_2(u_1 + Hu_2) - B_2u_2 + D\frac{\partial^2 u_2}{\partial x^2}, \quad (5.4b)$$

$$\frac{\partial w}{\partial t} = A - w - w(u_1 + u_2)(u_1 + Hu_2) + d\frac{\partial^2 w}{\partial x^2}, \quad (5.4c)$$

after dropping the  $\tilde{\cdot}$ 's for brevity, where

$$A = \frac{k_1^{(1)} \left( k_2^{(1)} \right)^{\frac{1}{2}} k_6}{k_7^{\frac{3}{2}}}, \quad B_1 = \frac{k_3^{(1)}}{k_7}, \quad B_2 = \frac{k_3^{(2)}}{k_7}, \quad S = \frac{k_4}{\left( k_2^{(1)} k_7 \right)^{\frac{1}{2}}},$$

$$F = \frac{k_1^{(2)}}{k_1^{(1)}}, \quad H = \frac{k_2^{(2)}}{k_2^{(1)}}, \quad D = \frac{k_5^{(2)}}{k_5^{(1)}}, \quad d = \frac{k_9}{k_5^{(1)}}.$$

The constants  $A$  and  $B_i$  are combinations of several of the original model's parameters, but represent rainfall and plant mortality, respectively. The ratios  $F$ ,  $H$  and  $D$  describe the differences in the plant species' water to biomass conversion rates, the effects on the soil's infiltration capacity and the diffusion coefficients, respectively. Finally,  $d$  quantifies the ratio of the rate of water diffusion to that of the diffusion of

Parameter	Units	Estimates	Description
$k_1^{(1)}$	(kg biomass) (kg H <sub>2</sub> O) <sup>-1</sup>	0.003 [99], 0.007 [16]	Water to biomass conversion rate for species $u_1$
$k_1^{(2)}$	(kg biomass) (kg H <sub>2</sub> O) <sup>-1</sup>	0.002 [99], 0.01 [16]	Water to biomass conversion rate for species $u_2$
$k_2^{(1)}$	m <sup>4</sup> year <sup>-1</sup> (kg biomass) <sup>-2</sup>	100 [99]	Effect of plant species $u_1$ on water infiltration into the soil
$k_2^{(2)}$	m <sup>4</sup> year <sup>-1</sup> (kg biomass) <sup>-2</sup>	1.5 [99]	Effect of plant species $u_2$ on water infiltration into the soil
$k_3^{(1)}$	year <sup>-1</sup>	1 [204], 1.8 [99]	Rate of plant loss for species $u_1$
$k_3^{(2)}$	year <sup>-1</sup>	0.023 [204], 0.18 [99], 1.2 [75]	Rate of plant loss for species $u_2$
$k_4$	m <sup>2</sup> year <sup>-1</sup> (kg biomass) <sup>-1</sup>	- (see text)	Interspecific competition (shading)
$k_5^{(1)}$	m <sup>2</sup> year <sup>-1</sup>	1 [99, 199], 36.5 [16]	Rate of diffusion of $u_1$
$k_5^{(2)}$	m <sup>2</sup> year <sup>-1</sup>	6.25 · 10 <sup>-4</sup> [75], 1 [99]	Rate of diffusion of $u_2$
$k_6$	(kg H <sub>2</sub> O) m <sup>-2</sup> year <sup>-1</sup>	250-750 [99], 0-1000 [75], 150-1200 [204], 0-365 [16]	Rainfall
$k_7$	year <sup>-1</sup>	2 [16], 4 [75, 99, 199], 8 [204]	Rate of evaporation
$k_9$	m <sup>2</sup> year <sup>-1</sup>	500 [199],	Rate of water diffusion
Parameter	Scaling	Estimates	Description
$A$	$k_1^{(1)}(k_2^{(1)})^{\frac{1}{2}}k_6k_7^{-\frac{3}{2}}$	0.94-2.8 [99]	Rainfall
$B_1$	$k_3^{(1)}k_7^{-1}$	0.125 [204], 0.45 [99]	Plant loss of $u_1$
$B_2$	$k_3^{(2)}k_7^{-1}$	0.0029 [204], 0.045 [99]	Plant loss of $u_2$
$F$	$k_1^{(2)}(k_1^{(1)})^{-1}$	0.1 [16], 0.67 [99]	Ratio of plants' water to biomass conversion rates
$H$	$k_2^{(2)}(k_2^{(1)})^{-1}$	0.015 [99]	Ratio of plants' effects on water infiltration into soil
$S$	$k_4(k_2^{(1)}k_7)^{-\frac{1}{2}}$	- (see text)	Shading effect
$D$	$k_5^{(2)}(k_5^{(1)})^{-1}$	0.1 [16, 75, 99]	Ratio of plant species' diffusion rates
$d$	$k_9(k_5^{(1)})^{-1}$	500 [199]	Ratio of water and plant species $u_1$ diffusion rates

Table 5.1: Overview of parameters in (5.3) and (5.4). Full caption overleaf.

Table 5.1 (cont.): Overview of parameters in (5.3) (upper half) and (5.4) (lower half). This table shows both the dimensional parameters in model (5.3) and the nondimensional parameters in (5.4), including their units (dimensional parameters) or scalings (nondimensional parameters), the estimated values that we use, and a brief description.

plant species  $u_1$ . Table 5.1 includes estimates for the nondimensional parameters.

In the analysis of the model we assume that  $u_1$  is a herbaceous species and allow  $u_2$  to vary between another grass species and a woody vegetation type. The parameters of  $u_1$  are fixed throughout the analysis and act as a reference point. To investigate how the difference between two plant species affects the plant-water dynamics of the system, the parameters of  $u_2$  are varied and comparisons to the fixed species  $u_1$  are made. For brevity we refer to the two plant densities as grass and trees, even if  $u_2$  differs only slightly from  $u_1$ . Parameter estimates (see Table 5.1) suggest that trees' rate of mortality is less than that of grasses ( $B_2 < B_1$ ), trees convert water into biomass less efficiently ( $F < 1$ ), trees affect the soil's water infiltration rate less severely per unit biomass ( $H < 1$ ) and trees disperse at a slower rate than grass ( $D < 1$ ). We further assume that the inhibitory effect of shading intensifies as the species difference increases. Thus only this parameter region is analysed. In particular, to define a measure of species difference we introduce a parameter  $\chi \in [0, 1]$  that describes the extent to which the species differ. Thus we set

$$\begin{aligned} B_2 &= B_1 - \chi(B_1 - b_2), & F &= 1 - \chi(1 - f), & H &= 1 - \chi(1 - h), \\ S &= s\chi, & D &= 1 - \chi(1 - D_0), \end{aligned} \tag{5.5}$$

where  $B_1$  is set to a typical mortality rate of a herbaceous species,  $b_2$  to that of a woody species and  $f, h$  and  $D_0$  to the smallest respective ratios between two differing species. If the species are the same (i.e.  $\chi = 0$ ), then  $B_2 = B_1$ ,  $F = H = D = 1$  and  $S = 0$ . In this case, (5.4) simplifies to

$$\frac{\partial(u_1 + u_2)}{\partial t} = w(u_1 + u_2)^2 - B_1(u_1 + u_2) + \frac{\partial^2(u_1 + u_2)}{\partial x^2}, \tag{5.6a}$$

$$\frac{\partial w}{\partial t} = A - w - w(u_1 + u_2)^2 + d\frac{\partial^2 w}{\partial x^2}, \tag{5.6b}$$

by adding (5.4a) and (5.4b). This simplified model is the extended Klausmeier model (5.1) in nondimensional form on flat ground for plant density  $u_1 + u_2$  and water density  $w$ .

## 5.4 Numerical Solutions of the Model

To motivate the analysis presented in Sections 5.5 and 5.6 we present some typical solutions of (5.4) that are obtained by numerical integration. Despite the inclusion of direct interspecific competition in (5.4) and the associated existence of a pair of equilibria in which both species coexist (see Section 5.6), the system converges to a single-species state for any choice of parameters. The nature of this long-term behaviour depends on the parameter values used in the integration and may be a uniform or patterned state of either species. The transient to such an equilibrium state in which only one of the plant types is present may, however, occur as a very slow process (exceeding  $10^3$  years in dimensional parameters) in which both species coexist in either a patterned configuration or uniformly in space. Such an unstable state which nevertheless persists as a solution for a very long time (compared to the time taken to emerge from some initial configuration) is referred to as a metastable state in this context.

In the parameter setting (5.5) two distinct initial configurations from which such metastable states arise are established. If the initial condition is set to a state in which both plant species and the water density are uniform in space with a random perturbation added, then the solution remains in a metastable configuration in which both species coexist for a long time. If the rainfall is sufficiently low, the solution develops a patterned appearance in all three variables during the long transient. Eventually the metastable state reduces to a stable single-species equilibrium. The type of this equilibrium depends on the choice of parameters and in particular on the level of rainfall (see Figure 5.1a). A sufficiently high level of rainfall leads to a spatially uniform solution, while lower amounts of precipitation cause convergence to a single-species pattern. The initial densities for the uniform state are chosen based on the steady states of the one-species Klausmeier model (5.1) [99].

A similar behaviour is exhibited by the model's solution if the initial condition of the system is set to a tree-only pattern that is obtained from the one-species Klausmeier model (5.1). To this configuration a low density of the grass variable  $u_1$  is added, as well as a random perturbation in all three variables. In this scenario, the grass density  $u_1$  quickly adopts a pattern that is in phase with the tree density  $u_2$ . The solution remains in this configuration for a long time, but a sharp reduction in tree density and changes to the wavelength of the pattern may occur. Eventually a transition to a grass-only equilibrium occurs. As described above, the choice of this grass-only equilibrium to which the system eventually converges depends on the precipitation parameter  $A$  (see Figure 5.1b).

Such metastable patterns are not only observed for the parameter values chosen in Figure 5.1, but occur for a wide range of parameters. This motivates a closer

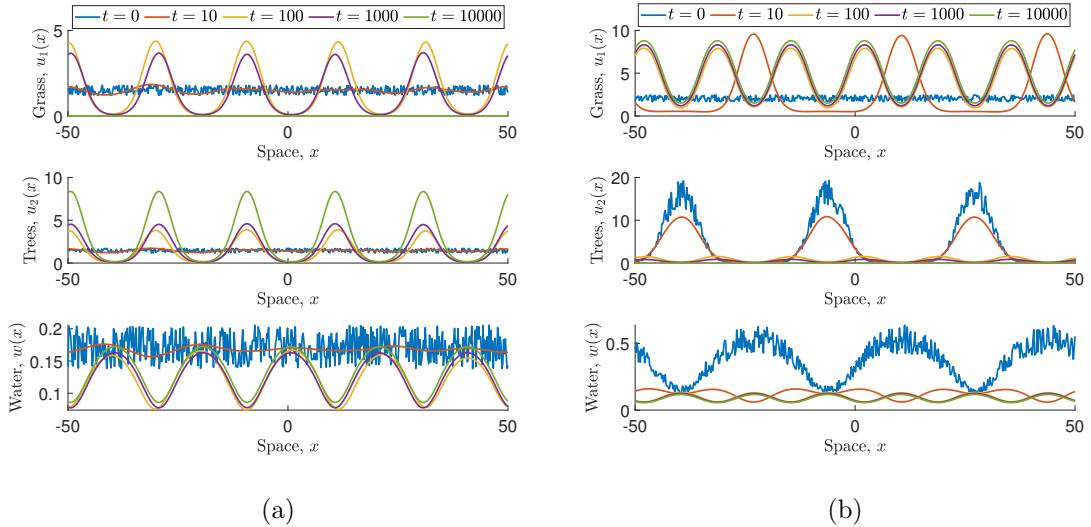


Figure 5.1: Numerical solution of the multi-species model (5.4) showing metastable patterns of species coexistence. The simulations are performed by discretising the space domain into  $M \in \mathbb{N}$  equidistant points, which yields a system of  $3M$  ordinary differential equations. Periodic boundary conditions are imposed on the endpoints of the domain. The resulting system is integrated using the MATLAB ODE solver `ode15s`. In (a),  $A = 1.5$  and  $\chi = 0.2$  and the system is initially perturbed randomly from a state in which all densities are uniform in space. In (b)  $A = 2.4$  and  $\chi = 0.8$  and the simulation is started from a tree-pattern to which a random perturbation is added. Both initial conditions are obtained from results of the one-species extended Klausmeier model (5.1). The other parameter values in all of the figures are  $B_1 = 0.45$ ,  $b_2 = 0.0055$ ,  $f = 0.01$ ,  $h = 0.01$ ,  $s = 10^{-3}$ ,  $d = 500$  and  $M = 2^9$ .

investigation of the coexistence patterns and in particular their metastability. One possibility to gain a comprehensive understanding of the patterns' properties would be a systematic numerical investigation of the whole parameter space. Such an approach could involve the tracking of the time the system spends in the coexistence state under variations of both single parameters and combinations of multiple parameters, as well as a closer investigation of the pattern's properties such as its wavelength. However, the number of different parameters in the model poses a significant challenge for this approach. Instead, linear stability analysis can be used to study the existence and stability of such patterns, which is presented in Sections 5.5 and 5.6.

## 5.5 Metastable coexistence patterns arising from stable one-species patterns

A common tool to study pattern formation in reaction-diffusion systems is linear stability analysis. Motivated by the simulation visualised in Figure 5.1b, we use linear stability analysis to discuss the emergence of metastable patterns in which

both species coexist from a stable one-species Turing-type pattern into which a new species is introduced.

Linear stability analysis is based on the growth/decay of perturbations to equilibria of the system. Depending on the choice of parameters (5.6) has up to seven spatially homogeneous steady states; a trivial state describing desert which is stable in the whole parameter space, and pairs of semi-trivial single-species steady states as well as a pair of equilibria that correspond to coexistence of both species. To differentiate between the two types of patterns addressed in this section, we strictly refer to a pattern to be of Turing-type if it emerges from a steady state that is linearly stable to spatially uniform perturbations and becomes unstable upon introduction of spatial variation in the perturbation. An equilibrium of (5.6) is linearly stable to spatially homogeneous perturbations if all eigenvalues  $\lambda_u \in \mathbb{C}$  of the system's Jacobian at the steady states satisfy  $\Re(\lambda_u) < 0$ . For (5.4), the Jacobian is given by  $J(u_1, u_2, w) = (j(u_1, u_2, w)_{k\ell})$ ,  $k, \ell = 1, 2, 3$ , where

$$j(u_1, u_2, w)_{11} = (Hw - S)u_2 + 2u_1w - B_1,$$

$$j(u_1, u_2, w)_{12} = u_1(Hw - S),$$

$$j(u_1, u_2, w)_{13} = u_1(u_1 + Hu_2),$$

$$j(u_1, u_2, w)_{21} = Fu_2w,$$

$$j(u_1, u_2, w)_{22} = 2Fw\left(\frac{u_1}{2} + Hu_2\right) - B_2, \quad (5.7)$$

$$j(u_1, u_2, w)_{23} = Fu_2(u_1 + Hu_2),$$

$$j(u_1, u_2, w)_{31} = -w(2u_1 + (1 + H)u_2),$$

$$j(u_1, u_2, w)_{32} = -w((1 + H)u_1 + 2Hu_2),$$

$$j(u_1, u_2, w)_{33} = -u_1^2 - (1 + H)u_1u_2 - Hu_2^2 - 1.$$

For an equilibrium that is linearly stable to spatially uniform perturbations, Turing-type patterns emerge if there exists a wavenumber  $k > 0$  such that at least one eigenvalue  $\lambda_s \in \mathbb{C}$  of  $J - \text{diag}(k^2, Dk^2, dk^2)$  has positive real part, i.e.  $\max_{k \geq 0, \lambda_s} \{\Re(\lambda_s)\} > 0$ .

Although  $\max_{k \geq 0, \lambda_s} \{\Re(\lambda_s)\} > 0$  is a necessary condition for the development of a pattern from a spatial perturbation,  $\max_{\lambda_u} \{\Re(\lambda_u)\} < 0$  is not necessarily required. Spatial patterns also form if  $0 < \max_{\lambda_u} \{\Re(\lambda_u)\} \ll \max_{k \geq 0, \lambda_s} \{\Re(\lambda_s)\}$ . In this case a pattern (and the corresponding equilibrium) is unstable but the difference in the

growth rates gives rise to a transient pattern but the solution eventually tends to a stable state. In particular, if  $\max_{\lambda_u} \{\Re(\lambda_u)\} \ll 1$ , this transient occurs at a slow rate as visualised in Figure 5.1 and the pattern is metastable.

### 5.5.1 Turing-type patterns

Investigation of the existence of such metastable patterns requires a understanding of the model's single-species Turing-type patterns. Due to the nature of the model, the linear stability analysis of the single-species equilibria is almost identical to that of the extended Klausmeier model on flat ground, in which patterns emerge from a Turing bifurcation. The considerations for (5.4) only differ from those of the Klausmeier model through the existence of an additional condition that determines the stability to the introduction of the second species. Moreover, in case of the tree-only equilibria the parameters  $F$ ,  $H$  and  $D$  alter the stability conditions quantitatively.

For each plant species, there exists a pair of semi-trivial steady states in which only one plant species prevails. Provided  $A > A_{\min}^G := 2B_1$ , the grass equilibrium is

$$\left( \bar{u}_1^{G,\pm}, 0, \bar{w}^{G,\pm} \right) = \left( \frac{A \pm \sqrt{A^2 - 4B_1^2}}{2B_1}, 0, \frac{2B_1^2}{A \pm \sqrt{A^2 - 4B_1^2}} \right),$$

where the superscript  $G$  identifies it as a single-species grass state and  $\pm$  indicates the choice of sign. Similarly, the pair of steady states describing a tree-only state is given by

$$\left( 0, \bar{u}_2^{T,\pm}, \bar{w}^{T,\pm} \right) = \left( 0, \frac{\xi_{\pm}}{2B_2H}, \frac{2B_2^2}{F\xi_{\pm}} \right),$$

provided the precipitation parameter exceeds  $A_{\min,\text{ex}}^T := 2B_2F^{-1}H^{-(1/2)}$ , where  $\xi_{\pm} = AFH \pm \sqrt{A^2F^2H^2 - 4B_2^2H}$ .

### Stability to Spatially Uniform Perturbations

The initial step in determining conditions for the existence of Turing-type patterns is linear stability analysis in a spatially uniform setting. Assuming no space dependence in (5.4), an equilibrium's stability is determined by the eigenvalues of the Jacobian with entries (5.7) evaluated at the equilibrium. For the grass-only steady

state  $(\bar{u}_1^{G,\pm}, 0, \bar{w}^{G,\pm})$  the Jacobian is

$$J^{G,\pm} = \begin{pmatrix} B_1 & \frac{2B_1^2H - SA - S\sqrt{A^2 - 4B_1^2}}{2B_1} & \frac{(A \pm \sqrt{A^2 - 4B_1^2})^2}{4B_1^2} \\ 0 & B_1F - B_2 & 0 \\ -2B_1 & -B_1(1 + H) & -\frac{A(A \pm \sqrt{A^2 - 4B_1^2})}{2B_1^2} \end{pmatrix}.$$

Thus, the eigenvalues  $\lambda_u^{G,\pm} \in \mathbb{C}$  satisfy

$$(B_1F - B_2 - \lambda_u^{G,\pm}) \det \begin{pmatrix} B_1 - \lambda_u^{G,\pm} & \frac{(A \pm \sqrt{A^2 - 4B_1^2})^2}{4B_1^2} \\ -2B_1 & -\frac{A(A \pm \sqrt{A^2 - 4B_1^2})}{2B_1^2} - \lambda_u^{G,\pm} \end{pmatrix} = 0. \quad (5.8)$$

The eigenvalue  $\lambda_{u,1}^{G,\pm} := B_1F - B_2$  accounts for the introduction of the tree species  $u_2$ , while the remaining two eigenvalues are independent of any parameters associated with  $u_2$ . Indeed, the matrix in (5.8) is identical with that of the corresponding matrix obtained in the linear stability analysis of the Klausmeier model in which only a single species is considered. Thus  $(\bar{u}_1^{G,+}, 0, \bar{w}^{G,+})$  is linearly stable to spatially homogeneous perturbations if  $A > A_{\min}^G$ ,  $B_2 > B_1F$  and  $B_1 < 2$ , while  $(\bar{u}_1^{G,-}, 0, \bar{w}^{G,-})$  is linearly unstable for any choice of parameters [99, 185].

Similar to the analysis of the grass steady state, the single-species tree equilibrium  $(0, \bar{u}_2^{T,-}, \bar{w}^{T,-})$  is linearly unstable in the whole parameter space, whereas  $(0, \bar{u}_2^{T,+}, \bar{w}^{T,+})$  is linearly stable to spatially homogeneous perturbations if  $A > A_{\min,\text{ex}}^T$ ,  $B_2 < 2$  and

$$S > \frac{2B_2H(B_2 - B_1F)}{F\xi_+}. \quad (5.9)$$

Similar to the stability conditions of the single-species grass equilibrium, only criterion (5.9) accounts for the stability of  $(0, \bar{u}_2^{T,+}, \bar{w}^{T,+})$  to the introduction of  $u_1$ . Thus, the stable (provided  $A > A_{\min,\text{ex}}^T$  and  $B_2 < 2$ ) single-species tree equilibrium becomes unstable to perturbations in the grass variable  $u_1$  if the shading parameter is sufficiently small (see the difference between Figures 5.2a and 5.2c). Rearranging (5.9) and combining it with the threshold  $A_{\min,\text{ex}}^T$  for existence of the steady state

yields that  $(0, \bar{u}_2^{T,+}, \bar{w}^{T,+})$  exists and is linearly stable if  $B_2 < 2$  and

$$A > A_{\min}^T := \begin{cases} \frac{2B_2}{F\sqrt{H}} & \text{if } S > S_c \\ \frac{B_2((B_1^2H + S^2)F^2 - 2B_1B_2FH + B_2^2H)}{(B_2 - B_1F)F^2HS} & \text{if } S < S_c \end{cases}, \quad (5.10)$$

where  $S_c := \sqrt{H}(B_2 - B_1F)F^{-1}$ . This lower bound is derived through calculation of the eigenvalues  $\lambda_u^{T,\pm} \in \mathbb{C}$  of the Jacobian at  $(0, \bar{u}_2^{T,\pm}, \bar{w}^{T,\pm})$  which satisfy

$$\left( \frac{2B_2H(B_2 - B_1F) - SF\xi_\pm}{2FHB_2} - \lambda_u^{T,\pm} \right) \det(J^{T,\pm} - \lambda_u^{T,\pm}I_2) = 0,$$

where

$$J^{T,\pm} = \begin{pmatrix} B_2 & \frac{F\xi_\pm^2}{4B_2^2H} \\ -\frac{2B_2}{F} & -\frac{AF\xi_\pm}{2B_2^2} \end{pmatrix},$$

and  $I$  is the identity matrix. Imposing a negativity condition on the root  $\lambda_u^{C,+}$  given by the first factor of this product yields (5.9), while the remaining two eigenvalues are both negative if and only if  $\text{tr}(J^{T,\pm}) < 0$  and  $\det(J^{T,\pm}) > 0$ . For  $(0, \bar{u}_2^{T,-}, \bar{w}^{T,-})$ ,  $\det(J^{T,-}) < 0$  for any choice of parameters yielding its instability, while for  $(0, \bar{u}_2^{T,+}, \bar{w}^{T,+})$ ,  $\det(J^{T,+}) > 0$ . Finally, stability requires  $\text{tr}(J^{T,+}) > 0$  which holds for all  $B_2 < 2$ .

Bistability of the tree-only steady state and the grass-only steady state requires stability of both semi-trivial equilibria to the introduction of the other species. Stability of the single-species grass equilibrium  $(\bar{u}_1^{G,+}, 0, \bar{w}^{G,+})$  to the introduction of the tree species  $u_2$ , i.e.  $B_2 > B_1F$ , occurs if the grass species has a superior water to biomass conversion to mortality rate, which we define to be a measure of a species' average fitness. To balance this disadvantage, stability of the tree-only state  $(0, \bar{u}_2^{T,+}, \bar{w}^{T,+})$  to the introduction of the grass species  $u_1$  necessitates the shading effect to be sufficiently large. Indeed, if  $B_2 > B_1F$  and  $S < S_c$ , then

$$A_{\min}^T = \frac{B_2((B_1^2H + S^2)F^2 - 2B_1B_2FH + B_2^2H)}{(B_2 - B_1F)F^2HS},$$

which is decreasing in  $S$  below the threshold  $S_c$ . Thus, in the parameter region in which the grass-only steady state is stable, a decrease in the inhibitory shading effect of trees on grass increases the precipitation requirement for bistability of the tree-only and grass-only steady state. This is visualised in Figures 5.2a and 5.2c. The threshold  $S_c$  defined in (5.10), which is of the same order of magnitude as the average fitness difference  $B_2 - B_1F$  between the species, describes the intensity of

shading above which the tree equilibrium  $(0, \bar{u}_2^{T,+}, \bar{w}^{T,+})$  is stable to the introduction of the grass-species  $u_1$  for any precipitation levels that guarantee the existence of the steady state. In other words, if the shading effect of  $u_2$  on  $u_1$  is sufficiently large, then  $(0, \bar{u}_2^{T,+}, \bar{w}^{T,+})$  is always linearly stable to the introduction of the grass-species  $u_1$ .

The bounds on the plant mortality parameters in the derivations above are sufficient but not necessary. However, parameter estimates consistently indicate that  $B_1 < 2$  and  $B_2 < 2$  [99, 204] and thus we restrict the analysis to this region.

### Conditions for the formation of Turing-type patterns

Having established stability conditions for the single-species equilibria in a spatially uniform setting, we turn to spatially non-uniform perturbations of the steady states to determine the loci of Turing bifurcations. Initially, we do this in the context of the single-species model obtained by setting one of the plant densities to zero. This reduces the multispecies model to the one-species Klausmeier model with water diffusion (up to the constants  $F$ ,  $H$  and  $D$  in case of  $(0, \bar{u}_2^{T,+}, \bar{w}^{T,+})$ ), for which patterns form due to a diffusion-driven instability.

More precisely, for  $(\bar{u}_1^{G,+}, 0, \bar{w}^{G,+})$  (5.4) reduces to

$$\begin{aligned}\frac{\partial u_1}{\partial t} &= wu_1^2 - B_1u_1 + \frac{\partial^2 u_1}{\partial x^2}, \\ \frac{\partial w}{\partial t} &= A - w - wu_1^2 + d\frac{\partial^2 w}{\partial x^2},\end{aligned}$$

which is the extended Klausmeier model on flat ground. The typical linear stability analysis approach outlined above yields that a pattern-forming instability occurs for

$$A_{\min}^G < A < A_{\max}^{G,+} :=$$

$$\frac{B_1^{\frac{3}{2}}d^{\frac{1}{2}} \left( 3B_1^2d^2 + 7B_1d - 8 - 2\sqrt{2B_1^4d^4 + 6B_1^3d^3 - 8B_1d} \right)^{\frac{1}{2}}}{dB_1 + 1}, \quad (5.11)$$

provided  $d > B_1^{-1}$ . If  $d < B_1^{-1}$  then  $A_{\max}^{G,+} \in \mathbb{C}$  and no Turing bifurcation occurs.

Similarly, setting  $u_1 = 0$  in (5.4), i.e. considering the tree-only steady state

$(0, \bar{u}_2^{T,+}, \bar{w}^{T,+})$ , yields

$$\frac{\partial u_2}{\partial t} = FHwu_2^2 - B_2u_2 + D\frac{\partial^2 u_2}{\partial x^2}, \quad (5.12a)$$

$$\frac{\partial w}{\partial t} = A - w - Hwu_2^2 + d\frac{\partial^2 w}{\partial x^2}. \quad (5.12b)$$

Considerations identical to those in the analysis of the extended Klausmeier model show that an instability leading to the formation of a tree pattern occurs if

$$A_{\min,\text{ex}}^T < A < A_{\max}^{T,+} :=$$

$$\frac{B_2^{\frac{3}{2}}d^{\frac{1}{2}} \left( 3B_2^2d^2 + 7DB_2d - 8D^2 - 2\sqrt{2B_2^4d^4 + 6DB_2^3d^3 - 8D^3B_2d} \right)^{\frac{1}{2}}}{D^{\frac{1}{2}}FH^{\frac{1}{2}}(dB_2 + D)}, \quad (5.13)$$

provided  $d > DB_2^{-1}$ . If  $d < DB_2^{-1}$ , then  $A_{\max}^{T,+} \in \mathbb{C}$  and no Turing bifurcation occurs.

Condition (5.13) is equivalent to the ratio  $d/D$  of the diffusion coefficients exceeding a critical threshold. Thus, a lower rate of diffusion of the woody species increases the size of the parameter region supporting pattern formation. This phenomenon is visualised in the stability diagrams 5.2a and 5.2b. It is important to emphasise that the bifurcation point  $A_{\max}^{T,+}$  is obtained by considering perturbations in  $u_2$  and  $w$  only. The calculation of  $A_{\max}^{T,+}$  does not take into account a possible introduction of the grass species  $u_1$ . Indeed, as the difference between Figure 5.2a and 5.2c visualises, if the shading parameter  $S$  is sufficiently small, then there exists a parameter region in which a single-species tree pattern is stable only in the context of a single-species model. The instability to an introduction of the grass species  $u_1$  occurs due to an increase of  $A_{\min}^T$ , given by (5.10), for decreasing  $S$ . For sufficiently small  $S$  this causes  $A_{\min}^T > A_{\min,\text{ex}}^T$  and thus a tree-only pattern cannot form for  $A_{\min,\text{ex}}^T < A < A_{\min}^T$  if the assumption of  $u_1 = 0$  is relaxed. Similarly, the pattern forming condition (5.11) obtained for  $(\bar{u}_1^{G,+}, 0, \bar{w}^{G,+})$  only applies if the steady state is stable to perturbations in  $u_2$ , i.e. if  $B_2 > B_1F$ . In the stability diagrams in Figure 5.2 a state is only assumed to be stable if the introduction of the second species does not cause destabilisation. Even though this restricts the bistability region of both single-species equilibria, the numerical simulations presented in Section 5.4 suggest that this restriction does not apply to metastable patterns in which both species coexist. In particular, the simulation visualised in Figure 5.1b, which corresponds to the  $(\beta)$  marker in Figure 5.2c, lies outside the bistability region. Indeed, the parameter region  $A_{\min,\text{ex}}^T < A < A_{\min}^T$ , i.e. the region in which the tree-pattern is stable in the one-species model but unstable to the introduction to the grass species,

gives rise to a metastable pattern such as that shown in Figure 5.1b and is closely examined in Section 5.5.2.

To address the effects caused by the difference between two plant species, we put particular emphasis on the parameter region given by (5.5), where the difference is described by a single parameter  $0 < \chi < 1$  for simplicity. To focus on the possible coexistence of both plant types, we further restrict the parameter region to that of the grass-only steady state's stability, i.e.  $A > 2B_1$  and  $B_2 > FB_1$ . The latter condition holds for all  $0 < \chi < 1$  if  $b_2 > fB_1$ . The lowest levels of precipitation beyond the threshold  $A = 2B_1$  that separates the parameter region in which only the trivial desert equilibrium is stable from bistability or tristability regions of plant states and the bare soil state, only support grass patterns. For a sufficiently small difference  $\chi < \chi_1$  between the grass and tree species, an increase of rainfall along the precipitation gradient leads to a region in which the two patterned states are stable, before the uniform grass-only steady state gains stability and eventually also the uniform tree equilibrium becomes stable to form a parameter region in which there is bistability of both uniform steady states. If the difference between the species is larger than the threshold  $\chi_1$ , then no bistability of both patterned states is possible. Instead, the uniform grass steady state becomes stable at rainfall levels that are lower than those required for a tree pattern to form (Figures 5.2a, 5.2b and 5.2c). Finally, if  $\chi > \chi_2 > \chi_1$ , where the threshold  $\chi_2$  may be larger than unity, the system does not support the formation of tree patterns and there is a direct transition from the parameter region that supports only the uniform grass equilibrium to the region in which bistability of both uniform steady states occurs (Figure 5.2c).

### 5.5.2 Metastable Patterns

The results of the preceding linear stability analysis not only show the existence of single-species Turing patterns, but in the parameter region  $A_{\min,\text{ex}}^T < A < A_{\min}^T$  also that of metastable patterns, such as the pattern visualised in Figure 5.1b, in which both species coexist.

Provided it exists ( $A > A_{\min,\text{ex}}^T$ ), the tree-only equilibrium  $(0, \bar{u}_2^{T,+}, \bar{w}^{T,+})$  is stable to spatially uniform perturbations in the tree density  $u_2$  and the water density  $w$  for all biologically relevant parameter values and tree patterns emerge from the steady state due to a Turing-type instability for sufficiently low precipitation levels. An additional stability condition (5.9) arises from the introduction of the grass species  $u_1$ . If  $(0, \bar{u}_2^{T,+}, \bar{w}^{T,+})$  is unstable to the introduction of  $u_1$  ( $A < A_{\min}^T$ ), the eigenvalue  $\lambda_{u,1}^{T,+}$  corresponding to spatially uniform perturbations is of small size and thus gives rise to a metastable solution as shown in Figure 5.1b. If in addition  $\Re(\lambda_{s,1}^{G,+}(k)) \gg \lambda_{u,1}^{T,+}$ , where  $\lambda_{s,1}^{T,+}(k) \in \mathbb{C}$  is the growth rate corresponding to a spatial

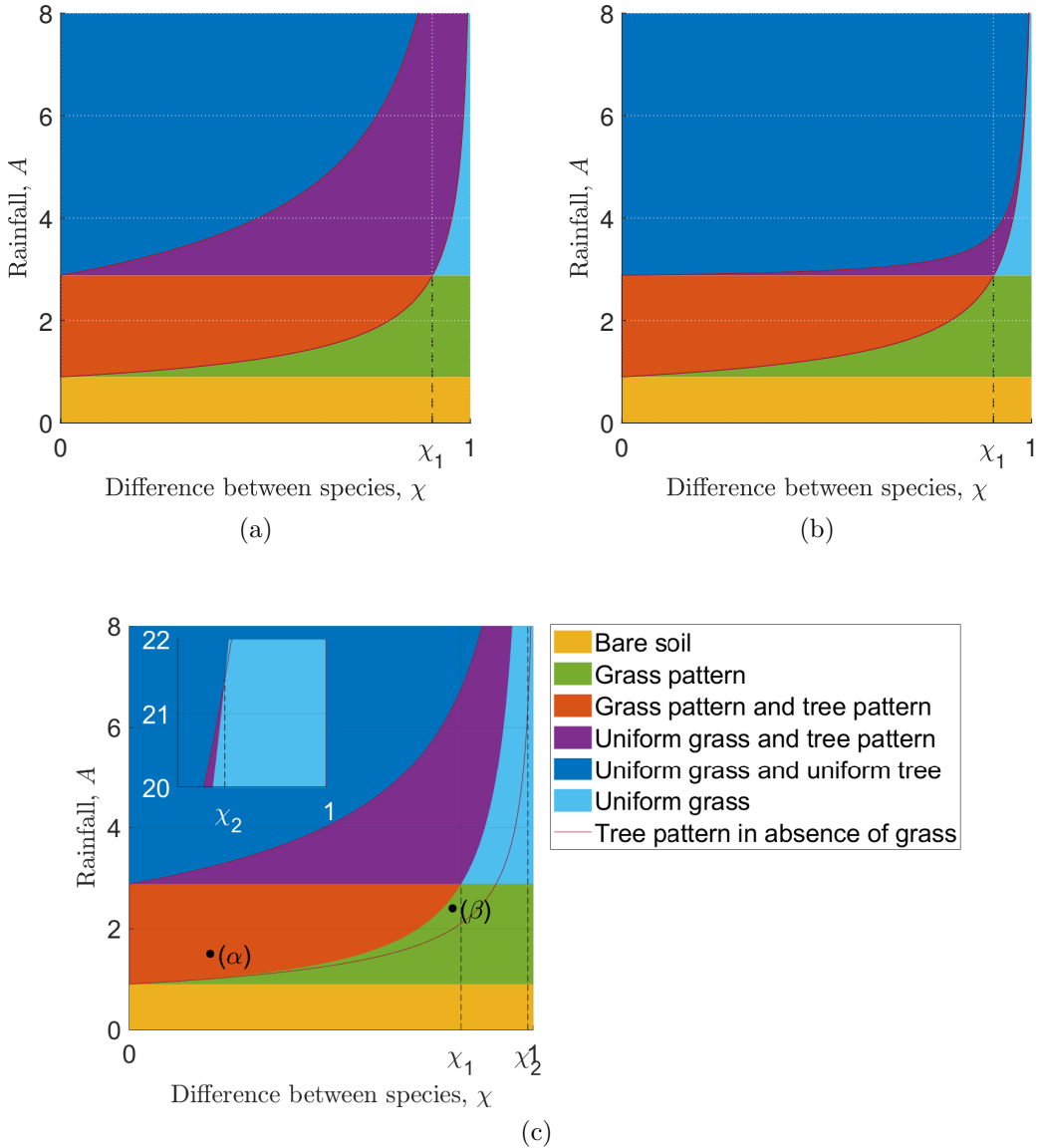


Figure 5.2: Stability diagram for the semi-trivial steady states. The coloured areas combine the results of the linear stability analysis of the full model to spatially homogeneous perturbations and the respective one-species models in which spatially heterogeneous perturbations of the semi-trivial steady states lead to patterns in the parameter region (5.5). The solid line indicates the parameter region in which tree patterns form in the one-species model (5.12). The difference between (a) and (c) shows that this does not coincide with the corresponding parameter region in the multispecies model if  $S$  is small. The desert steady state is stable in the whole parameter plane. The area indicated in the figure only shows the region in which it is the only stable state. In (a)  $s = 1$  and  $D = 1 - \chi(1 - 0.01)$ , which gives  $S < S_c$  for all  $0 < \chi < 1$ ; in (b)  $s = 1$  and  $D = 1$ ; and in (c)  $s = 10^{-3}$  and  $D = 1 - \chi(1 - 0.01)$ . The inset in (c) shows the behaviour around  $\chi = \chi_2$ . The other parameter values in all of the figures are  $B_1 = 0.45$ ,  $b_2 = 0.0055$ ,  $f = 0.01$ ,  $h = 0.01$  and  $d = 500$ . The markers ( $\alpha$ ) and ( $\beta$ ) refer to the parameter values used in the simulations presented in Figure 5.1.

perturbation with mode  $k > 0$ , the grass species quickly (compared to the time it takes to reach the stable grass-only state) adopts a patterned appearance in phase with the tree pattern during this transition. Indeed,

$$\lambda_{u,1}^{T,+} = \frac{2B_2H(B_2 - B_1F)}{F\left( AFH + \sqrt{A^2F^2H^2 - 4B_2^2F^2H} \right)} - S \leq \frac{2B_2}{AF^2}(B_2 - B_1F) \ll 1, \quad (5.14)$$

because tree mortality  $B_2$  is of small size (see Table 5.1). Further, the condition  $\Re(\lambda_{s,1}^{G,+}(k)) \gg \lambda_{u,1}^{T,+}$  is satisfied unless parameter values are close to the grass-only steady state's Turing bifurcation locus. Thus, if a grass population is introduced into a stable tree pattern and causes destabilisation of this pattern as shown in Figure 5.1b, the small size of the eigenvalue (if positive) yields a slow transition to the stable grass-only state. The difference  $B_2 - B_1F$  plays a crucial role in the metastability property as it is the cause of the pattern's slow rate of destabilisation. Ecologically the small size of this difference corresponds to similar average fitness of both species. It is this balance that enables the coexistence of both species. The significance of  $B_2 - B_1F$  is not a special feature of this particular case but also causes the metastability of patterns originating from spatially uniform initial conditions such as that used in the simulation visualised in Figure 5.1a. This is discussed in more detail in Section 5.6.

Similar considerations suggest the possibility of metastable coexistence patterns that arise from the introduction of the tree species into a stable grass pattern that consequently becomes unstable. In this situation, however, the eigenvalue  $\lambda_{u,1}^{G,+} = B_1F - B_2$  that corresponds to the introduction of the tree species is not necessarily small. Unless  $\lambda_{u,1}^{G,+} \ll 1$ , a perturbation of a grass pattern through the introduction of trees yields a quick transition to a tree pattern as a positive but not small value of  $B_1F - B_2$  corresponds to a larger average fitness of the tree-species.

## Wavelength

A key feature of any regular pattern is its wavelength. While an extensive study of pattern wavelength requires tools from nonlinear analysis, linear stability analysis provides an insight into the wavelength of the patterns close to the bifurcation locus. Then the pattern wavelength is typically determined by the wavenumber that corresponds to the largest growth rate. Given such a wavenumber  $k_{\max}$  calculated in the derivation of the Turing bifurcation points, the corresponding pattern has wavelength  $L = 2\pi/k_{\max}$ .

From the preceding linear stability analysis we find that the wavelength of the tree species is increasing with the parameter  $\chi$ . Thus, for a constant level of precipitation, the more tree-like a species is, the longer is its pattern wavelength (Figure

5.3c). Such a comparison requires bistability of both patterned states, which is not necessarily the case for all  $0 \leq \chi \leq 1$ , as indicated in Figure 5.3. The wavelength of both species further increases with decreasing rainfall, which is in agreement with results for the Klausmeier model on sloped terrain [185, 191].

The most unstable wavenumber is not necessarily the mode that is selected in a pattern. Hysteresis is known to occur in the single-species Klausmeier model [188, 199] and may cause the selected mode to differ from the most unstable mode. It is thus informative to obtain bounds on the wavelength from linear stability analysis. These bounds show that both an increase in species difference and lower precipitation increase the range of possible wavelengths (Figures 5.3a and 5.3b).

## 5.6 Metastable coexistence patterns originate from a coexistence equilibrium

The analysis in Section 5.5 only explains patterns in which both species coexist in the parameter region  $A_{\min,\text{ex}}^T < A < A_{\min}^T$ . The simulations presented in Section 5.4, however, suggest that metastable coexistence patterns occur in a wider range of the precipitation parameter  $A$ . In this section we show that Turing-type patterns of the tree species  $u_2$  are not the only origin of metastable patterns. Additionally, metastable patterns of species coexistence can arise from an equilibrium in which both species coexist, which is the subject of this section.

Besides the trivial and semi-trivial equilibria discussed in Section 5.5, (5.4) also admits a pair of coexistence steady states  $(\bar{u}_1^{C,\pm}, \bar{u}_2^C, \bar{w}^{C,\pm})$ , where similar to the notation used for the single species states the superscript  $C$  identifies the equilibrium as a coexistence state. The equilibria satisfy

$$\begin{aligned}\bar{u}_1^{C,\pm} &= \frac{1}{2B_2} (AF - B_2(1+F)\bar{u}_2^C \\ &\quad \pm \sqrt{(AF + B_2(1+F)\bar{u}_2^C)^2 - 4B_2(-AFH\bar{u}_2^C + B_2(1+H(\bar{u}_2^C)^2))}), \\ \bar{u}_2^C &= \frac{B_2 - FB_1}{SF}, \quad \bar{w}^{C,\pm} = A - \frac{B_2}{F} (\bar{u}_1^{C,\pm} + \bar{u}_2^C),\end{aligned}$$

under suitable conditions that ensure their existence and biological relevance. For  $(\bar{u}_1^{C,-}, \bar{u}_2^C, \bar{w}^{C,-})$  these are  $B_2 > B_1F$  and

$$\max \left\{ \frac{B_2(\bar{u}_2^C(1-H)+2)}{F}, \frac{B_2\bar{u}_2^C(1+F)}{F} \right\} < A < \frac{B_2(1+H(\bar{u}_2^C)^2)}{FH\bar{u}_2^C},$$

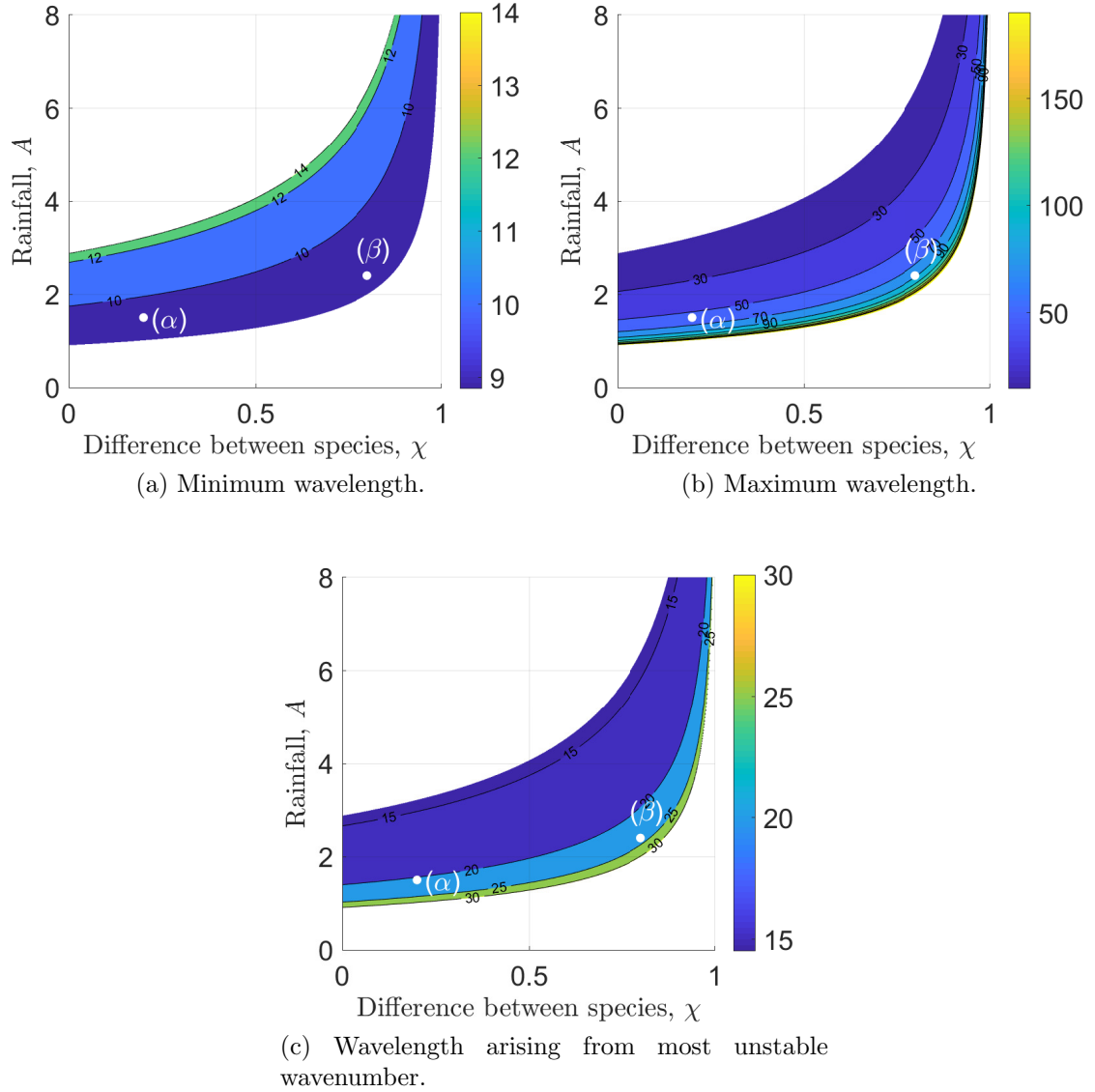


Figure 5.3: Single species pattern wavelength. This figure visualises the pattern wavelengths of both single-species patterns calculated through linear stability analysis. The contours show the wavelength of the pattern of species  $u_2$  as its difference from the grass species  $u_1$  increases, while the values on the  $A$ -axis correspond to the wavelength of the grass pattern. Minimum (a), maximum (b) and wavelengths corresponding to the most unstable mode (c) are shown. The parameter values are  $B_1 = 0.45$ ,  $b_2 = 0.0055$ ,  $f = 0.01$ ,  $h = 0.01$ ,  $D_0 = 0.01$ , and  $d = 500$ . The markers  $(\alpha)$  and  $(\beta)$  refer to the parameter values used in the simulations presented in Figure 5.1. For a comparison to the wavelengths of the coexistence pattern see Figure 5.7.

while the corresponding conditions for  $(\bar{u}_1^{C,+}, \bar{u}_2^C, \bar{w}^{C,+})$  are  $B_2 > B_1 F$  and

$$A > A_{\min}^{C,+} :=$$

$$\max \left\{ \frac{B_2 (\bar{u}_2^C (1 - H) + 2)}{F}, \min \left\{ \frac{B_2 \bar{u}_2^C (1 + F)}{F}, \frac{B_2 (1 + H (\bar{u}_2^C)^2)}{FH \bar{u}_2^C} \right\} \right\}. \quad (5.15)$$

Visualisations in this chapter are shown for the special parameter setting (5.5) and  $F = H$ . In this situation changes to  $\chi$  do not affect the nature of how the equilibrium loses its relevance. If  $s > b_2 - B_1 f$ , then  $(\bar{u}_1^{C,+}, \bar{u}_2^C, \bar{w}^{C,+})$  ceases to exist at  $A = A_{\min}^{C,+}$ , while otherwise  $A = A_{\min}^{C,+}$  represents the threshold at which  $\bar{u}_1^{C,+}$  becomes negative (see Figure 5.4). Similar considerations hold for  $(\bar{u}_1^{C,-}, \bar{u}_2^C, \bar{w}^{C,-})$ . This equilibrium, however, does not exhibit the metastability property which is the main focus of this study and is therefore not considered further. It is noteworthy that there is nothing special about the choice of  $F = H$  and results are robust to changes in  $F$  and  $H$ , provided the rainfall minimum  $A_{\min}^{C,+}$  remains in the biologically relevant parameter region. Results presented in this chapter are also robust to changes in  $s$ . Finally, we remark that the size of the shading parameter  $S$  needs to be similar to that of the average fitness difference between both species  $B_2 - B_1 F$  for the equilibrium to remain in a biologically relevant region, as large (small) shading effects only support coexistence at equilibrium if the density of  $u_2$  is low (high).

An initial conclusion that is drawn from calculation of the existence region of the coexistence equilibria is that their existence is not required for metastable patterns in which both species coexist to form and patterns outside the existence region of  $(\bar{u}_1^{C,\pm}, \bar{u}_2^C, \bar{w}^{C,\pm})$  truly originate from a stable tree-only pattern as discussed in Section 5.5. In particular, the simulation shown in Figure 5.1b is obtained by using parameter values for which the coexistence steady states do not exist (see the  $(\beta)$  marker in Figure 5.4a). The parameter region considered in this section may, however, overlap with that considered in Section 5.5, and no general statement on the sizes of  $A_{\min}^T$  and  $A_{\min}^{C,+}$  can be made.

To gain a better understanding of the effects caused by the difference in both plant types, it is essential to understand the steady states' behaviour if the species

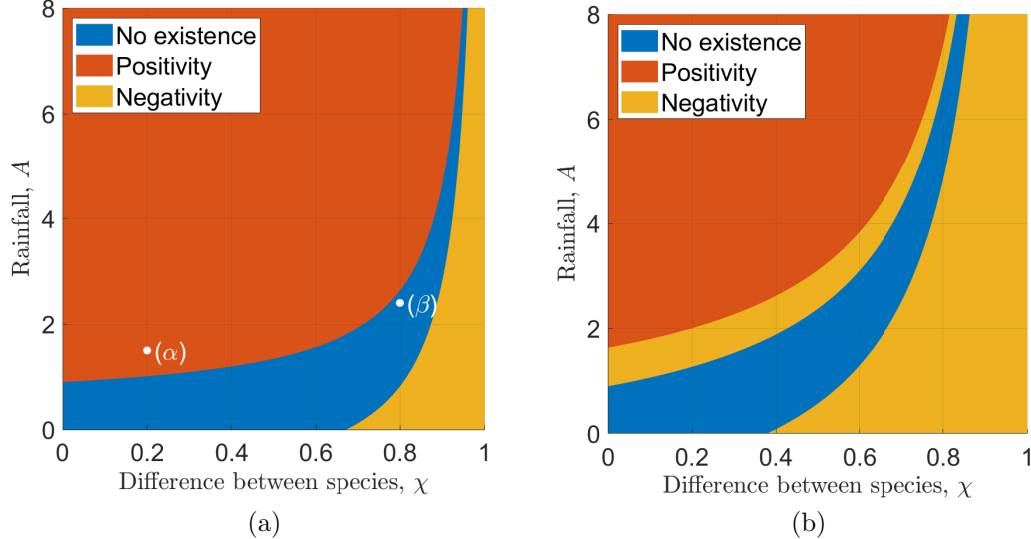


Figure 5.4: Existence and positivity of the coexistence steady state. Visualisation of the parameter regions in which the coexistence steady state  $(\bar{u}_1^{C,+}, \bar{u}_2^C, \bar{w}^{C,+})$  exists and is biologically relevant (positive) in the  $\chi$ - $A$  parameter plane for different levels of shading. In (a)  $s = 10^{-3}$ , while in (b)  $s = 3 \cdot 10^{-4}$ . The other parameter values used in this visualisation are  $B_1 = 0.45$ ,  $b_2 = 0.0055$ ,  $f = 0.01$  and  $h = 0.01$ . The legend of (a) also applies to (b). The markers  $(\alpha)$  and  $(\beta)$  in (a) refer to the parameter values used in the simulations presented in Figure 5.1.

are identical. At  $\chi = 0$ , the coexistence steady state is

$$\left( \bar{u}_1^{C,\pm}, \bar{u}_2^C, \bar{w}^{C,\pm} \right) = \left( \frac{\left( A \pm \sqrt{A^2 - 4B_1^2} \right)}{2B_1} - \frac{b_2 - B_1 f}{s}, \frac{b_2 - B_1 f}{s}, \frac{2B_1^2}{A \pm \sqrt{A^2 - 4B_1^2}} \right). \quad (5.16)$$

As remarked in Section 5.3, for  $\chi = 0$ , the densities  $u_1 + u_2$  and  $w$  satisfy the extended Klausmeier model. Thus, the sum  $u_1 + u_2$  gives rise to a continuum of steady states that satisfy

$$u_1 + u_2 = \frac{A \pm \sqrt{A^2 - 4B_1^2}}{2B_1^2}, \quad \text{and} \quad w = \frac{2B_1^2}{A \pm \sqrt{A^2 - 4B_1^2}}.$$

The coexistence steady state  $(\bar{u}_1^{C,\pm}, \bar{u}_2^C, \bar{w}^{C,\pm})$  maps to one member of this continuum whose choice depends on the model parameters as given by (5.16).

### 5.6.1 Stability to spatially uniform perturbations

Similar to the analysis in Section 5.5, linear stability analysis can be used to investigate the existence of patterns arising from the spatially uniform coexistence steady state  $(\bar{u}_1^{C,\pm}, \bar{u}_2^C, \bar{w}^{C,\pm})$ . The algebraic complexity of the Jacobian with entries (5.7) evaluated at both coexistence equilibria does not allow an analytic derivation of stability conditions similar to those for the single-species states in Section 5.5. Instead, we performed a systematic numerical investigation of the Jacobian's eigenvalues  $\lambda_u^{C,\pm} \in \mathbb{C}$  that determine the steady states' stability to spatially uniform perturbations in the respective positivity regions. This suggests that both steady states are unstable. The instability of  $(\bar{u}_1^{C,+}, \bar{u}_2^C, \bar{w}^{C,+})$ , however, is caused by an eigenvalue of small size, denoted by  $\lambda_{u,1}^{C,+}$ , i.e.  $0 < \max_{\lambda_u} \{\Re(\lambda_u^{C,+})\} = \Re(\lambda_{u,1}^{C,+}) \ll 1$ , where the maximum is taken over all eigenvalues  $\lambda_u^{C,+}$  of the Jacobian  $J^{C,+} = (j)_{k\ell}^{C,+}$ ,  $k, \ell = 1, 2, 3$  evaluated at the steady state (see Figure 5.5a). The metastability associated with the small size of  $\Re(\lambda_{u,1}^{C,+})$  is, as in the case discussed in Section 5.5, due to the species' similar average fitness, i.e. the small difference of  $B_2 - B_1F$ . Indeed, an application of determinant-preserving elementary row operations shows

$$\begin{aligned} \det(J^{C,+}) &= \det \begin{pmatrix} j_{11}^{C,+} & j_{12}^{C,+} & j_{13}^{C,+} \\ 0 & B_2 - B_1F & 0 \\ j_{31}^{C,+} & j_{32}^{C,+} & j_{33}^{C,+} \end{pmatrix} \\ &= (B_2 - B_1F) \left( j_{11}^{C,+} j_{33}^{C,+} - j_{13}^{C,+} j_{31}^{C,+} \right) = O(B_2 - B_1F). \end{aligned}$$

The equilibrium is only of biological relevance if  $B_2 > B_1F$ . Thus, as discussed in Section 5.5.2, if  $|B_2 - B_1F| \ll 1$ , then  $|\det J| \ll 1$ . Since the determinant of a matrix is the product of its eigenvalues, this shows the small size of one of the Jacobian's eigenvalues. If  $B_2 - B_1F = 0$  but  $S \neq 0$ , then the coexistence steady state  $(\bar{u}_1^{C,\pm}, \bar{u}_2^C, \bar{w}^{C,\pm})$  reduces to the grass-only equilibrium  $(\bar{u}_1^{G,\pm}, 0, \bar{w}^{G,\pm})$  and the small eigenvalue  $\lambda_{u,1}^{C,+}$  of the coexistence state corresponds to  $\lambda_{u,1}^{G,\pm}$  which vanishes because  $B_2 - B_1F = 0$ .

#### Metastable States

For a system initially close to the coexistence steady state  $(\bar{u}_1^{C,+}, \bar{u}_2^C, \bar{w}^{C,+})$  the small size of the only positive real part of the Jacobian's eigenvalues leads to a slow transition away from the equilibrium in the spatially uniform setting. If spatially nonuniform perturbations of the steady state are considered, this transition occurs via metastable coexistence patterns of both species, subject to sufficiently low rainfall levels. This is quantified by linear stability analysis which shows that the

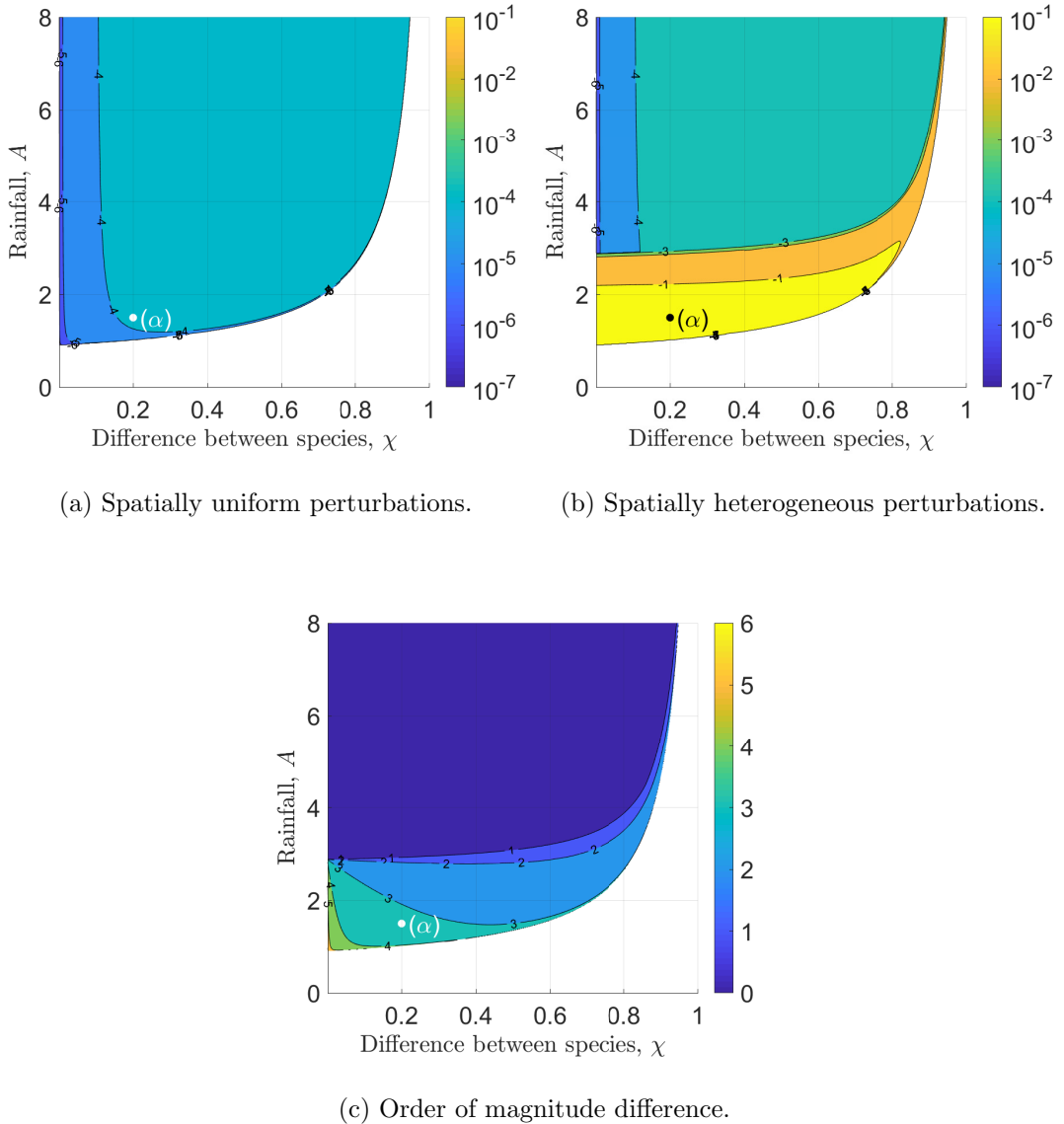


Figure 5.5: Largest real part of eigenvalues determining stability of the coexistence steady state. Visualisation of  $\max_{k>0}\{\Re(\lambda_{:,1}^{C,+})\}$  in the  $\chi$ - $A$  parameter plane for the coexistence equilibrium  $(\bar{u}_1^{C,+}, \bar{u}_2^C, \bar{w}^{C,+})$ , where  $\lambda_{:,1}^{C,+}$  denotes the eigenvalue with largest real part of the Jacobian with entries (5.7) evaluated at the steady state that determine its stability to spatially uniform ((a)) and spatially heterogeneous ((b)) perturbations. The order of magnitude difference between the results for spatially uniform and spatially heterogeneous perturbations is shown in (c). White areas indicate regions in which the steady state is negative or does not exist. The plots are obtained by evaluating  $\max_{k>0}\{\Re(\lambda_{:,1}^{C,+})\}$  for  $0 < A < 8$  and  $0 < \chi < 1$  with increments  $\Delta A = 0.01$  and  $\Delta \chi = 0.001$ . The parameters are  $s = 10^{-3}$ ,  $B_1 = 0.45$ ,  $b_2 = 0.0055$ ,  $f = 0.01$ ,  $h = 0.01$ ,  $D_0 = 0.01$ ,  $d = 500$ . The marker  $(\alpha)$  refers to the parameter values used in the simulations presented in Figure 5.1a.

maximum real part of the corresponding Jacobian's eigenvalues exceeds  $\Re(\lambda_{u,1}^{C,+})$  by several orders of magnitude (see Figures 5.5b and 5.5c for a visualisation). In other words,  $\max_{k \geq 0} \{\Re(\lambda_{s,1}^{C,+}(k^2))\} \gg \Re(\lambda_{u,1}^{C,+})$ , where  $\lambda_{s,1}^{C,+}(k^2)$  denotes the eigenvalue of  $J^{C,+} - \text{diag}(k^2, Dk^2, dk^2)$  with the largest real part. This leads to a quick establishment of a coexistence pattern about the steady state from a spatially non-uniform perturbation which then persists for a long time before transiting to a stable one-species state. The growth rate that causes the formation of spatial patterns is given by

$$\Re(\lambda_{s,1}^{C,+}(k^2)) = \alpha(k^2) + \Re\left(\frac{\left(\beta(k^2) + \sqrt{\gamma(k^2)}\right)^{\frac{2}{3}} + \delta(k^2)}{\left(\beta(k^2) + \sqrt{\gamma(k^2)}\right)^{\frac{1}{3}}}\right), \quad (5.17)$$

where  $\alpha$ ,  $\beta$ ,  $\gamma$  and  $\delta$  are polynomials in  $k^2$ . Due to the algebraic complexity of the eigenvalue, an analytic determination of the pattern-defining features is impractical. Instead, we studied it numerically to determine the existence and possible wavelengths of a metastable pattern.

As rainfall  $A$  increases from the minimum  $A_{\min}^{C,+}$ ,  $\max_{k \geq 0} \{\Re(\lambda_{s,1}^{C,+}(k^2))\}$  decreases and there exists a critical value of precipitation  $A_{\max}^{C,+}$  beyond which

$$\max_{k \geq 0} \{\Re(\lambda_{s,1}^{C,+}(A; k^2))\} = \Re(\lambda_{u,1}^{C,+}(A)),$$

as visualised in Figure 5.6a. In particular, there is a discontinuity in

$$k_{\max}^{C,+} := \arg \max_{k \geq 0} \{\Re(\lambda_{s,1}^{C,+}(k^2))\},$$

at  $A = A_{\max}^{C,+}$ , because the maximum real part of the eigenvalues attains its maximum at  $k = 0$  for  $A > A_{\max}^{C,+}$ , but  $k_{\max}^{C,+} \not\rightarrow 0$  as  $A \uparrow A_{\max}^{C,+}$ . This threshold is an upper bound for the existence of metastable coexistence patterns and is visualised in Figure 5.5c. For rainfall levels above this threshold, metastable coexistence of both plant species still occurs, albeit not as a pattern. Spatial heterogeneity does not cause the formation of patterns in this case as  $\Re(\lambda_{s,1}^{C,+}(A))$  attains its maximum at  $k = 0$ . The small size of  $\Re(\lambda_{u,1}^{C,+})$  still causes a solution slightly perturbed from the coexistence steady state to remain close to the equilibrium for a long time. This gives rise to a metastable state in which both vegetation types are present uniformly in space.

## Wavelength

Linear stability analysis further provides an insight into the wavelength of patterns. Typically the wavelength of a pattern is dominated by the wavenumber yielding the

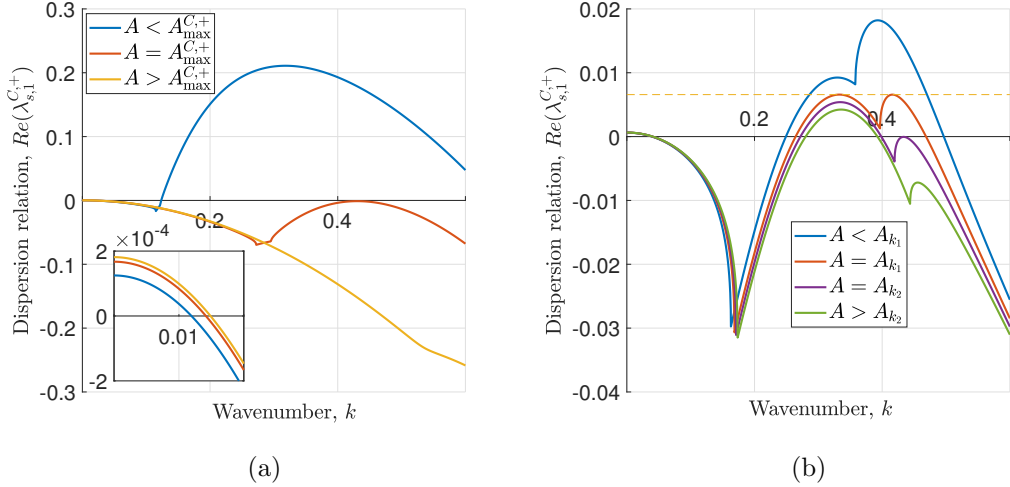


Figure 5.6: Dispersion relation for patterns with species coexistence. The dispersion relation is visualised for different rainfall levels  $A$  and fixed  $\chi = 0.2$  ((a)) and  $\chi = 0.86$  ((b)). The inset in (a) shows the behaviour close to the origin. The dotted line in (b) indicates the equality of the local maxima for  $A = A_{k_1}$ . The other parameters are  $s = 10^{-3}$ ,  $B_1 = 0.45$ ,  $b_2 = 0.0055$ ,  $f = 0.01$ ,  $h = 0.01$ ,  $D_0 = 0.01$ ,  $d = 500$ .

largest growth. However, since the wavelength of a pattern is an inherently nonlinear property, different modes may be selected due to effects such as hysteresis. In this case the roots of  $\Re(\lambda_{s,1}^{C,+}(k^2))$  provide an upper and lower bound for the wavelength. The numerical investigation of the dispersion relation shows that pattern wavelength increases with decreasing rainfall, in line with results shown in Section 5.5 and previous results on the single-species Klausmeier model on sloped ground [185, 191]. In other words, the distance between vegetation patches is larger in regions in which a smaller amount of the limiting water resource is available. An increase in the difference between the two plant species also causes an increase in the wavelength difference, but this increase is small compared to changes caused by precipitation fluctuations. A visualisation of the wavelength is given in Figure 5.7. A further complication in the calculation of the wavelength through linear stability analysis arises through the algebraic complexity of the dispersion relation (5.17) which causes a discontinuity in the most unstable mode and hence also the largest root in a subset of the parameter space considered in this analysis. The discontinuities arise from the existence of two local maxima of  $\Re(\lambda_{s,1}^{C,+}(k^2))$ , one of which occurs for  $k_1 < k < k_2$ , which is the positivity region of  $\gamma(k^2)$ , while the other local maximum is attained for  $k > k_2$ . Consequently, there exists a critical value of the precipitation parameter  $A_{k_1}$  at which there is a discontinuity in  $\arg \max_{k \geq 0} \Re(\lambda_{s,1}^{C,+}(k^2))$  because both local maxima coincide (see Figure 5.6b). Similarly, the rainfall value  $A_{k_2}$  at which  $\max_{k \geq k_2} \Re(\lambda_{s,1}^{C,+}(k^2)) = 0$ , causes a discontinuity in the largest root of the

dispersion relation and thus in the lower bound for the wavelength of the coexistence pattern.

## 5.7 Discussion

Our work predicts that coexistence of two plant species competing for the same limiting resource can occur as a long transient state, even if coexistence is inherently unstable. Such a metastable behaviour is characterised by the small size of the only positive eigenvalue of the equilibrium from which the coexistence arises. Coexistence of two species in such a metastable state is enabled by a balance of both species' average fitness which is measured by the ratio of a species' capability to convert water into new biomass to its mortality rate. In the nondimensional model parameters this balance corresponds to the small size of  $B_2 - B_1 F$ , the quantity that controls the size of the eigenvalue causing the instability.

In ecology, the understanding of transient states is of utmost importance as many ecosystems never reach an equilibrium state. Disturbances such as changes to grazing patterns or climate change interrupt the convergence to a steady state on a frequent basis, and thus keep systems in perpetual transients [200, 203]. The occurrence of such disequilibrium states is not specific to savanna and dryland biomes but also occurs in ecosystems of other climate zones [180]. While we have not investigated the system's response to changes in environmental conditions, such as variability in precipitation or a changes in water evaporation due to temperature fluctuations, the analysis presented in this study can provide an insight into the dynamics of such transient states by investigating their origin, fate and some of their properties.

We have established two possible origins of metastable states in the multispecies model (5.4): a spatially uniform equilibrium in which both species coexist (Section 5.6) and a one-species tree pattern that is unstable to the introduction of the herbaceous species (Section 5.5). For the latter, the consideration of the interspecific shading feedback is not necessary. The direct interspecific competition does, however, cause a further decrease in the unstable eigenvalue (5.14), by further reducing the average fitness difference between both species. Large shading effects may also tip that balance in favour of the tree species, stabilising the tree pattern and thus preventing the formation of a metastable coexistence pattern from an invasion-type scenario (see Figure 5.2).

On the other hand, the inclusion of the shading effect is essential for the existence of metastable states arising from a coexistence equilibrium as a direct interspecific competition term is necessary for the existence of such a steady state. Coexistence at equilibrium without the presence of a shading effect is only possible if the average

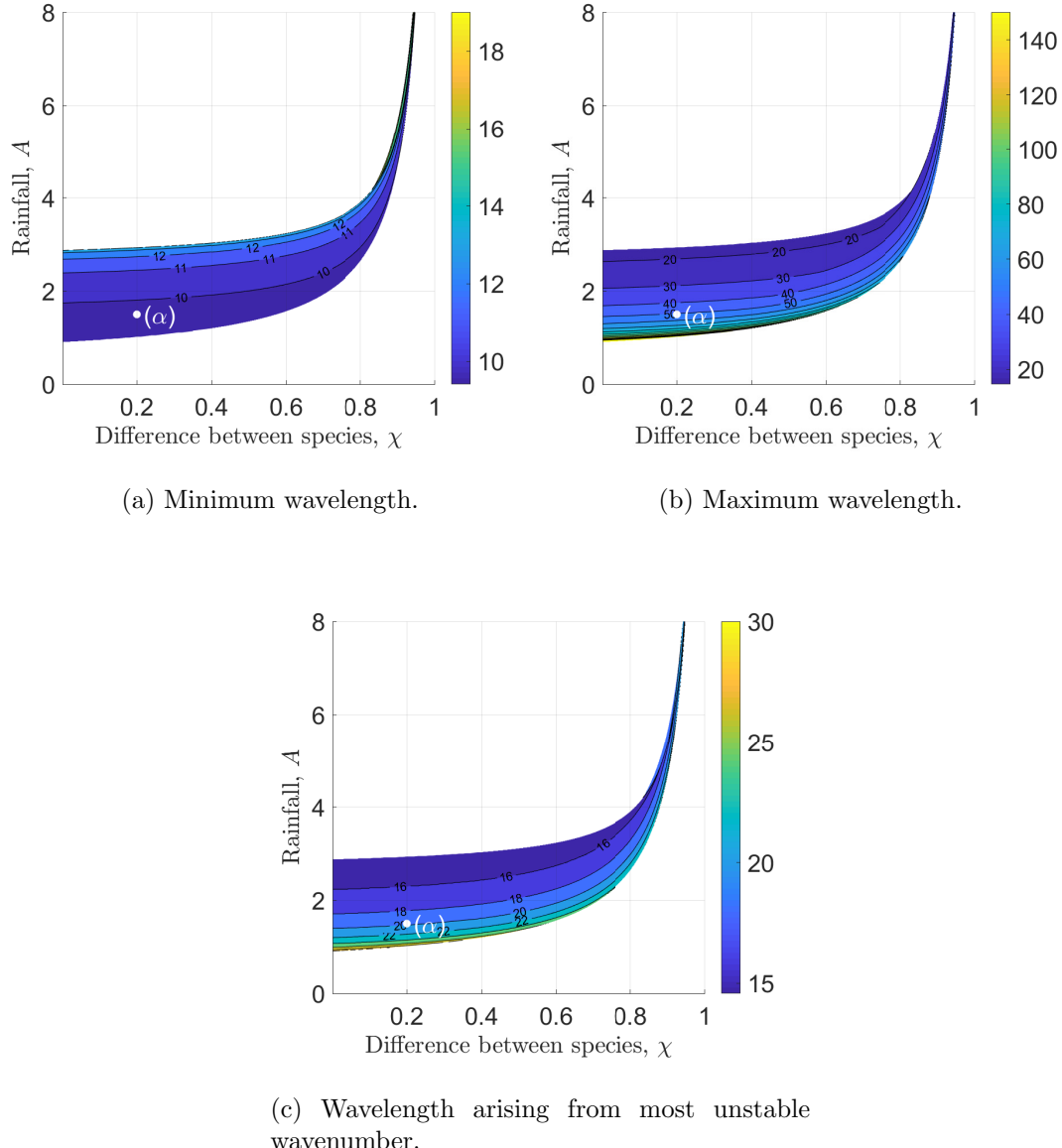


Figure 5.7: Wavelength of metastable coexistence patterns. This figure visualises contours of the wavelength associated with the wavenumber yielding the largest growth ( $c$ ) as well as lower ( $a$ ) and upper bounds ( $b$ ) that arise from linear stability analysis. For details on the creation of the plots and the parameter values see Figure 5.5. For a comparison to the wavelengths of the single-species pattern see Figure 5.3.

fitness of both species are equal, i.e.  $B_2 = B_1 F$ , a highly unlikely scenario unless both species are the same. Similar to a previous analysis of a multi-species model in dryland ecosystems by Nathan et al. [145] we did not consider this special case as it lacks biological relevance. Nevertheless, the lack of a shading feedback does not necessarily prevent the establishment of a coexistence pattern from perturbations to a spatially uniform configuration of both species similar to that visualised in Figure 5.1a. If the species differ in their dispersal behaviour, the faster dispersing species can establish a spatial pattern (provided precipitation is sufficiently low) and can act as an ecosystem engineer by redistributing the water resource to which the slow disperser can adapt and form a pattern itself. As discussed in slightly different settings by Nathan et al. [145] and Baudena and Rietkerk [16], this supports the existence of coexistence patterns. In particular, this pushes the system into a state to which the theory presented in Section 5.5 can be applied. Hence, if one of the two corresponding single-species states is unstable to the introduction of the competitor via a very small eigenvalue, the system remains in the coexistence pattern state for a long time. This observation emphasises the difficulty of inferring the origin of a metastable multi-species patterned state, which is beyond the scope of this study.

The wavelength of the pattern may provide a useful tool in predicting the fate of a coexistence pattern, but potential shortfalls (linearisation, neglection of hysteresis effects) in the determination of the wavelength need to be taken into account. Our analysis of the patterns' wavelengths shows that the wavelength of a single-species tree pattern (Figure 5.3) is very similar to that of a pattern in which the tree species coexists with the grass species (Figure 5.7). However, if both species differ significantly (the parameter  $\chi$  being close to unity), linear stability analysis predicts single-species grass patterns at a smaller wavelength than coexistence patterns. Thus, if a pattern in which both species coexist occurs at an atypical mode that differs from the results presented in Sections 5.5.2 and 5.6.1 and better fits the wavelength prediction of a one-species pattern (such as in the later stages of the solution visualised in Figure 5.1b), it can be concluded that the metastable pattern eventually reduces to a one-species pattern to which the observed wavelength corresponds.

We have restricted our analysis in this chapter to the two-species model (5.4) to focus on the analytical investigation of pattern existence. Numerical simulations of a three-species model similar to (5.2) with  $n = 3$ , but with the addition of multiple, hierarchical interspecific interaction terms, also yield metastable patterned solutions in which all three species coexist, provided their average fitness differences are small. Coexistence through metastability can further occur for just a subset of all species in the model. Indeed, our numerical experiments show that if one of the species has a lower average fitness, then the community of superior species outcompetes the in-

ferior species on a short timescale and forms a metastable coexistence state in which it remains on a long timescale. We thus hypothesise that the metastability property discussed in this chapter is not specific to the two-species model (5.4) but can be extended to a larger community of plant species in desert ecosystems. Moreover, our simulations of the three-species model indicate that the crucial condition for the existence of metastable solutions - small average fitness differences between species - is carried over to systems of more diverse plant communities.

The concept of a metastable solution to a system is not new. Metastability has, for example, been studied in the Cahn-Hilliard equation [11, 12], in chemotactic models [154] and microwave heating models [91]. The occurrence of a slow transient between two stable states has even been briefly commented on in the analysis of a more complex multi-species model of desert plants [76], without the attempt to provide a detailed investigation of the phenomenon. It is worth emphasising that we characterise metastability by the small size of the only positive eigenvalue of an equilibrium. In landscape ecology, however, the term metastability usually has a broader meaning as it describes a stable system whose single components are changing over time due to disturbance and recovery effects [248].

The model in this chapter is based on the Klausmeier model [99], which deliberately reduces the description of the dynamics responsible for the formation of vegetation patterns in arid environments to the infiltration feedback arising from a soil modification caused by plants. A range of more complex models exist (see [247] for a review of the most commonly used models) that capture a number of additional features of dryland ecosystems, such as nonlocal plant dispersal [3, 16, 61, 156, 157], different dynamics of soil and surface water [86, 163], nonlocal water uptake due to extended root networks [74], more realistic grazing/browsing effects [195, 197] or autotoxicity [120]. Simulation-based approaches have to some extent addressed the influence of these feedbacks on the coexistence of species [76, 103], but an analytical approach similar to that presented in this study may provide further insight into the way in which these additional assumptions affect coexistence mechanisms.

A natural extension of the work presented in this chapter would be an investigation of the metastability property in a two-dimensional space domain. The linear stability analysis from Sections 5.5 and 5.6 can be carried over to a higher space dimension, but does not provide any new information on the metastable behaviour of a patterned solution. Instead, numerical simulations could provide more insights into the coexistence pattern's properties away from the Turing bifurcation locus, such as a classification of its type (gap pattern, labyrinth pattern, stripe pattern or spot pattern) along the precipitation gradient [129]. The combination of adding an additional space dimension with the long runtimes required to capture the metastable behaviour of the system would, however, incur a significant computational

cost.

A final area of potential future work concerns variabilities in environmental conditions, which have not been addressed in this study. Effects such as rainfall seasonality [13, 80, 100], rainfall intermittency [13, 100, 198, 221], periodic variation in precipitation [217] or topographic heterogeneity [72] are known to be significant for vegetation patterns and have been studied using single-species models. It could therefore be of interest to extend those approaches to multi-species ecosystems to develop an understanding of how such heterogeneities affect the coexistence of species and in particular the metastability property of the model presented in this chapter. Indeed, simulations of our multispecies model under seasonal precipitation regimes suggest that rainfall seasons of intermediate length (150 - 250 days per year) prolong the time the system remains in a coexistence state. Initial simulations, however, also suggest that inherently nonlinear properties such as pattern wavelength have a significant effect on the system's transient behaviour under temporal variations of environmental conditions. A detailed investigation of this phenomenon is therefore beyond the scope of this study, but would present new valuable insights into coexistence of plant species in dryland ecosystems.

## Chapter 6

### Spatial self-organisation enables species coexistence in a model for savanna ecosystems

The contents of this chapter are published in [64].

#### 6.1 Author contribution

The authors of the published paper [64] are Lukas Eigentler and Jonathan A Sherratt. Lukas Eigentler conceptualised the research, formulated the mathematical model, performed both the analytical and numerical analyses of the model, wrote the paper draft and reviewed and edited the manuscript. Jonathan A Sherratt conceptualised the research, reviewed and edited the manuscript and provided supervision.

#### Abstract

The savanna biome is characterised by a continuous vegetation cover, comprised of herbaceous and woody plants. The coexistence of species in arid savannas, where water availability is the main limiting resource for plant growth, provides an apparent contradiction to the classical principle of competitive exclusion. Previous theoretical work using nonspatial models has focussed on the development of an understanding of coexistence mechanisms through the consideration of resource niche separation and ecosystem disturbances. In this chapter, we propose that a spatial self-organisation principle, caused by a positive feedback between local vegetation growth and water redistribution, is sufficient for species coexistence in savanna ecosystems. We propose a spatiotemporal ecohydrological model of partial differential equations, based on the Klausmeier reaction-advection-diffusion model for vegetation patterns, to investigate the effects of spatial interactions on species coexistence on sloped terrain. Our results suggest that species coexistence is a possible model outcome, if a balance is kept between the species' average fitness (a measure of a species' competitive abilities in a spatially uniform setting) and their colonisation abilities. Spatial heterogeneities in resource availability are utilised by the superior coloniser (grasses), before it is outcompeted by the species of

higher average fitness (trees). A stability analysis of the spatially nonuniform coexistence solutions further suggests that grasses act as ecosystem engineers and facilitate the formation of a continuous tree cover for precipitation levels unable to support a uniform tree density in the absence of a grass species.

## 6.2 Introduction

Savannas are characterised by the coexistence of herbaceous vegetation (*grasses*) and woody plant types (*shrubs* and *trees*) [176]. They are a dominating feature of many geographical regions worldwide, occupying over one eighth of the global land surface [176, 177]. Savannas stretch across a wide range of different climate zones, and in particular different aridity zones. If the total precipitation volume in savannas is low, they are referred to as water-limited or (semi-)arid savannas [173].

The coexistence of grass and trees in arid savannas, in which water is the main limiting resource for vegetation growth, has been of particular interest for many decades (see [244] for a review of mathematical models on the subject), as it provides an apparent contradiction to the classical competitive exclusion principle, which states that under competition for the same limiting resource only one species can survive (e.g. [88]). In broad terms, two different mechanisms that facilitate the coexistence of species in savannas have been established using mathematical modelling: resource niche differentiation and environmental disturbances. The former is based on Walter's hypothesis [234], which assumes niche differentiation into different root zones. According to this hypothesis, trees have exclusive access to water in deeper soil layers, while grasses are more efficient in their water uptake in the topsoil layer. Early modelling approaches used Walter's hypothesis to provide an explanation for the coexistence of grasses and trees in savannas [226, 232, 233].

However, empirical studies later suggested that Walter's hypothesis does not always hold in savannas so that it cannot be regarded as a universal mechanism responsible for species coexistence in water-limited ecosystems [19, 139, 178]. Modelling efforts consequently shifted towards other mechanisms, such as disturbances due to fires (e.g. [18, 201]), disturbances due to grazing and browsing (e.g. [175, 204]), asymmetric competitive effects that trees impose on grass (e.g. [213]), different competitive abilities of trees in different life stages [15, 43], or a combination thereof. The main characteristics in which existing models of the savanna biome differ are their representation of the state variables, water dynamics and disturbance occurrences. Many models (e.g. [215]) represent the plant state variables as area fraction covers, following the early model by Tilman [213]. However, to account for the fact that plant types are typically not mutually exclusive, other modelling frameworks (e.g. [17]) characterise plant variables by the plants' biomass per unit area. The

model by Tilman and many of its extensions incorporate the plant species' competition for water implicitly, but extensions (e.g. [1]) consider water dynamics explicitly in an ecohydrological framework. The occurrence of fire or grazing/browsing disturbances is described either in a probabilistic (e.g. [42]) or a deterministic sense. Models assuming the latter either provide a time-continuous (e.g. [245]), a time-discrete ([85]) or a time-impulsive ([206, 207, 242, 243]) description of the ecosystem dynamics.

Existing models describing savannas mostly use systems of ordinary differential equations or impulsive differential equations, with the spatiotemporal model for tree cover in mesic savannas by Martinez-Garcia et al. [123] being a notable exception. Such models are nonspatial and do not take into account any spatial effects that affect the plant populations. However, spatial self-organisation of plants into patterns of alternating patches of high biomass and bare soil are known to be an essential element in the survival of plants in drylands [47, 222]. The formation of patterns is usually induced by a positive feedback between local vegetation growth and water redistribution, caused, for example, by the formation of infiltration-inhibiting soil crusts that induce overland water flow towards existing biomass patches [130, 166]. A very common type of patterned vegetation is stripes that occur on sloped ground (up to 2% gradient) parallel to the terrain contours [222]. Similar to savanna ecosystems, coexistence of trees and grasses (on the level of single vegetation patches) also occurs in patterned vegetation [41, 179]. In striped vegetation, grass species are usually observed to dominate the uphill region of a stripe, while woody vegetation is more dominant towards the centre and downslope end of a stripe [41, 179].

Spatially explicit mathematical modelling using partial differential equations (PDEs) has explored different mechanisms that enable species coexistence in patterned ecosystems of dryland vegetation. For example, if a pattern-forming species and a non-pattern forming (in the absence of any competitors) species are considered, the pattern-forming species can act as an *ecosystem engineer* by altering the environmental conditions (in particular the availability of water) and thus facilitate coexistence with a non-pattern-forming species superior in its water uptake and dispersal capabilities [16, 145]. A different mechanism that provides a possible explanation for the stability of coexistence patterns is the plant species' adaptation to different soil moisture levels, using the stabilising effect of resource niche differentiation, similar to the early savanna models based on Walter's hypothesis [27, 221]. Coexistence of species in patterned form may not necessarily be observed as a stable solution of the system, but can also as a long transient, often referred to as a metastable state [63, 76] (Chapter 5). Such metastable patterns occur if the facilitative effects that cause the formation of patterns occur on a much shorter timescale than the competitive effects that yield the eventual extinction of the inferior spe-

cies. In-phase spatial patterns are not the only context in which coexistence of plant species in patterned form is studied in mathematical models of dryland ecosystems. Alternatively, coexistence of species can occur through the existence of a multitude of localised patterns of one species in an otherwise uniform solution of a competitor (homoclinic snaking) [103] in a model that assumes a trade-off between root and shoot growth and the associated competition for water and light.

Most models describing species coexistence in dryland ecosystems are extensions of either the Gilad et al. model [74, 75] or the Klausmeier model [99], which are both phenomenological single-species models that capture the formation of vegetation patterns in water-limited ecosystems. The latter in particular stands out due to its deliberately basic description of the plant-water dynamics and thus provides an excellent framework for mathematical analysis and model extensions (e.g. [10, 20, 34, 35, 61, 63, 120, 184–186, 188, 190–192, 194, 195, 197, 199, 221, 236, 237]). Other modelling frameworks that address the dynamics of vegetation patterns exist (see [21, 124] for reviews), but, to the best of our knowledge, have not been utilised to address species coexistence.

In this chapter, we introduce a spatially explicit ecohydrological PDE model to investigate the role of spatial self-organisation principles in the stable coexistence of trees and grasses on sloped terrain in savannas (Sec. 6.3). To solely focus on the effects of spatial heterogeneities caused by a pattern formation feedback, we deliberately assume that both species only differ in their basic parameters, but not in any of their functional responses. We base our model on the Klausmeier model for vegetation patterns and find stable solutions of the multispecies model in which both species coexist, representing a savanna biome. More precisely, these stable solutions are periodic in space, but, unlike in the single-species Klausmeier model, plant densities in the troughs of the pattern are not close to zero. Instead, both plant densities oscillate between two non-zero values. In Sec. 6.4 we perform a bifurcation analysis of the model to disentangle the origins of the coexistence state and establish key conditions required for the existence of coexistence patterns. We augment our results on pattern existence by an analysis of their stability in Sec. 6.5 and address the phase difference between the oscillations in both plant densities in Sec. 6.6. Our analysis is restricted to a one-dimensional space domain which is assumed to represent a sloped terrain, as the inclusion of a term describing the flow of water in the downhill direction facilitates the application of a numerical continuation method to study pattern existence and stability. We briefly comment on model solutions on a flat spatial domain in Sec. 6.7 and discuss the relevance and implications of our results. Sec. 6.8 provides an outline of the numerical continuation methods used in our bifurcation and stability analysis.

### 6.3 The model

In this section, we present the modelling framework used in this chapter to study the coexistence of plant species in water-deprived ecosystems. Our model is based on the reaction-advection-diffusion model by Klausmeier [99], which in nondimensional form reads

$$\frac{\partial u}{\partial t} = \underbrace{u^2 w}_{\text{plant growth}} - \underbrace{B u}_{\text{plant loss}} + \underbrace{\frac{\partial^2 u}{\partial x^2}}_{\text{plant dispersal}}, \quad (6.1a)$$

$$\frac{\partial w}{\partial t} = \underbrace{A}_{\text{rainfall}} - \underbrace{w}_{\substack{\text{evaporation and} \\ \text{drainage}}} - \underbrace{u^2 w}_{\substack{\text{water uptake} \\ \text{by plants}}} + \nu \underbrace{\frac{\partial w}{\partial x}}_{\substack{\text{water flow} \\ \text{downhill}}} + d \underbrace{\frac{\partial^2 w}{\partial x^2}}_{\text{water diffusion}}. \quad (6.1b)$$

The density  $u(x, t)$  denotes the dry biomass per unit area, and  $w(x, t)$  quantifies the mass of water per unit area at time  $t > 0$  at a space point  $x \in \mathbb{R}$  on a one-dimensional infinite spatial domain, on which  $x$  increases in the uphill direction if the terrain is considered to be sloped. It is assumed that rainfall is continuous and that both biomass density and water density decay due to plant mortality and water drainage and evaporation, respectively, at constant rates. The nonlinearity in the terms describing water consumption by plants and the consequential increase in biomass accounts for part of the positive feedback between local vegetation growth and the redistribution of water. Water uptake is the product of the consumer density ( $u$ ), the resource density ( $w$ ) and a term that accounts for the infiltration of water into soil layers where roots are present ( $u$ ). The latter's dependence on the biomass density stems from the plants' infiltration-enhancing soil modifications and the formation of soil crusts in regions of low biomass. Both densities undergo diffusion and water flow in the downhill direction is modelled by an advection term, if the model is considered on sloped terrain. Diffusion of water was not part of Klausmeier's original model, but is a well-established addition to account for water flow on flat terrain (e.g. [95, 199, 225, 247]). The parameters  $A$ ,  $B$ ,  $\nu$  and  $d$  are combinations of several dimensional parameters, but represent precipitation, plant mortality rate, the speed of water flow downhill and the ratio of the diffusion coefficients, respectively.

In a previous chapter (Chapter 5) [63], we have extended the single-species Klausmeier model (6.1) by separating the biomass density  $u$  into two species,  $u_1$  and  $u_2$  with differing growth and mortality rates, diffusion coefficients and water infiltration enhancement strengths. In this chapter, we follow a similar approach and analyse the two-species model, which, after a suitable nondimensionalisation (see

[63] (Chapter 5)<sup>1</sup>), is

$$\frac{\partial u_1}{\partial t} = \underbrace{wu_1(u_1 + Hu_2)}_{\text{plant growth}} - \underbrace{B_1 u_1}_{\text{plant mortality}} + \underbrace{\frac{\partial^2 u_1}{\partial x^2}}_{\text{plant dispersal}}, \quad (6.2a)$$

$$\frac{\partial u_2}{\partial t} = \underbrace{Fwu_2(u_1 + Hu_2)}_{\text{plant growth}} - \underbrace{B_2 u_2}_{\text{plant mortality}} + \underbrace{D \frac{\partial^2 u_2}{\partial x^2}}_{\text{plant dispersal}}, \quad (6.2b)$$

$$\frac{\partial w}{\partial t} = \underbrace{A}_{\text{rainfall}} - \underbrace{w}_{\text{evaporation and drainage}} - \underbrace{w(u_1 + u_2)(u_1 + Hu_2)}_{\text{water uptake by plants}} + \underbrace{\nu \frac{\partial w}{\partial x}}_{\text{water flow downhill}} + \underbrace{d \frac{\partial^2 w}{\partial x^2}}_{\text{water diffusion}}. \quad (6.2c)$$

As in (6.1),  $u_i(x, t)$ ,  $i = 1, 2$  and  $w(x, t)$  denote the respective plant densities and the water density at time  $t > 0$  and point  $x \in \mathbb{R}$ , where the space coordinate increases in the uphill direction of the sloped terrain. The modelling assumptions are identical to those in the single-species model, i.e. all three densities diffuse, where the nondimensional diffusion coefficients  $D$  and  $d$  are ratios of the respective dimensional diffusion coefficient and the diffusion coefficient of species  $u_1$ ; water flows downhill; plant loss of both species occurs at constant rates  $B_i$ ; evaporation and drainage effects reduce the water density at a constant rate; and precipitation continuously supplies the system with water at a constant rate, represented by the nondimensional precipitation parameter  $A$ . The water uptake term is composed of the total consumer density  $(u_1 + u_2)$ , the resource density  $(w)$ , and the enhancement of water infiltration caused by plants  $(u_1 + Hu_2)$ . The constant  $H$  accounts for the unequally strong effects of different plant species on the soil's permeability. Plant growth of species  $u_1$  directly corresponds to the resource consumption by  $u_1$  and thus occurs at rate  $w(u_1 + Hu_2)$ . Similarly, the biomass of species  $u_2$  increases at rate  $Fw(u_1 + Hu_2)$ , where  $F$  is the ratio of the species' water to biomass conversion coefficients. The multispecies model (6.2) is a simple extension of the single-species Klausmeier model (6.1). The plant species only differ in their parameters, with all functional responses being identical. In particular, each species satisfies the single-species model (6.1) in the absence of its competitor.

While the multispecies model (6.2) is similar to the model analysed in Chapter 5 [63], the results presented in this chapter address a solution type with applications to a fundamentally different ecosystem. In Chapter 5 [63], we focussed on species coexistence in vegetation patterns, which are characterised by a mosaic of colonised ground and bare soil. In this context, we found that coexistence can occur as a meta-

---

<sup>1</sup>The advection parameter  $\nu$  is not given in the nondimensionalisation in [63] (Chapter 5), but  $\nu = \tilde{\nu}(k_1 k_2)^{-1/2}$ , where  $\tilde{\nu}$ ,  $k_1$  and  $k_2$  are dimensional parameters describing water flow speed, diffusion of species  $u_1$  and water evaporation rate, respectively.

stable state, that is an inherently unstable state which appears as a long transient in the system. The novelty of the work presented in this study is twofold. Firstly, we address the effect of spatial interactions on species coexistence in savannas, an ecosystem in which plant cover is continuous, but not necessarily uniform. With the notable exception of [123], spatial effects on savanna ecosystems have not been considered in mathematical models before. Secondly, we are able to show that, unlike in the context of patterned vegetation considered in Chapter 5 [63], coexistence states of the multispecies model (6.2) that represent a savanna biome are stable solutions.

The model introduced in Chapter 5 [63] further includes an asymmetric direct competition term through which one species increases the mortality rate of its competitor (e.g. due to shading). However, the inclusion of such a direct competition term in either or both of the equations does not yield any qualitative differences in the results on species coexistence presented in this study (but may, in general, add to the richness of solution types in the system). Quantitative effects of direct interspecific competition include changes to the notion of the *local average fitness* of a species, but in the interest of providing a basic representation of the self-organisation principle as a coexistence mechanism, we do not consider any direct interaction between the plant species in (6.2). Instead, the two plant species only compete indirectly through the depletion of the limiting resource.

The main focus of this chapter is a description of coexistence of grass and trees or shrubs in water-deprived ecosystems. Thus, we henceforth consider  $u_1$  to be a herbaceous species and  $u_2$  to be of woody type. This assumption allows for qualitative statements on the parameters in the system. For example, mortality rates can be inferred from the lifespan of a species. The difference in the typical lifespans of grasses and trees yields that grasses die at a faster rate ( $B_1 > B_2$ ) [1]. Similarly, plant growth parameters can be deduced from the time necessary for a plant population to reach its equilibrium density. Grasses require significantly shorter periods to attain steady steady state biomass levels than trees, which suggests that grasses are superior in their water-to-biomass conversion ( $F < 1$ ) [1]. If other system parameters are known, the strength of a plant species' enhancement of water infiltration into the soil can be estimated from its equilibrium density [99]. As steady state biomass densities for tree species are in general much higher than those of grass species in dryland ecosystems, this yields that grasses cause a larger increase in soil permeability per unit biomass than trees ( $H < 1$ ) [125]. The plant species' diffusion coefficients relate the spatial spread of vegetation with time. The longer generation time of trees suggests slower dispersal of trees ( $D < 1$ ).

All our parameter estimates are based on previous modelling studies (e.g. [99, 199]), as there is a lack of empirical data that would allow for an accurate parameter estimation. However, all our assumptions on parameter differences between tree and

grass species are in agreement with parameter estimates in previous multispecies models (e.g. [16, 75]). Unless otherwise stated, we set  $B_1 = 0.45$ ,  $B_2 = 0.0486$ ,  $D = 0.109$ ,  $F = 0.109$ ,  $H = 0.109$ ,  $\nu = 50$  and  $d = 500$ .

## 6.4 Existence and onset of patterns in which species coexistence occurs

In this section, we discuss the existence of solutions of (6.2) in which both species coexist. Such solutions are periodic travelling waves, i.e. spatially periodic solutions that move in the uphill direction of the domain at a constant speed. Numerical continuation shows that the branches of periodic travelling waves, in which both plant species are strictly positive, terminate at a single-species pattern at either end. The key ingredient in understanding the onset and existence of coexistence states is information on the single-species patterns' stability. An investigation of the essential spectrum of the single-species pattern reveals that bifurcations to coexistence states occur as a single-species pattern loses/gains stability to the introduction of its competitor.

### 6.4.1 Stability of spatially uniform equilibria

The starting point of our bifurcation analysis is the equilibrium states in a spatially uniform setting. Depending on the level of precipitation, the multispecies model (6.2) has up to five spatially uniform steady states: a trivial desert steady state  $(0, 0, \bar{w}^D) = (0, 0, A)$  which exists and is stable in the whole parameter space; a pair of single-species grass equilibria  $(\bar{u}_1^{G,\pm}, 0, \bar{w}^{G,\pm})$  that exist for sufficiently high rainfall volumes  $A > A_{\min}^G$ ; and a pair of single-species tree states  $(0, \bar{u}_2^{T,\pm}, \bar{w}^{T,\pm})$  that exist for  $A > A_{\min}^T$ . In both cases, the pair of single-species equilibria meet in a fold at their respective existence thresholds, and the lower branches, here denoted by a minus sign in the superscripts, are unstable. The remaining single-species grass equilibrium  $(\bar{u}_1^{G,+}, 0, \bar{w}^{G,+})$  is linearly stable to spatially uniform perturbations if  $B_2 - FB_1 > 0$  and  $B_1 < 2$ , while the tree steady state  $(0, \bar{u}_2^{T,+}, \bar{w}^{T,+})$  is linearly stable to spatially homogeneous perturbations if  $B_2 - FB_1 < 0$  and  $B_2 < 2$ . [63] (Chapter 5). Parameter estimates consistently imply that plant mortality is sufficiently low to assume  $B_i < 2, i = 1, 2$ .

These two stability criteria emphasise the critical role of the quantity  $B_2 - FB_1$  in the system, as  $B_2 - FB_1 = 0$  is a separatrix of the stability regions of the single species equilibria in the spatially uniform setting. We thus refer to  $B_2 - FB_1$  as the *average fitness difference* between the two species, because its sign determines the single-species state to which the system converges in the absence of any spatial interactions (provided the precipitation level  $A$  is sufficiently high). In dimensional parameters, the average fitness of a species in the model is the ratio between its

water-to-biomass conversion capabilities (growth rate) and its mortality rate [63] (Chapter 5).

#### 6.4.2 Single-species patterns

If spatial interactions are included, the multispecies model (6.2) admits single-species patterns that move in the uphill direction of the domain at a constant speed. Such regularly patterned solutions moving through the spatial domain are classified as periodic travelling waves, an important solution type for reaction-advection-diffusion equations and other partial differential equations. Periodic travelling waves can be represented by a single variable  $z = x - ct$  only, where  $c \in \mathbb{R}$  is the migration speed of the periodic solution, and  $u_1(x, t) = U_1(z)$ ,  $u_2(x, t) = U_2(z)$  and  $w(x, t) = W(z)$ . This coordinate transformation reduces the PDE system (6.2) to the corresponding travelling wave ODE system

$$WU_1(U_1 + HU_2) - B_1U_1 + c\frac{dU_1}{dz} + \frac{d^2U_1}{dz^2} = 0, \quad (6.3a)$$

$$FWU_2(U_1 + HU_2) - B_2U_2 + \frac{dU_2}{dz} + D\frac{d^2U_2}{dz^2} = 0, \quad (6.3b)$$

$$A - W - W(U_1 + U_2)(U_1 + HU_2) + (c + \nu)\frac{dW}{dz} + d\frac{d^2W}{dz^2} = 0. \quad (6.3c)$$

Patterned solutions of the PDE system (6.2) correspond to limit cycles of (6.3). In the PDE setting of (6.2), we would typically investigate the interval of a given control parameter, here the precipitation parameter  $A$ , in which patterned solution exist. Moreover, the transformation to the comoving frame introduces an additional parameter: the migration speed  $c$ . If a patterned solution of (6.2) exist for a given set of the PDE parameters, limit cycles of (6.3) exist for a range of values of the migration speed  $c$ . We thus need to consider a pattern forming region in the  $(A, c)$  parameter plane, instead of an interval of  $A$  only.

The existence of single-species patterns is examined using the numerical continuation software AUTO-07p [53] and form part of the bifurcation diagrams visualised in Fig. 6.3. In particular, since the multispecies model (6.2) reduces to the single-species Klausmeier model (6.1) in the absence of one of the species, the bifurcation structure of the system's single-species states is identical to that of the single-species Klausmeier model. More precisely, the pair of spatially uniform single-species grass equilibria  $(\bar{u}_1^{G,\pm}, 0, \bar{w}^{G,\pm})$  meet in a fold. In the spatial model, the branch stable to spatially uniform perturbations loses its stability at a Turing-Hopf bifurcation. This is the onset locus of the single-species pattern. A multitude of stable and unstable patterned states at different wavelengths and migration speeds exist (only

one solution branch is shown in the bifurcation diagrams 6.3), which all originate at a Hopf-bifurcation and terminate in a homoclinic orbit as the control parameter  $A$  is decreased [194]. Due to the symmetry in the model, identical considerations hold true for the single-species tree states.

### 6.4.3 Multispecies patterns

Even though there is no spatially uniform equilibrium in which both plant species coexist, numerical simulations of the full system (Fig. 6.1) suggest the existence of stable patterned solutions of (6.2) in which species coexistence occurs. Such solutions also move in the uphill direction, but are distinctly different from the single-species patterns that occur in both the single-species Klausmeier model (6.1) and the multispecies model (6.2). In single-species patterned solutions, the plant density oscillates between a high level of biomass and a biomass level close to zero (Fig. 6.6 (a) and (b)). Ecologically, such solutions represent a transect of a striped vegetation pattern in which patches of high biomass alternate with regions of bare soil. By contrast, in the multispecies patterns, both plant densities oscillate between two nonzero levels (Fig. 6.1 and Fig. 6.6 (c) and (d)). In this solution type, there are no patches devoid of biomass, as occurs in a savanna ecosystem.

### Onset of multispecies patterns

Branches of single-species periodic travelling waves originate from bifurcations of the spatially uniform equilibria. Further bifurcations may occur along those solution branches, and these are the origin of other solution branches in which both plant species coexist (with non-negative densities) in a patterned state. An insight into the onset of these coexistence patterns is gained through a stability analysis of the single-species patterns in both the single-species Klausmeier model (6.1) and the multispecies model (6.2). The stability of a periodic travelling wave can be determined through a calculation of its essential spectrum.

The essential spectrum  $\mathcal{S} \subset \mathbb{C}$  of a periodic travelling wave solution determines the leading order behaviour of small perturbations to the periodic travelling wave. Since periodic travelling waves are translation invariant, the origin is always part of the essential spectrum. Hence, the origin is excluded from the following definition of stability. If the essential spectrum lies entirely in the  $\Re(\lambda) < 0, \lambda \in \mathbb{C}$  half-plane, then the periodic travelling wave is spectrally stable, otherwise it is spectrally unstable. The essential spectrum can be calculated using the numerical continuation method by Rademacher et al. [160] and we provide a brief outline of how the method is applied to (6.3) in Sec. 6.8.

To understand the onset of coexistence patterns, the essential spectrum of a

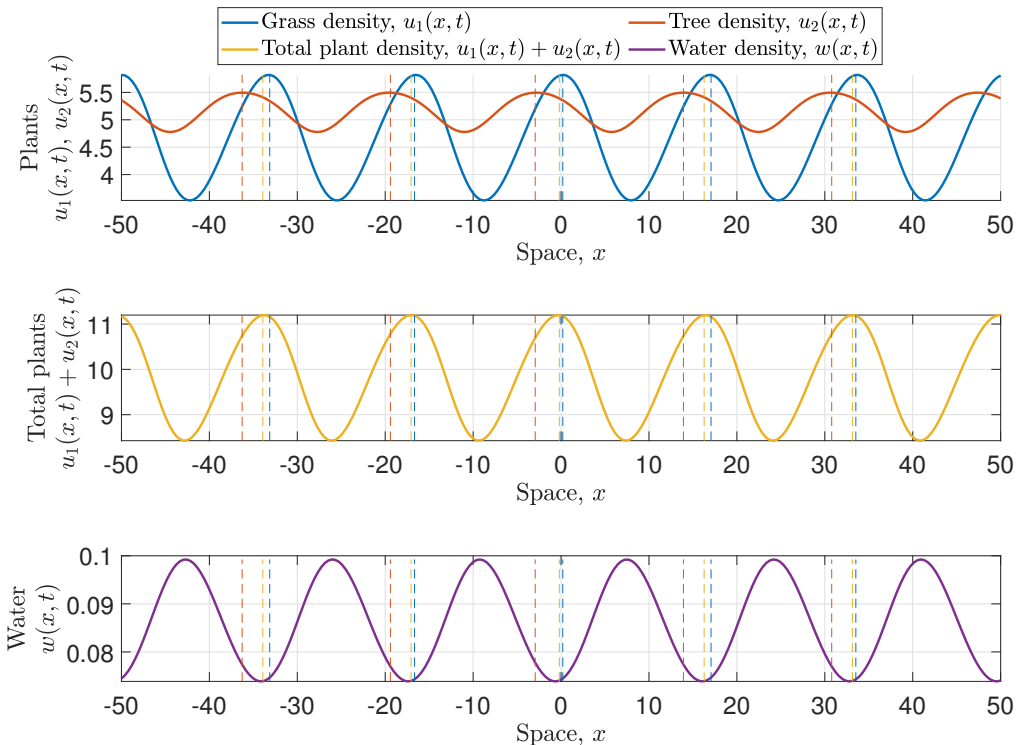


Figure 6.1: Numerical simulation of the multispecies model. This figure shows a typical patterned solution of (6.2) in which both species coexist. The red, blue and yellow vertical lines indicate the location of local minima of the grass density  $u_1$ , the tree density  $u_2$  and the total plant density  $u_1 + u_2$  respectively, and highlight that the total plant density and the water density are antiphase, as well as the existence of a phase difference between the plant patterns. The solution is obtained through a numerical simulations with precipitation parameter  $A = 4.5$ .

given pattern in the single-species Klausmeier model (6.1) is compared with that of the same single-species solution of the multispecies model (6.2) (Fig. 6.2). The spectrum of the pattern in the multispecies model includes additional components that describe the behaviour of perturbations in the plant type absent in the single species pattern. The bifurcation to the coexistence patterns occurs where the single species pattern loses stability to the introduction of the competitor species. This does not necessarily correspond to a stability change of the single species pattern, since it may be unstable in the single-species model either side of the bifurcation. In more formal words, if  $\mathcal{S}_1$  denotes the spectrum of a single-species pattern in the single-species model (6.1) (Fig. 6.2a) and  $\mathcal{S}_2$  denotes the spectrum of the same solution in the multispecies model (6.2) (Fig. 6.2b), then  $\mathcal{S}_1 \subset \mathcal{S}_2$  and the bifurcation to the coexistence pattern occurs as  $\max\{\Re(\lambda) : \lambda \in \mathcal{S}_2 \setminus \mathcal{S}_1\} = 0$ , i.e. as  $\mathcal{S}_2 \setminus \mathcal{S}_1$  crosses the imaginary axis  $\Re(\lambda) = 0$  (Fig. 6.2c). Due to the symmetry in the model, these considerations hold for both species in the model.

The coexistence solution branches either connect both single-species solution branches or connect two bifurcations along the same single-species pattern branch. However, coexistence patterns do not originate or terminate at these bifurcations. Instead, the plant density which is zero at the bifurcation changes its sign and the coexistence solution branch continues beyond the bifurcation but is biologically irrelevant (not shown in Fig. 6.3). We henceforth use *coexistence pattern* to describe those with positive densities in both species only, and with a slight abuse of terminology refer to the branching points along the single species pattern solution branches as their *origins* or *termini*. The exception to the considerations detailed above is large migration speeds  $c$ , for which only one of the single-species pattern exists. In this case, the branch of patterned coexistence solutions terminates in a homoclinic orbit.

### Existence of multispecies patterns

A critical requirement for the existence of coexistence patterns is a sufficiently slow (compared to its competitor) growth rate of the species with superior average fitness. If  $B_2 - FB_1 < 0$  ( $u_2$  has higher average fitness) then coexistence patterns of a fixed migration speed  $c$  only occur if  $F$  is below a critical threshold  $F_{\text{exist}}$ . A second significant change of the bifurcation structure occurs at  $F = F_{\text{split}} < F_{\text{exist}}$ , at which the precipitation interval in which coexistence patterns occur is split into two disjoint intervals. Assuming that the average fitness difference  $B_2 - FB_1$  and the migration speed  $c$  are kept constant, changes to the system's bifurcation structure under increases in  $F$  (and associated decreases in  $B_2$ ) can be characterised as follows (Fig. 6.3):

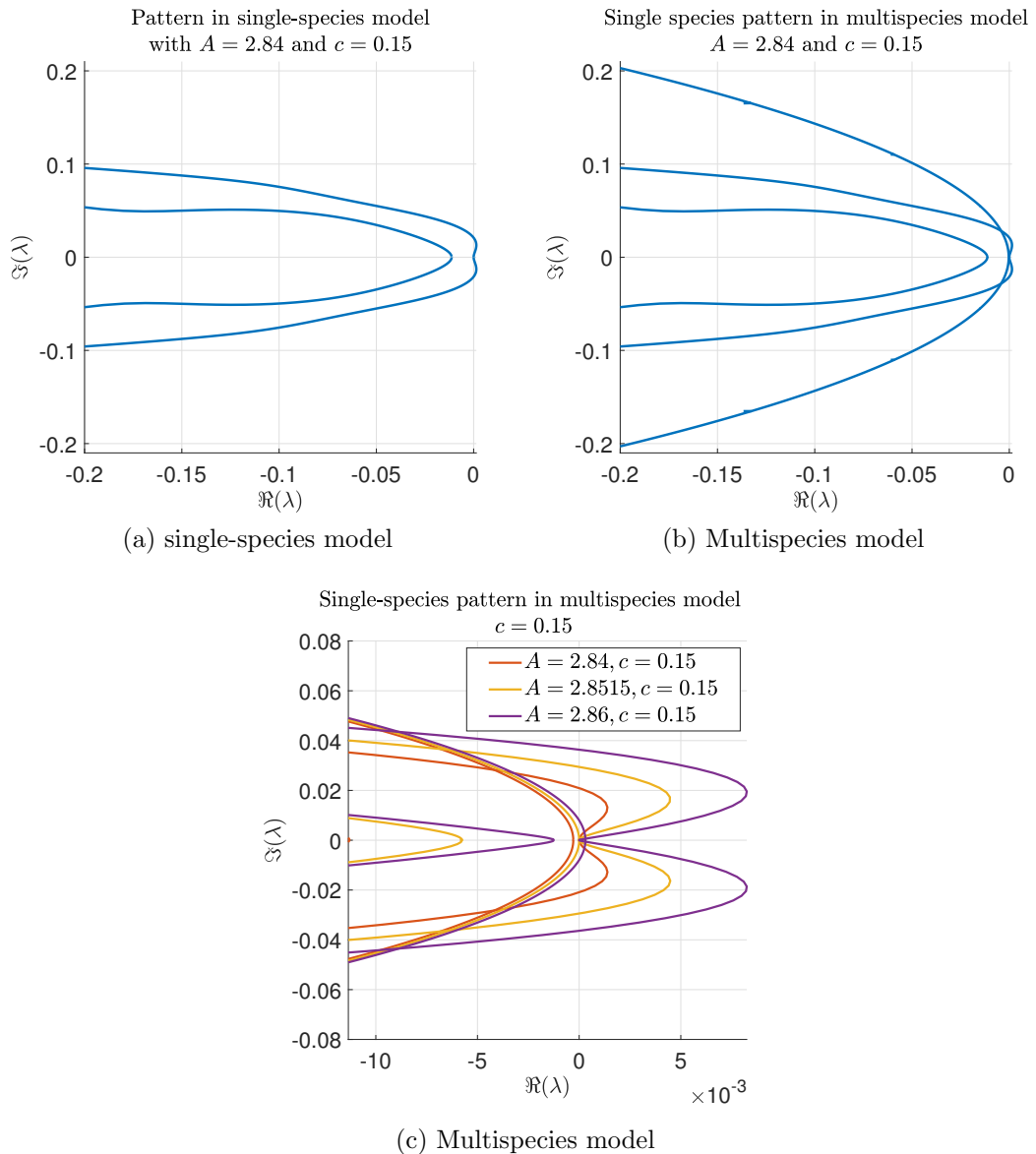


Figure 6.2: Spectra of single-species patterns. The visualisations in (a) and (b) compare the spectrum of a patterned solution in the single-species Klausmeier model to that of the identical periodic travelling wave in the multispecies model. The pattern's spectrum in the single-species model is a subset of its the pattern's spectrum in the multispecies model, as the latter contains additional components corresponding to perturbations in the plant density absent in the single species pattern. In (c), the spectra of a single-species pattern in the multispecies model is shown around the origin for different values of the precipitation parameter  $A$  (either side of and at the bifurcation to the multispecies pattern) to visualise that the bifurcation to coexistence patterns occurs as the single-species loses/gains stability to the introduction of a second species.

$F \ll F_{\text{split}}$ : For sufficiently small  $F$ , there is only one branch of periodic travelling waves in which both species coexist, which connects branching points on either branch of the single species patterns (Fig. 6.3 (a)).

$F \approx F_{\text{split}}$  **and**  $F < F_{\text{split}}$ : As the growth rate ratio  $F$  is gradually increased, a second pair of branching points moves along each of the single species pattern branches from the homoclinic solution towards the Turing-Hopf bifurcation and a second branch of coexistence patterns connects both branching points (Fig. 6.3 (b)).

$F_{\text{split}} < F < F_{\text{exist}}$ : A further increase of  $F$  causes a significant change in the bifurcation structure. At the critical threshold  $F = F_{\text{split}}$  both coexistence solution branches coincide for some precipitation level. For  $F > F_{\text{split}}$  the origins and termini of the solution branches are exchanged and each solution branch connects both branching points on the same single species pattern branch (Fig. 6.3 (c)). This breaks up the existence interval of the coexistence solutions into the union of two disjoint intervals.

$F \approx F_{\text{exist}}$  **and**  $F < F_{\text{exist}}$ : Further increases of  $F$  increase the gap between the existence intervals and consequently reduce the size of the existence region (Fig. 6.3 (d)). Increases in  $F$  also reduce the distance between both branching points along the single species branch, until they meet in a fold at a threshold  $F = F_{\text{exist}}^{(i)}$ ,  $i = 1, 2$ , where  $F_{\text{exist}}^{(1)}$  and  $F_{\text{exist}}^{(2)}$  may differ and depend on other parameters in the model, in particular the diffusion rate ratio  $D$ .

$F > F_{\text{exist}}$ : For  $F > F_{\text{exist}}^{(i)}$ , no branching points along the respective single species pattern branch exist. For the species of inferior average fitness ( $u_1$ ) this is due to the instability of the single-species pattern to the introduction of the second species  $u_2$  caused by the combination of the competitor's higher average fitness and sufficiently fast growth rate. In terms of the essential spectrum, this is characterised by the subset  $\mathcal{S}_2 \setminus \mathcal{S}_1$  of the essential spectrum of the single-species pattern, which always extends into the  $\Re(\lambda) > 0$  half-plane, i.e.  $\max\{\Re(\lambda) : \lambda \in \mathcal{S}_2 \setminus \mathcal{S}_1\} > 0$  along the whole solution branch if  $F > F_{\text{exist}}^{(1)}$ . Vice versa,  $\max\{\Re(\lambda) : \lambda \in \mathcal{S}_2 \setminus \mathcal{S}_1\} < 0$  for the species of higher average fitness ( $u_2$ ) along the branch of single species pattern, if  $F > F_{\text{exist}}^{(2)}$ , corresponding to the pattern's stability to the introduction of  $u_1$ . Thus, patterned solutions in which both species coexist cease to occur at  $F = F_{\text{exist}} := \max\{F_{\text{exist}}^{(i)}\}$ . The level of  $F_{\text{exist}}$  depends on the dispersal behaviour of both plant species and increases monotonically with  $|\log(D)|$ . In particular, if  $D = 1$ , i.e. the species' diffusion coefficients are equal,  $F_{\text{exist}} = F_{\text{exist}}^{(1)} = F_{\text{exist}}^{(2)} = 1$  and coexistence patterns cease to occur if both species growth rates are equal.

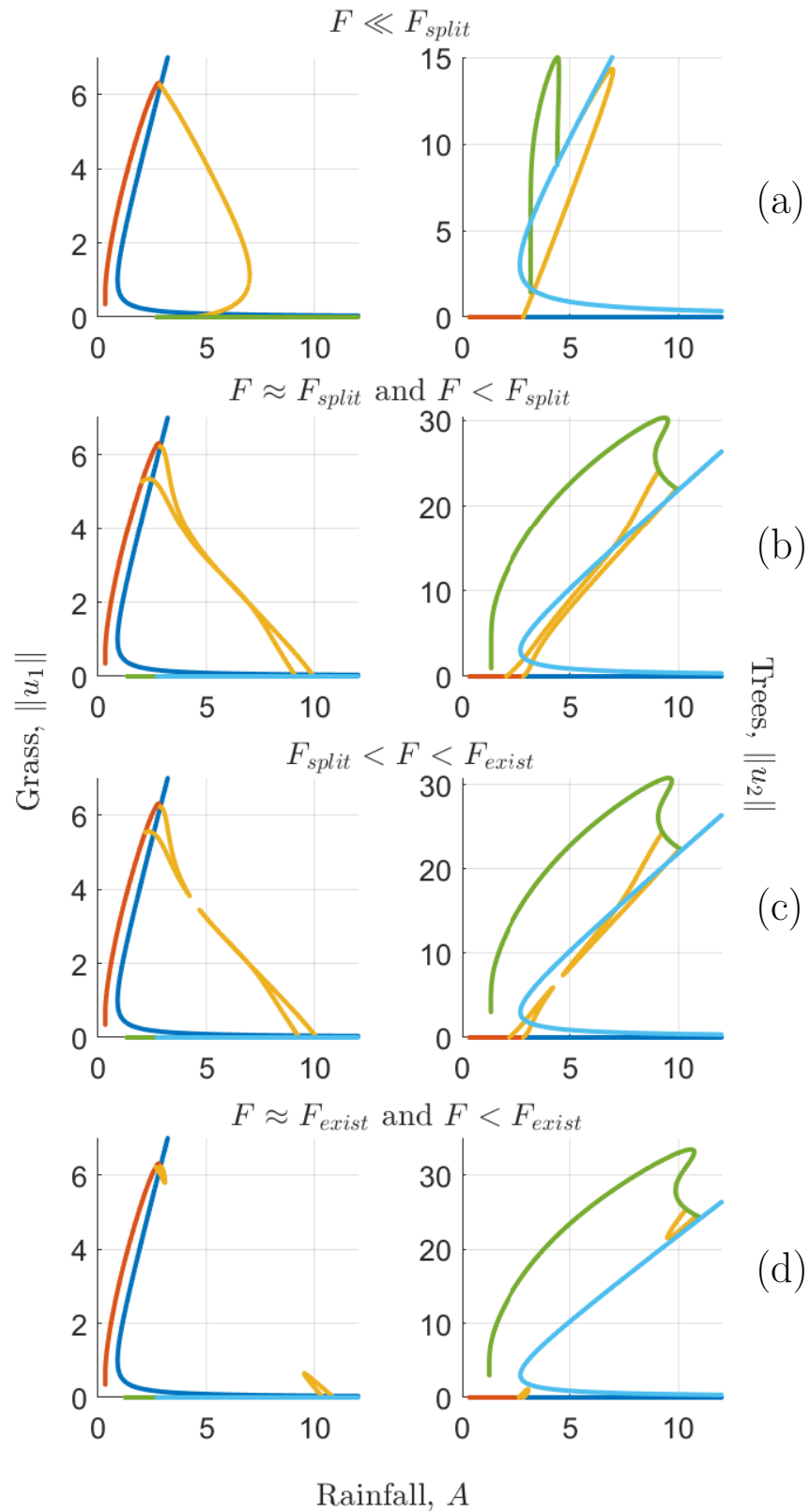


Figure 6.3: Bifurcation diagrams under varying growth rate ratio  $F$  and constant average fitness. The full figure caption and legend are displayed overleaf.

	uniform $u_1$
	uniform $u_2$
	single species pattern $u_1$
	single species pattern $u_2$
	coexistence pattern $u_1, u_2$

Figure 6.3 (cont.): Overleaf, bifurcation diagrams for a number of different values of  $F$  and  $B_2$ , keeping the average fitness difference  $B_2 - FB_1 < 0$  constant, are shown. For sufficiently small  $F$ , i.e. a sufficiently slow growth rate of the species of higher average fitness, only one branch of coexistence patterns occurs (a). Increases in  $F$  cause the appearance of a second branch (b), before the precipitation interval in which patterns exist is split into two (c). Further increases of  $F$  reduce the size of the parameter region in which coexistence patterns occur (d), before the coexistence state ceases to exist as  $F$  passes through a critical threshold (not shown). Solution branches of patterned states are only shown for fixed migration speed  $c = 0.15$  and no stability information is shown. The chosen values of the growth rate ratio  $F$  are  $F = 0.109$  (in (a)),  $F = 0.73$  (in (b)),  $F = 0.7543$  (in (c)) and  $F = 0.9$  (in (d)). Note the difference to the bifurcation diagrams presented in Fig. 6.4, in which only  $B_2$  is varied and the average fitness difference undergoes changes.

The crucial role of the balance between the average fitness difference  $B_2 - FB_1$  and the growth rate ratio  $F$  is further emphasised by an analysis of the bifurcation structure under changes to the average fitness difference if the growth rate ratio  $F$  is fixed. If  $B_2 - FB_1 < 0$  and  $F$  is sufficiently small, i.e.  $u_2$  has superior average fitness but a slower growth rate than  $u_1$ , then coexistence pattern occur, as outlined above (Fig. 6.5 (a)). If the average fitness is gradually increased, the branching points, at which the coexistence patterns originate, move along the single species branch towards the Turing-Hopf bifurcation and cease to exist at  $B_2 - FB_1 = 0$  (Fig. 6.5 (b)). Hence, no coexistence patterns occur if the faster growing species has superior average fitness (Fig. 6.5 (c)). In terms of the essential spectrum of the single-species pattern, this is because  $\mathcal{S}_2 \setminus \mathcal{S}_1$  does not extend into the  $\Re(\lambda) > 0$  half-plane for any precipitation levels. This corresponds to the pattern's stability to the introduction of a competitor with slower growth rate and inferior average fitness.

Moreover, the amplitudes of all densities in the coexistence pattern tend to zero as  $B_2 - FB_1 \rightarrow 0$ . In other words, the coexistence pattern approaches a spatially uniform state as the average fitness difference tends to zero. If a coexistence pattern is a stable solution of (6.2) for  $B_2 - FB_1 < 0$  (but see Sec. 6.5 for more details on stability), then it automatically loses its stability at  $B_2 - FB_1 = 0$  as no coexistence equilibrium state is admitted for  $B_2 - FB_1 > 0$ . The further evolution of such a solution as  $B_2 - FB_1 > 0$  was addressed in Chapter 5 [63] for a slightly different model. Those differences (flat ground instead of sloped terrain and an additional

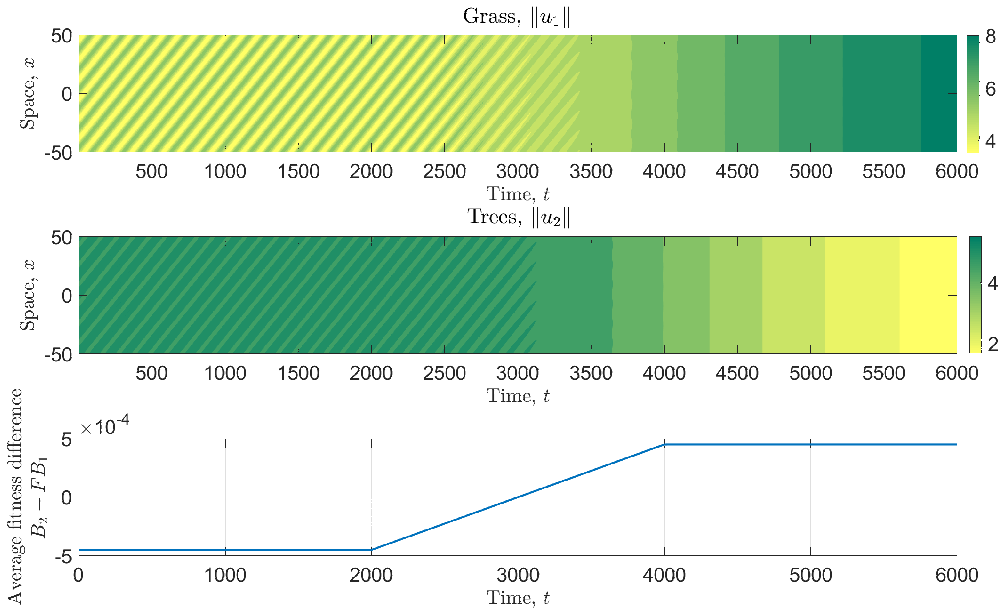


Figure 6.4: Behaviour of a solution as the average fitness difference changes its sign. This illustration shows the decrease in solution amplitudes of a patterned solution of (6.2) in which both species coexist, as the average fitness difference  $B_2 - FB_1$  gradually tends to zero from below. At  $B_2 - FB_1 = 0$  the solution loses its stability, but no rapid regime shift to a stable single-species state occurs. Instead, both species continue to coexist in a spatially uniform metastable state. The precipitation parameter used in the simulation is  $A = 4.5$ . The average fitness difference is changed by variations in  $B_2$  only.

term accounting for an asymmetric interspecific competition), however, do not qualitatively affect the relevant results presented here. If the average fitness difference  $B_2 - FB_1 > 0$  remains sufficiently small, then coexistence of both plant species occurs as a metastable state. A metastable solution is a long transient state which eventually converges to a stable single-species state. Hence, a coexistence solution of (6.2) remains in a coexistence state for a significant amount of time after it ceases to exist at  $B_2 - FB_1 = 0$ , provided that  $B_2 - FB_1 \ll 1$  (see Fig. 6.4).

## 6.5 Stability of coexistence pattern

The analysis presented in the previous section provides an insight into the existence of patterned coexistence solutions of (6.2). Ecologically, however, it is key to gain an understanding of the stability of such solutions. In Sec. 6.4, we investigated pattern onset and existence for fixed migration speed  $c$ . In this section, however, we present stability (and existence) results in the whole  $(A, c)$  plane to gain a comprehensive understanding of a pattern's behaviour under changes of the precipitation parameter  $A$ .

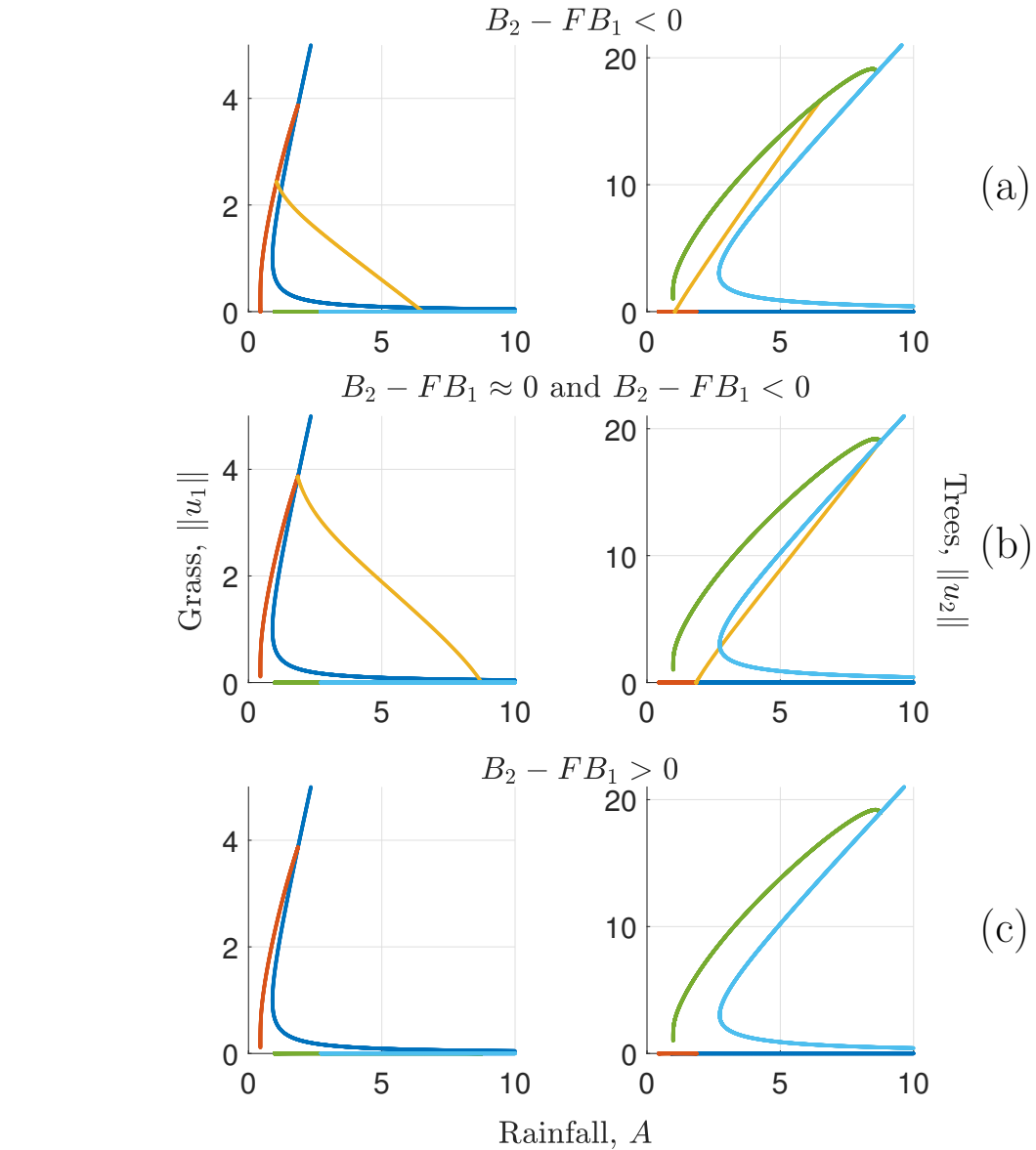


Figure 6.5: Bifurcation diagrams under changing average fitness difference. Bifurcation diagrams for different values of the average fitness difference  $B_2 - FB_1$  are shown. As the average fitness difference increases, the origin of coexistence patterns moves along the single species pattern branches towards the Hopf bifurcation at which the single-species pattern originate. No coexistence pattern occur for  $B_2 - FB_1 > 0$ . The average fitness difference is varied by changes in  $B_2$ . Plant mortality of the tree species is  $B_2 = 0.0486$  (in (a)),  $B_2 = 0.04904$  (in (b)) and  $B_2 = 0.04906$  (in (c)). Note the difference to the bifurcation diagrams shown in Fig. 6.3, in which both  $F$  and  $B_2$  are varied to keep the average fitness difference constant.

The (in)stability of a pattern with given precipitation level  $A$  and migration speed  $c$  can be determined through a calculation of its essential spectrum. To avoid the computationally expensive calculation of a large number of essential spectra on a fine grid in the  $(A, c)$  parameter plane, an extension of the numerical continuation method by Rademacher et al. [160, 189] can be used to trace stability boundaries in parameter space (see Sec. 6.8 and [160, 189] for more details). Stability changes of periodic travelling waves under variations of either the PDE parameters or the migration speed  $c$  can be classified into two types [159]. A stability change of Eckhaus (sideband) type is characterised by a sign change of the curvature of the spectrum at the origin, which is always part of the spectrum due to translation invariance of periodic travelling waves. If instead a pair of folds in the essential spectrum crosses the imaginary axis with nonzero real imaginary part, then the stability change is said to be of Hopf type. Tracing both Eckhaus and Hopf stability boundaries allows us to create a map of stability in the  $(A, c)$  plane, often referred to as the *Busse balloon* [26]. Such a Busse balloon for the coexistence patterns in (6.2) is shown in Fig. 6.7, where it is embedded into the solution type's existence region. The boundaries for pattern existence in the  $(A, c)$  are also obtained by numerical continuations of pattern onset loci and folds along the solution branches. Note that due to the existence of folds in the solution branches of coexistence patterns, an  $(A, c)$  pair does not necessarily uniquely define a member of the coexistence pattern solution family. However, our stability analysis indicates that if more than one periodic travelling wave solution of (6.2) exists for a given  $(A, c)$  pair, then only a maximum of one of the solutions is stable. For simplicity, we make no distinction between  $(A, c)$  pairs that uniquely define a stable pattern and parameter values for which additional unstable patterns exist in our definition of the Busse balloon. Hence, a pair  $(A, c)$  is a member of the stability region in the visualisations (Fig. 6.7 and 6.8), even if additional unstable patterns exist.

A crucial ecological aspect of patterned solutions of (6.2) is their behaviour as they become unstable due to changes in precipitation. To gain some information on the evolution of a solution under changing rainfall, it is instructive to superimpose wavelength contours on the stability diagram (Fig. 6.7). Given a stable pattern with given wavelength  $L$ , the solution follows the wavelength contour if the precipitation parameter is varied, until it reaches a stability boundary. Unlike in previous work on pattern stability in ecological systems [20, 44], we do not observe any qualitative differences between the effects of an instability caused by crossing an Eckhaus boundary and a destabilisation that occurs after a stability boundary of Hopf type is crossed. As the stability boundary is crossed, a new wavelength is selected. Significantly, wavelength selection for the coexistence patterns differs from that of both single species patterns. In the case of a single-species solution,

a decrease of precipitation across a stability boundary causes a switch to a higher wavelength pattern, increasing the size of the gaps of bare ground between the vegetation stripes (Fig. 6.6(a) and (c)). Conversely, a destabilisation of a coexistence pattern due to decreasing precipitation causes the selection of a shorter wavelength pattern (Fig. 6.6(b) and (d)). To understand this difference, it is worth recalling a key difference between the two solution types. The troughs of single species patterns in (6.2) attain values close to  $u_i = 0$  and represent alternating areas of high biomass and bare ground regions, while the coexistence patterned solutions oscillate between two nonzero biomass levels, corresponding to a savanna-like state. The selection of a smaller wavelength in the coexistence pattern for decreasing precipitation is associated with a simultaneous decrease of the relative pattern amplitude  $(\max u_i - \min u_i)/\|u_i\|$ ,  $i = 1, 2$  in both species. A reduction in the relative amplitude allows for a compensation of the higher density of vegetation peaks associated with a shorter wavelength to achieve the overall reduction in biomass caused by a decrease in the rainfall parameter  $A$ .

A second key difference between coexistence and single-species patterns in the system is the patterns' migration speed close to stability boundaries for decreasing precipitation  $A$ . Single-species patterns experience a decrease in their migration speed  $c$  before a destabilisation due to decreasing rainfall occurs. This behaviour is an example of a warning sign of an imminent deterioration of the ecosystem that may be used in predicting regime shifts towards desert in water limited ecosystems [39, 45, 78, 96, 164, 170]. Such a reduction in uphill movement is not in general observed for patterned solutions in which both species coexist. Depending on a pattern's wavelength, its migration speed may be increasing or decreasing as the wavelength contour passes through a stability boundary and no clear parametric trends of the uphill movement of the pattern close to a wavelength change can be deduced.

A further significant result obtained from a comparison of stability regions for the three patterned solution types in (6.2) is that key features of the coexistence pattern, such as its wavelength and migration speed, are dominated by and very similar to those of the single-species pattern of the species with faster growth rate (Fig. 6.8). Moreover, if  $F$  is sufficiently small, i.e. the species with higher average fitness is growing sufficiently slowly, the Busse balloon of the coexistence patterns and the single-species patterns of the fast-growing species do not overlap, as coexistence patterns are stable for precipitation levels that are higher than those in which the single-species patterns are stable. By contrast, the rainfall levels in which coexistence patterns are stable and the single-species patterns of the slow growing species are stable in the context of the single-species model, overlap. An important implication of this is a facilitative effect of the fast growing species on the species with a slower

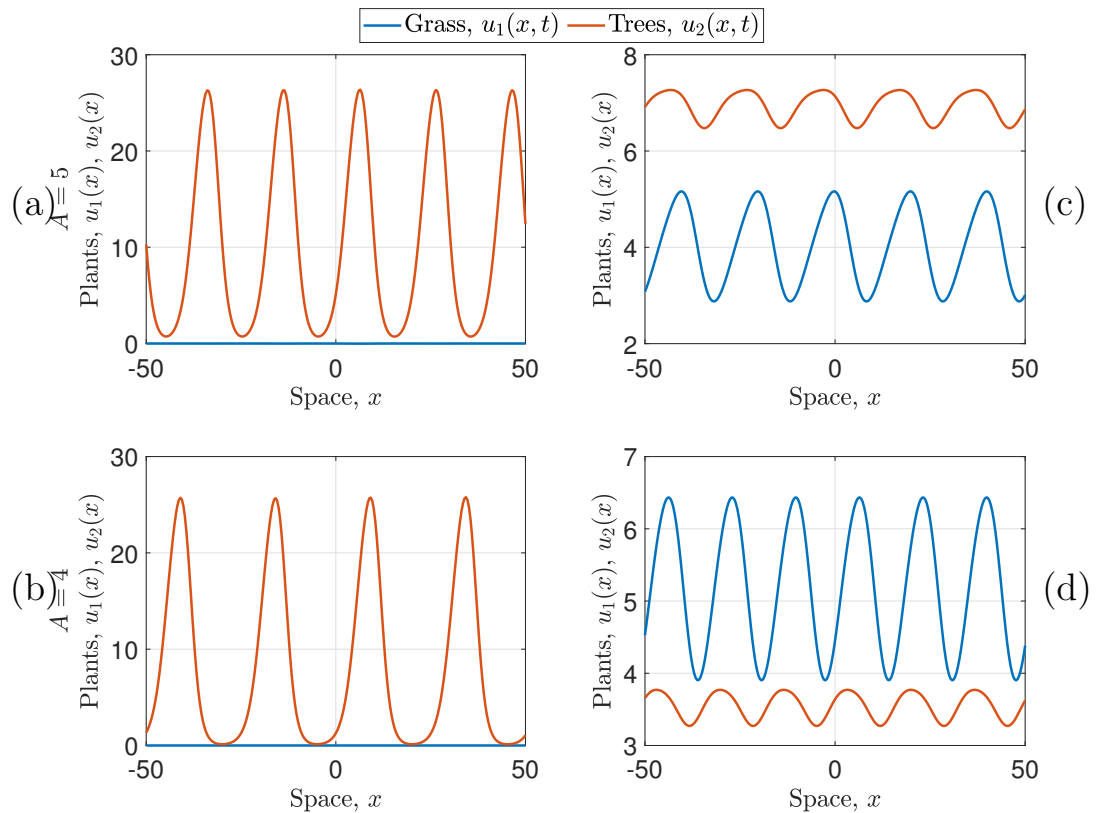


Figure 6.6: Wavelength changes due to decreasing precipitation. Single-species patterns ((a) and (c)) and multispecies patterns ((b) and (d)) are shown for different precipitation levels to visualise the difference in the wavelength selection at destabilisations due to decreasing rainfall. The first row shows stable patterns for  $A = 5$ . As  $A$  is gradually decreased to  $A = 4$ , both patterns lose their stability. The single-species pattern ((a) and (c)) selects a solution of higher wavelength, while the multispecies pattern ((b) and (d)) assumes a pattern of lower wavelength.

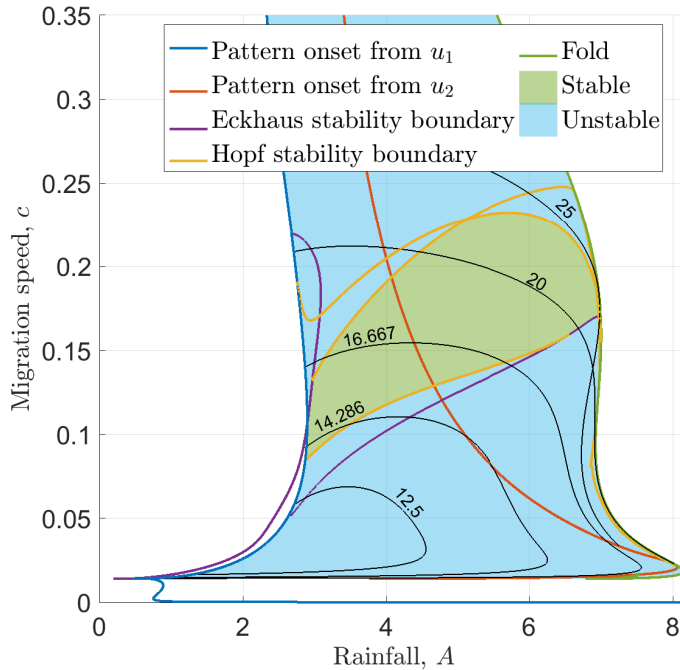


Figure 6.7: Existence and stability of coexistence patterns. The Busse balloon (parameter region of stable patterns) of patterned solutions of (6.2) in which both species coexist is shown embedded in the existence regions of such solutions in the  $(A, c)$  parameter plane. Existence and stability boundaries are computed using the numerical continuation methods outlined in Sec. 6.8. Wavelength contours are visualised using black solid lines. Note that stability boundaries may extend into regions that are neither marked as stable nor unstable, since biologically irrelevant coexistence patterns with negative densities occur outside the shaded parameter region.

growth rate. More precisely, there exist precipitation levels in which, in the absence of a second species, the slow growing species assumes a patterned state with  $u_2$  close to zero in the troughs of the pattern, but in which also coexistence patterns are stable. Hence, while  $\min u_2 \ll \|u_2\|$  in the absence of a competitor,  $\min u_2 \approx \|u_2\|$  if a faster growing species is present in the system. Thus,  $u_2$  can attain relatively high densities throughout the whole domain, if it coexists with a faster growing species, instead of appearing as an oscillation between a high density and a biomass level close to zero. This facilitative effect is a case of *ecosystem engineering*, a term coined to describe changes to environmental conditions caused by a species that creates a habitat for other species [93].

## 6.6 Phase difference

A striking feature of periodic travelling wave solutions of (6.2) in which both species coexist (see e.g. Fig. 6.1) is a slight phase difference between the oscillations of the

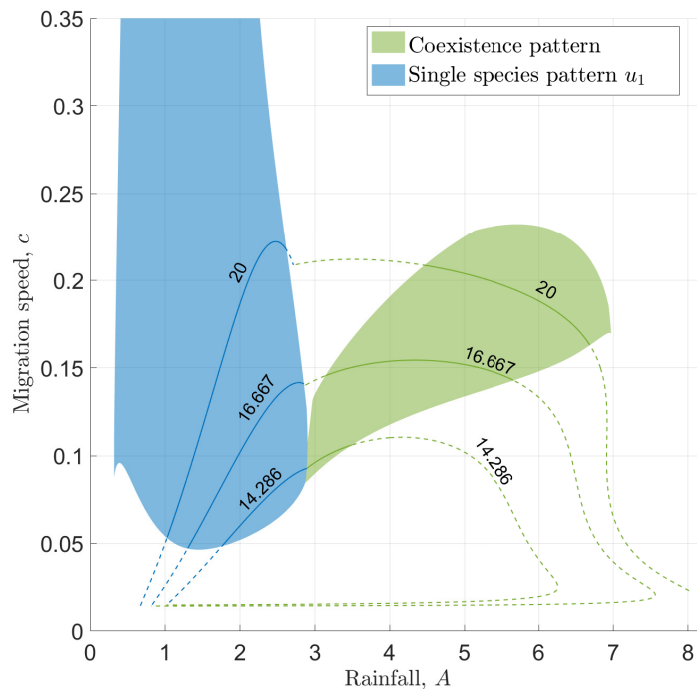


Figure 6.8: Busse balloons of patterns in the system. This figure visualises the Busse balloons (regions of stable patterns) for the coexistence patterns and the single species grass patterns that occur as solutions of (6.2). For the parameter values chosen in this visualisation, patterns of  $u_2$  are always unstable. Wavelength contours are given as solid lines, and their colour indicates the solution type they represent. Solid lines correspond to stable solutions (inside the respective Busse balloon), dashed lines to unstable patterns.

two plant species. All model parameters affect the slight shift in the solution profile, but the ratio of the plant species' diffusion coefficients  $D$  is found to play the most significant role, as it determines which plant species has higher biomass in the uphill direction.

In the one-species Klausmeier model, the plant density and water density of a patterned solution are typically antiphase (i.e. the peaks in the plant density are at the same locations as the troughs of the water density and vice versa) [98, 186]. Similarly, in the multispecies model (6.2), the total plant density  $u_1 + u_2$  and the water density  $w$  are also antiphase. The two components of the total plant density (i.e. the grass density  $u_1$  and the tree density  $u_2$ ), however, are slightly out of phase. In the solution shown in Fig. 6.1, for example, local maxima of the grass density  $u_1$  are located a short distance in the uphill direction (increasing  $x$ ) away from the corresponding local maxima in the tree density  $u_2$ .

Numerical continuation can be used to obtain an insight into the effects of variations in the PDE parameters on the phase difference (Fig. 6.9). Changes in parameters can have large effects on the period of the patterned solution. We therefore consider the relative phase difference  $\phi := (\arg \max(u_1) - \arg \max(u_2))/L$ , where the maxima are taken over one period  $0 < x < L$ , instead of the absolute distance between the two maxima. The tracking of the relative phase difference in solutions obtained through numerical continuation shows that the diffusion coefficient  $D$ , which describes the ratio of the two plant species' diffusion coefficients, has the most significant effect on the phase difference between the species. If the phase difference  $\phi$  is defined as above, then it decreases monotonically with increasing  $D$ . In particular, it changes its sign close to  $D = 1$ . In other words, if both plant species have similar diffusion coefficients, then their phase difference is small. Note that  $\phi = 0$  does not necessarily occur at  $D = 1$ , as other model parameters affect the phase difference. The sign change of  $\phi$  corresponds to a change in the species which leads the uphill movement of the pattern. Neglecting the phase difference's behaviour in the immediate vicinity of  $D = 1$ , it can be summarised that over one period, the faster dispersing species' maximum and minimum is located a small distance ahead in the uphill direction of the spatial domain.

## 6.7 Discussion

Previous modelling of the savanna biome using nonspatial ODE and impulsive differential equations models (see [244] for a review) has successfully identified a range of different mechanisms that stabilise species coexistence based on key differences between grasses and trees. Examples include disturbances that affect species asymmetrically, such as different functional responses in the description of grazing and

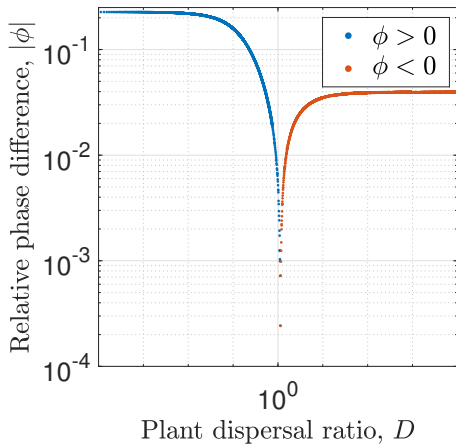


Figure 6.9: Phase difference between the plant species. This figure visualises the absolute value of the relative phase difference in coexistence solutions of (6.2) under changes to the diffusion coefficient  $D$ , obtained through numerical continuation. The colours indicate the sign of  $\phi$ , which changes at  $D \approx 1$ , i.e. when the species' dispersal behaviour is similar. Note the logarithmic scale. The precipitation parameter is  $A = 4.5$  and the migration speed is set to  $c = 0.15$ .

browsing [204] or variations in the species' susceptibility to fires [245]; an age structure of trees with different competitive abilities of tree seedlings and adult trees [15, 43]; or resource niche separation [226]. Model results presented in this chapter suggest that the consideration of spatial interactions in savanna ecosystems can provide an alternative mechanism for species coexistence, as spatial self-organisation principles can facilitate the stable coexistence of grasses and trees in savannas. The novelty of the tree-grass coexistence in model solutions presented in this study is that both species considered in our multispecies model (6.2) differ only in basic parameters, such as growth rate and mortality rate, and, in particular, satisfy the same single-species model (6.1) for their respective parameter sets.

Solutions of (6.2) in which both species coexist occur, provided that the species with inferior average fitness has a sufficiently large growth rate (Sec. 6.4). The average fitness difference  $B_2 - FB_1$  between the species only depends on the species' growth and mortality rates and determines the system's behaviour in a spatially uniform setting. In particular,  $B_2 - FB_1 = 0$  separates the disjoint stability regions of the system's spatially uniform single-species equilibria. The consideration of spatial interactions enables species coexistence as it allows for the capture of effects caused by a positive feedback between local vegetation growth and water redistribution. Patterns of biomass and water densities in the multispecies model (6.2) and the single-species Klausmeier model (6.1) are antiphase (i.e. high water densities in regions of low biomass densities and vice versa). This is due to the depletion of water in regions of high biomass due to the nonlinear dependence of water uptake on the plant densities. The species with faster growth rate (but inferior average fitness) can utilise the higher resource densities in regions of lower biomass through a fast increase in its density in such regions. In the long term, however, it is outcompeted by the species of higher average fitness. This balance between local facilitation by the species of higher average fitness and the fast colonisation ability of the species

with larger growth rate creates a balance in which coexistence of both species is possible.

This result is at odds with those by Durrett and Levin [56], who show that the interplay of local competitiveness and dispersal behaviour it is not sufficient to explain species coexistence in a general competition model, even though it has significant effects on the asymptotic behaviour of the system. A crucial difference between the model by Durrett and Levin and our multispecies ecohydrological model (6.2) is the lack of spatial self-organisation principles in the former. Indeed, if the pattern-inducing feedback is removed from (6.2), i.e. the infiltration enhancement terms ( $u_2 + Hu_2$ ) are set to unity, no species coexistence occurs in the model. This further emphasises that stable coexistence of the two species is indeed enabled by the spatial heterogeneity in the environmental conditions (water density), which is itself caused by the positive feedback between local plant growth and water redistribution towards high density biomass patches.

The model presented in this study can capture two distinct spatially nonuniform outcomes. Single-species patterns of either species are stable solutions of the system and resemble bands of vegetation that alternate with stripes of bare soil on sloped terrain. In terms of the biomass density, the plant density oscillates between a high level and a level close to zero. By contrast, the second stable patterned solution type features oscillations of both plant species between two non-zero biomass levels. This resembles a savanna state, as plant cover is continuous and no regions of bare soil exist. For typical parameter values of a grass species  $u_1$  and a tree species  $u_2$ , the precipitation intervals of stable (in the sense of the single species model (6.1)) single-species tree patterns and stable savanna solutions overlap. This results in the existence of precipitation volumes in which grasses have a local facilitative effect on trees. Under such rainfall regimes and in the absence of a grass species, trees can only attain a patterned state in which the tree density oscillates between a high level of biomass and biomass level close to zero. However, if additionally a grass species is considered in the system, trees can coexist with grasses in the whole space domain without the troughs of the oscillations being close to zero. While the total tree biomass decreases if trees coexist with grass, grasses have local facilitative effects on trees as they cause local increases in the tree density. Facilitation occurs due to improvements in environmental conditions. Grasses increase water infiltration into the soil and thus increase resource availability which is utilised by trees, if they are the superior species in a spatially uniform setting. This type of facilitation due to alterations in environmental conditions is referred to as *ecosystem engineering* [93]. It is well documented in both empirical (e.g. [140, 158]) and modelling studies (e.g. [76, 133]) that trees can act as ecosystem engineers and facilitate the growth of grass in their vicinity. Our model results suggest that grasses may act as ecosystem

engineers too, a mechanism that was established to be the driving force of species coexistence in a model for dryland vegetation patterns by Baudena and Rietkerk [16] and backed up by field studies [5, 117].

The plant species' diffusion coefficients ratio  $D$  has a significant influence on the coexistence solution dynamics. In particular, it quantitatively affects the size of the parameter region giving species coexistence (Sec. 6.4). If both species diffuse at the same rate ( $D = 1$ ), then coexistence patterns occur if the species with superior average fitness has a slower growth rate. In this case, the inferiority of one species' competitive abilities is balanced by its advantage in its colonisation abilities. The requirement of this crucial balance for species coexistence has already been noted in the early savanna model by Tilman [213]. However, in any nonspatial model, spatial spread cannot be distinguished from local growth in the description of a species' colonisation abilities. In the PDE model in this study, a comparison of local growth rates is only equivalent to a comparison of the plant species' colonisation abilities if the plant species do not differ in their diffusion coefficients. If, however, the inferior competitor in the spatially uniform setting diffuses at a faster rate, then higher growth rates of the superior species are tolerated. Similarly, coexistence patterns also occur if the species of higher average fitness is also superior in its spatial spread, provided that its local growth rate is sufficiently small.

In the context of species coexistence in vegetation patterns, Nathan et al. [145] found that under the assumption that two species decay at an equal rate, coexistence requires a species that is superior in both its competitive (defined by plant growth only) and dispersal abilities, due to a trade-off between spatial spread and local growth. Our results on pattern existence attempt to bridge a gap between the apparent mismatch between the predictions by Tilman [213] and Nathan et al. [145]. We emphasise that it is essential to consider spatiotemporal models that consider growth and death of plants separately, to gain an understanding of species coexistence. Our results show that, in this case, the complex system dynamics enable species coexistence in different parameter regimes that cover the predictions by both Tilman [213] and Nathan et al. [145]. In particular, the spatial self-organisation of plants that induces a nonlinear description of biomass growth, renders it insufficient to consider a plant species' competitive ability by one parameter only. The use of the notion of the average fitness of a plant species, comparing its growth rate to its mortality rate, as a measure of its competitive abilities instead, allows to overcome the proposed trade-off between spatial dispersal and local plant growth and enables coexistence of species if the superior competitor diffuses at a slower rate.

Coexistence of species as a model outcome is not limited to the parameter regions discussed above. If no solution with species coexistence occurs in the model, coexistence can occur as a long transient state (towards a stable single-species state),

provided that the average fitness difference between the two species is sufficiently small (Fig. 6.4). We have discussed the concept of metastability as a coexistence mechanism in Chapter 5 [63], using a model very similar to the multispecies model considered in this chapter. The differences between the two models do, however, not qualitatively affect the metastability property. Metastability is characterised by the small (but positive) growth rates of perturbations to a single-species equilibrium that becomes unstable as a competitor is introduced. The size of the growth rate is controlled by the average fitness difference between both species and thus coexistence can occur as a long transient state if the species' competitive abilities are similar, even if coexistence is unstable.

The metastability property is a feature of the spatially uniform model and thus independent of the slope parameter  $\nu$  [63] (Chapter 5). Hence, metastable coexistence also occurs in the system if the terrain is assumed to be flat. The analysis of the stable coexistence states in Sec. 6.4-6.6, however, is only valid on a sloped terrain, as the application of the numerical continuation techniques used in the bifurcation and stability analyses rely on the advection term in the equation for the water dynamics. Numerical integration of the PDE system, however, shows that a gradual decrease of the slope parameter to  $\nu = 0$  does not qualitatively change the behaviour of a stable coexistence state (in particular the phase difference between the total plant density and the water density). By contrast, PDE simulations starting from a randomly perturbed uniform state with the slope parameter fixed to  $\nu = 0$  yield coexistence solutions in which the pattern wavelength changes frequently. While there is a clear indication that coexistence of species is a potential model outcome on flat ground, the investigation of the system dynamics would require an application of different analytical tools, which is beyond the scope of this study.

A distinctive feature of spatially nonuniform solutions of our model is a slight phase difference between both species (Sec. 6.6). Such phase differences have been recorded in empirical studies on species coexistence in vegetation bands of semi-arid ecosystems, with grasses reported to be the dominant species in the uphill regions of a stripe, while trees were observed to attain their maximum densities in the central regions of a stripe [41]. Our model is unable to reproduce stable solutions that represent species coexistence in vegetation bands, but nevertheless predicts a phase difference between the two species coexisting in a spatially non-uniform savanna state. In particular, in the context of coexistence of grasses and trees (grasses disperse faster than trees), our analysis suggests that the biomass peaks of the herbaceous species are located in the upward direction of the biomass peaks of the woody species. While we are not aware of any data on species-specific biomass distribution in savanna ecosystems, this finding agrees with the empirical data that is available for banded vegetation patterns. [41]. In our model, we describe plant spread by

diffusion, which is a local mode of dispersal derived from a random walk, and characterise differences in the plant species dispersal behaviour by different diffusion coefficients only. In reality, however, nonlocal processes affect seed dispersal (e.g. [25]). Effects of nonlocal plant dispersal on vegetation in semi-arid environments has previously been studied in single-species models [20, 61, 156]. A similar approach could be used in an extension of the multispecies model presented in this chapter to gain more information on the biomass distribution of both species across a single vegetation stripe.

In this chapter, we investigated the facilitative effects of spatial heterogeneities on species coexistence in arid savannas. However, we restricted the extent of spatial heterogeneities to those in the availability of resources caused by a self-organisation principle in the plant populations. In doing so, we neglected potential heterogeneities in the topography of the spatial domain, which may have a significant influence on the ecosystem dynamics [72]. In particular, topographic nonuniformity may alter the dynamics of water flow and thus increase the heterogeneity in the resource availability. Such a promotion of resource niche creation could be exploited in a future model extension to extend the theory on the facilitative effects of spatial interactions in patterned vegetation and arid savannas.

The work presented in this study not only suggests a novel mechanism for species coexistence in savannas, but also provides insights into other properties of the ecosystem dynamics, such as the slow uphill movement of biomass peaks or the slight phase shift in the species distribution, as discussed above. To test these hypotheses, a comparison with empirical data would be desirable. However, data acquisition for dryland ecosystems is notoriously difficult. Some relevant types of data on dryland ecosystems are available. In particular, Deblauwe et al. [48] were able to estimate the uphill movement of vegetation stripes by comparing recent satellite images with those taken by spy satellites in the 1960's, but this relied on the clear contrast between vegetation and bare ground - changes in vegetation type within savannas are much more difficult to detect. Data on precipitation (both current and historical [193]) and on elevation (and hence slope) [202] are also available. But these are insufficient to provide an effective empirical test of model (6.2). However, advances in technologies (e.g. image processing) may in the future be utilised to extract more data from satellite images to estimate ecosystem properties of savannas, such as species composition or biomass densities, over large spatial scales.

The study of facilitation between species and mechanisms that promote coexistence is widespread across ecology. In particular, spatial self-organisation has been established as a key element promoting species coexistence in a variety of ecosystems. For example, self-organisation of a macrophyte species in streams enhances environmental conditions through deflection of water and thus facilitates other species

through a reduction in environmental stress [37]. Similarly, self-organised shellfish reefs (in particular mussel beds) are shown to cause a significant increase in species richness and diversity [32]. A detailed understanding of facilitative mechanisms caused by spatial self-organisation principles is therefore relevant not only in the vegetation dynamics of semi-arid environments, but also in a wide range of other ecosystems, as it can provide valuable information for restoration and conservation efforts [37].

## 6.8 Methods of calculating pattern existence and stability

In this section we outline the numerical continuation method by Rademacher et al. [160] to calculate the essential spectrum of a periodic travelling wave and trace stability boundaries of periodic travelling waves in a parameter plane, which we utilised in our bifurcation and stability analysis in Sec. 6.4 and 6.5. We provide an overview of the implementation of the method to (6.2), but refer the reader to [160, 187, 189] for full details. The method described below is implemented using the numerical continuation software AUTO-07p [53].

### 6.8.1 Single-species pattern existence

Single-species patterns of both the multispecies model (6.2) and the single-species Klausmeier model (6.1) originate at a Hopf bifurcation and terminate in a homoclinic orbit. Numerical continuation of the Hopf locus in the  $(A, c)$  parameter plane is straightforward. The homoclinic orbits, yielding the lower bounds on the precipitation parameter  $A$  for pattern existence, may also be calculated by means of numerical continuation [29]. In this context, however, it suffices to approximate homoclinic orbits by periodic travelling waves of large period  $L$ . Up to some constants in the equilibria and the parameter bounds, identical considerations hold for the second plant species  $u_2$ , due to the symmetry in the model.

### 6.8.2 Calculation of the essential spectrum

The starting point for the calculation of the essential spectrum of a patterned solution of (6.2) is the travelling wave system (6.3), i.e.

$$f(U_1, U_2, W) + c \frac{dU_1}{dz} + \frac{d^2U_1}{dz^2} = 0, \quad (6.4a)$$

$$g(U_1, U_2, W) + \frac{dU_2}{dz} + D \frac{d^2U_2}{dz^2} = 0, \quad (6.4b)$$

$$h(U_1, U_2, W) + (c + \nu) \frac{dW}{dz} + d \frac{d^2W}{dz^2} = 0, \quad (6.4c)$$

where

$$f(U_1, U_2, W) = WU_1(U_1 + HU_2) - B_1U_1,$$

$$g(U_1, U_2, W) = FWU_2(U_1 + HU_2) - B_2U_2,$$

$$h(U_1, U_2, W) = A - W - W(U_1 + U_2)(U_1 + HU_2).$$

To determine the essential spectrum, it is further convenient to rewrite the PDE system (6.2) in terms of  $z$  and  $t$ . Denoting  $\hat{u}_1(z, t) = u_1(x, t)$ ,  $\hat{u}_2(z, t) = u_2(x, t)$  and  $\hat{w}(z, t) = w(x, t)$  thus yields

$$\frac{\partial \hat{u}_1}{\partial t} = f(\hat{u}_1, \hat{u}_2, \hat{w}) + c \frac{\partial \hat{u}_1}{\partial z} + \frac{\partial^2 \hat{u}_1}{\partial z^2}, \quad (6.5a)$$

$$\frac{\partial \hat{u}_2}{\partial t} = g(\hat{u}_1, \hat{u}_2, \hat{w}) + \frac{\partial \hat{u}_2}{\partial z} + D \frac{\partial^2 \hat{u}_2}{\partial z^2}, \quad (6.5b)$$

$$\frac{\partial \hat{w}}{\partial t} = h(\hat{u}_1, \hat{u}_2, \hat{w}) + (c + \nu) \frac{\partial \hat{w}}{\partial z} + d \frac{\partial^2 \hat{w}}{\partial z^2}. \quad (6.5c)$$

Given a periodic travelling wave solution  $\bar{V}(z) = (\bar{U}_1(z), \bar{U}_2(z), \bar{W}(z))$  of (6.5) (i.e. a triplet  $(\bar{U}_1(z), \bar{U}_2(z), \bar{W}(z))$  that satisfies (6.4)), its stability is determined by the behaviour of small perturbations to the periodic travelling wave. Under the assumptions that temporal perturbations to  $\bar{V}(z)$  are proportional to  $\exp(\lambda t)$ ,  $\lambda \in \mathbb{C}$ , i.e. setting  $\tilde{v}(z, t) = \bar{V}(z) + \exp(\lambda t)\tilde{V}(z)$ , and linearising (6.5) about the travelling wave solution  $\bar{V}(z)$  yields that the leading order behaviour of perturbations is determined by the eigenvalue problem

$$\lambda \tilde{V}(z) = J \tilde{V}(z) + c \tilde{V}'(z), \quad (6.6)$$

where the prime denotes differentiation with respect to  $z$  and  $J$  is the Jacobian of the right hand side of (6.5) with respect to  $\hat{v}$  and its derivatives, i.e.

$$J = \begin{pmatrix} \frac{\partial f}{\partial \hat{u}_1} + c \frac{d}{dz} + \frac{d^2}{dz^2} & \frac{\partial f}{\partial \hat{u}_2} & \frac{\partial f}{\partial \hat{w}} \\ \frac{\partial g}{\partial \hat{u}_1} & \frac{\partial g}{\partial \hat{u}_2} + c \frac{d}{dz} + D \frac{d^2}{dz^2} & \frac{\partial g}{\partial \hat{w}} \\ \frac{\partial h}{\partial \hat{u}_1} & \frac{\partial h}{\partial \hat{u}_2} & \frac{\partial h}{\partial \hat{w}} + (c + \nu) \frac{d}{dz} + d \frac{d^2}{dz^2} \end{pmatrix},$$

evaluated at the periodic travelling wave solution  $\bar{V}$ .

The eigenvalue problem (6.6) is formulated over one period  $L$  of the travelling wave solution  $\bar{V}(z)$  and needs to be equipped with boundary conditions. By definition,  $\bar{V}(0) = \bar{V}(L)$ . The eigenfunction  $\tilde{V}(z)$ , however, is not necessarily periodic. The amplitude of  $\tilde{V}(z)$  needs to be conserved to prevent growth to  $\pm\infty$ , but phase shifts are admissible. An appropriate boundary condition thus is

$$\tilde{V}(0) = \tilde{V}(L)e^{\gamma i}, \quad (6.7)$$

for  $\gamma \in \mathbb{R}$  which can be derived using Floquet theory [50, 160, 172].

The spectral stability of periodic travelling wave solutions  $\bar{V}$  can then be determined by finding the set of eigenvalues  $\lambda$  for which the eigenvalue problem (6.6) with boundary condition (6.7) has a nontrivial solution. To do this, it suffices to find the essential spectrum of the periodic travelling wave, as the point spectrum is always empty [172].

The calculation of the essential spectrum is performed in two stages. First, the special (and simpler) case of periodic boundary conditions (i.e.  $\gamma = 0$ ) is considered. This simplification allows for a transformation of the eigenvalue problem (6.6) into a matrix eigenvalue problem by discretising the domain and approximating the derivatives through finite differences. The matrix eigenvalue problem can be solved by standard means and provides a starting point for a numerical continuation in  $\gamma$  to complete the computation of the essential spectrum.

To implement the numerical continuation, it is convenient to rewrite the eigenvalue problem (6.6) as the first order system

$$\tilde{\tilde{V}}(z)' = (Y(z) + \lambda X) \tilde{\tilde{V}}(z), \quad \tilde{\tilde{V}}(0) = \tilde{\tilde{V}}(L)e^{i\gamma},$$

where

$$Y(z) = \begin{pmatrix} 0 & 1 & 0 & 0 & 0 & 0 \\ -\frac{\partial f}{\partial U_1} & -c & -\frac{\partial f}{\partial U_2} & 0 & -\frac{\partial f}{\partial W} & 0 \\ 0 & 0 & 0 & 1 & 0 & 0 \\ -\frac{1}{D} \frac{\partial g}{\partial U_1} & 0 & -\frac{1}{D} \frac{\partial g}{\partial U_2} & -\frac{c}{D} & -\frac{1}{D} \frac{\partial g}{\partial W} & 0 \\ 0 & 0 & 0 & 0 & 0 & 1 \\ -\frac{1}{d} \frac{\partial h}{\partial U_1} & 0 & -\frac{1}{d} \frac{\partial h}{\partial U_2} & 0 & -\frac{1}{d} \frac{\partial h}{\partial W} & -\frac{c+\nu}{d} \end{pmatrix},$$

evaluated at the periodic travelling wave solution  $\bar{V}$  and

$$X = \begin{pmatrix} 0 & 0 & 0 & 0 & 0 & 0 \\ 1 & 0 & 0 & 0 & 0 & 0 \\ 0 & 0 & 0 & 0 & 0 & 0 \\ 0 & 0 & \frac{1}{D} & 0 & 0 & 0 \\ 0 & 0 & 0 & 0 & 0 & 0 \\ 0 & 0 & 0 & 0 & \frac{1}{d} & 0 \end{pmatrix}.$$

The boundary condition is transformed into a periodic boundary condition by setting  $\tilde{\tilde{V}}(z) = \exp(i\gamma z/L)\alpha(z)$ . Together with the normalisation  $z = L\xi$  of the domain, this yields

$$\alpha'(\xi) = (L(Y(\xi) + \lambda X) - i\gamma I)\alpha(\xi), \quad \alpha(0) = \alpha(1), \quad (6.8)$$

where  $I$  is the identity matrix. Implementation in AUTO requires separation of real and imaginary parts of (6.8). This yields

$$\Re(\alpha)' = (L(Y + \Re(\lambda)X))\Re(\alpha) + (\gamma I - L\Im(\lambda)X)\Im(\alpha), \quad (6.9a)$$

$$\Im(\alpha)' = (L(Y + \Re(\lambda)X))\Im(\alpha) + (-\gamma I + L\Im(\lambda)X)\Re(\alpha), \quad (6.9b)$$

$$\Re(\alpha(0)) = \Re(\alpha(1)), \quad \Im(\alpha(0)) = \Im(\alpha(1)). \quad (6.9c)$$

The eigenvalue problem (6.8) is not sufficient to uniquely determine the eigenfunctions  $\alpha$ . The periodic boundary conditions allow for arbitrary phase shifts. Thus, (6.8) is supplemented with the phase fixing condition

$$\Im(\langle \alpha_{\text{old}}, \alpha \rangle) = \int_0^1 (\Re(\alpha_{\text{old}}) \cdot \Im(\alpha) - \Im(\alpha_{\text{old}}) \cdot \Re(\alpha)) d\xi = 0, \quad (6.10)$$

where  $\alpha_{\text{old}}$  is the eigenfunction  $\alpha$  at any previous step of the numerical continuation or the initial eigenfunction from which the continuation is started, and the inner product is defined by

$$\langle \alpha_1, \alpha_2 \rangle = \int_0^1 \alpha_1 \cdot \alpha_2^* d\xi,$$

where the asterisk denotes the complex conjugation. Further, the eigenfunction is normalised by imposing the integral condition

$$\langle \alpha, \alpha \rangle = \int_0^1 (\Re(\alpha) \cdot \Re(\alpha) + \Im(\alpha) \cdot \Im(\alpha)) d\xi = 1. \quad (6.11)$$

Similar to the phase fixing condition (6.10) for the eigenfunction  $\alpha$ , also the periodic travelling wave solution  $V = (U_1, U'_1, U_2, U'_2, W, W')$  of (6.4) with periodic boundary conditions requires a phase fixing condition to prevent arbitrary translations in  $z$ . The appropriate integral condition is

$$\int_0^1 V'_{\text{old}} \cdot (V_{\text{old}} - V) dz = 0. \quad (6.12)$$

Given a solution of the eigenvalue problem (6.6) with periodic boundary conditions (i.e.  $\gamma = 0$ ), the full essential spectrum can then be found by continuing the travelling wave equation (6.4) with periodic boundary conditions and the eigenfunction equation (6.9) with the integral constraints (6.10), (6.11) and (6.12), starting from each of the eigenvalues  $\lambda$  and corresponding eigenfunctions  $\alpha$  obtained from the matrix eigenvalue problem for  $\gamma = 0$ . The principal continuation parameter is  $0 < \gamma < 2\pi$ , while  $\Re(\lambda)$ ,  $\Im(\lambda)$  and  $L$  are chosen as secondary continuation parameters. In practise, not the whole essential spectrum needs to be computed to determine the spectral stability of a given periodic travelling wave solution. It is sufficient to perform the numerical continuation starting only from the, say 20, largest eigenvalues obtained form the matrix eigenvalue problem for  $\gamma = 0$ .

### 6.8.3 Numerical continuation of stability boundaries

The method described in the previous section allows for the calculation of the essential spectrum of a periodic travelling wave solution for a set of given parameters. The algorithm can further be extended to trace stability boundaries of periodic travelling waves in a parameter plane, such as  $(A, c)$ . Full details of this algorithm are found in [160, 189].

To locate and trace stability boundaries, derivatives of the eigenfunctions  $\alpha$  with

respect to  $\gamma$  are required. Implicit differentiation of (6.8) with respect to  $\gamma$  gives

$$\alpha'_\gamma = (L(Y + \lambda X) - i\gamma I) \alpha_\gamma + (L\lambda_\gamma X - iI) \alpha, \quad \alpha_\gamma(0) = \alpha_\gamma(1), \quad (6.13)$$

where the prime denotes derivatives with respect to  $\xi$  and the subscript  $\gamma$  derivatives with respect to  $\gamma$ . Further implicit differentiation yields

$$\alpha'_{\gamma\gamma} = (L(Y + \lambda X) - i\gamma I) \alpha_{\gamma\gamma} + 2(L\lambda_\gamma X - iI) \alpha_\gamma + L\lambda_{\gamma\gamma} X \alpha, \quad \alpha_{\gamma\gamma}(0) = \alpha_{\gamma\gamma}(1). \quad (6.14)$$

As previously discussed, implementation in AUTO requires separation of real and imaginary parts. This yields

$$\begin{aligned} \Re(\alpha'_\gamma) &= L(Y + \Re(\lambda)X) \Re(\alpha_\gamma) + (-L\Im(\lambda)X + \gamma I) \Im(\alpha_\gamma) \\ &\quad + L\Re(\lambda_\gamma) X \Re(\alpha) + (-L\Im(\lambda_\gamma) X + I) \Im(\alpha), \end{aligned} \quad (6.15a)$$

$$\begin{aligned} \Im(\alpha'_\gamma) &= (L\Im(\lambda)X - \gamma I) \Re(\alpha_\gamma) + L(Y + \Re(\lambda)X) \Im(\alpha_\gamma) \\ &\quad + (L\Im(\lambda_\gamma) X - I) \Re(\alpha) + L\Re(\lambda_\gamma) X \Im(\alpha), \end{aligned} \quad (6.15b)$$

$$\Re(\alpha_\gamma(0)) = \Re(\alpha_\gamma(1)), \quad \Im(\alpha_\gamma(0)) = \Im(\alpha_\gamma(1)), \quad (6.15c)$$

and

$$\begin{aligned} \Re(\alpha'_{\gamma\gamma}) &= L(Y + \Re(\lambda X)) \Re(\alpha_{\gamma\gamma}) + (-L\Im(\lambda)X + \gamma I) \Im(\alpha_{\gamma\gamma}) \\ &\quad + 2L\Re(\lambda_\gamma) X \Re(\alpha_\gamma) + 2(-L\Im(\lambda_\gamma) X + I) \Im(\alpha_\gamma) \\ &\quad + L\Re(\lambda_{\gamma\gamma}) X \Re(\alpha) - L\Im(\lambda_{\gamma\gamma}) X \Im(\alpha), \end{aligned} \quad (6.16a)$$

$$\begin{aligned} \Im(\alpha'_{\gamma\gamma}) &= (L\Im(\lambda)X - \gamma I) \Re(\alpha_{\gamma\gamma}) + L(Y + \Re(\lambda X)) \Im(\alpha_{\gamma\gamma}) \\ &\quad + 2(L\Im(\lambda_\gamma) X - I) \Re(\alpha_\gamma) + 2L\Re(\lambda_\gamma) X \Im(\alpha_\gamma) \\ &\quad + L\Im(\lambda_{\gamma\gamma}) X \Re(\alpha) + L\Re(\lambda_{\gamma\gamma}) X \Im(\alpha), \end{aligned} \quad (6.16b)$$

$$\Re(\alpha_{\gamma\gamma}(0)) = \Re(\alpha_{\gamma\gamma}(1)), \quad \Im(\alpha_{\gamma\gamma}(0)) = \Im(\alpha_{\gamma\gamma}(1)), \quad (6.16c)$$

respectively.

The equations given in (6.13) and (6.14) cannot determine the derivatives  $\alpha_\gamma$  and  $\alpha_{\gamma\gamma}$  uniquely, as they may contain components in the nullspace of (6.8). Hence,

they are equipped with integral conditions given by

$$\langle \alpha, \alpha_\gamma \rangle = 0 \quad (6.17)$$

and

$$\langle \alpha, \alpha_{\gamma\gamma} \rangle = 0 \quad (6.18)$$

A stability change of Eckhaus (sideband) type is detected through a numerical continuation of the travelling wave equation (6.4), the eigenfunction equation (6.9), the imaginary part of the eigenvalue equation differentiated with respect to  $\gamma$  (6.15b) and the real part of the eigenvalue equation differentiated twice with respect to  $\gamma$  (6.16a) with the corresponding boundary and integral conditions. The continuation is started at the eigenvalue  $\lambda = 0$  and its corresponding eigenfunction obtained from the matrix eigenvalue problem that is solved in the initial stage of the algorithm. The principal continuation parameter is the migration speed  $c$  (or the PDE parameter  $A$ ), and the five secondary continuation parameters must include  $\Re(\lambda_{\gamma\gamma})$ . If a locus with  $\Re(\lambda_{\gamma\gamma}) = 0$  is found, a stability change of Eckhaus type is detected. The secondary continuation parameter  $\Re(\lambda_{\gamma\gamma})$  is then replaced by the PDE parameter  $A$  (or the migration speed  $c$ ) to trace out the stability boundary in the  $(A, c)$  parameter plane.

The continuation of a stability change of Hopf type follows the same idea, but contains some caveats. First, a fold in the spectrum is detected by a numerical continuation of the travelling wave equation (6.4), the eigenfunction equation (6.9) and both the real and imaginary parts of the eigenvalue equation differentiated with respect to  $\gamma$  (6.15) with the corresponding boundary and integral conditions. The spectrum may contain many folds, but only the fold with largest real part is of interest and the continuation must start sufficiently close to that fold. The principal continuation parameter is  $\gamma$  and the five secondary continuation parameters must include  $\Re(\lambda_\gamma)$ . A fold in the spectrum is located, when a zero of  $\Re(\lambda_\gamma)$  is found. The zero of  $\Re(\lambda_\gamma)$  is subsequently fixed and the migration speed  $c$  (or the PDE parameter  $A$ ) is then chosen as the principal continuation parameter. The equations are continued in this parameter until a zero of  $\Re(\lambda)$ , which needs to be one of the secondary continuation parameters, is found. This corresponds to a stability change of Hopf type. Finally,  $\Re(\lambda)$  is replaced as a secondary continuation parameter by the PDE parameter  $A$  (or the migration speed  $c$ ) to trace out the locus of the stability change of Hopf type in the  $(A, c)$  plane.

## Chapter 7

### Species coexistence in vegetation patterns facilitated by the interplay of spatial self-organisation and intraspecific competition

The contents of this chapter are submitted for publication and a preprint is available [60].

#### 7.1 Author contribution

The submitted paper [60] is a single-authored paper by Lukas Eigentler.

#### Abstract

The exploration of mechanisms that enable species coexistence under competition for a sole limiting resource is widespread across ecology. Two examples of such facilitative processes are intraspecific competition and spatial self-organisation. A classical example of an ecosystem governed by the latter is dryland vegetation patterns. Previous theoretical investigations have explained coexistence in patterned vegetation by making strong assumptions on the differences between species (e.g. contrasting dispersal behaviours or different functional responses to soil moisture). In this chapter, I show that the interplay between the competitive effects of intraspecific competition and the facilitative nature of self-organisation forms a coexistence mechanism that does not rely on species-specific assumptions. I use an ecohydrological reaction-advection-diffusion system that captures the interactions of two plant species with an explicitly modelled resource to show that coexistence relies on a balance between species' colonisation abilities and their local competitiveness, provided intraspecific competition is sufficiently strong. Crucially, the requirements on species' self-limitation for coexistence to occur differ on opposite ends of the precipitation (resource input) spectrum. For low resource levels, coexistence is facilitated by strong intraspecific competition dynamics of the species superior in its colonisation abilities, but for larger volumes of resource input, strong intraspecific competition of the locally superior species enables coexistence. Results presented in this chapter also capture the em-

pirically observed spatial species distribution within bands of vegetation and propose differences in plants' dispersal behaviour as its cause.

Keywords: banded vegetation; semi-arid ecosystems; reaction-advection-diffusion model; mathematical modelling; competition and coexistence; pattern formation.

## 7.2 Introduction

A classical result of coexistence theory states that species coexistence in ecological and biological systems cannot occur if species compete for a single limiting resource; this is often referred to as Tilman's  $R^*$  rule [212]. For any given species,  $R^*$  denotes the smallest resource level at which that species is able to persist. The species that can depress the resource to its lowest level (i.e. has the smallest  $R^*$  value) is able to monopolise the limiting resource and outcompete all other species, according to Tilman's  $R^*$  rule. Nevertheless, it is evident that this principle is an oversimplification and is insufficient to fully describe the outcome of competition as species coexistence occurs in many ecosystems despite competition for a single resource. Hence, this suggests that other processes prevent resource monopolisation by one species and thus enable coexistence [127].

One such mechanism that has been singled out as a common facilitator of species coexistence is intraspecific competition (e.g. [30, 127]). The inclusion of self-limitation due to negative density-dependent effects is an integral part of investigating coexistence through Lotka-Volterra competition models (e.g. [30]). More recently, such dynamics have also been added to Rosenzweig-MacArthur-type models in which interactions of consumer species with a sole limiting resource are explicitly modelled [127]. The impact of self-limitation on consumer competition dynamics is that, if sufficiently strong, it limits the abundance of each species so that no single species is able to monopolise the resource in the sense of Tilman's  $R^*$  rule. This allows the limiting resource to be shared among two or more species and thus enables coexistence.

A different mechanism that has been found to promote species coexistence is spatial self-organisation. As opposed to local intraspecific competition, self-organisation principles are characterised by positive density-dependent effects on short spatial scales in combination with long-range competition for resources [166]. The formation of spatial patterns of consumer species due to such scale-dependent feedbacks can create spatial heterogeneities in environmental conditions (e.g. resource availability) in otherwise homogeneous environments [37, 64] (Chapter 6). Such heterogeneous landscapes lead to spatial separation of competitive and facilitative interactions between different consumer species, which creates a balance that enables species coexistence [37]. This mechanism is not unique to self-organised consumer com-

munities, but has also been attributed to enrich species richness in other ecological systems where the underlying spatial heterogeneities are not induced by the species themselves [223].

A classical example of a self-organised ecosystem in which species coexistence occurs is dryland vegetation patterns [179, 222]. This state is characterised by alternating patches of high biomass and areas of bare soil and forms an interface along the precipitation gradient between full deserts and arid savannas, where plants form a continuous biomass cover. The self-organisation of plants into mosaics of vegetated patches and regions of bare soil is induced by a positive feedback between local vegetation growth and water redistribution towards areas of high biomass [71, 166]. This is caused, for example, by the formation of biogenic soil crusts on bare soil which inhibit water infiltration and induce overland water flow, or by the combination of laterally extended root systems with a soil type that facilitates fast water diffusion and hence causes resource redistribution below-ground [130]. As a consequence, plants facilitate their growth on short spatial scales, but compete for water across long spatial scales. This results in a scale-dependent feedback due to which self-organisation occurs.

Vegetation patterns occur in a range of different shapes, including regular stripes parallel to contours of gentle slopes [222]. Long-term field studies indicate that such vegetation stripes gradually move upslope over a generational timescale [48]. This uphill migration occurs because the water run-off from low-permeability inter-band regions aggregates near the top edges of existing stripes, creating a heterogeneous resource landscape within vegetation bands that causes upslope expansion and downslope contraction [38]. Transects through vegetation bands typically feature a group of species dominating the upslope edges of each band (typically annual grasses), and a group of plant types mostly confined to the centre and downslope regions of the stripes (typically perennial grasses, shrubs and trees) [179]. The former are often regarded as the driving force of the bands' uphill migration and are therefore commonly referred to as *coloniser species*.

In this chapter, I use banded vegetation as a case study to unite the two strands of coexistence theory discussed above (intraspecific competition and spatial self-organisation) in a theoretical framework. Dryland vegetation represents an ideal candidate for such an approach, since its ecosystem dynamics have been the subject of countless mathematical modelling studies over the last three decades [21, 124, 247]. The existing modelling frameworks provide a good foundation for further theoretical investigations of the ecosystem dynamics and in particular species coexistence.

This chapter is not the first mathematical model to investigate species coexistence in dryland vegetation patterns. Baudena and Rietkerk [16] have shown that

coexistence can be induced by facilitation of a species unable to form spatial patterns by a self-organising species. Similarly, Ursino and Callegaro [27, 220] have included the adaptation of plant species to different soil moisture niches in a theoretical framework to successfully capture coexistence. However, a shortfall of both these approaches is that they rely on the assumption that the plant species fundamentally differ in their interaction with the environment and are thus not applicable to a general setting.

In a previous chapter, I have shown that self-organisation is a sufficient mechanism to enable coexistence in arid savannas, where no segregation between vegetated and bare patches occurs [64] (Chapter 6). Crucially however, I have also argued that other processes must be involved in the facilitation of coexistence in vegetation patterns if species do not differ in their functional responses to the environment. This hypothesis is based on a description of the resource-consumer dynamics of two species (or two groups of species) whose difference from each other only manifests itself quantitatively through different parameter estimates of basic properties (e.g. growth and death rates) but not qualitatively through different functional responses to the environment. In this setting, coexistence occurs if one (group of) species is superior in its colonisation abilities but is outcompeted locally by a second (group of) species. Consequently, the former are referred to as *colonisers* and the later as the *locally superior species*, a terminology that will be carried over to this chapter. This mechanism only gives insights into the coexistence of both species groups. Coexistence within those groups may occur due to other facilitative processes that are independent of spatial self-organisation principles. For brevity, I will refer to such species groups as single species in the remainder of the chapter.

This previous study functions as the baseline case of the unification of spatial self-organisation and intraspecific competition dynamics in coexistence theory of vegetation patterns presented in this chapter. I argue that the inclusion of self-limitation is crucial to capture coexistence of a coloniser species with a locally superior species in vegetation patterns that occur under severe water scarcity. Moreover, the importance of spatial self-organisation in the coexistence of dryland vegetation is reinforced by the result that strong intraspecific competition of different species facilitates coexistence at different ends of the precipitation (resource input) spectrum. Finally, this unified approach is the first to capture the spatial species distribution within vegetation bands, confirming verbal arguments that the patterns' uphill migration is indeed driven by the coloniser species [179].

This chapter focusses on the ecological implications obtained through a comprehensive model analysis of the system presented in Sec. 7.3 below. As such, only stable model outcomes are considered. Nevertheless, the mathematical model also admits unstable solutions, an analysis of which aids greatly to the understanding

of the bifurcations in the system. A comprehensive bifurcation analysis aimed at a more mathematics-oriented readership and an analysis of the impact of intraspecific competition dynamics in single-species ecosystems are presented in a separate chapter [59] (Chapter 8).

### 7.3 Model & Methods

A well-established mathematical model describing the ecohydrological dynamics of vegetation stripes on sloped terrain is the single-species reaction-advection-diffusion system by Klausmeier [99]. This phenomenological model stands out due to its deliberate simplicity and thus provides a rich framework for model extensions (e.g. [20, 35, 58, 61, 62, 120, 195]). One recent extension has introduced a second plant species to the system, based on the assumption that plant species only differ from each other quantitatively in their basic parameters but not qualitatively in any of their functional responses [63, 64] (Chapters 5 and 6). This model forms the basis of the theoretical framework presented below.

#### 7.3.1 Model details

The per capita growth rates of both plant species in the multispecies model presented in [63, 64] (Chapters 5 and 6) are

$$\begin{aligned} G_{\infty}^{u_1} &= w(u_1 + Hu_2), \\ G_{\infty}^{u_2} &= Fw(u_1 + Hu_2), \end{aligned} \tag{7.1}$$

where  $u_1 = u_1(x, t)$  and  $u_2 = u_2(x, t)$  denote the nondimensional (see the supplementary material for a nondimensionalisation) plant densities at time  $t \geq 0$  at the space point  $x \in \mathbb{R}$ . The rate of plant growth not only increases with the resource density  $w = w(x, t)$ , describing water availability, but also with both plant densities  $u_1$  and  $u_2$ . This positive density-dependence represents the short-range facilitative effects of plants on each other which is caused, for example, by increases of soil permeability in vegetated areas. The strength of facilitation differs between the two species and is accounted for by the nondimensional constant  $H$ . The nondimensional constant  $F$  describes the ratio of the two species' water-to-biomass conversion capabilities.

To account for intraspecific competition dynamics among plant species in the theoretical framework, I convert the growth rates (7.1) into logistic-growth-type

terms by setting

$$\begin{aligned} G_{k_1}^{u_1} &= w(u_1 + Hu_2) \left(1 - \frac{u_1}{k_1}\right), \\ G_{k_2}^{u_2} &= Fw(u_1 + Hu_2) \left(1 - \frac{u_2}{k_2}\right). \end{aligned} \quad (7.2)$$

The parameters  $k_1$  and  $k_2$  denote the maximum standing biomasses of both species. In this context, self-limitation does not refer to intraspecific competition for water, as the ecohydrological dynamics are explicitly modelled. Instead, the strength of intraspecific competition depends on other factors, such as the maximum biomass of a single individual, which limit the total biomass a species can reach in a fixed area [145]. The per capita growth rates (7.2) capture both the intraspecific facilitation and intraspecific competition that occur in dryland ecosystems (Fig. 7.1). For low biomass densities, the per capita growth rate of a species increases with that species' density (facilitation), but decreases for higher biomass densities (competition).

Replacing the plant growth rates (7.1) in the multispecies model presented in [63, 64] (Chapters 5 and 6) by (7.2) yields

$$\frac{\partial u_1}{\partial t} = \underbrace{wu_1(u_1 + Hu_2) \left(1 - \frac{u_1}{k_1}\right)}_{\text{plant growth}} - \underbrace{B_1 u_1}_{\text{plant mortality}} + \underbrace{\frac{\partial^2 u_1}{\partial x^2}}_{\text{plant dispersal}}, \quad (7.3a)$$

$$\frac{\partial u_2}{\partial t} = \underbrace{Fwu_2(u_1 + Hu_2) \left(1 - \frac{u_2}{k_2}\right)}_{\text{plant growth}} - \underbrace{B_2 u_2}_{\text{plant mortality}} + \underbrace{D \frac{\partial^2 u_2}{\partial x^2}}_{\text{plant dispersal}}, \quad (7.3b)$$

$$\frac{\partial w}{\partial t} = \underbrace{A}_{\text{rainfall}} - \underbrace{w}_{\text{evaporation and drainage}} - \underbrace{w(u_1 + u_2)(u_1 + Hu_2)}_{\text{water uptake by plants}} + \underbrace{\nu \frac{\partial w}{\partial x}}_{\text{water flow downhill}} + \underbrace{d \frac{\partial^2 w}{\partial x^2}}_{\text{water diffusion}}, \quad (7.3c)$$

where time  $t \geq 0$  and the space variable  $x \in \mathbb{R}$  increases in the uphill direction of the one-dimensional domain, representing sloped terrain. The consideration of a one-dimensional space domain instead of an ecologically more intuitive two-dimensional domain is justified by the appearance of vegetation patterns as regular stripes parallel to the contours of the slope. Solution profiles of (7.3) thus represent a transversal cut along the gradient of the terrain.

Water is added to the system at a constant rate  $A$  and is removed through evaporation and drainage processes that are assumed to be proportional to the water density. Water is consumed by plants, represented by the third term on the right hand side of (7.3c). The rate of water uptake by plants does not only depend

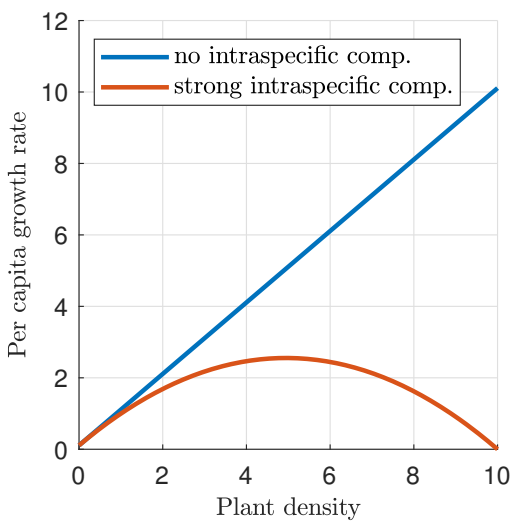


Figure 7.1: Per capita plant growth rates. Sketches of a plant species' growth rate in the absence of intraspecific competition ( $G_\infty$ , blue curve) and with the inclusion of self-limitation ( $G_{10}$ , red curve) are shown. Even if intraspecific competition is considered, the growth rate captures facilitative intraspecific effects of plants on each other for low biomass densities. For larger plant densities, the negative density-dependent effects dominate and the species' growth rate decreases. Densities of  $u_2$  and  $w$  are kept constant in this visualisation.

on the total consumer density ( $u_1 + u_2$ ), but also on the enhancement of the plants' water consumption capabilities in areas of high biomass ( $u_1 + Hu_2$ ), as discussed above. Plant mortality is assumed to be proportional to plant density and occurs at rates  $B_1$  and  $B_2$ , respectively. Finally, all three densities undergo diffusion, and water is assumed to flow downhill on the sloped terrain. The description of the latter by advection is based on the assumption that the slope does not exceed gradients of a few percent, consistent with field observations of striped vegetation patterns [222]. The diffusion parameters  $D$  for species  $u_2$  and  $d$  for water, as well as the advection speed  $\nu$  compare the respective dimensional parameters to the diffusion coefficient of species  $u_1$ .

In the following, I assume that  $u_1$  and  $u_2$  represent a *coloniser species* and a *locally superior species*, respectively. A number of theoretical models on dryland vegetation have been proposed over the last three decades and therefore all parameter values in (7.3) are obtained from previous models. Details on how parameter estimation for those models is performed are presented in [1, 99, 125]. The distinction between a coloniser and a locally superior species yields qualitative assumptions on the model parameters [64] (Chapter 6). The coloniser both grows and dies at a faster rate ( $F < 1, B_1 > B_2$ , but see comment below), has a stronger impact on the soil's permeability per unit biomass ( $H < 1$ ) and disperses faster ( $D < 1$ ) [64] (Chapter 6). The locally superior species is assumed to outcompete the coloniser species in a spatially uniform setting in the absence of any self-limitation. This requires  $B_2 < FB_1$  [63] (Chapter 5) and I assume that this relation holds throughout the chapter.

### 7.3.2 Model analysis

Typically, both single-species solutions and coexistence solutions of (7.3) are either spatially constant or spatially patterned. In the latter case, these are periodic travelling waves, i.e. spatially periodic functions that move in the uphill direction of the domain at a constant speed. The uphill migration speed is an emergent property of model solutions, but can be made explicit through a change of coordinates that transforms (7.3) into a travelling wave framework. In travelling wave coordinates, spatio-temporal patterned solutions can be represented by a single variable only (see supplementary material). This facilitates a bifurcation analysis (the study of qualitative changes to the solution structure under variations of system parameters), which is performed by a combination of analytical tools and numerical continuation (see supplementary material). In particular, the stability calculations of the periodic travelling wave solutions of the system are performed using a numerical continuation method for the calculation of essential spectra by Rademacher et al. [160].

Numerical simulations of the PDE system (7.3) are obtained using the method of lines, with the resulting system being solved by a standard numerical solver for ordinary differential equations (ODEs) (e.g. `ode15s` in MATLAB).

The spatial distribution of species in a single vegetation band is quantified by the linear correlation between both plant species' solution components. The linear correlation is given by

$$\rho(U_1, U_2) = \frac{\text{cov}(U_1, U_2)}{\sigma(U_1)\sigma(U_2)},$$

where  $U_1$  and  $U_2$  are two vectors obtained by discretising the spatial domain in space and evaluating the plant densities  $u_1$  and  $u_2$  on this mesh. Here,  $\text{cov}(\cdot, \cdot)$  denotes the covariance of two vectors, and  $\sigma(\cdot)$  the standard deviation. The linear correlation satisfies  $-1 \leq \rho(U_1, U_2) \leq 1$ , and a larger correlation corresponds to a more in-phase-like appearance of both plant patterns. Numerical continuation of model solutions using AUTO-07p [53] allows for an exhaustive calculation of the linear correlation in the parameter space.

## 7.4 Results

### 7.4.1 Spatially uniform coexistence

Depending on the precipitation volume, the multispecies model (7.3) has up to four biologically relevant spatially uniform equilibria: a desert steady state that is stable in the whole parameter space; a single-species equilibrium for each plant species; and a coexistence state. Under sufficiently high rainfall levels, the single-

species equilibria are stable in the absence of a second species, but may become unstable if a competitor is introduced. Stability to the introduction of a second species requires both sufficiently weak intraspecific competition and a higher local average fitness than the competitor. Moreover, the stability regions of both single-species equilibria do not overlap and it is straightforward to determine the species of higher local average fitness based on their parameter values. In particular, only changes to growth and mortality rates, but not variations in the strength of the intraspecific competition can change which species is of higher local average fitness (see supplementary material for more details).

As intraspecific competition of the locally superior species increases, its single-species equilibrium loses stability to the coexistence equilibrium. In other words, spatially uniform coexistence occurs if intraspecific competition among the locally superior species is sufficiently strong compared to the interspecific competition for water, which is quantified by the rainfall parameter (Fig. 7.2 and 7.3). The characterisation of the strength of interspecific competition through such a proxy is necessitated by the explicit modelling of the resource dynamics. This makes it impossible to directly quantify the competitive impact of one species on the other. In particular, this does not allow for a quantitative comparison with the strength of intraspecific competition dynamics, quantified by the carrying capacities  $k_1$  and  $k_2$ . Strong intraspecific competition reduces equilibrium densities and hence renders the locally superior species unable to utilise all of the available resource. This allows for the invasion of a second species and thus facilitates coexistence. The strength of intraspecific competition among the locally inferior species has no significant impact on the occurrence of spatially uniform coexistence.

For each of the non-desert equilibria of (7.3), there exists a complementary unstable steady state with the same species composition. Their instability for all biologically realistic parameter values causes them to bear no influence on the model outcomes discussed in this chapter. Nevertheless, details on unstable equilibria of (7.3) can be found in the supplementary material.

#### 7.4.2 Patterned species coexistence

Decreases in precipitation cause the spatially uniform states of (7.3) to lose stability to spatio-temporal patterns. Patterns either feature both plant species or consist of the coloniser species only. Single-species patterns of the locally superior species are always unstable to the introduction of the coloniser species, despite being stable in the absence of any competitor. In particular, a solution's species composition is not necessarily conserved across a transition from a spatially uniform to a spatially patterned state. For example, if intraspecific competition of the locally superior

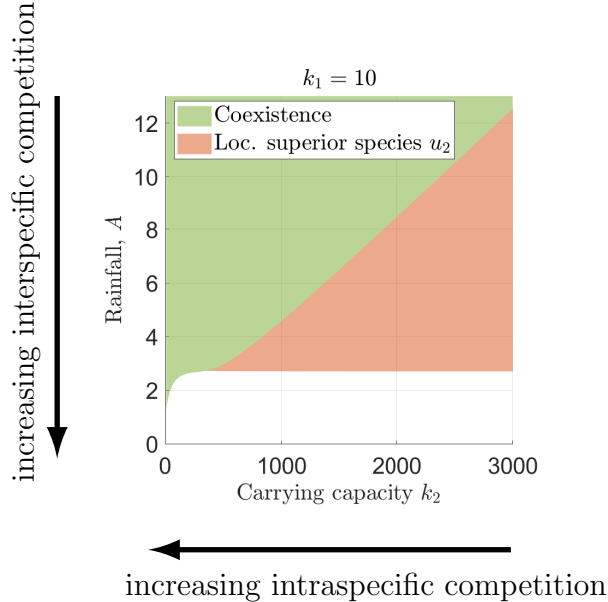


Figure 7.2: Stability of spatially uniform equilibria in the nonspatial model. Stability regions of the coexistence equilibrium and the equilibrium of the locally superior species are shown under changes to interspecific (rainfall parameter  $A$ ) and intraspecific (carrying capacity  $k_2$ ) competition. The equilibrium of the coloniser species is always unstable and the trivial desert steady state is stable in the whole parameter region (not shown). Parameter values are  $B_1 = 0.45$ ,  $B_2 = 0.05$ ,  $F = 0.11$ ,  $H = 0.11$ .

species is insufficient to stabilise spatially uniform coexistence, the spatially uniform single-species state nevertheless loses stability to a coexistence pattern (Fig. 7.3 (b)).

Moreover, the precipitation volume also determines if a solution represents a vegetation pattern or a spatially non-uniform savanna. The former state is attained for low rainfall levels at which plant densities oscillate between a level of high biomass and zero, corresponding to alternating bands of vegetation and bare soil. By contrast, spatially patterned savanna solutions occur for larger precipitation volumes and are characterised by oscillations between two non-zero biomass levels. Crucially, coexistence in a vegetation pattern state is only possible if intraspecific competition among the coloniser species is sufficiently strong (Fig. 7.3 (a) and (b)). If self-limitation of the coloniser species is weak, then the beneficial effects of its colonisation abilities outweigh the local superiority of its competitor for a wider range of precipitation volumes. The destabilisation of coexistence thus occurs at higher rainfall levels, where solutions represent a savanna state (Fig. 7.3 (c) and (d)).

Under high-volume rainfall regimes, a unique spatially uniform stable state exists for each value of the precipitation parameter, but multistability of stable equilibria occurs for lower rainfall amounts. Firstly, if a spatial pattern is a stable model outcome for a given precipitation volume, then a range of other patterned solutions are also stable. Such patterns differ in their wavelengths (distance between two consecutive biomass peaks) and their uphill migration speeds (Fig. 7.3 and Fig. 7.4 (a)).

Secondly, multistability of single-species and coexistence patterns, as well as coexistence patterns and spatially uniform states also occurs, especially if intraspecific competition among the coloniser species is strong (Fig. 7.3 (a) and (b)).

This singles out patterns' wavelengths and uphill migration speeds as crucial pieces of information in the understanding of transitions between species coexistence and single-species states. Typically, if a patterned state of a given wavelength loses its stability due to changes in precipitation, a transition, such as that depicted in Fig. 7.4 (c), to a pattern of a different wavelength occurs. The multistability of patterned states implies that the newly attained state is not necessarily close to destabilisation. Hence, such transitions cannot typically be reversed by simply increasing/decreasing the precipitation volume back to its original level.

A change in wavelength is not the only possible result of a pattern's destabilisation. If intraspecific competition of the coloniser species is strong, a large range of coexistence patterns lose their stability to a single-species pattern (of the coloniser) with the same wavelength as precipitation decreases. In such a case, destabilisation results in an extinction event, despite the stability of coexistence patterns at different wavelengths for the same environmental conditions (Fig. 7.3 (a) and (b) and Fig. 7.4). Thus, species richness in the system not only depends on precipitation volume and species properties but also on past states of the ecosystem. In particular, the resilience of coexistence patterns to increases in aridity depends on their wavelength and uphill migration speed. The phenomena outlined above are examples of hysteresis, a well-known feature of theoretical models of vegetation patterns and other patterned ecosystems [188].

Spatially uniform equilibria and regular spatio-temporal patterns are not the only stable outcomes of the model system (7.3). In the absence of strong intraspecific competition, no direct switch from regular coexistence pattern to a uniform state of the locally superior species occurs (Fig. 7.3 (d)). Instead, this transition takes place via a coexistence state, which lacks any regularity in space and time (example solution plot is shown in the supplementary material). Currently, I am unable to make any conclusive statements about this type of model solution and its ecological implications, but note that it relies on the intraspecific competition dynamics of both species being weak.

Similar to the spatially uniform states discussed in Sec. 7.4.1, stable patterned model outcomes of (7.3) are also complemented by unstable solutions. While in this context, unstable states do not have any ecological relevance, they are essential to understand the full solution structure of the mathematical model. Examples of bifurcation diagrams as well as more information on the bifurcations that occur in the system are given in the supplementary material.

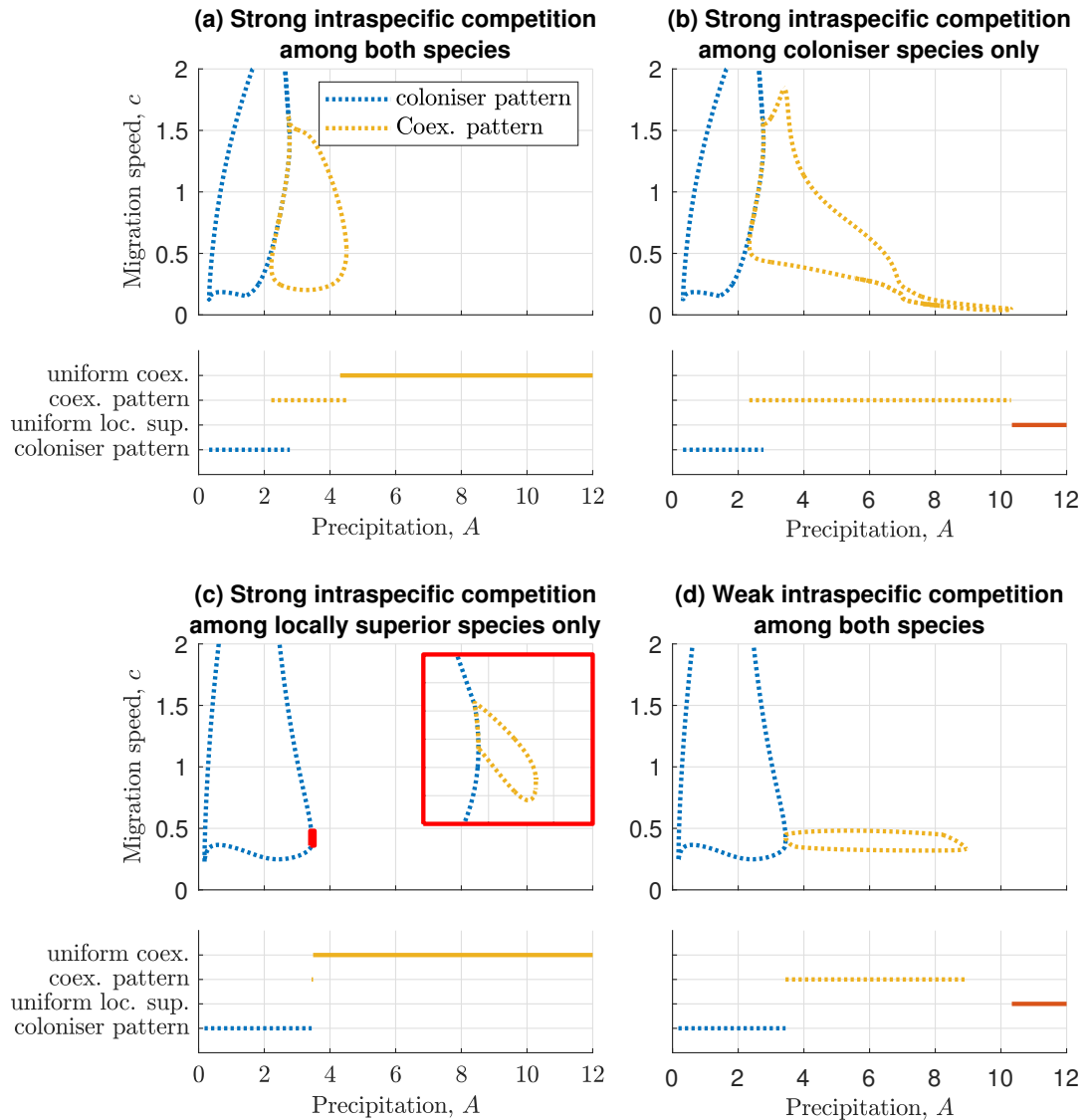
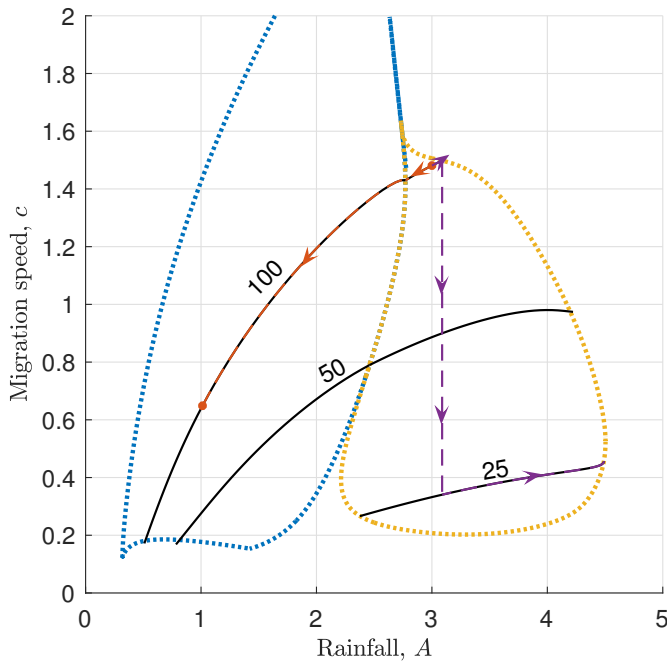
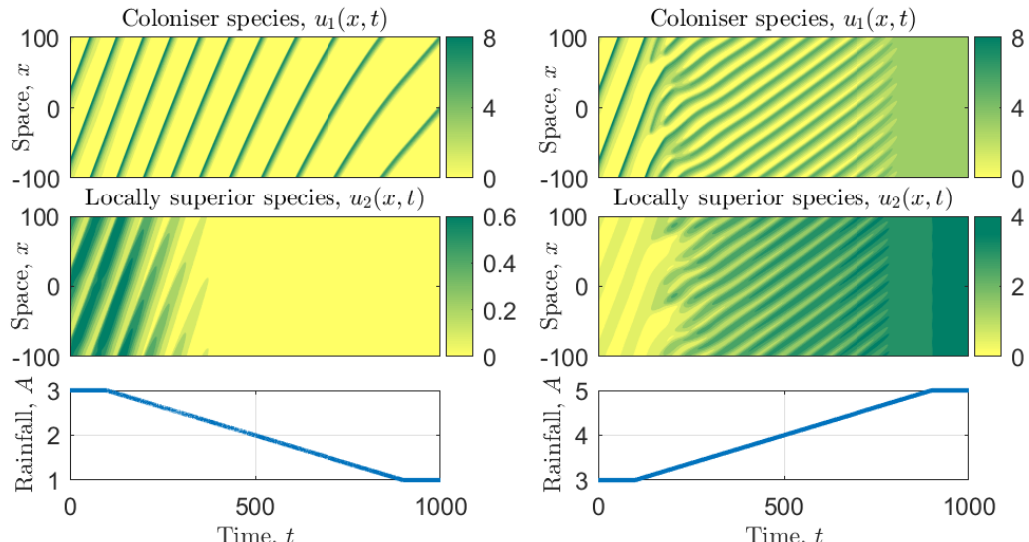


Figure 7.3: Overview of stable model outcomes for different combinations of species' intraspecific competition strengths. The lower panel in each quadrant provides a visualisation of the precipitation ranges in which spatially uniform (solid lines) and spatially patterned solutions (dotted lines) are stable model solutions. The top panel shows the stability boundaries of the patterned states in the  $(A, c)$  parameter plane and thus also provides information on the uphill migration speed of stable patterns. Increases in intraspecific competition strength of the locally superior species stabilises spatially uniform coexistence for lower precipitation volumes, while strong intraspecific competition among the coloniser species promotes patterned coexistence. The intraspecific competition strengths are  $k_1 = k_2 = 10$  in (a),  $k_1 = 10, k_2 = 10^4$  in (b),  $k_1 = 10^4, k_2 = 10$  in (c) and  $k_1 = k_2 = 10^4$  in (d), while other parameter values are  $B_1 = 0.45$ ,  $B_2 = 0.05$ ,  $F = H = 0.11$ ,  $\nu = 182.5$  and  $d = 500$  in (a)-(d).



(a) Wavelength contours of stable patterns.



(b) Transition to single-species pattern.

(c) Transition to uniform coexistence.

Figure 7.4: State transitions under changing precipitation. Transitions from patterned coexistence to a single-species pattern (b) and a uniform coexistence state (c) under changing precipitation volumes are shown. Both model solutions are initiated at rainfall volume  $A = 3$  and a wavelength of  $L = 100$ . Solutions follow wavelength contours (solid black curves in (a)) until they are destabilised and a pattern of a new stable wavelength is chosen. Red dashed lines in (a) indicate the dynamics of the solution shown in (b); purple dashed lines that of the model outcome visualised in (c). Parameter values correspond to those used in Fig. 7.3 (a).

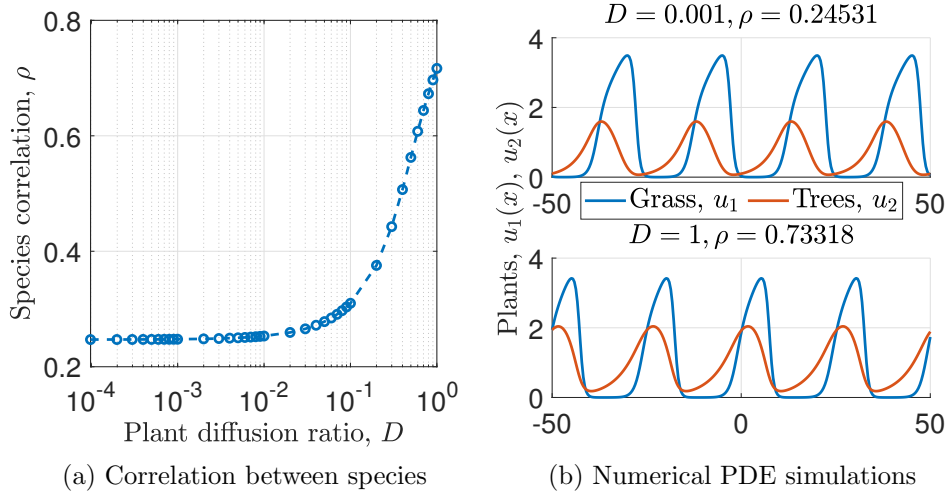


Figure 7.5: The spatial correlation between the two plant species components of model solutions under changes in the diffusion coefficient  $D$  are shown in (a). Part (b) visualises solution profiles ( $u_1, u_2$  only) for specific values of  $D$ . Correlation increases as dispersal behaviour becomes more similar. Other parameter values are  $B_1 = 0.45$ ,  $B_2 = 0.05$ ,  $F = H = 0.11$ ,  $\nu = 182.5$ ,  $d = 500$ ,  $k_1 = k_2 = 5$  and  $A = 2$ .

#### 7.4.3 Plant species' distribution

Depending on system parameters, the multispecies model (7.3) captures the spatial species distribution within vegetation stripes. In other words, the uphill edge of a single vegetation band is dominated by one species, while its competitor is mostly confined to a narrow region in the centre of the band.

The ratio of the plant species' diffusion coefficients  $D$  has the most significant impact on the correlation between both plant species (Fig. 7.5). If the species with slower growth rate also disperses at a slower rate, then the correlation between both species is small, as the uphill edge of each vegetation band features a high density of the faster disperser only. As the difference between the plant species' diffusion coefficients becomes smaller, the correlation between the plant densities increases. For  $D = 1$ , i.e. when both plant species diffuse at the same rate, both species feature near the top edge of each stripe at a high density. Nevertheless, solution components are not exactly in phase due to the faster growth and mortality dynamics of the coloniser species. (Fig. 7.5b).

### 7.5 Discussion

The exploration of coexistence mechanisms that prevent competitive exclusion in resource limited ecosystems has been a common research topic in theoretical ecology for many decades [30, 127, 212, 231]. The importance of considering intraspecific competition dynamics has been established early in the history of coexistence the-

ory (e.g. [115]). Self-limitation of species enables coexistence because it keeps their abundances sufficiently low to prevent resource monopolisation by any one species [30, 212]. More recently, heterogeneities caused by spatial self-organisation in otherwise homogeneous environments have been singled out as an alternative potential explanation of species coexistence under competition for a sole limiting resource [37, 64]. Interestingly, these processes are typically associated with opposite impacts on population growth in general: intraspecific competition corresponds to negative density-dependence in population growth, but spatial self-organisation involves local facilitation.

In the context of dryland vegetation, a classical example of a self-organisation principle in ecology, pattern formation on its own has been unable to explain species coexistence across a wide range of the precipitation (resource input) gradient [64, 157]. In this chapter, I show that the combination of facilitative self-organisation and self-limiting intraspecific competition in a theoretical framework provides more insights into the coexistence of a coloniser species with a locally superior species in states ranging from spatially uniform savannas to regular stripe patterns.

A widely applicable result of coexistence theory is that coexistence of two species can occur if each species' intraspecific competition is stronger than its impact on the competitor species (e.g. [30, 127]). Interestingly, the combination of intraspecific competition with spatial self-organisation dynamics show that different species' self-limitation is the facilitator of coexistence at opposite ends of the resource input spectrum. This phenomenon arises despite the assumption that both species do not qualitatively differ from each other in any of their functional responses to the environment. Under high resource availability, for which spatially uniform plant cover is possible, strong intraspecific competition of the locally superior species facilitates coexistence (Fig. 7.2). If self-limitation of the locally superior species is sufficiently strong, it cannot utilise all of the available resource and can thus allow for coexistence with a second species [127]. In this context, local superiority corresponds to a higher local average fitness, which is determined by the stability of spatially uniform single-species equilibria. While in the multispecies model presented in this chapter, the stability regions of these steady states do not overlap, complications in the definition of the locally superior species may arise in other modelling frameworks if bistability of single-species states occurs.

The impact of intraspecific competition changes significantly if resource availability is low. Under such environmental conditions, the spatial self-organisation principle destabilises spatially uniform states and leads to pattern formation. Firstly, species coexistence requires the locally superior species to be inferior in its colonisation abilities [64] (Chapter 6). This balance enables species coexistence due to spatial heterogeneities in the environment, caused by the spatial self-organisation.

The potential of intercepting resource run-off in uncolonised regions is high, which can be exploited by the coloniser. The redistribution of water towards areas of high biomass consequently facilitates the growth of the second species. Eventually, the locally superior species locally outcompetes the superior coloniser, thus creating a balance that facilitates coexistence. Secondly, coexistence in patterned form is facilitated by strong intraspecific competition of the coloniser species (Fig. 7.3 (b)). In contrast to the coexistence mechanism which applies under high resource availability and is discussed above, the intraspecific competition's impact on resource availability is not the cause of coexistence. Instead, coexistence under severe resource scarcity is enabled by the strengthening of the facilitative balance between the two species' colonisation abilities and local competitiveness. In the absence of intraspecific competition, the coloniser is able to tip that balance in its favour by being able to colonise new areas faster than being outcompeted locally by its competitor. Strong self-limitation prevents this and thus facilitates coexistence.

A different important aspect in the understanding of species coexistence in self-organised ecosystems highlighted by the results presented in this chapter is hysteresis. As is common with pattern-forming systems, multistability of stable states occur. In other words, given any set of parameters describing plant species and environmental conditions, no conclusive statement about the model outcome can be made. Instead, information about a pattern's history is required to obtain more information about its future dynamics. In particular, extinction events, i.e. the transition from a coexistence state to a single-species state, cannot be pinned down to a specific level of resource without having information about the ecosystem's current and past states (Fig. 7.4). Theoretical studies of history dependence in patterned vegetation in the context of only one species highlight that this property could be of crucial importance to advance our understanding of the ecosystem dynamics in general, not only of the transitions between coexistence and single-species states [44, 188]. Hysteresis is believed to be of crucial importance in many ecosystems [218], but empirical evidence of history dependence in patterned ecosystems is challenging to detect [49] and only limited empirical data on the phenomenon exists [216].

A novelty of results presented in this chapter is the proposal of a coexistence mechanism for dryland vegetation patterns that does not rely on species-specific assumptions. Previous theoretical models on the subject suggest that species coexistence in vegetation patterns is only possible if only one species contributes to the system's pattern-forming feedback loop [16, 145] or if plant species adapt to different soil moisture niches [27, 220]. By contrast, the coexistence mechanism presented in this chapter exclusively relies on comparative assumptions (e.g. one species being superior in its colonisation abilities while having a lower local average

fitness than its competitor). As a consequence, it applies to a wider combination of plant species and may be extended to other consumer-resource systems governed by self-organisation principles, for example shellfish reefs [32].

It is worth emphasising that the coexistence mechanism attributed to spatial self-organisation presented in this chapter differs from that proposed in a different class of models: rock-paper-scissor-type systems. In those models, coexistence is facilitated by competitive hierarchies of three or more species that follow the idea of the well-known children's game of the same name. Under such assumptions, spatial self-organisation occurs due to spatial segregation and leads to each coexisting species occupying its own habitat in a larger spatial domain [7, 97, 112, 161]. By contrast, the ecohydrological model presented in this chapter captures species coexistence within single patches of vegetation, in agreement with field observations [179, 222]. Moreover, it also captures both the uphill movement of vegetation stripes and the spatial species distribution within vegetation bands (Fig. 7.5b). Field observations of banded vegetation patterns report that the top edge of each stripe is dominated by annual grasses [179], thus coined to be the *coloniser species*, while other species are mostly confined to the centre and lower regions of each stripe. The comprehensive analysis of spatial correlation between both plant species in coexistence solutions of (7.3) shows that the spatial species distribution in a single vegetation band mainly depends on the plant species' dispersal behaviour. The faster the diffusion of the coloniser species in relation to its competitor, the more pronounced is its presence at the uphill edge of the stripe. This confirms the empirical hypothesis that the pioneering character of grasses in grass-tree coexistence is indeed caused by the faster dispersal of the coloniser species [179].

In the model presented in this chapter, all intraspecific dynamics are combined into one single parameter for each species. To gain a better understanding of how the balance between intraspecific and interspecific competition enables species coexistence, more information on these dynamics is needed. Promising first steps have been made through the explicit inclusion of (auto-)toxicity effects on interacting plant species [119]. These suggest potential avenues of further exploration in both the context of vegetation patterns and more general modelling frameworks for species coexistence within ecosystems in which both spatial self-organisation and intraspecific competition dynamics play a significant role.

## 7.6 Supplementary material

### 7.6.1 Dimensional model and its nondimensionalisation

The nondimensional multispecies model used in the manuscript is obtained from the dimensional model

$$\frac{\partial u_1}{\partial t} = \underbrace{\alpha_1^{(1)} w u_1 (\alpha_2^{(1)} u_1 + \alpha_2^{(2)} u_2) \left(1 - \frac{u_1}{\alpha_{10}^{(1)}}\right)}_{\text{plant growth}} - \underbrace{\alpha_3^{(1)} u_1}_{\text{plant mortality}} + \underbrace{\alpha_5^{(1)} \frac{\partial^2 u_1}{\partial x^2}}_{\text{plant dispersal}}, \quad (7.4a)$$

$$\frac{\partial u_2}{\partial t} = \underbrace{\alpha_1^{(2)} w u_2 (\alpha_2^{(1)} u_1 + \alpha_2^{(2)} u_2) \left(1 - \frac{u_2}{\alpha_{10}^{(2)}}\right)}_{\text{plant growth}} - \underbrace{\alpha_3^{(2)} u_2}_{\text{plant mortality}} + \underbrace{\alpha_5^{(2)} \frac{\partial^2 u_2}{\partial x^2}}_{\text{plant dispersal}}, \quad (7.4b)$$

$$\frac{\partial w}{\partial t} = \underbrace{\alpha_6}_{\text{rainfall}} - \underbrace{\alpha_7 w}_{\text{evaporation}} - \underbrace{w(u_1 + u_2)(\alpha_2^{(1)} u_1 + \alpha_2^{(2)} u_2)}_{\text{water uptake by plants}} + \underbrace{\alpha_8 \frac{\partial w}{\partial x}}_{\text{water flow downhill}} + \underbrace{\alpha_9 \frac{\partial^2 w}{\partial x^2}}_{\text{water diffusion}}. \quad (7.4c)$$

The model is based on the single-species reaction-advection-diffusion model by Klausmeier [99] and is an extension of the multispecies models used in [63, 64] (Chapters 5 and 6). The spatial domain is one-dimensional and  $x \in \mathbb{R}$  (units: m) increases in the uphill direction if the terrain is assumed to be sloped. Plant densities at time  $t \geq 0$  (years) and  $x \in \mathbb{R}$  are denoted by  $u_i(x, t)$  ( $\text{kg m}^{-1}$ ) and the water density by  $w(x, t)$  ( $\text{kg m}^{-1}$ ).

A constant amount of water is added to the system per unit time, represented by  $\alpha_6$  ( $\text{kg m}^{-1} \text{ years}^{-1}$ ) in the model. Water evaporation and drainage effects occur at rate  $\alpha_7$  ( $\text{years}^{-1}$ ). Water uptake is the product of three terms: the resource density  $w$ , the total consumer density  $u_1 + u_2$  and a term representing the increase in resource available for consumption in dense biomass patches  $\alpha_2^{(1)} u_1 + \alpha_2^{(2)} u_2$ . The constants  $\alpha_2^{(1)}$  and  $\alpha_2^{(2)}$  (both  $\text{m}^2 \text{ years}^{-1} \text{ kg}^{-2}$ ) account for the strength of each species' resource availability enhancement. In the absence of intraspecific competition, plant growth of each species directly corresponds to its water consumption and  $\alpha_1^{(1)}$  and  $\alpha_1^{(2)}$  (both dimensionless) quantify the species' water to biomass conversion ability. Further, plant growth is limited by density dependent effects, here modelled by a logistic growth-type term with carrying capacities  $\alpha_{10}^{(1)}$  and  $\alpha_{10}^{(2)}$  (both  $\text{kg m}^{-1}$ ), respectively. Plant mortality occurs at constant rates  $\alpha_3^{(1)}$  and  $\alpha_3^{(2)}$  (both  $\text{years}^{-1}$ ), respectively. Finally, both plant densities and the water density undergo diffusion with coefficients  $\alpha_5^{(1)}$ ,  $\alpha_5^{(2)}$  (both  $\text{m}^2 \text{ years}^{-1}$ ) and  $\alpha_9$  ( $\text{m}^2 \text{ years}^{-1}$ ), respectively. If the model is considered on sloped terrain, then water is assumed to flow downhill, modelled by advection with speed  $\alpha_8$  ( $\text{m years}^{-1}$ ).

A suitable nondimensionalisation of (7.4) is given by

$$\begin{aligned}
 u_1 &= \left( \frac{\alpha_7}{\alpha_2^{(1)}} \right)^{\frac{1}{2}} \tilde{u}_1, \quad u_2 = \left( \frac{\alpha_7}{\alpha_2^{(1)}} \right)^{\frac{1}{2}} \tilde{u}_2, \quad w = \frac{\alpha_7^{\frac{1}{2}}}{\alpha_1^{(1)} \left( \alpha_2^{(1)} \right)^{\frac{1}{2}}} \tilde{w}, \\
 x &= \left( \frac{\alpha_5^{(1)}}{\alpha_7} \right)^{\frac{1}{2}} \tilde{x}, \quad t = \frac{1}{\alpha_7} \tilde{t}, \quad A = \frac{\alpha_1^{(1)} \left( \alpha_2^{(1)} \right)^{\frac{1}{2}} \alpha_6}{\alpha_7^{\frac{3}{2}}}, \quad B_i = \frac{\alpha_3^{(i)}}{\alpha_7}, \quad F = \frac{\alpha_1^{(2)}}{\alpha_1^{(1)}}, \\
 H &= \frac{\alpha_2^{(2)}}{\alpha_2^{(1)}}, \quad k_i = \frac{\alpha_{10}^{(i)} \left( \alpha_2^{(1)} \right)^{\frac{1}{2}}}{\alpha_7^{-\frac{1}{2}}}, \quad D = \frac{\alpha_5^{(2)}}{\alpha_5^{(1)}}, \quad \nu = \frac{\alpha_8}{\left( \alpha_5^{(1)} \alpha_7 \right)^{\frac{1}{2}}}, \quad d = \frac{\alpha_9}{\alpha_5^{(1)}}.
 \end{aligned}$$

Substitution into (7.4) and dropping the tildes for brevity gives the nondimensional model (7.3).

### 7.6.2 Methods for model analysis

#### Transformation into travelling wave coordinates

Typically, model solutions of (7.3) are either spatially uniform or spatially patterned. In the latter case, they are periodic in space and move in the uphill direction of the spatial domain at a constant speed. Thus, spatial patterns in (7.3) belong to the class of periodic travelling waves, an important class of solutions for many reaction-advection-diffusion equations. Periodic travelling waves allow for a coordinate transformation to a comoving frame, as they can be represented by a single variable  $z = x - ct$ , where  $c \in \mathbb{R}$  is the migration speed of the solution profile. This coordinate transformation and setting  $u_1(x, t) = U_1(z)$ ,  $u_2(x, t) = U_2(z)$  and  $w(x, t) = W(z)$  reduces the PDE system (7.3) to the ODE system

$$WU_1(U_1 + HU_2) \left( 1 - \frac{U_1}{k_1} \right) - B_1 U_1 + c \frac{dU_1}{dz} + \frac{d^2 U_1}{dz^2} = 0, \quad (7.5a)$$

$$FWU_2(U_1 + HU_2) \left( 1 - \frac{U_2}{k_2} \right) - B_2 U_2 + c \frac{dU_2}{dz} + D \frac{d^2 U_2}{dz^2} = 0, \quad (7.5b)$$

$$A - W - W(U_1 + U_2)(U_1 + HU_2) + (c + \nu) \frac{dW}{dz} + d \frac{d^2 W}{dz^2} = 0. \quad (7.5c)$$

Spatially patterned solutions of the PDE system (7.3) correspond to limit cycles in the travelling wave ODE system (7.5). If a patterned solution exists in the PDE system (7.3) for a given value of the bifurcation parameter, here the precipitation volume  $A$ , then limit cycles in the ODE system (7.5) exist for a range of different

wavespeeds  $c$  at different wavelenghts.

### Bifurcation analysis

Properties of spatially uniform single-species states in the model are analytically tractable and an overview is provided below (Sec. 7.6.3) and can also be found in [59] (Chapter 8). Other properties of single-species states (pattern onset, pattern existence and pattern stability) as well as those of coexistence states (spatially uniform equilibria, pattern onset, pattern existence) are determined through numerical continuation using AUTO-07p [53]. Besides standard numerical continuation techniques, this also requires an understanding of the patterns' stability, which can be obtained from the patterns' essential spectra. Those are calculated using a numerical continuation method by Rademacher et al. [160]. I refer to [160, 187, 189] for full details on the method, and to [64] (Chapter 6) for details on the method's implementation for a model similar to (7.3).

#### 7.6.3 Stability of spatially uniform single-species states

The trivial and semi-trivial biologically relevant spatially uniform equilibria of (7.3) are the desert steady state  $(\overline{u}_1^D, \overline{u}_2^D, \overline{w}^D) = (0, 0, A)$ , the single-species state

$$\left(\overline{u}_1^\pm, 0, \overline{w}_1^\pm\right) = \left(\frac{A \pm \sqrt{A^2 - 4B_1 \left(B_1 + \frac{A}{k_1}\right)}}{2 \left(B_1 + \frac{A}{k_1}\right)}, 0, \frac{A}{1 + \left(\overline{u}_1^\pm\right)^2}\right),$$

of the coloniser species  $u_1$ , which exist provided

$$A > A_{\min}^{(1)} := 2B_1 \left(\frac{1}{k_1} + \sqrt{1 + \frac{1}{k_1^2}}\right),$$

and the single-species state

$$\left(0, \overline{u}_2^\pm, \overline{w}_2^\pm\right) = \left(0, \frac{FHA \pm \sqrt{(FHA)^2 - 4B_2 H \left(B_2 + \frac{FHA}{k_2}\right)}}{2H \left(B_2 + \frac{FHA}{k_2}\right)}, \frac{A}{1 + H \left(\overline{u}_2^\pm\right)^2}\right),$$

of the locally superior species, which exist provided

$$A > A_{\min}^{(2)} := \frac{2B_2}{FH} \left(\frac{1}{k_2} + \sqrt{H + \frac{1}{k_2^2}}\right).$$

Further, a pair of spatially uniform coexistence equilibria  $(\overline{u}_1^{C,\pm}, \overline{u}_2^{C,\pm}, \overline{w}^{C,\pm})$  ex-

ists. Even though a closed-form expression can be obtained, the equilibria's algebraic complexity makes any analytical approach infeasible and their properties are instead addressed through numerical continuation techniques.

The stability of trivial and semi-trivial spatially uniform equilibria to spatially uniform perturbations is determined by a standard linear stability approach. The desert steady state  $(\bar{u}_1^D, \bar{u}_2^D, \bar{w}^D)$  is always linearly stable (eigenvalues of Jacobian are  $-B_1, -B_2, -1$ ). The equilibrium  $(\bar{u}_1^+, 0, \bar{w}_1^+)$  of the coloniser species is stable for

$$A < A_u^{(1)} := \frac{B_2^2 + k_1^2 (B_2 - FB_1)^2}{Fk_1 (B_2 - FB_1)},$$

provided  $0 < B_2 - FB_1 < FB_1$  and  $k_1 > \sqrt{B_2(2FB_1 - B_2)}(B_2 - FB_1)^{-1}$ , and unstable otherwise. The single-species equilibrium  $(\bar{u}_1^-, 0, \bar{w}_1^-)$  is always unstable.

The equilibrium  $(0, \bar{u}_2^+, \bar{w}_2^+)$  of the locally superior species is stable for

$$A < A_u^{(2)} := \frac{F^2 B_1^2 + Hk_2^2 (B_2 - FB_1)^2}{FHk_2 (FB_1 - B_2)},$$

provided  $-B_2 < B_2 - FB_1 < 0$  and  $k_2 > \sqrt{B_1 FH(2B_2 - FB_1)}(H(FB_1 - B_2))^{-1}$ , and unstable otherwise. The single-species equilibrium  $(0, \bar{u}_2^-, \bar{w}_2^-)$  is always unstable.

Note that the stability regions of the single-species spatially uniform equilibria never overlap, because  $A_u^{(1)} A_u^{(2)} < 0$ . The sign of  $A_u^i$  is determined by  $B_2 - FB_1$ , the local average fitness difference between both species in the absence of intraspecific competition [63] (Chapter 5). Thus, only the single-species state of the species of higher local average fitness can be stable.

The instabilities that occur as  $A$  is increased are due to the introduction of the competitor species, which causes the single-species state to lose stability to the coexistence equilibrium. In the corresponding single-species models, both  $(\bar{u}_1^+, 0, \bar{w}_1^+)$  and  $(0, \bar{u}_2^+, \bar{w}_2^+)$  are stable for any precipitation value in their existence ranges if  $B_i < 2$ . Parameter estimates for dryland species consistently predict plant mortalities well below this threshold and thus  $B_i < 2$  is assumed throughout the analysis.

Existence and stability of the coexistence equilibrium  $(\bar{u}_1^{C+}, \bar{u}_2^{C+}, \bar{w}^{C+})$  are found using the numerical continuation software AUTO-07p [53] and are presented in the main text. Its complement  $(\bar{u}_1^{C-}, \bar{u}_2^{C-}, \bar{w}^{C-})$  is always unstable.

#### 7.6.4 Patterned model solutions

The stability diagrams presented in Fig. 3.2 of the main text only provide information on stable model solutions under changes to precipitation and intraspecific

competition strength. Nevertheless, unstable patterns provide useful information on how different stable states are connected in the system. Thus, a full bifurcation analysis can yield more insights into the model system. Fig. 7.6 in the supplementary material visualises corresponding bifurcation diagrams (for one fixed uphill migration speed only) obtained through numerical continuation. Note that the co-existence equilibrium may exist at negative densities of the inferior local competitor and this is visualised as *negative biomass* in Fig. 7.6. Further, single species states of  $u_1$  are shown as horizontal lines at  $u_2 = 0$  in the bifurcation diagrams for  $u_2$  and vice versa.

Bifurcation analysis of (7.3) establishes two different mechanisms as the cause of coexistence pattern onset; a Hopf bifurcation of the spatially uniform coexistence equilibrium, and a stability change of a single-species pattern due to the introduction of a competitor species. As a consequence, a coexistence pattern connects a single-species pattern to either the spatially uniform coexistence equilibrium (Fig. 7.6a and 7.6c) or the single-species pattern of its competitor (Fig. 7.6b) in the parameter space.

The onset of spatial patterns via a Hopf bifurcation of a spatially uniform equilibrium is a classical result of bifurcation theory (e.g. [142]). Coexistence pattern onset at such a bifurcation is inhibited (i.e. shifted to lower precipitation volumes) by both weak intraspecific competition of the superior coloniser and strong intraspecific competition of the locally superior species.

To understand the onset of coexistence patterns from a single-species pattern, information on the latter's stability is required. The stability properties can be split into two distinct and independent mechanisms. To be stable, a single-species pattern requires to be both stable in the absence of a second species and stable to the introduction of its competitor. Onset of coexistence patterns occurs if a single-species pattern loses/gains stability to the introduction of the second species [64] (Chapter 6).

A transition between the two mechanisms occurs if intraspecific competition of the locally superior species decreases. Such a decrease reduces the biomass of the locally inferior species in the coexistence equilibrium, and leads to an intersection of the coexistence equilibrium with the single-species equilibrium of the locally superior species. In particular, the Hopf bifurcations on both equilibria coincide for a critical level of the locally superior species' intraspecific competition. This intersection causes a switch in the onset mechanism of coexistence patterns, which hence connect both single-species solution branches for sufficiently weak intraspecific competition of the locally superior species (Fig. 7.6b).

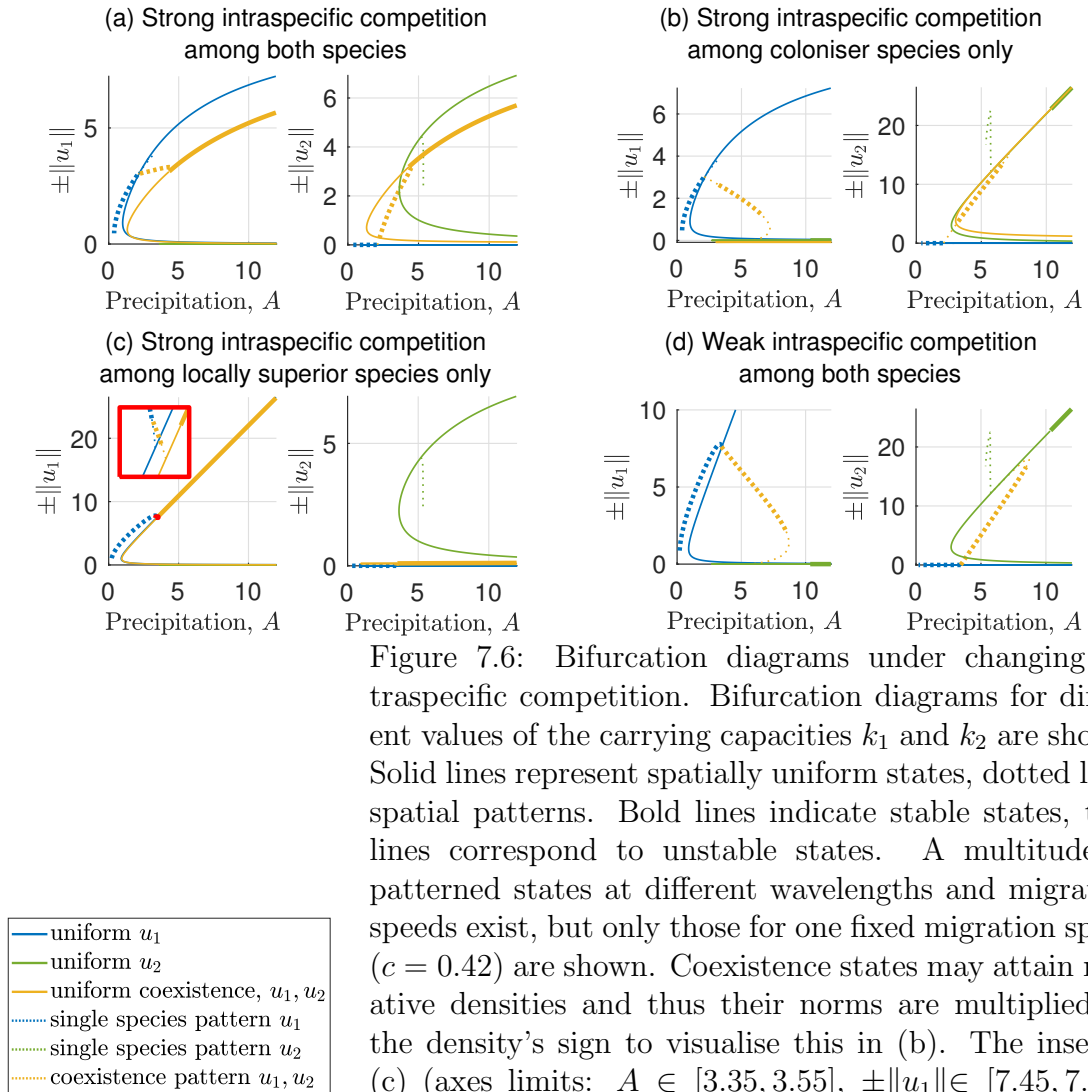


Figure 7.6: Bifurcation diagrams under changing intraspecific competition. Bifurcation diagrams for different values of the carrying capacities  $k_1$  and  $k_2$  are shown. Solid lines represent spatially uniform states, dotted lines spatial patterns. Bold lines indicate stable states, thin lines correspond to unstable states. A multitude of patterned states at different wavelengths and migration speeds exist, but only those for one fixed migration speed ( $c = 0.42$ ) are shown. Coexistence states may attain negative densities and thus their norms are multiplied by the density's sign to visualise this in (b). The inset in (c) (axes limits:  $A \in [3.35, 3.55]$ ,  $\pm \|u_1\| \in [7.45, 7.65]$ ) shows a blow-up of the small parameter region in which coexistence pattern occur. The intraspecific competition strengths are  $k_1 = k_2 = 10$  in (a),  $k_1 = 10, k_2 = 10^4$  in (b),  $k_1 = 10^4, k_2 = 10$  in (c) and  $k_1 = k_2 = 10^4$  in (d), while other parameter values are  $B_1 = 0.45$ ,  $B_2 = 0.05$ ,  $F = H = 0.11$ ,  $\nu = 182.5$  and  $d = 500$  in (a)-(d).

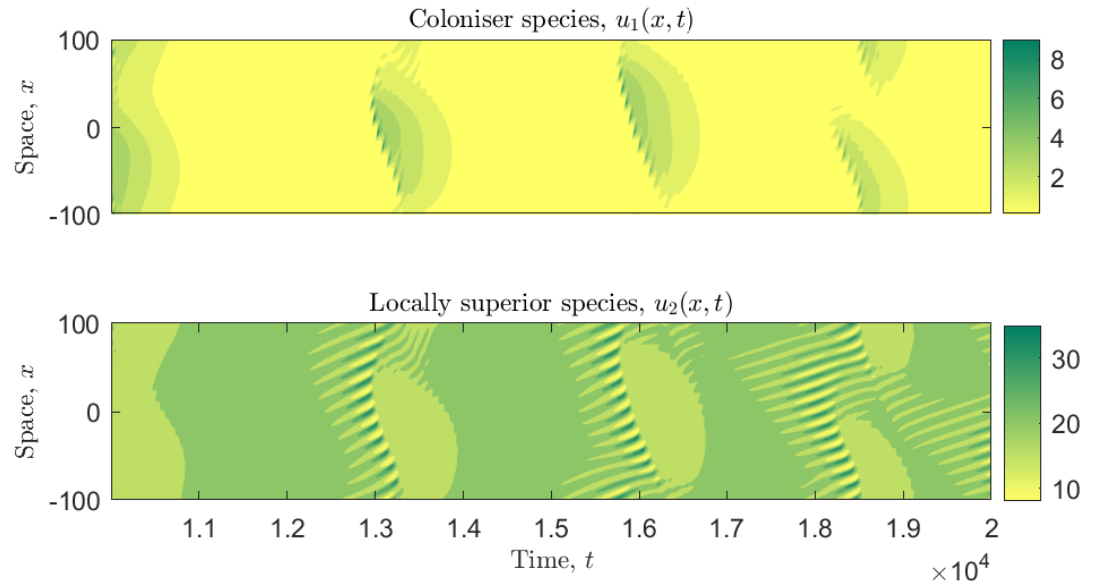


Figure 7.7: Transition between regular coexistence patterns and spatially uniform solution under weak intraspecific competition among both species. This figure shows the long-term behaviour of a model run for the parameter set  $A = 9.5$ ,  $B_1 = 0.45$ ,  $B_2 = 0.05$ ,  $k_1 = k_2 = 10^4$ ,  $F = H = 0.11$ ,  $\nu = 182.5$  and  $d = 500$ . This corresponds to the parameter region shown in Fig. 3.2 (d) of the main text in which neither a regular spatio-temporal nor a spatially uniform equilibrium is stable.

### 7.6.5 Other model solutions

Regular spatio-temporal patterns and spatially uniform states are not the only possible model outcomes of the multispecies model (7.3). In the absence of intraspecific competition, there exists an interval of the rainfall parameter in which neither of these solution types is stable. Instead, irregular coexistence solutions, such as that shown in Fig. 7.7 are outcomes of the model. My simulations suggest that this type of solution only occurs in a very small region of parameter space.

## Chapter 8

### Intraspecific competition in models for vegetation patterns: decrease in resilience to aridity and facilitation of species coexistence

The contents of this chapter are published in [59].

#### 8.1 Author contribution

The submitted paper [59] is a single-authored paper by Lukas Eigentler.

#### Abstract

Patterned vegetation is a characteristic feature of many dryland ecosystems. While plant densities on the ecosystem-wide scale are typically low, a spatial self-organisation principle leads to the occurrence of alternating patches of high biomass and patches of bare soil. Nevertheless, intraspecific competition dynamics other than competition for water over long spatial scales are commonly ignored in mathematical models for vegetation patterns. In this chapter, I address the impact of local intraspecific competition on a modelling framework for banded vegetation patterns. Firstly, I show that in the context of a single-species model, neglecting local intraspecific competition leads to an overestimation of a patterned ecosystem's resilience to increases in aridity. Secondly, in the context of a multispecies model, I argue that local intraspecific competition is a key element in the successful capture of species coexistence in model solutions representing a vegetation pattern. For both models, a detailed bifurcation analysis is presented to analyse the onset, existence and stability of patterns. Besides the strengths of local intraspecific competition, also the difference between two species has a significant impact on the bifurcation structure, providing crucial insights into the complex ecosystem dynamics. Predictions on future ecosystem dynamics presented in this chapter, especially on pattern onset and pattern stability, can aid the development of conservation programs.

## 8.2 Introduction

Approximately 40% of the Earth's land mass are classified as drylands [162]. The development of an understanding of ecosystem dynamics in water-deprived areas is of considerable socio-economic importance as a similar proportion of the total human population lives in arid and semi-arid climate zones, where agriculture is an integral part of the economy [51]. A characteristic feature of arid ecosystems is vegetation patterns, which form an interface between continuous vegetation cover and full deserts.

A mechanism commonly credited with the self-organisation of plants into alternating patches of biomass and bare soil is a positive feedback loop between local growth of vegetation and resource (water) distribution towards areas of high biomass. Several processes are the cause of such hydrological heterogeneities; for example the formation of biogenic soil crusts on bare ground that inhibit water infiltration into the soil and induce overland water flow, or the creation of soil moisture gradients due to vertically extended root systems in soil types that allow for fast water diffusion [130]. A common type of pattern is regular stripes that occur on hillslopes parallel to the contours of the terrain [222].

Ecosystem functioning heavily depends on plant populations as they constitute basal levels of food webs [132]. Changes to a vegetation pattern's properties, such as wavelength or recovery time from perturbations, can provide early warning signals of desertification processes, a major threat for economies in drylands [79, 170]. However, the large spatial and temporal scales associated with the ecohydrological dynamics of vegetation patterns restrict the acquisition of comprehensive high-quality data to specific properties (e.g. wavelength [48]) and to short time series. As a consequence, mathematical modelling, and in particular continuum approaches using systems of (potentially nonlocal) PDEs, have been established as a powerful tool to disentangle the complex ecosystem dynamics [132]. In broad terms, PDE models for patterned vegetation can be separated into two classes: kernel-based models that consist of a single equation describing the nonlocal plant interactions [105, 121, 122, 124]; and ecohydrological systems of two or more PDEs that explicitly account for the plants' interactions with the resource [74, 75, 86, 99, 163].

A subclass of kernel-based models captures the formation of vegetation patterns purely through nonlocal intraspecific competition among plants within a certain interaction range, whose size is determined by the horizontal extension of the plants' root network [121, 122]. By contrast, ecohydrological models explain the occurrence of spatiotemporal patterns through a scale dependent feedback between short-range facilitation and long-range competition for water [166]. Thereby, they commonly neglect any local intraspecific competition dynamics other than competition for wa-

ter, for example the release of autotoxic pathogens into the soil [126] or biomass limits in given areas due to the maximum biomasses of single individuals [76]. In particular, the majority of these theoretical frameworks assume that the rate of plant growth is either independent of the plant density or increasing with biomass. Combined with the pattern formation feedback in such models, this can result in solutions with biomass peaks of very high densities (e.g. [20]), a mathematically interesting but ecologically potentially irrelevant feature. A notable exception is the Gilad et al. model [74, 75], in which the rate of plant growth approaches zero as biomass density increases to its maximum value, and becomes negative for higher plant densities. Nevertheless, due to differences in the various modelling frameworks, the precise impact of local intraspecific competition for resources other than water on the ecosystem dynamics has not been previously addressed in the context of ecohydrological models for vegetation patterns.

It is a classical result from Lotka-Volterra competition models that the interplay between intraspecific and interspecific competition can facilitate species coexistence in resource-limited ecosystems, provided intraspecific competition among all species is sufficiently stronger than interspecific competition between them (e.g. [30]). In the context of patterned vegetation in drylands, coexistence of herbaceous (*grasses*) and woody (*shrubs and trees*) species is commonly observed, despite the species' competition for water [179]. Previous theoretical studies have successfully captured species coexistence in vegetation patterns by making the assumption that only one plant type contributes to the pattern-forming feedback [16, 145]. Such approaches, however, are based on strong assumptions on differences between plant species, such as contrasting functional responses to soil moisture, and may thus not be applicable in a general setting. In a previous chapter, I have shown that strong intraspecific competition of a species superior in its colonisation abilities can provide an alternative explanation for species coexistence that does not rely on such species-specific assumptions. I argued that a deeper understanding of the impact of intraspecific competition in spatially extended, resource-limited ecosystems can be a key ingredient in the explanation of species coexistence [60] (Chapter 7).

In this chapter, I closely investigate the impact of local intraspecific competition dynamics other than competition for water on solutions of an ecohydrological model for banded vegetation patterns in semi-arid environments. To distinguish these dynamics from long-range intraspecific competition for water, I use the term *local intraspecific competition* to refer to negative density-dependent effects that are unaffected by plants at other space locations. The chapter is split into two major parts. Firstly, I assess the effects of intraspecific competition on pattern onset, existence and stability in the context of a single-species model by comparing results to those obtained for the corresponding model which only takes into account intraspe-

cific competition for water (Sec. 8.3). Secondly, I extend the results presented in [60] and Chapter 7 to provide more insights into how local intraspecific competition can enable species coexistence under competition for a sole limiting resource by performing a comprehensive bifurcation analysis of a multispecies model (Sec. 8.4). In [60] and Chapter 7, I mainly focus on the impact of changes to local intraspecific competition strength of either species on the occurrence of coexistence patterns. By contrast, in this chapter, I present details on how results relate to earlier modelling studies that only consider intraspecific competition for water. In particular, I investigate how the bifurcation structure, especially the onset mechanisms for coexistence patterns, changes under simultaneous and separate variations of local intraspecific competition strengths of both species. Moreover, I address how the similarity between two species affects their ability to coexist. This contrasts with the analysis presented in [60] and Chapter 7 which is restricted to grass-tree coexistence, a parameter setting which corresponds to large species difference in the context of this chapter. Finally, in Sec. 8.5, I provide an interpretation and discussion of my results.

### 8.3 Single-species model

#### 8.3.1 Model

Several modelling frameworks to describe the ecohydrological dynamics in vegetation patterns have been proposed over the last two decades (see [124, 247] for reviews). One system that stands out due to its simplicity is the extended Klausmeier model [99], a phenomenological reaction-advection-diffusion system which has been the basis for many model extensions (e.g. [35, 58, 61, 62, 72, 120, 195]). To investigate the impact of local intraspecific competition dynamics other than those for water on the ecosystem dynamics, I adjust the plant growth rate in the Klausmeier model to account for negative effects of crowding. The resulting model describes the dynamics between the plant density  $u(x, t)$  and the water density  $w(x, t)$ , where the space coordinate  $x \in \mathbb{R}$  increases in the uphill direction of the domain and time  $t \geq 0$ . After a suitable nondimensionalisation [99, 185]<sup>1</sup>, the model is

---

<sup>1</sup>the nondimensionalisations in [99, 185] do not include  $k = \alpha_1 \alpha_2^{1/2} \alpha_3^{-1/2}$ , where  $\alpha_1$ ,  $\alpha_2$ ,  $\alpha_3$  are the strength of the plant species' local intraspecific competition, the constant quantifying the plants' enhancement of resource availability and the water's evaporation rate, respectively.

$$\frac{\partial u}{\partial t} = \underbrace{u^2 w \left(1 - \frac{u}{k}\right)}_{\text{plant growth}} - \underbrace{B u}_{\text{plant loss}} + \underbrace{\frac{\partial^2 u}{\partial x^2}}_{\text{plant dispersal}}, \quad (8.1a)$$

$$\frac{\partial w}{\partial t} = \underbrace{A}_{\text{rainfall}} - \underbrace{w}_{\text{evaporation and drainage}} - \underbrace{u^2 w}_{\text{water uptake by plants}} + \underbrace{\nu \frac{\partial w}{\partial x}}_{\text{water flow downhill}} + \underbrace{d \frac{\partial^2 w}{\partial x^2}}_{\text{water diffusion}}. \quad (8.1b)$$

The only modification to the extended Klausmeier model occurs in the plant growth term. In the extended Klausmeier model, plant growth is proportional to water consumption by plants, modelled by  $u^2 w$ . The nonlinearity arises due to the short-range facilitation by plants and thus is crucial in capturing the formation of spatiotemporal patterns in the model. The term is the product of the consumer density ( $u$ ), the resource density ( $w$ ), and a term that describes the enhancement of resource availability in existing biomass patches ( $u$ ), e.g. due to an increase in soil permeability caused by plants. While water uptake remains unaffected by the model extension, the rate of plant growth in (8.1) is not assumed to increase without bound as the plant density increases. Instead it is mediated by a logistic growth-type term, which accounts for local intraspecific competition among the plant species. This type of intraspecific competition may occur due to plant properties, such as maximum standing biomasses of single individuals [145] or the release of autotoxic compounds into the soil [126], but does not correspond to intraspecific competition for water; those dynamics are accounted for explicitly through the interactions with the water density. Moreover, in both the extended Klausmeier model and the extension (8.1), water is added to the system at a constant rate representing precipitation, both evaporation/drainage and plant mortality effects occur at constant rates and plant dispersal is modelled through diffusion. Finally, the water transport terms are derived from shallow-water theory, resulting in an advection (if the terrain is sloped) and diffusion term [74]. The diffusion of water was not included in the model's original formulation [99], but has become a commonly used addition (e.g. [199, 247]), which leads to the model being referred to as the *extended* Klausmeier model. In principle, the derivation of the flux from shallow-water theory yields a nonlinear diffusion term, but evidence that model outcomes do not significantly depend on the exact functional form has led to the simpler linear term being well-established [145]. The parameters  $A$ ,  $k$ ,  $B$ ,  $\nu$  and  $d$  are nondimensional parameters that can be interpreted as rainfall volume, strength of local intraspecific competition, rate of plant mortality, speed of water flow downhill and the water diffusion coefficient, respectively. Typical parameter estimates (e.g. [99]) suggest that  $\nu \approx 200$  is large compared to other model parameters, as it reflects the difference between the rate

of water advection and the rate of plant diffusion. The terrain's slope, however, is not steep itself. The derivation of water flow using shallow-water theory is only valid as long as water flow occurs as sheet flow and thus (8.1) does not apply if the terrain's gradient exceeds a few percent, consistent with topological data from field observations of banded vegetation patterns [222].

The (extended) Klausmeier model neglecting local intraspecific competition can be obtained from (8.1) by taking  $k \rightarrow \infty$ . This limiting case has been the subject of extensive mathematical analyses, in particular on the onset, existence and stability of spatial patterns [191]. Onset of patterned solutions in PDE systems usually occurs at either a Hopf bifurcation of a spatially uniform equilibrium or at a homoclinic solution (but see Sec. 8.4.4 for an exception). Typically, onset loci also form the boundaries of the parameter regions in which patterns exist, unless a fold in the solution branch occurs. The transition from uniform to patterned vegetation due to increases in aridity occurs at a Hopf bifurcation of a spatially uniform equilibrium, while at low rainfall volumes, patterned solutions terminate in a homoclinic solution [191]. The homoclinic solution also provides a lower bound for the pattern existence region, while the upper bound may occur at higher precipitation levels than those of the Hopf bifurcation due to the occurrence of a fold. A powerful tool in the analytical derivation of the patterns' features is the utilisation of the size of the advection parameter  $\nu$ , which allows for asymptotic approximations valid to leading order in  $\nu$  as  $\nu \rightarrow \infty$ .

The addition of local intraspecific competition does not have a qualitative impact on pattern onset, existence and stability in the model but noteworthy quantitative impacts are observed as detailed below. Besides the desert steady state  $\mathbf{v}_s^D = (0, A)$ , which exists and is stable in the whole parameter space, (8.1) admits a pair of vegetated spatially uniform equilibria given by

$$\mathbf{v}_s^\pm = (\bar{u}^\pm, \bar{w}^\pm) = \left( \frac{A \pm \sqrt{A^2 - 4B(B + \frac{A}{k})}}{2(B + \frac{A}{k})}, \frac{A}{1 + (\bar{u}^\pm)^2} \right),$$

which exist provided

$$A > A_{\min}^G := 2B \left( \frac{1}{k} + \sqrt{1 + \frac{1}{k^2}} \right).$$

The lower branch  $\mathbf{v}_s^-$  is unstable, while the upper branch  $\mathbf{v}_s^+$  is stable to spatially uniform perturbations if  $B < 2$ . Parameter estimates consistently suggest that plant mortality  $B$  remains well below this threshold, and thus the case  $B \geq 2$  is not con-

sidered in the analysis. As is expected, the plant density of the biologically relevant spatially uniform steady state  $\mathbf{v}_s^+$  decreases as the strength of local intraspecific competition increases (decrease in  $k$ ).

### 8.3.2 Pattern onset, existence & stability

Onset of spatial patterns due to a decrease in precipitation  $A$  occurs as  $\mathbf{v}_s^+$  loses stability to spatially nonuniform perturbations. This is referred to as a Turing-Hopf bifurcation and different methods to analytically calculate an asymptotic approximation of the rainfall threshold exist [61] (Chapter 2). In this context, this is best performed in travelling wave coordinates; patterned solutions of (8.1) are periodic travelling waves, i.e. solutions that are periodic in space and move in the uphill direction of the domain at a constant speed  $c \in \mathbb{R}$ , and motivate this approach. The transformation into a comoving frame is achieved by setting  $z := x - ct$ ,  $U(z) := u(x, t)$  and  $W(z) := w(x, t)$ , which yields the travelling wave ODE system

$$WU^2 \left(1 - \frac{U}{k}\right) - BU + c \frac{dU}{dz} + \frac{d^2U}{dz^2} = 0, \quad (8.2a)$$

$$A - W - WU^2 + (c + \nu) \frac{dW}{dz} + d \frac{d^2W}{dz^2} = 0. \quad (8.2b)$$

Patterned solutions of the PDE system (8.1) correspond to limit cycles of the ODE system (8.2). In the PDE setting, the patterns' features, such as their existence, would typically be investigated in a one-dimensional parameter space of a chosen control parameter, here the precipitation volume  $A$ . However, the transformation into travelling wave coordinates introduces an additional parameter, the migration speed  $c$ . If patterns exist for a given rainfall level in (8.1), then limit cycles with a range of different migration speeds exist in (8.2) for the same precipitation volume. As a consequence, the patterns' features need to be addressed in a two-dimensional parameter space in the travelling wave coordinates, comprised of the chosen PDE bifurcation parameter and the uphill migration speed  $c$ .

A convenient tool to investigate pattern onset, existence and stability is numerical continuation, but the size of the slope parameter  $\nu$  also allows for an analytical derivation of some properties valid to leading order in  $\nu$  as  $\nu \rightarrow \infty$ . A significant challenge of this approach is posed by the dependence of the parameter region in which patterns exist on the slope parameter  $\nu$ . In particular, the dependence of both  $A$  and  $c$  on  $\nu$  throughout the parameter region covers several orders of magnitude. For the standard Klausmeier model, an extensive analysis of these dynamics exists [184, 186, 190–192]. The focus of this chapter is on  $c = O_s(1)$

$(x = O_s(y) \iff x = O(y)$  but not  $x = o(y)$ ) as  $\nu \rightarrow \infty$  but the pattern dynamics in (8.1) for both small and large migration speeds are expected to be qualitatively similar to those of the model without local intraspecific competition.

The rainfall level the Turing-Hopf bifurcation causing pattern onset due to a destabilisation of the spatially uniform equilibrium is  $A = O_s(\sqrt{\nu})$  [192]. An asymptotic approximation of this critical threshold is found by calculating the corresponding Hopf bifurcation in the travelling wave framework and determining the maximum rainfall level on the loci of Hopf bifurcations in the  $(A, c)$  plane. The method follows that used for the (extended) Klausmeier model in [61, 192] (Chapter 2). The rescaling  $U = A/BU^*$ ,  $W = B^2/AW^*$ ,  $z = 1/\sqrt{B}z^*$ ,  $c = \sqrt{B}c^*$ ,  $\Gamma = A^2/(B^{5/2}\nu)$ ,  $\kappa = Bk/A$  and the assumption that  $A = O_s(\sqrt{\nu})$  yields

$$U' = \tilde{U}, \quad (8.3a)$$

$$\tilde{U}' = -c\tilde{U} - WU^2 \left( 1 - \frac{U}{\kappa} \right) + U, \quad (8.3b)$$

$$W' = -\Gamma (1 - U^2 W), \quad (8.3c)$$

valid to leading order in  $\nu$  as  $\nu \rightarrow \infty$ , after dropping the asterisks for brevity. The Hopf locus in the  $(A, c)$  parameter plane is calculated through a linear stability analysis. The eigenvalues  $\lambda \in \mathbb{C}$  of the Jacobian matrix of (8.3) are assumed to be purely imaginary, i.e.  $\lambda = i\omega$ ,  $\omega \in \mathbb{R}$ . This allows the Jacobian's characteristic polynomial to be split into its real and imaginary parts and for  $\omega$  to be eliminated. The resulting condition implicitly describes the Hopf-locus. Implicit differentiation facilitates the explicit calculation of the rainfall threshold at which the Turing-Hopf bifurcation occurs.

Investigation of this rainfall threshold shows that increases in local intraspecific competition shift the Turing-Hopf bifurcation to lower rainfall levels (Fig. 8.1). The stabilisation of the spatially uniform vegetated state is caused by a reduction in plant equilibrium density under strong local intraspecific competition which reduces the water requirements of the spatially uniform state.

The subset of the  $(A, c)$  parameter plane in which patterned solutions of (8.1) exist can be mapped out using numerical continuation. In terms of the PDE control parameter  $A$ , the pattern existence region is bounded from below by a homoclinic solution. Methods for calculating the location of homoclinic solutions exist [29], but for the analysis presented in this chapter it suffices to approximate homoclinic solutions by patterned solutions of large wavelength, say  $L = 1000$ . The upper precipitation bound of the pattern existence parameter region is given by either the

Hopf locus or the location of a fold in the solution branch, if such a fold occurs. The impact of local intraspecific competition is a reduction in the size of the parameter region in which patterns exist. As discussed above, the Hopf bifurcation occurs at lower rainfall levels if local intraspecific competition is strong and the locus of the fold mimics this behaviour. By contrast, the homoclinic solution is located at higher precipitation values if local intraspecific competition is strong (Fig. 8.1).

The stability of patterned solutions of (8.1) is determined through a calculation of the essential spectrum of the corresponding periodic travelling wave solution in (8.2). The essential spectrum  $\mathcal{S} \subset \mathbb{C}$  of a periodic travelling wave describes the leading order behaviour of perturbations to it. Due to translation invariance of periodic travelling waves, the origin is excluded from the following definition of stability. If  $\mathcal{S}$  lies entirely in  $\{z \in \mathbb{C} : \Re(z) < 0\}$ , then the corresponding pattern is stable, otherwise it is unstable. The essential spectrum is calculated through a numerical continuation algorithm by Rademacher et al. [160], and I refer to [160, 187, 189] for full details on the method and to [64] (Chapter 6) for an overview of an implementation to a related system. In particular, the algorithm also facilitates the tracking of stability boundaries, such as that displayed in Fig. 8.1 based on a numerical continuation of the spectra.

An application of this algorithm to (8.1) yields that strong local intraspecific competition stabilises patterned solutions at slower uphill migration speeds (Fig. 8.1). However, combined with the results on pattern existence discussed above, this also shows that the transition from patterned states to a full desert state occurs at higher rainfall levels if local intraspecific competition is strong (Fig. 8.1). Thus, neglect of intraspecific competition dynamics other than those for water in the model causes an overestimation of both the patterns' existence and stability ranges, in particular if a species carrying capacity is small (Fig. 8.1c).

## 8.4 Multispecies model

### 8.4.1 Model

Species coexistence in dryland ecosystems has previously been addressed in several modelling frameworks. Both Baudena and Rietkerk [16] and Nathan et al. [145] have successfully explained tree-grass coexistence in patterned form by assuming that only one of the two species induces a pattern-forming feedback loop. The assumption that plant species significantly differ in their functional responses to the environment, however, imposes a restriction on the applicability to a general setting. To overcome this, I have introduced a modelling framework to investigate species coexistence that does not rely on such an assumption in a previous chapter [63] (Chapter 5).

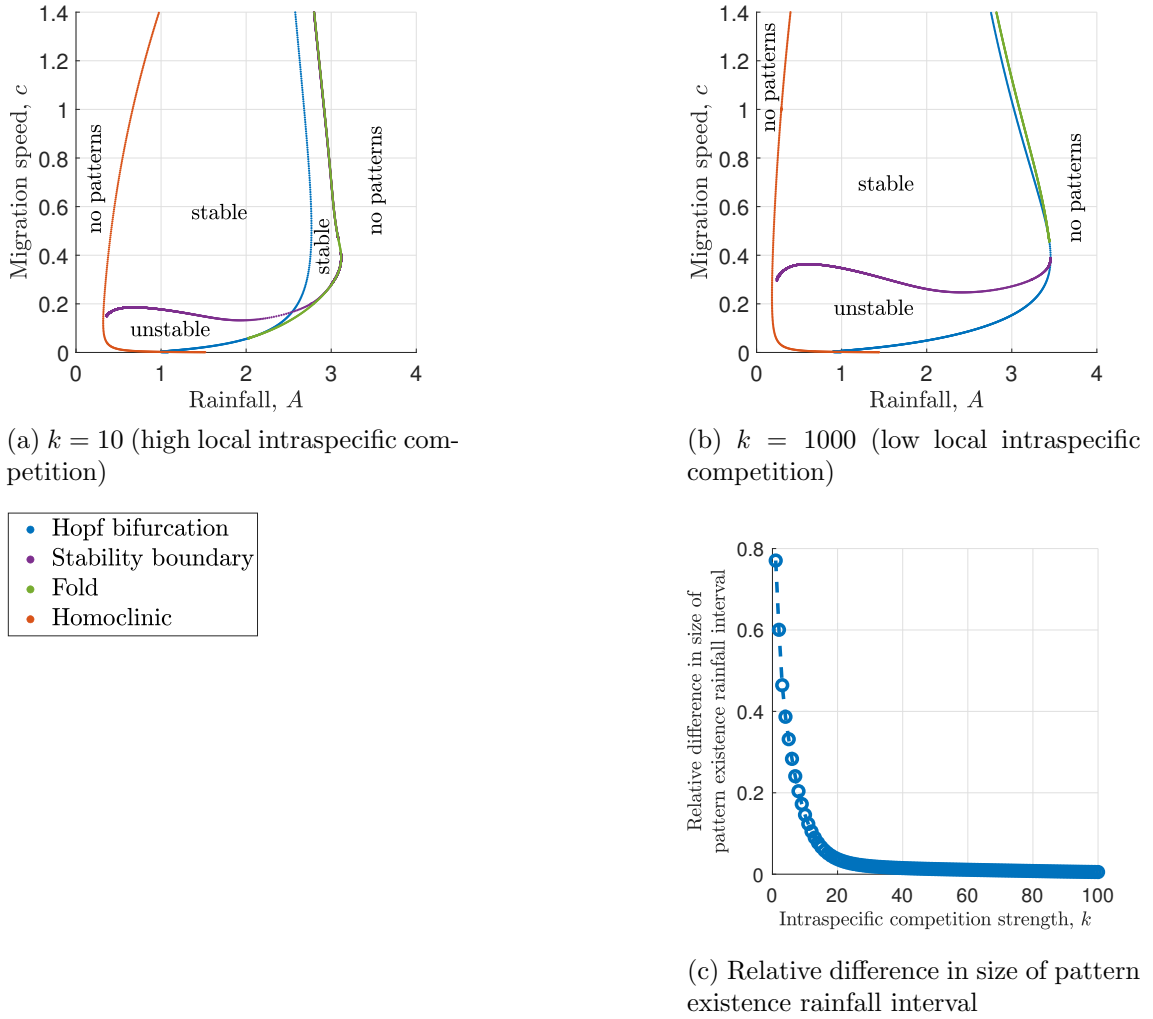


**Figure 8.1: Local intraspecific competition stabilises spatially uniform solutions and patterns at lower migration speeds.** Onset, existence and stability parameter regions of patterned solutions of (8.1) are shown in the  $(A, c)$  parameter plane. Onset at high precipitation values occurs at a Hopf bifurcation, while onset at low values occurs at a homoclinic solution. The existence region of patterns is bounded below by the homoclinic solution and bounded above by either the Hopf bifurcation or a fold in the solution branch, if it exists. Part (a) corresponds to strong local intraspecific competition, (b) to weak local intraspecific competition. The loci of both the Hopf bifurcation and the fold in the patterned solution branches are shifted to lower precipitation volumes if local intraspecific competition is strong, while the homoclinic solution occurs at higher rainfall levels. Hence, the length of the rainfall interval in which patterns exist decreases with increasing local intraspecific competition. Shown in (c), the relative difference in the size of the pattern existence rainfall interval is given by  $(\bar{A}_\infty - \bar{A}_k)/\bar{A}_\infty$ , where  $\bar{A}_\infty$  and  $\bar{A}_k$  are the lengths of the pattern existence rainfall interval in the absence of local intraspecific competition and for local intraspecific competition dynamics with carrying capacity  $k$ , respectively. Moreover, strong local intraspecific competition stabilises patterns at lower migration speeds.

If intraspecific competition dynamics are restricted to the plant's competition for water, this model successfully captures species coexistence as long transient states in both a spatially uniform and a vegetation pattern state, provided that species are of similar average fitness [63] (Chapter 5). Moreover, coexistence is also possible in a *spatially nonuniform savanna state* if there is a balance between the species' local competitiveness and their colonisation abilities [64] (Chapter 6). The term *savanna* is ambiguous and a variety of different definitions of savanna ecosystems exist [176, 205]. In this chapter, *spatially nonuniform savanna* refers to a state that is represented by periodic travelling wave solutions in which both species coexist, their solution profiles are approximately in phase (but see Sec. 8.4.5) and the total plant density oscillates between two nonzero biomass level. If additionally local intraspecific competition dynamics are taken into account, then coexistence is possible in a vegetation pattern state (periodic travelling wave solutions in which the total plant density oscillates between a high biomass level and zero), provided local intraspecific competition among the superior coloniser is sufficiently large [60] (Chapter 7). In this chapter, I provide more information on the impact of local intraspecific competition on the origin and existence of patterned model solutions in which species coexist.

To do so, the model used in the analysis is

$$\frac{\partial u_1}{\partial t} = \underbrace{wu_1(u_1 + Hu_2)}_{\text{plant growth}} \left(1 - \frac{u_1}{k_1}\right) - \underbrace{B_1 u_1}_{\text{plant mortality}} + \underbrace{\frac{\partial^2 u_1}{\partial x^2}}_{\text{plant dispersal}}, \quad (8.4a)$$

$$\frac{\partial u_2}{\partial t} = \underbrace{Fwu_2(u_1 + Hu_2)}_{\text{plant growth}} \left(1 - \frac{u_2}{k_2}\right) - \underbrace{B_2 u_2}_{\text{plant mortality}} + \underbrace{D \frac{\partial^2 u_2}{\partial x^2}}_{\text{plant dispersal}}, \quad (8.4b)$$

$$\frac{\partial w}{\partial t} = \underbrace{A}_{\text{rainfall}} - \underbrace{w}_{\text{evaporation and drainage}} - \underbrace{w(u_1 + u_2)(u_1 + Hu_2)}_{\text{water uptake by plants}} + \underbrace{\nu \frac{\partial w}{\partial x}}_{\text{water flow downhill}} + \underbrace{d \frac{\partial^2 w}{\partial x^2}}_{\text{water diffusion}}, \quad (8.4c)$$

after a suitable nondimensionalisation [60] (Chapter 7). The model is based on the single-species model (8.1) presented in Sec. 8.3 and consequently all modelling assumptions are identical to those taken in the single-species model. In particular, water uptake of species  $u_i$  is given by  $wu_i(u_1 + Hu_2)$  and summing over both species yields the third term in (8.4c). In other words, each species not only facilitates its own water consumption (and hence growth) but also that of its competitor. However, the strength of facilitation (for example due to increases soil permeability) differs between species and this is accounted for by the nondimensional constant

$H$ . As in the single-species model (8.1), plant growth of a species in the absence of local intraspecific competition dynamics is proportional to water consumption of that species. However, to account for local intraspecific competition among species, negative density-dependence is also included in the growth terms. The constants  $k_1$  and  $k_2$  are the maximum standing biomasses of species  $u_1$  and  $u_2$ , respectively. Note that  $u_1$  has no direct competitive impact on  $u_2$  and vice versa. Interspecific competition only occurs due to competition for water. The negative density dependence in the growth rates thus strictly correspond to intraspecific competition, for example due to the release of autotoxic pathogens into the soil [126]. The parameter  $B_1$  of species  $u_1$  corresponds to  $B$  in the single-species model (8.1), while the additional parameters  $F$ ,  $B_2$  and  $D$  are all related to the newly introduced species  $u_2$  and represent its growth, death rate and dispersal coefficient, respectively.

Moreover, the single species model (8.1) can be obtained from (8.4) by setting one of the plant densities to zero. In the case of  $u_1 = 0$  this further requires a rescaling. As a consequence, results presented in Sec. 8.3 also hold for the multispecies model (8.4) in the absence of a competitor species. The introduction of a second species nevertheless has an impact on the single-species states of the system, which is discussed below.

The model only accounting for intraspecific competition for water is analysed in [64] and Chapter 6. It is obtained from (8.4) by taking the limit  $k_1, k_2 \rightarrow \infty$ . This limiting behaviour motivates a comparison of results presented in this chapter with those in [64] (Chapter 6), to address what impact the consideration of local intraspecific competition dynamics has on the modelling framework. I present results for  $k_1 = k_2$  to make such a comparison, but also discuss the effects of varying  $k_1$  and  $k_2$  separately.

The main purpose of this chapter is to discuss the impact of local intraspecific competition and further develop the understanding of coexistence of herbaceous species and woody species in dryland ecosystems. Due to the symmetry in the model, I assume, without loss of generality, that  $u_1$  and  $u_2$  represent a grass and tree/shrub species, respectively. Event though the lack of detailed empirical data does not allow for an accurate parameter estimation, model parameters can be obtained from previous theoretical work (e.g. [99, 199]). Moreover, the distinction between a grass and a tree species allows for qualitative assumptions on some model parameters. For example, a plant species' water-to-biomass conversion abilities can be deduced from the time a population requires to attain its steady state density in the absence of any resource scarcity or competition. Grasses reach their equilibrium densities on a much shorter timescale than shrubs and trees, which suggests that they are superior in their ability to convert water into new biomass ( $F < 1$ ) [1]. Similarly, a species' mortality rate can be inferred from its average lifespan. Typically, grasses have a

much shorter lifespan than shrubs and trees which leads to a higher mortality rate in the mathematical model ( $B_1 > B_2$ ) [1]. The diffusion operators in (8.4a) relate the spatial spread of each species with time. Typically, the time from germination to the first dispersal of viable seeds is much longer for shrubs and trees, which suggests a lower diffusion coefficient ( $D < 1$ ) [64] (Chapter 6). Finally, if other parameters are known, the constant describing local facilitation can be deduced from a species' equilibrium density. This is typically higher for shrubs and trees which yields that grasses' facilitative impact per unit biomass is stronger ( $H < 1$ ) [99]. As a consequence of these qualitative assumptions, the grass species  $u_1$  is superior in its colonisation abilities and is thus referred to as the *coloniser species* or *pioneer species*. In the absence of local intraspecific competition, species coexistence occurs as a state representing a savanna biome if the inferior coloniser  $u_2$  is the *superior local competitor* [64] (Chapter 6), quantified by the average local fitness difference  $B_2 - FB_1$  being negative [63] (Chapter 5). In this chapter, I focus on this parameter setting to explore the role of local intraspecific competition and species difference in the coexistence of species in vegetation patterns. For the latter, I follow the approach of [63] (Chapter 5) and set

$$\begin{aligned} B_2 &= B_1 - \chi(B_1 - \widetilde{B}_2), & F &= 1 - \chi(1 - \widetilde{F}), & H &= 1 - \chi(1 - \widetilde{H}), \\ D &= 1 - \chi(1 - \widetilde{D}), \end{aligned} \tag{8.5}$$

where  $\widetilde{B}_2$ ,  $\widetilde{F}$ ,  $\widetilde{H}$  and  $\widetilde{D}$  are typical parameter estimates for a tree species. Thus, the difference between  $u_1$  and  $u_2$  is quantified by a single parameter  $0 \leq \chi \leq 1$ . Note that the local intraspecific competition strengths  $k_1$  and  $k_2$  are not included in this definition as their impact is addressed separately. Unless otherwise stated, I set  $B_1 = 0.45$ ,  $\widetilde{B}_2 = 0.004$ ,  $\widetilde{F} = \widetilde{H} = \widetilde{D} = 0.01$ ,  $k_1 = 10$ ,  $k_2 = 10$ ,  $d = 500$  and  $\nu = 182.5$  and  $\chi = 0.9$ . The precipitation volume  $A$  is the main bifurcation parameter of the system.

#### 8.4.2 Stability in spatially uniform model

As for the single-species model (8.1), an understanding of patterned solutions requires knowledge of the system's dynamics in a spatially uniform setting. The system has up to seven spatially uniform equilibria, as visualised in Fig. 8.2. The desert steady state  $\overline{\mathbf{v}_m^d} = (0, 0, A)$ , the pair of single-species grass equilibria  $\overline{\mathbf{v}_m^{g,\pm}} = (\overline{u_1^{g,\pm}}, 0, \overline{w^{g,\pm}})$ , where  $\overline{u_1^{g,\pm}} = \overline{u^\pm}$  and  $\overline{w^{g,\pm}} = \overline{w^\pm}$  and the latter's existence threshold  $A > A_{\min}^g := A_{\min}$  are identical with those of the single-species model presented in Sec. 8.3. Due to the symmetry in the model, (8.4) also admits a pair

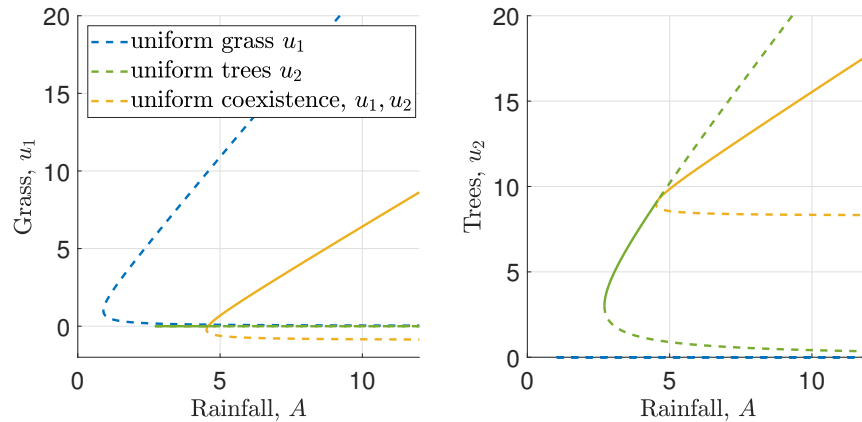


**Figure 8.2: Linear stability of spatially uniform equilibria.** The spatially uniform equilibria of (8.4) and their stability under changes to the precipitation volume  $A$  are shown. Solid lines indicate stable states, dashed lines unstable states. For high precipitation values, the coexistence equilibrium  $\bar{\mathbf{v}}_m^{c,+}$  is stable because interspecific competition for water is sufficiently lower than intraspecific competition. A decrease in  $A$  causes  $\bar{\mathbf{v}}_m^{c,+}$  to lose stability to the single-species tree equilibrium  $\bar{\mathbf{v}}_m^{t,+}$ . For the parameters used in the visualisation the stability change occurs where both equilibria intersect, but this need not be the case. Also note that at the intersection of equilibria, the coexistence steady state becomes ecologically irrelevant, as one of the plant densities becomes negative. Nevertheless, this steady state can be instructive for mathematical understanding of the dynamics. The grass equilibrium  $\bar{\mathbf{v}}_m^{g,+}$  is unstable for all  $A$ , because changes in rainfall cannot change which species is of higher local average fitness. Here  $k_1 = k_2 = 1000$  to keep local intraspecific competition sufficiently weak. For significantly smaller values of  $k_1 = k_2$  only the coexistence equilibrium is stable.

of single-species tree equilibria, given by

$$\begin{aligned}\overline{\mathbf{v}_m^{t,\pm}} &:= \left(0, \overline{u_2^{t,\pm}}, \overline{w^{t,\pm}}\right) \\ &= \left(0, -\frac{FHA \pm \sqrt{(FHA)^2 - 4B_2H(B_2 + \frac{FHA}{k_2})}}{2H(B_2 + \frac{FHA}{k_2})}, \frac{A}{1 + H(\overline{u_2^{t,\pm}})^2}\right),\end{aligned}$$

which exist provided

$$A > A_{\min}^t := \frac{2B_2}{FH} \left( \frac{1}{k_2} + \sqrt{H + \frac{1}{k_2^2}} \right).$$

Finally, a pair of coexistence spatially uniform steady states  $\overline{\mathbf{v}_m^{c,\pm}} := (\overline{u_1^{c,\pm}}, \overline{u_2^{c,\pm}}, \overline{w^{c,\pm}})$  exists, provided precipitation is sufficiently large. While it is possible to obtain a closed-form expression for  $\overline{\mathbf{v}_m^{c,\pm}}$ , its algebraic complexity renders any analytical approach to study its properties impracticable.

The desert steady state  $\overline{\mathbf{v}_m^d}$  is always linearly stable (the eigenvalues of its Jacobian are  $-B_1, -B_2, -1$ ). The grass equilibrium  $\overline{\mathbf{v}_m^{g,+}}$  is linearly stable for

$$A < A_u^G := \frac{B_2^2 + k_1^2(B_2 - FB_1)^2}{Fk_1(B_2 - FB_1)},$$

provided  $0 < B_2 - FB_1 < FB_1$  and  $k_1 > \sqrt{B_2(2FB_1 - B_2)}(B_2 - FB_1)^{-1}$ , and unstable otherwise. The second grass equilibrium  $\overline{\mathbf{v}_m^{g,-}}$  is unstable. The tree equilibrium  $\overline{\mathbf{v}_m^{t,+}}$  is stable for

$$A < A_u^T := \frac{F^2B_1^2 + Hk_2^2(B_2 - FB_1)^2}{FHk_2(FB_1 - B_2)},$$

provided  $-B_2 < B_2 - FB_1 < 0$  and  $k_2 > \sqrt{B_1FH(2B_2 - FB_1)}(H(FB_1 - B_2))^{-1}$ , and unstable otherwise. The second tree equilibrium  $\overline{\mathbf{v}_m^{t,-}}$  is unstable. Existence and stability of the coexistence equilibria  $\overline{\mathbf{v}_m^{c,\pm}}$  are found using the numerical continuation software AUTO-07p [53]. The lower branch  $\overline{\mathbf{v}_m^{c,-}}$  is always unstable, while  $\overline{\mathbf{v}_m^{c,+}}$  is stable if intraspecific competition is sufficiently stronger than interspecific competition. In particular, the local intraspecific competition of the locally superior species needs to be sufficiently strong for coexistence to be stable, while that of the

locally inferior species only has a negligible effect on the stability of the equilibrium.

The upper bounds on the rainfall parameter and other constraints required for stability of the spatially uniform single-species equilibria are a crucial difference to the stability results for the single-species model (8.1). As precipitation is increased, the single-species equilibria lose their stability to the coexistence equilibrium  $\overline{\mathbf{v}_m^{c,+}}$ , because an increase in resource availability causes a reduction in the strength of interspecific competition (Fig. 8.2). In the absence of local intraspecific competition, no coexistence equilibrium exists and no upper bound on the rainfall parameter for stability of the single-species equilibria exists.

Moreover, both in (8.4) and in the absence of local intraspecific competition, no bistability of the single-species equilibria can occur, as the upper precipitation bounds satisfy  $A_u^g A_u^t < 0$  (Fig. 8.2). The quantity  $B_2 - FB_1$ , which determines the signs of  $A_u^g$  and  $A_u^t$ , denotes the local average fitness difference between both species in the absence of any local intraspecific competition [63] (Chapter 5). A definition of local average fitness in (8.4) is not as straightforward as in the model with no local intraspecific competition, but the stability thresholds  $A_u^G$  and  $A_u^T$  highlight that local intraspecific competition cannot change which species is of higher local average fitness.

#### 8.4.3 Single-species patterns

Onset and existence of single-species patterns remain independent of the introduction of a second species, i.e. results presented for the single species model (8.1) also hold for the multispecies model (8.4). By contrast, stability of single-species patterns is significantly affected by the introduction of a competitor species and is also related to the onset of coexistence patterns.

As for the single species model (8.1), patterned solutions of (8.4) are limit cycles of the corresponding travelling wave ODE system

$$WU_1(U_1 + HU_2) \left(1 - \frac{U_1}{k_1}\right) - B_1 U_1 + c \frac{dU_1}{dz} + \frac{d^2 U_1}{dz^2} = 0, \quad (8.6a)$$

$$FWU_2(U_1 + HU_2) \left(1 - \frac{U_2}{k_2}\right) - B_2 U_2 + c \frac{dU_2}{dz} + D \frac{d^2 U_2}{dz^2} = 0, \quad (8.6b)$$

$$A - W - W(U_1 + U_2)(U_1 + HU_2) + (c + \nu) \frac{dW}{dz} + d \frac{d^2 W}{dz^2} = 0, \quad (8.6c)$$

which is obtained from the PDE model (8.4) by setting  $u_1(x, t) = U_1(z)$ ,  $u_2(x, t) = U_2(z)$  and  $w(x, t) = W(z)$  for  $z = x - ct$ ,  $c \in \mathbb{R}$ . As in the single-species model (8.1), this introduces a new parameter, the uphill migration speed  $c$ , and the bifurc-

ation analysis is performed in the  $(A, c)$  parameter plane. However, for illustrative purposes, I fix the migration speed in the presentation of the bifurcation diagrams, but emphasise that the results do not qualitatively depend on the choice of  $c$ , unless otherwise stated. The transformation into the travelling wave framework enables the calculation of a pattern's essential spectrum to determine its stability using the numerical continuation method by Rademacher et al. [160], and I again refer to [160, 187, 189] for full details on the method and to [64] (Chapter 6) for an overview on how this algorithm is implemented for (8.4) in the limit  $k_1, k_2 \rightarrow \infty$ .

Unlike pattern onset and existence, the stability of single-species patterns of (8.4) is affected by the second species in the system. For a single-species pattern to be stable in the multispecies model (8.4), it needs to be stable in the context of the single-species model (8.1) and stable to the introduction of the competitor species, two conditions that are independent of each other. The stability of a single-species pattern to the introduction of the competitor species is determined by a comparison of its essential spectrum in the multispecies model with that of the same solution in the single-species model (Fig. 8.3). The spectrum of the periodic travelling wave in the single-species model is a subset of that of the solution in the multispecies model. The additional elements in the latter describe the leading order behaviour of perturbations due to the introduction of the competitor species. Thus, a pattern that is stable in the corresponding single-species model may be unstable in the multispecies model (8.4) due to its interaction with a competitor species.

#### 8.4.4 Onset and existence of coexistence patterns

Onset of coexistence patterns can occur through three different mechanisms. As for the single-species patterns discussed in Sec. 8.3, two potential causes of pattern onset are a homoclinic solution and a Turing-Hopf bifurcation of the spatially uniform coexistence equilibrium  $v_m^{c,+}$ . Onset of coexistence patterns can further occur on a solution branch of a single-species pattern as it loses/gains stability to the introduction of the second species. As outlined in the previous section, such a bifurcation can be detected through a comparison of the single-species pattern's essential spectra in the context of the single-species model (8.1) and the multispecies model (8.4). The same mechanism also causes pattern onset if only intraspecific competition for water is considered [64] (Chapter 6). Onset at a homoclinic solution or at a Turing-Hopf bifurcation of a spatially uniform equilibrium, however, cannot occur if local intraspecific competition dynamics are neglected, as no spatially uniform equilibria exist. In (8.4), solution branches of coexistence patterns either connect two single-species patterns (the only mechanism that occurs in the absence of local intraspecific competition), a single-species pattern with the spatially uni-

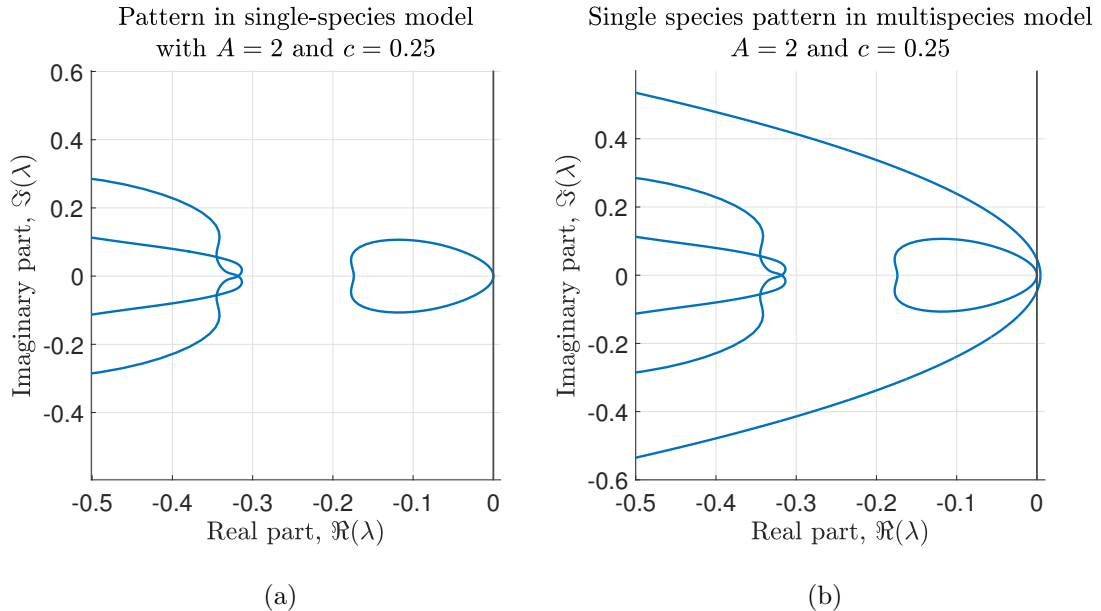


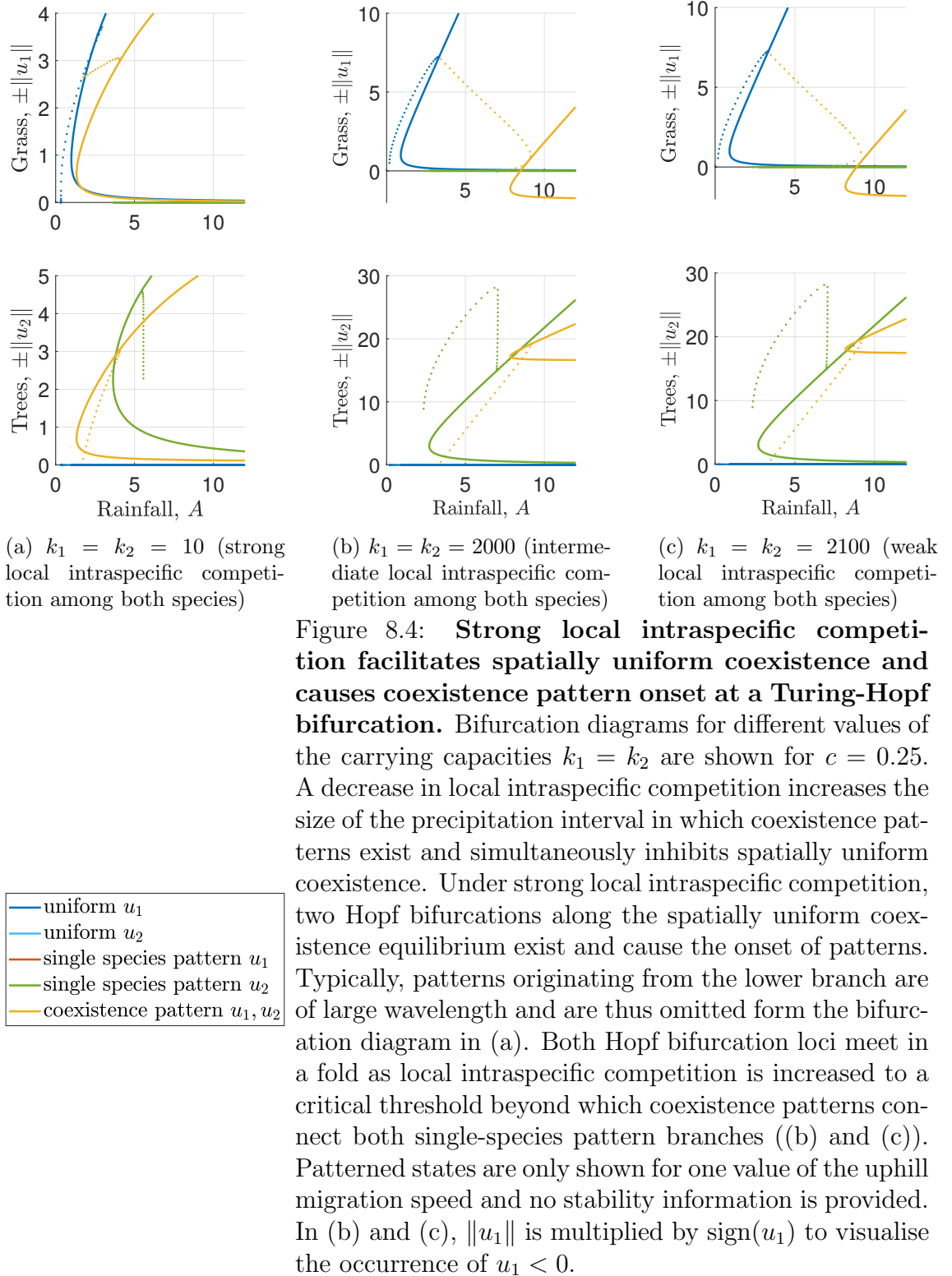
Figure 8.3: **Introduction of a second species affects stability of single-species patterns.** A comparison of the essential spectra of a single-species pattern in the single-species model (8.1) (a) and the multispecies model (8.4) (b) are shown. The spectrum in the single-species model is a subset of the spectrum in the multispecies model. The additional elements of the spectrum correspond to the leading order behaviour of perturbations in the density of the second species. Note that the spectra yield that the corresponding single-species pattern is stable in the single-species model, but unstable in the multispecies model due to the introduction of the competitor species. The vertical lines visualise the imaginary axis. The parameter values are  $A = 2$  and  $c = 0.25$ . For this visualisation, a pattern of species  $u_1$  was chosen, but identical considerations hold for single-species patterns of species  $u_2$ .

form coexistence state, or the spatially uniform coexistence state with a homoclinic solution. The choice of which of these three mechanisms occurs depends on both the strength of local intraspecific competition and the difference between both species, as is outlined below.

### The role of local intraspecific competition

If  $k_1 = k_2$  is small and species difference is sufficiently large so that  $u_1$  and  $u_2$  represent a typical grass and tree species, respectively, two Hopf bifurcations on the spatially uniform coexistence equilibria occur and are the origins of coexistence pattern solution branches that connect to either of the single-species pattern branches. (Fig. 8.4a). Typically, one of the Hopf bifurcations occurs on  $\mathbf{v}_m^{c,-}$  and patterns originating there are of very large wavelength, beyond the  $L = 1000$  threshold used to approximate homoclinic solutions in this bifurcation analysis. Note that the Hopf bifurcation on  $\mathbf{v}_m^{c,-}$  does not cause a stability change of the equilibrium because a third eigenvalue with positive real part exists. As  $k_1 = k_2$  increases, the spatially uniform coexistence equilibrium is shifted to higher precipitation volumes and one of its biomass components may attain ecologically irrelevant negative values. Moreover, the Hopf bifurcation on  $\mathbf{v}_m^{c,-}$  moves along the solution branch, through the fold, and onto the  $\mathbf{v}_m^{c,+}$  branch (Fig. 8.4b). A further increase in  $k_1 = k_2$  reduces the distance between both Hopf bifurcations, until they coincide. Beyond this threshold, no Hopf bifurcation along the spatially uniform coexistence equilibrium exists. However, coexistence patterns continue to occur. As in the analysis shown in [64] and Chapter 6 (the  $k_1, k_2 \rightarrow \infty$  limit of the model in this chapter), one coexistence pattern solution branch connects both single-species pattern branches for sufficiently large  $k_1 = k_2$  (Fig. 8.4c). In other words, local intraspecific competition shifts the existence region of both the spatially uniform coexistence equilibrium and the spatially patterned coexistence state to lower precipitation levels and enables coexistence pattern onset at a Hopf bifurcation on the spatially uniform equilibrium.

An investigation with one of the species' local intraspecific competition strengths being fixed, gives more insight into the different roles of both parameters. A decrease in local intraspecific competition of the coloniser species (i.e. increase in  $k_1$ ) reduces the size of the parameter region for which coexistence patterns occur (Fig. 8.6c). As is discussed in [60] (Chapter 7) and visualised in Fig. 8.6a and 8.6b, strong local intraspecific competition among the coloniser species facilitates coexistence patterns because it shifts the upper rainfall threshold at which pattern onset occurs to higher levels, while only having a negligible impact on the onset at low precipitation volumes. This causes an increase in the size of the parameter region in which coexistence patterns exist. Variations in  $k_2$ , however, have a very



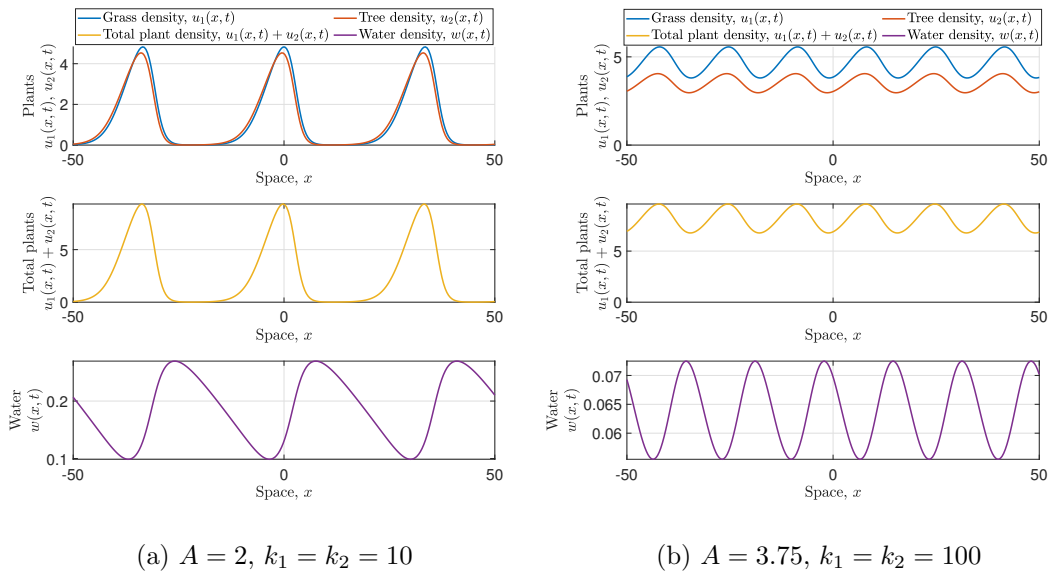


**Figure 8.5: Local intraspecific competition facilitates species coexistence in vegetation patterns.** Two coexistence solutions are shown. In (a), local intraspecific competition is strong and the solution represents a vegetation pattern, while in (b) a solution corresponding to a savanna state is visualised, which occurs due to weak local intraspecific competition. Note the different values of the precipitation parameter. A decrease in local intraspecific competition destabilises the coexistence state at lower rainfall volumes. The species difference parameter is  $\chi = 0.3$ .

similar effect as in the case of  $k_1 = k_2$  (Fig. 8.6a and 8.6b). A reduction in local intraspecific competition increases the size of the pattern existence region. In contrast to the  $k_1 = k_2$  case, the Hopf bifurcation on the lower branch of the spatially uniform coexistence equilibrium has no impact on the structure of ecologically relevant solutions, as it exclusively occurs for parameter values at which one of the plant densities of the coexistence equilibrium is negative. Nevertheless, a transition to a bifurcation structure in which the coexistence pattern solution branch connects both single-species patterns occurs as follows. As  $k_2$  increases the  $u_1$  density of the spatially uniform coexistence equilibrium decreases and becomes negative after intersecting the single-species tree equilibrium. Consequently, the Hopf bifurcation on the equilibrium occurs for lower densities of  $u_1$  as  $k_2$  increases (Fig. 8.6a). At a critical threshold, the Hopf bifurcation crosses  $u_1 = 0$ , where it coincides with the Hopf bifurcation on the single-species tree equilibrium. For  $k_2$  larger than this threshold, ecologically relevant patterns connect the Hopf bifurcations on the single-species equilibria and do not extend to the Hopf bifurcation on the coexistence equilibrium solution branch, as this occurs for  $u_1 < 0$  (Fig. 8.6b).

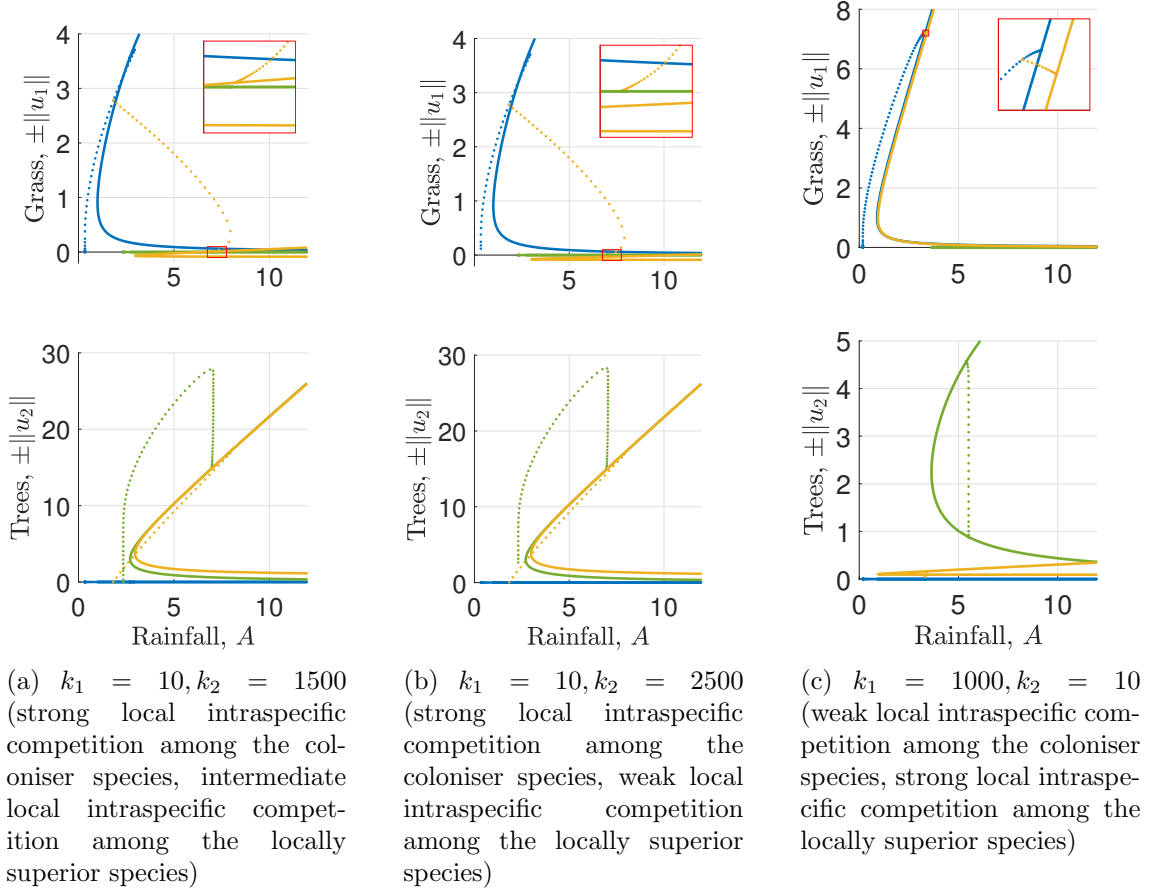


**Figure 8.6: Strong local intraspecific competition of the coloniser species and weak local intraspecific competition of the locally superior species promote patterned coexistence.** Bifurcation diagrams under changing local intraspecific competition of one-species only are shown. Both strong local intraspecific competition among the coloniser species  $u_1$  and weak local intraspecific competition among the locally superior species  $u_2$  increase the size of the parameter region in which coexistence patterns exist. The insets in (a) and (b) (axes limits:  $A \in [6.75, 7.75]$ ,  $\pm \|u_1\| \in [-0.1, 0.1]$ ) show the onset of coexistence patterns close to  $u_1 = 0$  to highlight the transition from onset at the spatially uniform coexistence equilibrium to onset at the single-species  $u_2$  pattern as local intraspecific competition among  $u_2$  decreases. The inset in (c) (axes limits:  $A \in [3.2, 3.5]$ ,  $\pm \|u_1\| \in [7.1, 7.3]$ ) shows a blow-up of the parameter region in which coexistence pattern exist. The pattern migration speed is  $c = 0.25$ . In (a) and (b),  $\|u_1\|$  is multiplied by sign( $u_1$ ) to visualise the occurrence of  $u_1 < 0$ . For an interpretation of colours and line styles used in the visualisation, see the legend of Fig. 8.4.

## Transition from a savanna to a patterned vegetation state

Strong local intraspecific competition also changes the solution behaviour by facilitating species coexistence in a state representing vegetation patterns. As discussed above, increases in local intraspecific competition strength shift the parameter interval in which coexistence patterns occur to lower precipitation volumes (Fig. 8.4). Associated with this is a transition from a solution-type that represents a savanna biome to a solution type that represents a vegetation pattern. Both these solution types are periodic travelling waves, but the biomass components of the former oscillate between two non-zero levels, while those of the latter oscillate between a nonzero plant density and zero (Fig. 8.5a and 8.5b). In general, the transition between the two solution types is a gradual process. However, it may be accelerated by a destabilisation and associated change in wavelength of a pattern. The savanna state patterned solution also occurs in the  $k_1, k_2 \rightarrow \infty$  limit as discussed in [64] (Chapter 6).

## The role of species difference

The difference between both plant species, quantified by the parameter  $\chi$  in the parameter setting (8.5), also has a significant impact on the bifurcation structure of the system. In the results presented above, the difference between both species is set to a large value so that  $u_1$  and  $u_2$  represent a grass and tree species, respectively. Under this assumption, the onset of coexistence patterns at the lower precipitation bound for pattern existence always occurs along the single-species grass pattern. Decreases in the species difference  $\chi$ , corresponding to simultaneous changes in parameters of species  $u_2$  that make it more similar to species  $u_1$ , cause the pattern onset locus to move along the single-species pattern branch in a decreasing precipitation direction towards the homoclinic solution of  $u_1$ . At a critical threshold of  $\chi$ , the homoclinic  $u_1$  solution coincides with the homoclinic coexistence solution and a transition of the pattern onset type occurs. For lower values of the species difference parameter  $\chi$ , onset at low precipitation values thus occurs at the homoclinic solution (Fig. 8.7).

### 8.4.5 The effects of plant dispersal

As is discussed in [60] (Chapter 7), the ratio of the plant species' diffusion coefficients  $D$  has a significant impact on the model solutions. Plant components of the patterned model solutions are not exactly in phase. Depending on the parameters in the system, the uphill edges (and to a lesser extent the downhill edges) of the travelling wave solutions are dominated by one species, while its competitor is mostly confined to narrow regions in the centre of the bands. This behaviour can be quantified through the linear correlation

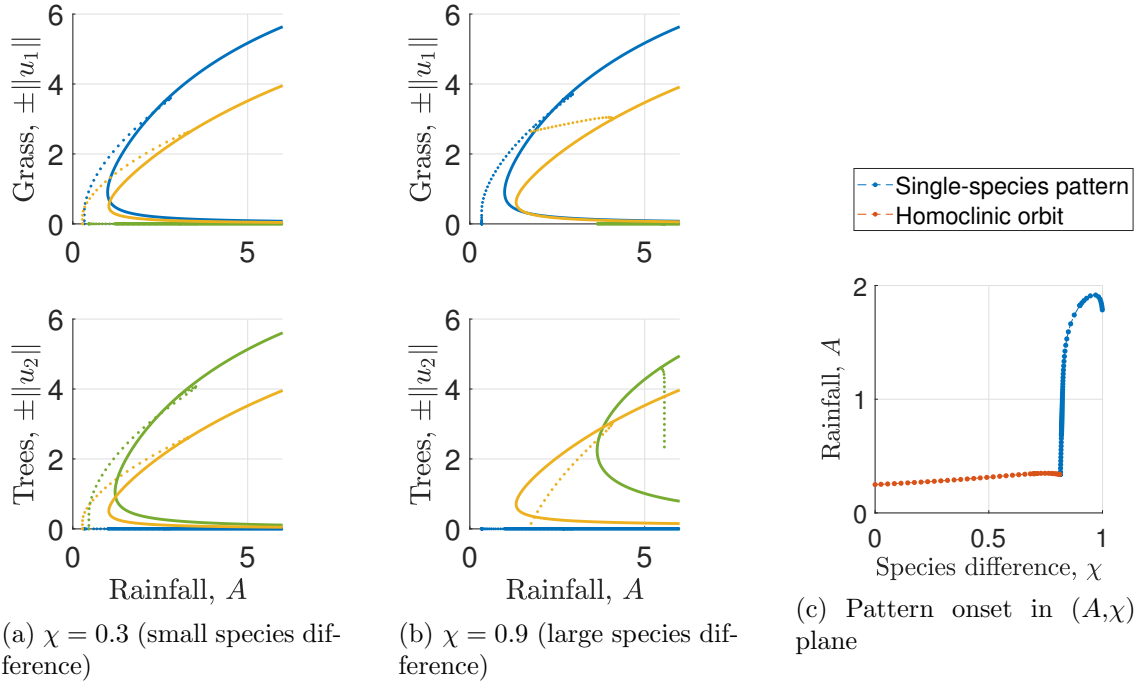


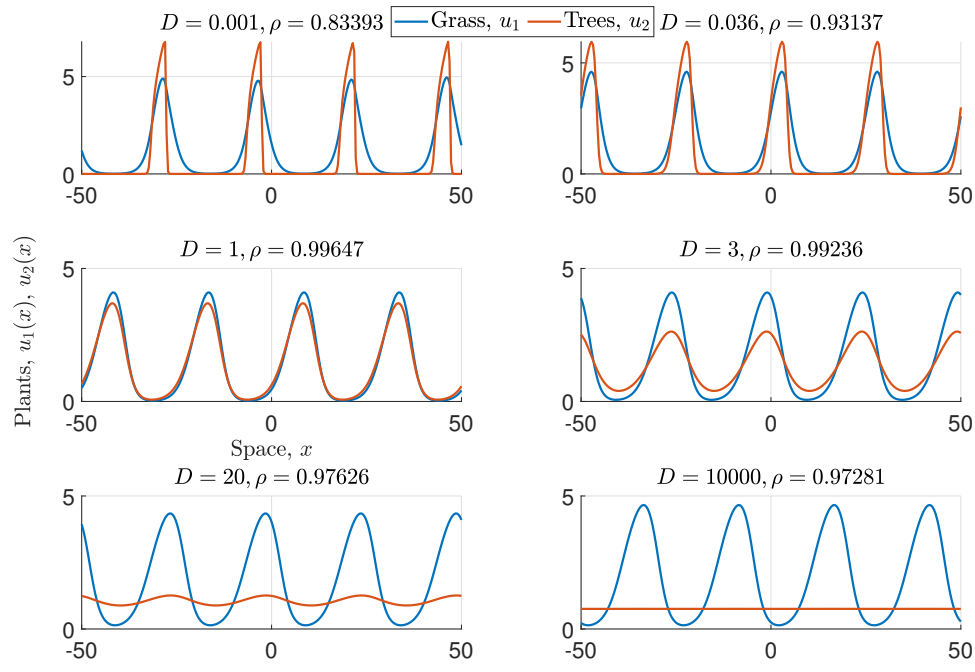
Figure 8.7: **A transition from coexistence pattern onset at a single-species pattern to onset at a homoclinic solution occurs due to increases in species similarity.** Bifurcation diagrams for different values of the species difference parameter  $\chi$  are shown in (a) and (b). A transition from coexistence pattern onset at a homoclinic solution to onset at the single-species grass pattern occurs as species difference increases. The type of onset point and the precipitation level at which onset occur are tracked in (c). The pattern migration speed is  $c = 0.25$ . For an interpretation of colours and line styles used in (a) and (b), see the legend of Fig. 8.4.

$$\rho(U_1, U_2) = \frac{\text{cov}(\widetilde{U}_1, \widetilde{U}_2)}{\sigma(\widetilde{U}_1)\sigma(\widetilde{U}_2)},$$

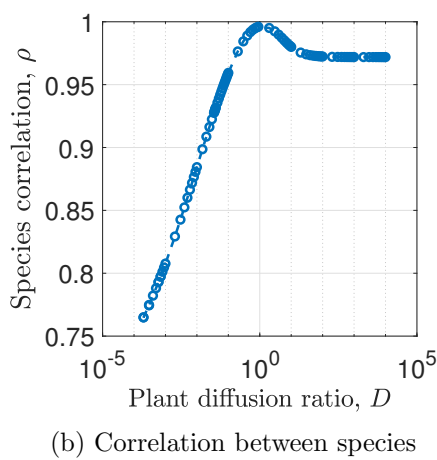
between both plant densities, where  $\text{cov}(\cdot, \cdot)$  denotes the covariance of two vectors, and  $\sigma(\cdot)$  the standard deviation. The vectors  $\widetilde{U}_1$  and  $\widetilde{U}_2$  are obtained by discretising the spatial domain and evaluating the plant densities  $u_1$  and  $u_2$  on this mesh. Note that the linear correlation takes values  $-1 \leq \rho(U_1, U_2) \leq 1$ , and a larger correlation corresponds to a more in-phase-like appearance of both plant patterns.

An exhaustive calculation of the linear correlation in the parameter space can be performed, as numerical continuation allows for an easy generation of model solutions. The ratio of the plant species' diffusion coefficients  $D$  has the most significant impact on the correlation (Fig. 8.8). To specifically focus on the coexistence of grasses and trees, I have outlined in [60] (Chapter 7) that if the species with slower growth also disperses at a slower rate (i.e.  $(F - 1)(D - 1) > 0$ ), then larger differences in the diffusion coefficients yield smaller spatial correlations, as the uphill edge of each vegetation band features a high density of the faster disperser only. In this parameter setting, that species can be referred to as the *pioneer species*, as it is responsible for the colonisation of the bare ground in the uphill direction, before its competitor species utilises the increased resource availability in the newly colonised ground. It is noteworthy that the species correlation of solutions of (8.4) is always positive. In particular, the plant densities never occur in antiphase, i.e. no complete spatial segregation of species takes place in the system. Increases in the similarities of the species' dispersal behaviour causes an increase in the spatial correlation. In particular, the correlation attains its maximum value close to  $D = 1$ , i.e. where both plant species diffuse at the same rate. For  $D = 1$ , the solution profile shows both plant species to be approximately in phase (Fig. 8.8a), but the influence of other parameters prevents the species from appearing exactly in phase. Nevertheless, changes to other parameters do not have any qualitative impact on species correlation in solutions of (8.4).

By contrast, if the assumption that one species both grows and disperses at a faster rate is dropped (i.e. if  $(F - 1)(D - 1) < 0$ ), then the correlation between the plant species does not decrease significantly from its maximum close to  $D = 1$  (Fig. 8.8b). However, the solution changes significantly. Instead of occurring in a patterned configuration with its competitor, the faster dispersing species attains a spatially uniform state, while the faster growing species (and slower disperser) remains in a patterned state (Fig. 8.8a).



(a) Numerical PDE simulations



(b) Correlation between species

**Figure 8.8: Plant dispersal influences spatial species distribution and enables coexistence of a spatially uniform fast disperser with a patterned slow disperser.** The spatial correlation between plant species is shown in (b) and some example solutions are displayed in (a). Note that the spatial correlation peaks close to  $D = 1$  but does not reach unity due to the plant species differing in other parameters. No other parameters have any qualitative impact on correlation. In particular, species correlation is unaffected by changes in the strengths of local intraspecific competition, which are set to  $k_1 = k_2 = 10$  for visualisation purposes. For  $D > 1$ , coexistence of the locally superior species (which also disperses faster) in a spatially uniform state with a patterned state of the superior coloniser (but slower disperser) is possible. The species difference is set to  $\chi = 0.3$  and the wavelength  $L$  is fixed to  $L = 25$  in the numerical continuation with the uphill migration speed allowed to vary.

## 8.5 Discussion

The inclusion of local intraspecific competition dynamics in the modelling framework of the Klausmeier model for dryland vegetation patterns has a significant impact on the model solutions. In the context of the single-species model (8.1), only considering intraspecific competition for water that acts on a long spatial scale leads to an overestimation of the precipitation range in which patterns occur, while in the multispecies model (8.4), local intraspecific competition is a key ingredient in the successful capture of species coexistence in a solution type that represents patterned vegetation.

In the single-species Klausmeier model, the rate of plant growth grows without bound as the plant density increases [99]. One possible motivation for this simplistic description is the type of ecosystem the modelling framework is describing. Dryland vegetation is limited by the low volumes of precipitation in arid ecosystems and thus total biomass is commonly low. Thus, intraspecific competition among plants is generally only associated with long-range competition for water and any negative density-dependent effects on the rate of plant growth caused by local intraspecific competition are neglected in the Klausmeier model and similar modelling frameworks [86, 99, 163]. However, even though total biomass on the ecosystem-wide scale is low, the spatial self-organisation of plants leads to the occurrence of localised patches in which biomass is high, thus raising a potential issue for the assumption to neglect local intraspecific competition.

Indeed, model solutions of the Klausmeier model and its extensions typically undergo several wavelength changes in their transition from a uniformly vegetated state to a desert state along the precipitation gradient. Towards the lower end of the rainfall range supporting stable patterns, the solutions' wavelength become large and biomass may locally increase to biologically unrealistic levels [20]. The consideration of local intraspecific competition dynamics in the single-species model (8.1) presented in this chapter does not allow for such solutions due to the existence of an upper bound, the maximum standing biomass, on the plant density at every space point. As a consequence, the patterned state loses stability (and existence) to the desert equilibrium at higher precipitation volumes than in the model without local intraspecific competition (Fig. 8.1). Hence, it can be concluded that models that only consider intraspecific competition for water overestimate the resilience of vegetation patterns to increasing aridity and that an understanding of intraspecific competition dynamics is essential to make predictions on desertification processes in ecosystems.

A characteristic feature of banded vegetation is the uphill migration of vegetation stripes [48]. Model solutions of the Klausmeier model consistently predict a

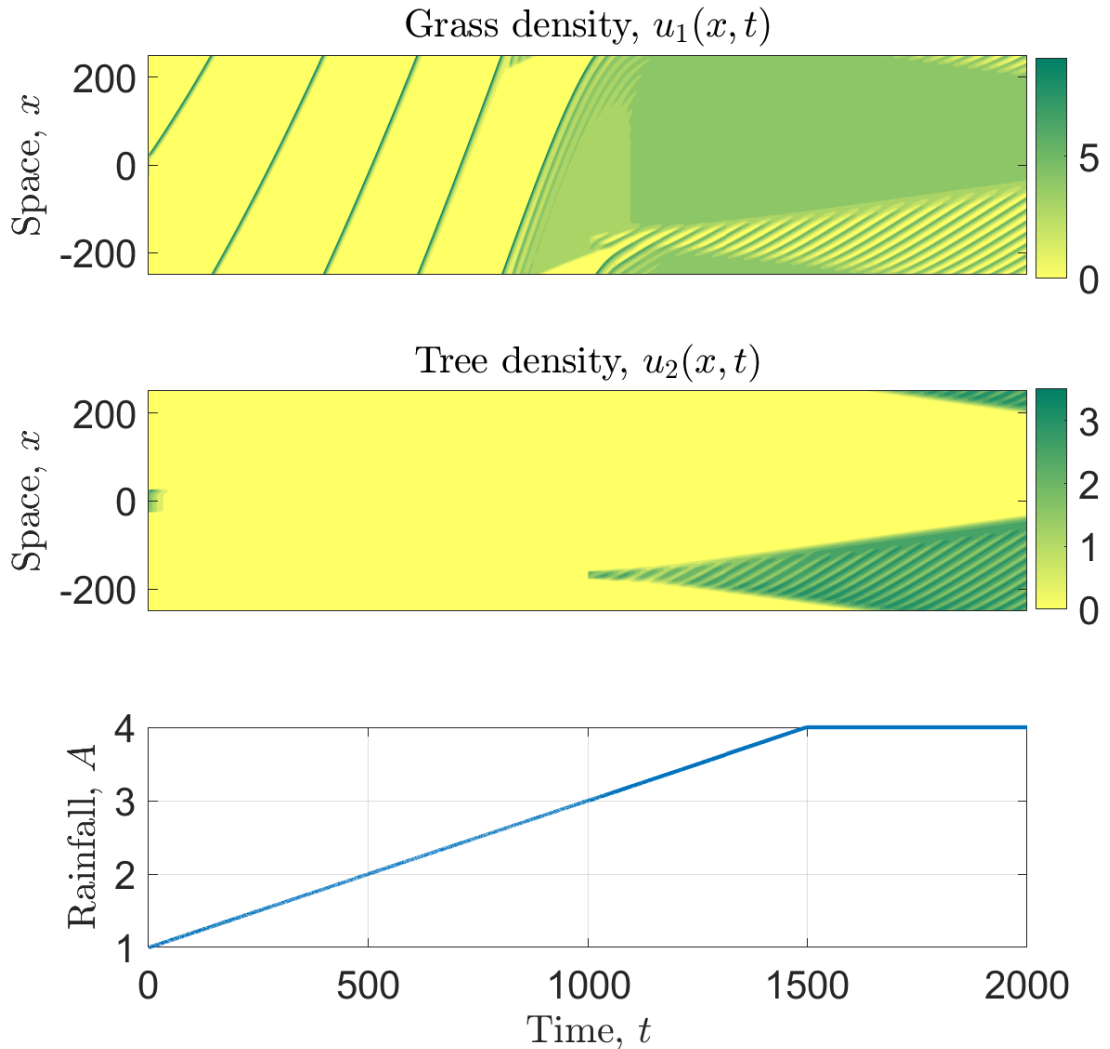


**Figure 8.9: Large species difference inhibits coexistence onset from desert.** Grass density  $u_1$  and tree density  $u_2$  of a model solution of (8.4) are shown in the  $(t, x)$  under increasing precipitation volume  $A$ . Initially, both biomass densities are set to zero, apart from a region in the centre of the domain. The tree species becomes extinct and onset of a single-species grass pattern occurs. Onset of a coexistence pattern is only possible after a reintroduction of species  $u_2$  at  $t = 1000$ , following a sufficient increase in precipitation  $A$ . A further increase in  $A$  causes a transition from the single-species grass pattern to a spatially uniform single-species state, but the coexistence pattern eventually invades. The parameter values are consistent with the bifurcation diagram shown in Fig. 8.7b.

reduction in uphill migration speed before a destabilisation due to increasing aridity occurs [20, 188], a property that can be used for early detection of degradation processes. While the introduction of local intraspecific competition to the single-species Klausmeier model decreases the size of the rainfall range supporting stable patterns, it stabilises patterned solutions with slower uphill migration speeds (Fig. 8.1). This further emphasises the importance of taking local intraspecific competition dynamics into account when developing methods of predicting future ecosystem developments, as they have a significant impact on ecologically important properties of model solutions.

The impact of local intraspecific competition in the framework of the multispecies model (8.4) is even more significant, because it stabilises species coexistence in both a spatially uniform state and in a state representing vegetation patterns (i.e. oscillations between a high level of biomass and zero). In the absence of local intraspecific competition dynamics, species coexistence can only occur in a spatially nonuniform savanna-type state (i.e. oscillations between two nonzero biomass levels) [64] (Chapter 6). The main mechanism that enables coexistence in both (8.4) and the model neglecting local intraspecific competition is the spatial self-organisation of vegetation, which causes heterogeneities in the environmental conditions and thus gives rise to the existence of two behavioural niches (e.g. [240]); that of colonisation and that of local superiority. In other words, coexistence is possible if the species which is locally inferior is superior in its colonisation abilities. The latter allows the species to utilise the spatial heterogeneities in the resource availability to colonise new ground, before eventually being outcompeted locally by a second species [64] (Chapter 6). With intraspecific competition dynamics restricted to competition for water, such a balance is only maintained for relatively high volumes of precipitation, thus giving rise to the savanna-type model solution. As precipitation decreases, the coexistence state loses its stability to a single-species state of the coloniser species, as the beneficial effects of the coloniser's ability to self-organise itself into patterns tips the balance in its favour [64] (Chapter 6). If local intraspecific competition of the coloniser species is sufficiently strong, however, its advantages due to its self-organisation abilities decline as the maximum density in single plant patches declines. This stabilises the coexistence state at lower rainfall volumes at which it represents a vegetation pattern state (Fig. 8.6). This stabilisation of coexistence is related to classical results from nonspatial Lotka-Volterra competition models which state that coexistence is possible if intraspecific competition among all species is stronger than interspecific competition between them (e.g. [30]). The crucial difference is that due to the spatial self-organisation in the system, strong local intraspecific competition of one species only suffices to explain species coexistence [60] (Chapter 7).

Variations in the strength of local intraspecific competition of both species further have an impact on the system's bifurcation structure, and in particular on the onset of patterns. Decreases in local intraspecific competition strength cause a transition of the pattern onset mechanism at high precipitation levels from a Hopf bifurcation of the spatially uniform coexistence equilibrium to a stability change of a single-species pattern to the introduction of a second species (Fig. 8.4b and 8.4c). As a consequence, model results predict that under weak local intraspecific competition no transition from a spatially uniform coexistence state to a patterned state can occur. Instead, one species' biomass decreases to zero as aridity increases, causing a transition to a spatially uniform single-species state. Only a reintroduction of the extinct species after a further decrease in precipitation can result in a patterned coexistence state.

The mechanism causing onset of coexistence patterns at the lower end of the precipitation range supporting their existence mainly depends on the difference between both species. If species are sufficiently similar, onset occurs at a homoclinic solution, while otherwise onset occurs due to a stability change of a single-species pattern to the introduction of a competitor (Fig. 8.7). This has significant ecological consequences as this predicts that the introduction of two significantly differing species into a desert state under sufficiently high precipitation volumes will not result in a successful invasion of the coexistence state. Instead, one species will become extinct and only a single-species pattern will prevail (Fig. 8.9). A transition to a coexistence state only becomes possible after a further increase in rainfall and a reintroduction of the second species. This, combined with the insights into ecosystem resilience presented above, highlights that mathematical modelling can be a powerful aid for the development of conservation programs in drylands.

The various hypotheses proposed by both (8.4) and (8.1) could be tested using empirical data. However, the acquisition of data from vegetation patterns that are of sufficiently high quality and quantity is a significant challenge yet to be addressed by ecologists. Exceptions, for example on the uphill migration speed of vegetation stripes in various sites worldwide, exist [48] but in isolation such datasets are not sufficient to provide empirical tests for the models presented in this chapter. Methods for data collection (in particular image processing) are expected to improve and thus such tests may become possible in the future.

While the modelling framework presented in this chapter leads to the successful capture of species coexistence in banded vegetation patterns, its counterpart neglecting local intraspecific competition dynamics only captures one out of many different types of savanna states [176]. Indeed, a comprehensive analysis of species correlation in coexistence solutions throughout the whole parameter space shows that both species' biomass densities are always approximately in phase (Fig. 8.8a).

An exception occurs if the species with lower biomass yield per unit water consumed disperses significantly faster than its competitor. In this case, that species attains a spatially uniform solution but its competitor species remains in a spatial pattern. This is reminiscent of a different common savanna state: isolated clusters of trees within grasslands [174]. However, under the assumptions taken in the modelling framework presented in this chapter, my analysis predicts that such a state is only attained if woody species are superior in their water-to-biomass conversion abilities ( $F > 1$ ). Parameter estimates for dryland vegetation predict that grasses can convert water into new biomass more efficiently than trees or have a faster growth rate [1, 99] and I thus argue that the modelling framework presented by (8.4) is unable to capture such a type of savanna state. Instead, a potential mechanism causing this kind of coexistence is the competition for a second limiting resource (e.g. light). Competition for two resources can both prevent competitive exclusion (e.g. [30]) and cause multistability of single-species equilibria in mathematical frameworks. This can lead to the occurrence of localised patterns of one species within an otherwise uniform state of the second species, representing isolated clusters of trees within grasslands [103].

The local intraspecific competition dynamics among plant species are incorporated into the modelling framework in a general way by combining them into one single variable, the maximum standing biomass, for each species. The significant impact of strong local intraspecific competition proposed by the results presented in this chapter motivates a more detailed investigation of its details in the future. Promising first steps have been taken through the explicit modelling of toxic soil compounds produced by plants which inhibit their growth [119]. In the absence of water scarcity, these dynamics are sufficient to create a pattern-inducing feedback and give rise to yet another spatially patterned solution type typically referred to as a savanna state: spatial segregation of species, i.e. patterns that are anti-phase. Even though this approach cannot make any statements about coexistence in water-deprived banded vegetation, it highlights the importance of local intraspecific competition dynamics. Moreover, it could be the foundation for a more detailed investigation of their impact on the competition and coexistence dynamics, potentially resulting in a modelling framework that unifies existing hypothesis on coexistence in vegetation patterns and savannas and thus allows for better predictions of future ecosystem dynamics.

The modelling framework presented in this chapter is very general and provides a deliberately simple description of a self-organisation principle in ecology. Moreover, results presented in this chapter only depend on basic species properties but do not rely on any species-specific assumptions. This suggests that results may be extended to a host of different consumer-resource ecosystems in which coexistence

of consumer species occurs. Indeed, the significant impact of self-organisation in such ecosystems has been addressed in recent years through both empirical and theoretical approaches [32, 37], which emphasise that pattern formation can play a significant role in species coexistence and suggest more detailed theoretical studies of the phenomenon in the future to advance our understanding of species coexistence.

## Chapter 9

### Conclusion

The use of mathematical modelling in the description of dryland vegetation patterns has thrived over the past three decades [21, 124, 132, 247]. Among a number of different modelling approaches, the Klausmeier reaction-advection-diffusion model [99] stands out due to its deliberate simplicity, making itself accessible for the application of powerful tools from mathematical analysis to disentangle the complex ecosystem dynamics. As a consequence, it provides a promising framework for model extensions to investigate the impact of specific processes, such as various grazing regimes [68, 195, 197] or autotoxicity [120] on the ecosystem-wide dynamics. The chapters of this thesis follow this general idea and present extensions of the Klausmeier model to address the impact of nonlocal seed dispersal (Chapter 2, but also Chapters 3 and 4) and temporal variability in precipitation regimes (Chapters 3 and 4) on vegetation patterns and to propose different mechanisms that enable species coexistence under competition for a sole limiting resource in vegetation patterns and arid savannas (Chapters 5 to 8).

For simplicity, plant dispersal is commonly described through diffusion in PDE models for dryland vegetation patterns. However, diffusion is a local process that neglects any nonlocal mechanisms involved in the dispersal of seeds. As a consequence, empirical evidence does not support this mathematical description and it is difficult to estimate diffusion coefficients from the available data. By contrast, comprehensive empirical data on seed dispersal kernels, probability density functions describing the distribution of seed dispersal distances, is available [25]. In Chapter 2, I investigate the impact of changes to seed dispersal kernels on the onset of vegetation patterns. A similar approach is also followed in Chapters 3 and 4, although the main focus of those chapters lies on the impact of temporal variability in precipitation regimes.

The overarching conclusion of Chapters 2 to 4 is that longer seed dispersal distances stabilise uniformly vegetated states for lower precipitation volumes and thus inhibit the onset of spatial patterns (e.g. Figs. 2.6, 3.4a and 4.6a). Interestingly, empirical studies suggest that plant species in drylands have developed traits, so called antitelechoric mechanisms, that inhibit long-range dispersal of seeds [66, 227]. As a

consequence, seed dispersal dynamics in drylands have evolved to be characterised by narrow seed dispersal kernels. On first glance, this contradicts the modelling results presented in Chapters 2 to 4 from an evolutionary perspective (assuming that uniform vegetation cover is an evolutionary beneficial outcome). However, the development of antitelechoric seed dispersal behaviour is commonly caused by the evolution of protective mechanisms that enhance seed survival rates and thus (in the simplified terms of the mathematical models presented in this thesis) reduce plant mortality [66]. In other words, this suggests an evolutionary trade-off between seed dispersal distances and plant mortality or plant fecundity. Depending on the exact form of such a trade-off, modelling results presented in this thesis can indeed explain this behaviour from an eco-evolutionary perspective (Figs. 2.9 and 3.5).

Results presented in Chapter 2 focus on the onset of spatiotemporal patterns at high precipitation values, i.e. the transition from a uniformly vegetated state to a spatially patterned state due to a decrease in rainfall volume. This chapter has formed the basis of an investigation of pattern existence and pattern stability in the nonlocal Klausmeier model (2.2) by Bennett and Sherratt [20], utilising numerical continuation techniques similar to those presented in Section 6.8 of this thesis. In particular, their analysis shows that the nonlocal Klausmeier model (2.2) presented in Chapter 2 proposes a potential resolution of the contradicting empirical observations regarding the uphill movement of banded vegetation patterns. A number of field studies report an upslope migration [48], while some do not find evidence of such a behaviour [55]. The inclusion of nonlocal seed dispersal in the modelling framework of the Klausmeier model shows that the model system captures both migrating solutions and spatial patterns with negligible uphill migration speed, if seed dispersal distances are sufficiently large [20]. Thus, this extension of the results presented in Chapter 2 further highlights the importance of the inclusion of nonlocal seed dispersal dynamics.

The modelling frameworks presented in Chapters 3 and 4 investigate the impact of temporal variability in precipitation on the onset of vegetation patterns. In Chapter 3, I present an integrodifference model that captures a seasonal rainfall regime in which seed dispersal is assumed to occur either during the dry season or synchronised with the beginning of the wet season, while in Chapter 4, I utilise an impulsive model (combination of PDEs with time-discrete maps) to account for intermittent rainfall regimes in which pulses of biological processes are caused by short precipitation events of high intensity. Both these approaches are based on historical rainfall data that show that rainfall in drylands occurs intermittently, seasonally, or as a combination thereof [148], and therefore provide a more realistic description of precipitation regimes than PDE models that assume continuous addition of water at a constant rate. Nevertheless, the deterministic nature of the models presented

in Chapters 3 and 4 neglects any randomness in precipitation regimes. Indeed, an appropriate (but still idealised) mathematical description of precipitation in drylands is the use of a Poisson process to model the arrival of rainfall pulses, with exponentially distributed intensities [167]. However, current modelling frameworks, including the impulsive model (4.5) presented in Chapter 4, are not suitable to be equipped with probabilistic rainfall regimes. Solutions would eventually be pushed onto trajectories leading to plant extinction by the occurrence of time periods during which total rainfall volume is significantly below its mean. This causes plant extinction, because modelling frameworks lack mechanisms that would allow plants to recover from low biomass densities once environmental conditions improve. In reality, however, vegetation has developed such features, for example seed banks that allow seeds to remain dormant below-ground until environmental conditions are favourable for germination [109]. The inclusion of such energy storage mechanisms in one of the current modelling frameworks would be an important step towards an investigation of the impact of probabilistic rainfall regimes on the ecohydrological dynamics of dryland vegetation and is thus a promising direction of potential future work.

The mathematical models presented in Chapters 5 to 8 all address the question, *How can species coexist in vegetation patterns despite their competition for a sole limiting resource?* The papers forming Chapters 5 to 8 of this thesis are not the first to provide partial answers to this question. Previously, Baudena and Rietkerk [16] and Nathan et al. [145] successfully captured the coexistence of two plant species in mathematical models for vegetation patterns by assuming that only one species contributes to the pattern-forming feedback. The pattern forming species acts as an ecosystem engineer and facilitates a second species which is both the locally superior species and the faster disperser, but is unable to self-organise into a spatial pattern itself [145]. Species coexistence in vegetation bands is also captured by Ursino and Callegaro [27, 220] through the assumption that plant species are adapted to different soil moisture niches, resulting in different functional responses of plant growth to soil moisture. All these approaches are fundamentally based on the assumption that plant species significantly differ from each other, in particular in their functional responses to the environment. Thus, the crucial novelty of the multispecies modelling framework presented in Chapters 5 to 8 is that both plant species only differ in their basic parameter values (e.g. growth rates, mortality rates), but not in any of their functional responses. Nevertheless, the model successfully captures species coexistence in solutions both representing arid savannas (Chapters 5 and 6) and vegetation patterns (Chapters 5, 7 and 8). The two main conclusions of Chapters 5 to 8 addressing the research question posed above are as follows. Firstly, the spatial self-organisation principle that governs the separation of plants into patches of

high biomass and patches of bare soil also facilitates species coexistence by creating a spatially heterogeneous resource landscape, if a balance is kept between species' colonisation abilities and local competitiveness (Chapters 6 to 8). Secondly, the results presented in Chapter 5 emphasise that the principle of competitive exclusion (e.g. [88]) does not necessarily prohibit coexistence, if species are of a similar average fitness. In this case, coexistence can occur as a long transient. Such a state is mathematically characterised by a metastable solution, a state originating from an unstable equilibrium, whose instability is caused by only one small positive eigenvalue. This highlights the importance of considering out-of-equilibrium solutions to gather a comprehensive understanding of a mathematical model. The only exception to the assumption of symmetry between both plant species in the multispecies model is the shading term in (5.4). However, while the shading dynamics enrich the solution behaviour, its omission does not affect the basic concept of the metastability property (Chapter 5).

The multispecies models in Chapters 5 to 8 present results for two different plant types interacting with a limiting resource (water). This is motivated by the distinction of vegetation into two types; one that dominates in the *pioneer zones* (annual grasses) and one that forms the *thicket cores* (perennial grasses, shrubs, trees) of vegetation bands, rather than into individual species [179]. Nevertheless, it would be interesting to investigate if the coexistence mechanisms proposed in this thesis can be extended to theoretical models for more than two vegetation types, such as (5.2).

Indeed, the metastability property presented in Chapter 5 can be easily extended to a larger number of species, in particular if shading effects are neglected. This coexistence mechanism only depends on the local average fitness of each species, which, in the simplified setting of the dimensional model (5.2) is defined to be the ratio of a plant species' water to biomass conversion rate to its mortality rate. As such, its computation is not affected by the number of other species in the system. The analytical derivation of growth rates of perturbations to equilibria (Sections 5.5 and 5.6) becomes infeasible if a higher dimensional model is considered, but can be replaced by numerical calculations of matrix eigenvalues. This suggests that the metastability property can be extended to an arbitrary number of species. In other words, metastable solutions of (5.2) containing an arbitrary number of species can occur, provided all species are of similar average fitness.

An extrapolation of the coexistence mechanism proposed in Chapters 6 to 8 appears to be less straightforward. The mechanism relies on the interactions of a species superior in its colonisation abilities with a species that is locally superior. It is not immediately clear from the results presented in Chapters 6 to 8 how this can be extended if a third (or more) species are considered in the dynamics. Nevertheless,

the same mathematical techniques could be utilised to investigate coexistence in models of more than two plant species. For example, the method to determine the bifurcation leading to the onset of two-species coexistence patterns from a single-species pattern in the two-species model (Fig. 6.2) could also be used to screen the parameter space for the onset of a three-species pattern in a three-species model. Identically to the method presented in Chapter 6, this would involve a comparison between the spectra of the same two-species pattern in the two-species model and the three-species model. While I hypothesise that a further bifurcation can be found using this method, I am not able to make any predictions about the properties of the solution branch originating from such a bifurcation. It is neither clear if this solution features all three species or if one species is replaced by the newly introduced vegetation type, nor can any statements regarding pattern stability be made. Thus, a significant amount of work with associated challenges (e.g. increased computational cost) would be needed to verify if results of Chapters 6 to 8 can be extended to systems with more than two plant types.

The results presented in Chapters 6 to 8 also highlight the importance of the plant types' dispersal behaviours on the coexistence mechanism. In the multispecies models used in Chapters 6 to 8, plant dispersal is modelled through diffusion. By contrast, results presented in Chapter 2 (and the extension by Bennett and Sherratt [20]) emphasise the importance of considering nonlocal plant dispersal in models for vegetation patterns. Thus, a natural question arises that may feature in a further extension of the theory: how does nonlocal plant dispersal affect species coexistence? Nonlocal dispersal was previously included in a multispecies model by Baudena and Rietkerk [16] without an attempt to investigate its impact. Such an extension would create the significant challenge of adapting the numerical continuation procedures to perform a bifurcation analysis. Numerical continuation using AUTO-07p cannot be applied to models with nonlocal terms. Instead, such systems need to be rewritten as local models. For the Laplace kernel, this can be done by introducing a new variable representing the nonlocal convolution term and differentiating twice in space [20, 22, 77, 128]. The only option for other kernel functions is a discretisation of the domain, incurring a significant computational cost [20].

A final area of potential extensions of all topics presented in this thesis is the consideration of a two-dimensional spatial domain. The restriction to a one-dimensional spatial domain in the models presented in this thesis is motivated by the original formulation of the Klausmeier model, solutions of which represent a transversal cut orthogonal to the terrain contours through regular banded vegetation [99]. Nevertheless, an analysis on an ecologically more realistic, two-dimensional spatial domain could provide more insights into the models' solution structures and the impact of the considered processes. On flat terrain in particular, vegetation patterns can

occur as gap patterns, labyrinth patterns or spot patterns, depending on the hydrological conditions [129]. It is of crucial importance to understand the dynamics of phase transitions between those different pattern types to gain more information on desertification and other degradation processes in drylands. Even in models describing the ecohydrological processes on sloped terrain, the inclusion of a second space dimension can yield valuable new information on the ecosystem dynamics. For example, Siero et al. [196] have shown that the restriction to a one-dimensional spatial domain in the Klausmeier model leads to an overestimation of the size of the precipitation interval in which striped patterns are stable. Similar dynamics are assumed to occur in the models presented in this thesis and therefore suggest to extend spatial domains in future analyses of mathematical models of vegetation patterns.

The long-term goal of the study of dryland vegetation patterns by both ecologists and mathematical modellers is the development of predictive frameworks that provide forecasts of future developments of such ecosystems, in particular to combat the threat of irreversible desertification processes. A basic ingredient for this is the understanding of the effects of basic ecological mechanisms on the ecosystem dynamics. The chapters presented in this thesis provide examples of theoretical investigations into the impact of such processes. The mathematical models used are phenomenological and consequently only provide qualitative insights into the ecohydrological dynamics. A key future step to enhance our knowledge of vegetation patterns would be to unify phenomenological modelling work with data-driven approaches. Promising first steps include the inference of a pattern's history from the relation between its wavelength and the terrain's slope [193], the confirmation of the occurrence of multistability (i.e. the existence of several stable patterned states) predicted by models through empirical data [10] and the establishment of a relation between arcing of vegetation stripes and terrain curvature [72]. Nevertheless, key challenges, such as the modelling of water redistribution during rainfall events or the development of more accurate precipitation forecasts, remain to be addressed before the long-term goal of predicting future ecosystem developments in drylands can be achieved.

## Bibliography

- [1] Accatino, F., De Michele, C., Vezzoli, R., Donzelli, D. and Scholes, R. J.: Tree–grass co-existence in savanna: interactions of rain and fire. *J. Theor. Biol.* 267.2 (2010), pp. 235–242. DOI: [10.1016/j.jtbi.2010.08.012](https://doi.org/10.1016/j.jtbi.2010.08.012).
- [2] Akhmet, M., Beklioglu, M., Ergenc, T. and Tkachenko, V.: An impulsive ratio-dependent predator–prey system with diffusion. *Nonlinear Anal. Real World Appl.* 7.5 (2006), pp. 1255–1267. DOI: [10.1016/j.nonrwa.2005.11.007](https://doi.org/10.1016/j.nonrwa.2005.11.007).
- [3] Alfaro, M., Izuhara, H. and Mimura, M.: On a nonlocal system for vegetation in drylands. *J. Math. Biol.* 77.6-7 (2018), pp. 1761–1793. DOI: [10.1007/s00285-018-1215-0](https://doi.org/10.1007/s00285-018-1215-0).
- [4] Allen, E. J., Allen, L. J. S. and Gilliam, X.: Dispersal and competition models for plants. *J. Math. Biol.* 34.4 (1996), pp. 455–481. DOI: [10.1007/BF00167944](https://doi.org/10.1007/BF00167944).
- [5] Anthelme, F. and Michalet, R.: Grass-to-tree facilitation in an arid grazed environment (Air Mountains, Sahara). *Basic Appl. Ecol.* 10.5 (2009), pp. 437–446. DOI: [10.1016/j.baae.2008.10.008](https://doi.org/10.1016/j.baae.2008.10.008).
- [6] Aronson, J., Kigel, J. and Shmida, A.: Reproductive allocation strategies in desert and mediterranean populations of annual plants grown with and without water stress. *Oecologia* 93.3 (1993), pp. 336–342. DOI: [10.1007/BF00317875](https://doi.org/10.1007/BF00317875).
- [7] Avelino, P. P., Oliveira, B. F. de and Trintin, R. S.: Predominance of the weakest species in Lotka–Volterra and May–Leonard formulations of the rock–paper–scissors model. *Physical Review E* 100.4 (2019). DOI: [10.1103/physreve.100.042209](https://doi.org/10.1103/physreve.100.042209).
- [8] Bastiaansen, R., Carter, P. and Doelman, A.: Stable planar vegetation stripe patterns on sloped terrain in dryland ecosystems. *Nonlinearity* 32.8 (2019), pp. 2759–2814. DOI: [10.1088/1361-6544/ab1767](https://doi.org/10.1088/1361-6544/ab1767).

## BIBLIOGRAPHY

- [9] Bastiaansen, R., Doelman, A., Eppinga, M. B. and Rietkerk, M.: The effect of climate change on the resilience of ecosystems with adaptive spatial pattern formation. *Ecol. Lett.* 23.3 (2020). Ed. by Etienne, R., pp. 414–429. DOI: [10.1111/ele.13449](https://doi.org/10.1111/ele.13449).
- [10] Bastiaansen, R., Jaibi, O., Deblauwe, V., Eppinga, M. B., Siteur, K., Siero, E., Mermoz, S., Bouvet, A., Doelman, A. and Rietkerk, M.: Multistability of model and real dryland ecosystems through spatial self-organization. *Proc. Natl. Acad. Sci.* (2018), pp. 11256–11261. DOI: [10.1073/pnas.1804771115](https://doi.org/10.1073/pnas.1804771115).
- [11] Bates, P. and Xun, J.: Metastable patterns for the Cahn-Hilliard equation, part I. *Journal of Differential Equations* 111.2 (1994), pp. 421–457. DOI: [10.1006/jdeq.1994.1089](https://doi.org/10.1006/jdeq.1994.1089).
- [12] Bates, P. and Xun, J.: Metastable patterns for the Cahn-Hilliard equation: part II. layer dynamics and slow invariant manifold. *Journal of Differential Equations* 117.1 (1995), pp. 165–216. DOI: [10.1006/jdeq.1995.1052](https://doi.org/10.1006/jdeq.1995.1052).
- [13] Baudena, M., Boni, G., Ferraris, L., Hardenberg, J. von and Provenzale, A.: Vegetation response to rainfall intermittency in drylands: results from a simple ecohydrological box model. *Adv. Water Resour.* 30.5 (2007), pp. 1320–1328. DOI: [10.1016/j.advwatres.2006.11.006](https://doi.org/10.1016/j.advwatres.2006.11.006).
- [14] Baudena, M. and Provenzale, A.: Rainfall intermittency and vegetation feedbacks in drylands. *Hydrol. Earth Syst. Sci.* 12.2 (2008), pp. 679–689. DOI: [10.5194/hess-12-679-2008](https://doi.org/10.5194/hess-12-679-2008).
- [15] Baudena, M., D’Andrea, F. and Provenzale, A.: An idealized model for tree–grass coexistence in savannas: the role of life stage structure and fire disturbances. *J. Ecol.* 98.1 (2010), pp. 74–80. DOI: [10.1111/j.1365-2745.2009.01588.x](https://doi.org/10.1111/j.1365-2745.2009.01588.x).
- [16] Baudena, M. and Rietkerk, M.: Complexity and coexistence in a simple spatial model for arid savanna ecosystems. *Theor. Ecol.* 6.2 (2013), pp. 131–141. DOI: [10.1007/s12080-012-0165-1](https://doi.org/10.1007/s12080-012-0165-1).
- [17] Beckage, B., Gross, L. J. and Platt, W. J.: Grass feedbacks on fire stabilize savannas. *Ecol. Model.* 222.14 (2011), pp. 2227–2233. DOI: [10.1016/j.ecolmodel.2011.01.015](https://doi.org/10.1016/j.ecolmodel.2011.01.015).
- [18] Beckage, B., Platt, W. and Gross, L.: Vegetation, fire, and feedbacks: a disturbance-mediated model of savannas. *Am. Nat.* 174.6 (2009), pp. 805–818. DOI: [10.1086/648458](https://doi.org/10.1086/648458).
- [19] Belsky, A. J.: Influences of trees on savanna productivity: tests of shade, nutrients, and tree-grass competition. *Ecology* 75.4 (1994), pp. 922–932. DOI: [10.2307/1939416](https://doi.org/10.2307/1939416).

## BIBLIOGRAPHY

- [20] Bennett, J. J. R. and Sherratt, J. A.: Long-distance seed dispersal affects the resilience of banded vegetation patterns in semi-deserts. *J. Theor. Biol.* 481 (2018), pp. 151–161. DOI: [10.1016/j.jtbi.2018.10.002](https://doi.org/10.1016/j.jtbi.2018.10.002).
- [21] Borgogno, F., D’Odorico, P., Laio, F. and Ridolfi, L.: Mathematical models of vegetation pattern formation in ecohydrology. *Rev. Geophys.* 47:RG1005 (2009). DOI: [10.1029/2007RG000256](https://doi.org/10.1029/2007RG000256).
- [22] Britton, N. F.: Spatial structures and periodic travelling waves in an integro-differential reaction-diffusion population model. *SIAM J. Appl. Math.* 50.6 (1990), pp. 1663–1688. DOI: [10.1137/0150099](https://doi.org/10.1137/0150099).
- [23] Bromley, J., Brouwer, J., Barker, A., Gaze, S. and Valentine, C.: The role of surface water redistribution in an area of patterned vegetation in a semi-arid environment, south-west Niger. *J. Hydrol.* 198.1 (1997), pp. 1–29. DOI: [10.1016/S0022-1694\(96\)03322-7](https://doi.org/10.1016/S0022-1694(96)03322-7).
- [24] Buis, E., Veldkamp, A., Boeken, B. and van Breemen, N.: Controls on plant functional surface cover types along a precipitation gradient in the Negev Desert of Israel. *J. Arid. Environ.* 73.1 (2009), pp. 82–90. DOI: [10.1016/j.jaridenv.2008.09.008](https://doi.org/10.1016/j.jaridenv.2008.09.008).
- [25] Bullock, J. M., González, L. M., Tamme, R., Götzenberger, L., White, S. M., Pärte, M. and Hooftman, D. A. P.: A synthesis of empirical plant dispersal kernels. *J. Ecol.* 105.1 (2017), pp. 6–19. DOI: [10.1111/1365-2745.12666](https://doi.org/10.1111/1365-2745.12666).
- [26] Busse, F. H.: Non-linear properties of thermal convection. *Rep. Prog. Phys.* 41.12 (1978), pp. 1929–1967. DOI: [10.1088/0034-4885/41/12/003](https://doi.org/10.1088/0034-4885/41/12/003).
- [27] Callegaro, C. and Ursino, N.: Connectivity of niches of adaptation affects vegetation structure and density in self-organized (dis-connected) vegetation patterns. *Land Degradation & Development* 29.8 (2018), pp. 2589–2594. DOI: [10.1002/ldr.2759](https://doi.org/10.1002/ldr.2759).
- [28] Carter, P. and Doelman, A.: Traveling stripes in the Klausmeier model of vegetation pattern formation. *SIAM J. Appl. Math.* 78.6 (2018), pp. 3213–3237. DOI: [10.1137/18m1196996](https://doi.org/10.1137/18m1196996).
- [29] Champneys, A. R., Kuznetsov, Y. A. and Sandstede, B.: A numerical toolbox for homoclinic bifurcation analysis. *Int. J. Bifur. Chaos* 06.05 (1996), pp. 867–887. DOI: [10.1142/s0218127496000485](https://doi.org/10.1142/s0218127496000485).
- [30] Chesson, P.: Mechanisms of maintenance of species diversity. *Annu. Rev. Ecol. Syst.* 31 (2000), pp. 343–366.

## BIBLIOGRAPHY

- [31] Chesson, P., Gebauer, R. L. E., Schwinning, S., Huntly, N., Wiegand, K., Ernest, M. S. K., Sher, A., Novoplansky, A. and Weltzin, J. F.: Resource pulses, species interactions, and diversity maintenance in arid and semi-arid environments. *Oecologia* 141.2 (2004), pp. 236–253. DOI: [10.1007/s00442-004-1551-1](https://doi.org/10.1007/s00442-004-1551-1).
- [32] Christianen, M., van der Heide, T., Holthuijsen, S., van der Reijden, K., Borst, A. and Olff, H.: Biodiversity and food web indicators of community recovery in intertidal shellfish reefs. *Biol. Conserv.* 213 (2017), pp. 317–324. DOI: [10.1016/j.biocon.2016.09.028](https://doi.org/10.1016/j.biocon.2016.09.028).
- [33] Clark, J. S., Lewis, M., McLachlan, J. S. and HilleRisLambers, J.: Estimating population spread: what can we forecast and how well? *Ecology* 84.8 (2003), pp. 1979–1988. DOI: [10.1890/01-0618](https://doi.org/10.1890/01-0618).
- [34] Consolo, G., Currò, C. and Valenti, G.: Supercritical and subcritical Turing pattern formation in a hyperbolic vegetation model for flat arid environments. *Physica D* 398 (2019), pp. 141–163. DOI: [10.1016/j.physd.2019.03.006](https://doi.org/10.1016/j.physd.2019.03.006).
- [35] Consolo, G. and Valenti, G.: Secondary seed dispersal in the Klausmeier model of vegetation for sloped semi-arid environments. *Ecol. Model.* 402 (2019), pp. 66–75. DOI: [10.1016/j.ecolmodel.2019.02.009](https://doi.org/10.1016/j.ecolmodel.2019.02.009).
- [36] Cooley, J. W., Lewis, P. A. W. and Welch, P. D.: The fast Fourier transform and its applications. *IEEE Trans. Educ.* 12.1 (1969), pp. 27–34. DOI: [10.1109/TE.1969.4320436](https://doi.org/10.1109/TE.1969.4320436).
- [37] Cornacchia, L., van de Koppel, J., van der Wal, D., Wharton, G., Puijalon, S. and Bouma, T. J.: Landscapes of facilitation: how self-organized patchiness of aquatic macrophytes promotes diversity in streams. *Ecology* 99.4 (2018), pp. 832–847. DOI: [10.1002/ecy.2177](https://doi.org/10.1002/ecy.2177).
- [38] Cornet, A., Delhoume, J. and Montaña, C.: Dynamics of striped vegetation patterns and water balance in the Chihuahuan Desert. During, H., Werger, M. and Willem, H. *Diversity and pattern in plant communities*. The Hague: SPB Academic Publishing, 1988, pp. 221–231.
- [39] Corrado, R., Cherubini, A. M. and Pennetta, C.: Early warning signals of desertification transitions in semiarid ecosystems. *Phys. Rev. E: Stat., Non-linear, Soft Matter Phys.* 90 (2014), p. 062705. DOI: [10.1103/PhysRevE.90.062705](https://doi.org/10.1103/PhysRevE.90.062705).
- [40] Cosner, C., Dávila, J. and Martínez, S.: Evolutionary stability of ideal free nonlocal dispersal. *J. Biol. Dyn.* 6.2 (2012), pp. 395–405. DOI: [10.1080/17513758.2011.588341](https://doi.org/10.1080/17513758.2011.588341).

## BIBLIOGRAPHY

- [41] d'Herbès, J.-M., Valentin, C., Tongway, D. J. and Leprun, J.-C.: Banded vegetation patterns and related structures. *Banded vegetation patterning in arid and semiarid environments: ecological processes and consequences for management*. Ed. by Tongway, D. J., Valentin, C. and Seghieri, J. New York, NY: Springer New York, 2001, pp. 1–19. DOI: [10.1007/978-1-4613-0207-0\\_1](https://doi.org/10.1007/978-1-4613-0207-0_1).
- [42] D'Odorico, P., Laio, F. and Ridolfi, L.: A probabilistic analysis of fire-induced tree-grass coexistence in savannas. *Am. Nat.* 167.3 (2006), E79–E87. DOI: [10.1086/500617](https://doi.org/10.1086/500617).
- [43] D'Onofrio, D., Baudena, M., D'Andrea, F., Rietkerk, M. and Provenzale, A.: Tree-grass competition for soil water in arid and semiarid savannas: the role of rainfall intermittency. *Water Resour. Res.* 51.1 (2015), pp. 169–181. DOI: [10.1002/2014WR015515](https://doi.org/10.1002/2014WR015515).
- [44] Dagbovie, A. S. and Sherratt, J. A.: Pattern selection and hysteresis in the Rietkerk model for banded vegetation in semi-arid environments. *Journal of The Royal Society Interface* 11.99 (2014), p. 20140465. DOI: [10.1098/rsif.2014.0465](https://doi.org/10.1098/rsif.2014.0465).
- [45] Dakos, V., Kéfi, S., Rietkerk, M., van Nes, E. H. and Scheffer, M.: Slowing down in spatially patterned ecosystems at the brink of collapse. *Am. Nat.* 177.6 (2011), E153–E166. DOI: [10.1086/659945](https://doi.org/10.1086/659945).
- [46] Deblauwe, V.: Modulation des structures de végétation auto-organisées en milieu aride. PhD Thesis. Université Libre de Bruxelles, 2010.
- [47] Deblauwe, V., Barbier, N., Couteron, P., Lejeune, O. and Bogaert, J.: The global biogeography of semi-arid periodic vegetation patterns. *Global Ecol. Biogeogr.* 17.6 (2008), pp. 715–723. DOI: [10.1111/j.1466-8238.2008.00413.x](https://doi.org/10.1111/j.1466-8238.2008.00413.x).
- [48] Deblauwe, V., Couteron, P., Bogaert, J. and Barbier, N.: Determinants and dynamics of banded vegetation pattern migration in arid climates. *Ecol. Monogr.* 82.1 (2012), pp. 3–21. DOI: [10.1890/11-0362.1](https://doi.org/10.1890/11-0362.1).
- [49] Deblauwe, V., Couteron, P., Lejeune, O., Bogaert, J. and Barbier, N.: Environmental modulation of self-organized periodic vegetation patterns in Sudan. *Ecography* 34.6 (2011), pp. 990–1001. DOI: [10.1111/j.1600-0587.2010.06694.x](https://doi.org/10.1111/j.1600-0587.2010.06694.x).
- [50] Deconinck, B. and Kutz, J. N.: Computing spectra of linear operators using the Floquet–Fourier–Hill method. *J. Comput. Phys.* 219.1 (2006), pp. 296–321. DOI: [10.1016/j.jcp.2006.03.020](https://doi.org/10.1016/j.jcp.2006.03.020).

## BIBLIOGRAPHY

- [51] Dickovick, J. T.: *Africa 2014-2015. World Today* (Stryker). Rowman & Littlefield Publishers, 2014. 374 pp.
- [52] Dieulin, C., Mahé, G., Paturel, J.-E., Ejjiyar, S., Tramblay, Y., Rouché, N. and Mansouri, B. E.: A new 60-year 1940/1999 monthly-gridded rainfall data set for Africa. *Water* 11.2 (2019), p. 387. DOI: [10.3390/w11020387](https://doi.org/10.3390/w11020387).
- [53] Doedel, E. J., Oldeman, B. E., Champneys, A. R., Dercole, F., Fairgrieve, T., Kuznetsov, Y., Paenroth, R., Sandstede, B., Wang, X. and Zhang, C.: *AUTO-07p: Continuation and Bifurcation Software for Ordinary Differential Equations*. Tech. rep. 2012.
- [54] Dunkerley, D.: Banded vegetation in some Australian semi-arid landscapes: 20 years of field observations to support the development and evaluation of numerical models of vegetation pattern evolution. *Desert* 23.2 (2018), pp. 165–187.
- [55] Dunkerley, D. and Brown, K.: Oblique vegetation banding in the Australian arid zone: implications for theories of pattern evolution and maintenance. *J. Arid. Environ.* 51.2 (2002), pp. 163–181. DOI: [10.1006/jare.2001.0940](https://doi.org/10.1006/jare.2001.0940).
- [56] Durrett, R. and Levin, S.: Spatial aspects of interspecific competition. *Theor. Popul. Biol.* 53.1 (1998), pp. 30–43. DOI: [10.1006/tpbi.1997.1338](https://doi.org/10.1006/tpbi.1997.1338).
- [57] Easterling, D. R., Meehl, G. A., Parmesan, C., Changnon, S. A., Karl, T. R. and Mearns, L. O.: Climate extremes: observations, modeling, and impacts. *Science* 289.5487 (2000), pp. 2068–2074. DOI: [10.1126/science.289.5487.2068](https://doi.org/10.1126/science.289.5487.2068).
- [58] Eigentler, L. and Sherratt, J. A.: Effects of precipitation intermittency on vegetation patterns in semi-arid landscapes. *Physica D* 405 (2020), p. 132396. DOI: [10.1016/j.physd.2020.132396](https://doi.org/10.1016/j.physd.2020.132396).
- [59] Eigentler, L.: Intraspecific competition in models for vegetation patterns: decrease in resilience to aridity and facilitation of species coexistence. *Ecol. Complexity* 42 (2020), p. 100835. DOI: [10.1016/j.ecocom.2020.100835](https://doi.org/10.1016/j.ecocom.2020.100835).
- [60] Eigentler, L.: Species coexistence in vegetation patterns facilitated by the interplay of spatial self-organisation and intraspecific competition. *bioRxiv preprint* (2020). DOI: [10.1101/2020.01.13.903179](https://doi.org/10.1101/2020.01.13.903179).
- [61] Eigentler, L. and Sherratt, J. A.: Analysis of a model for banded vegetation patterns in semi-arid environments with nonlocal dispersal. *J. Math. Biol.* 77.3 (2018), pp. 739–763. DOI: [10.1007/s00285-018-1233-y](https://doi.org/10.1007/s00285-018-1233-y).

## BIBLIOGRAPHY

- [62] Eigentler, L. and Sherratt, J. A.: An integrodifference model for vegetation patterns in semi-arid environments with seasonality (2019). arXiv: 1911.10964 [q-bio.PE].
- [63] Eigentler, L. and Sherratt, J. A.: Metastability as a coexistence mechanism in a model for dryland vegetation patterns. *Bull. Math. Biol.* 81.7 (2019), pp. 2290–2322. DOI: 10.1007/s11538-019-00606-z.
- [64] Eigentler, L. and Sherratt, J. A.: Spatial self-organisation enables species coexistence in a model for savanna ecosystems. *J. Theor. Biol.* 487 (2020), p. 110122. DOI: 10.1016/j.jtbi.2019.110122.
- [65] Eldridge, D., Zaady, E. and Shachak, M.: Infiltration through three contrasting biological soil crusts in patterned landscapes in the Negev, Israel. *CATENA* 40.3 (2000), pp. 323–336. DOI: 10.1016/S0341-8162(00)00082-5.
- [66] Ellner, S. and Shmida, A.: Why are adaptations for long-range seed dispersal rare in desert plants? *Oecologia* 51.1 (1981), pp. 133–144. DOI: 10.1007/BF00344663.
- [67] Fan, Y., Li, X., Wu, X., Li, L., Li, W. and Huang, Y.: Divergent responses of vegetation aboveground net primary productivity to rainfall pulses in the Inner Mongolian Plateau, China. *J. Arid. Environ.* 129 (2016), pp. 1–8. DOI: 10.1016/j.jaridenv.2016.02.002.
- [68] Fernandez-Oto, C., Escaff, D. and Cisternas, J.: Spiral vegetation patterns in high-altitude wetlands. *Ecol. Complexity* 37 (2019), pp. 38–46. DOI: 10.1016/j.ecocom.2018.12.003.
- [69] Fravolini, A., Hultine, K. R., Brugnoli, E., Gazal, R., English, N. B. and Williams, D. G.: Precipitation pulse use by an invasive woody legume: the role of soil texture and pulse size. *Oecologia* 144.4 (2005), pp. 618–627. DOI: 10.1007/s00442-005-0078-4.
- [70] Friedman, J., Gunderman, N. and Ellis, M.: Water response of the hydrochastic skeletons of the true rose of jericho (*Anastatica hierochuntica* L.) *Oecologia* 32.3 (1978), pp. 289–301. DOI: 10.1007/BF00345108.
- [71] Gandhi, P., Iams, S., Bonetti, S. and Silber, M.: Vegetation pattern formation in drylands. *Dryland ecohydrology*. Springer International Publishing, 2019, pp. 469–509. DOI: 10.1007/978-3-030-23269-6\_18.
- [72] Gandhi, P., Werner, L., Iams, S., Gowda, K. and Silber, M.: A topographic mechanism for arcing of dryland vegetation bands. *Journal of The Royal Society Interface* 15.147 (2018), p. 20180508. DOI: 10.1098/rsif.2018.0508.

## BIBLIOGRAPHY

- [73] Geritz, S. A. and Kisdi, É.: On the mechanistic underpinning of discrete-time population models with complex dynamics. *J. Theor. Biol.* 228.2 (2004), pp. 261–269. DOI: [10.1016/j.jtbi.2004.01.003](https://doi.org/10.1016/j.jtbi.2004.01.003).
- [74] Gilad, E., Hardenberg, J. von, Provenzale, A., Shachak, M. and Meron, E.: Ecosystem engineers: from pattern formation to habitat creation. *Phys. Rev. Lett.* 93:098105 (2004). DOI: [10.1103/PhysRevLett.93.098105](https://doi.org/10.1103/PhysRevLett.93.098105).
- [75] Gilad, E., Hardenberg, J. von, Provenzale, A., Shachak, M. and Meron, E.: A mathematical model of plants as ecosystem engineers. *J. Theor. Biol.* 244.4 (2007), pp. 680–691. DOI: [j.jtbi.2006.08.006](https://doi.org/10.1016/j.jtbi.2006.08.006).
- [76] Gilad, E., Shachak, M. and Meron, E.: Dynamics and spatial organization of plant communities in water-limited systems. *Theor. Popul. Biol.* 72.2 (2007), pp. 214–230. DOI: [10.1016/j.tpb.2007.05.002](https://doi.org/10.1016/j.tpb.2007.05.002).
- [77] Gourley, S. A., Chaplain, M. A. J. and Davidson, F. A.: Spatio-temporal pattern formation in a nonlocal reaction-diffusion equation. *Dyn. Syst.* 16.2 (2001), pp. 173–192. DOI: [10.1080/14689360116914](https://doi.org/10.1080/14689360116914).
- [78] Gowda, K., Chen, Y., Iams, S. and Silber, M.: Assessing the robustness of spatial pattern sequences in a dryland vegetation model. *Proc. R. Soc. Lond. A* 472:20150893 (2016). DOI: [10.1098/rspa.2015.0893](https://doi.org/10.1098/rspa.2015.0893).
- [79] Gowda, K., Iams, S. and Silber, M.: Signatures of human impact on self-organized vegetation in the Horn of Africa. *Sci. Rep.* 8 (2018), pp. 1–8. DOI: [10.1038/s41598-018-22075-5](https://doi.org/10.1038/s41598-018-22075-5).
- [80] Guttal, V. and Jayaprakash, C.: Self-organization and productivity in semi-arid ecosystems: implications of seasonality in rainfall. *J. Theor. Biol.* 248.3 (2007), pp. 490–500. DOI: [10.1016/j.jtbi.2007.05.020](https://doi.org/10.1016/j.jtbi.2007.05.020).
- [81] Hardenberg, J. von, Kletter, A. Y., Yizhaq, H., Nathan, J. and Meron, E.: Periodic versus scale-free patterns in dryland vegetation. *Proc. R. Soc. Lond. B* 277.1688 (2010), pp. 1771–1776. DOI: [10.1098/rspb.2009.2208](https://doi.org/10.1098/rspb.2009.2208).
- [82] Heisler-White, J. L., Knapp, A. K. and Kelly, E. F.: Increasing precipitation event size increases aboveground net primary productivity in a semi-arid grassland. *Oecologia* 158.1 (2008), pp. 129–140. DOI: [10.1007/s00442-008-1116-9](https://doi.org/10.1007/s00442-008-1116-9).
- [83] Hemming, C. F.: Vegetation arcs in Somaliland. *J. Ecol.* 53.1 (1965), pp. 57–67. DOI: [10.2307/2257565](https://doi.org/10.2307/2257565).

## BIBLIOGRAPHY

- [84] Heras, M. M. las, Saco, P. M., Willgoose, G. R. and Tongway, D. J.: Variations in hydrological connectivity of Australian semiarid landscapes indicate abrupt changes in rainfall-use efficiency of vegetation. *J. Geophys. Res., G: Biogeosci.* 117:G03009 (2012). DOI: 10.1029/2011JG001839.
- [85] Higgins, S. I., Scheiter, S. and Sankaran, M.: The stability of African savannas: insights from the indirect estimation of the parameters of a dynamic model. *Ecology* 91.6 (2010), pp. 1682–1692. DOI: 10.1890/08-1368.1.
- [86] HilleRisLambers, R., Rietkerk, M., van den Bosch, F., Prins, H. H. T. and de Kroon, H.: Vegetation pattern formation in semi-arid grazing systems. *Ecology* 82.1 (2001), pp. 50–61. DOI: 10.2307/2680085.
- [87] Huang, Q., Wang, H. and Lewis, M. A.: A hybrid continuous/discrete-time model for invasion dynamics of zebra mussels in rivers. *SIAM J. Appl. Math.* 77.3 (2017), pp. 854–880. DOI: 10.1137/16m1057826.
- [88] Hutchinson, G. E.: The paradox of the plankton. *Am. Nat.* 95.882 (1961), pp. 137–145. DOI: 10.1086/282171. eprint: <https://doi.org/10.1086/282171>.
- [89] Hutson, V., Martinez, S., Mischaikow, K. and Vickers, G.: The evolution of dispersal. *J. Math. Biol.* 47.6 (2003), pp. 483–517. DOI: 10.1007/s00285-003-0210-1.
- [90] IPCC, 2014: *Climate Change 2014: Synthesis Report. Contribution of Working Groups I, II and III to the Fifth Assessment Report of the Intergovernmental Panel on Climate Change*. Ed. by Core Writing Team, Pachauri, R. and Meyer, L. Geneva, Switzerland, 2014.
- [91] Iron, D. and Ward, M. J.: The stability and dynamics of hot-spot solutions to two one-dimensional microwave heating models. *Analysis and Applications* 02.01 (2004), pp. 21–70. DOI: 10.1142/s0219530504000291.
- [92] Johnson, W. C.: Estimating dispersability of acer, fraxinus and tilia in fragmented landscapes from patterns of seedling establishment. *Landscape Ecol.* 1.3 (1988), pp. 175–187. DOI: 10.1007/BF00162743.
- [93] Jones, C. G., Lawton, J. H. and Shachak, M.: Organisms as ecosystem engineers. *Oikos* 69.3 (1994), p. 373. DOI: 10.2307/3545850.
- [94] Kao, C.-Y., Lou, Y. and Shen, W.: Random dispersal vs non-local dispersal. *Discret. Contin. Dyn. Syst.* 26.2 (2010), pp. 551–596. DOI: 10.3934/dcds.2010.26.551.

## BIBLIOGRAPHY

- [95] Kealy, B. J. and Wollkind, D. J.: A nonlinear stability analysis of vegetative Turing pattern formation for an interaction–diffusion plant–surface water model system in an arid flat environment. *Bull. Math. Biol.* 74.4 (2012), pp. 803–833. DOI: [10.1007/s11538-011-9688-7](https://doi.org/10.1007/s11538-011-9688-7).
- [96] Kéfi, S., Rietkerk, M., Alados, C. L., Pueyo, Y., Papanastasis, V., ElAich, A. and de Ruiter, P.: Spatial vegetation patterns and imminent desertification in Mediterranean arid ecosystems. *Nature* 449.7159 (2007), pp. 213–217. DOI: [10.1038/nature06111](https://doi.org/10.1038/nature06111).
- [97] Kerr, B., Riley, M. A., Feldman, M. W. and Bohannan, B. J. M.: Local dispersal promotes biodiversity in a real-life game of rock–paper–scissors. *Nature* 418.6894 (2002), pp. 171–174. DOI: [10.1038/nature00823](https://doi.org/10.1038/nature00823).
- [98] Kinast, S., Zelnik, Y. R., Bel, G. and Meron, E.: Interplay between Turing mechanisms can increase pattern diversity. *Phys. Rev. Lett.* 112.7 (2014). DOI: [10.1103/physrevlett.112.078701](https://doi.org/10.1103/physrevlett.112.078701).
- [99] Klausmeier, C. A.: Regular and irregular patterns in semiarid vegetation. *Science* 284.5421 (1999), pp. 1826–1828. DOI: [10.1126/science.284.5421.1826](https://doi.org/10.1126/science.284.5421.1826).
- [100] Kletter, A., von Hardenberg, J., Meron, E. and Provenzale, A.: Patterned vegetation and rainfall intermittency. *J. Theor. Biol.* 256.4 (2009), pp. 574–583. DOI: [10.1016/j.jtbi.2008.10.020](https://doi.org/10.1016/j.jtbi.2008.10.020).
- [101] Köppen, W.: *Das geographische System der Klimate*. Vol. 1.C. Handbuch der Klimatologie. Verlag von Gebrüder Bornträger, Berlin, 1936.
- [102] Kot, M. and Schaffer, W. M.: Discrete-time growth-dispersal models. *Math. Biosci.* 80.1 (1986), pp. 109–136. DOI: [10.1016/0025-5564\(86\)90069-6](https://doi.org/10.1016/0025-5564(86)90069-6).
- [103] Kyriazopoulos, P., Nathan, J. and Meron, E.: Species coexistence by front pinning. *Ecol. Complexity* 20 (2014), pp. 271–281. DOI: [10.1016/j.ecocom.2014.05.001](https://doi.org/10.1016/j.ecocom.2014.05.001).
- [104] Laio, F., Porporato, A., Ridolfi, L. and Rodriguez-Iturbe, I.: Plants in water-controlled ecosystems: active role in hydrologic processes and response to water stress: II. probabilistic soil moisture dynamics. *Adv. Water Resour.* 24.7 (2001), pp. 707–723. DOI: [10.1016/S0309-1708\(01\)00005-7](https://doi.org/10.1016/S0309-1708(01)00005-7).
- [105] Lefever, R. and Lejeune, O.: On the origin of tiger bush. *Bull. Math. Biol.* 59.2 (1997), pp. 263–294. DOI: [10.1007/bf02462004](https://doi.org/10.1007/bf02462004).
- [106] Lefever, R., Barbier, N., Couderon, P. and Lejeune, O.: Deeply gapped vegetation patterns: on crown/root allometry, criticality and desertification. *J. Theor. Biol.* 261.2 (2009), pp. 194–209. DOI: [10.1016/j.jtbi.2009.07.030](https://doi.org/10.1016/j.jtbi.2009.07.030).

## BIBLIOGRAPHY

- [107] Lejeune, O., Couteron, P. and Lefever, R.: Short range co-operativity competing with long range inhibition explains vegetation patterns. *Acta Oecol.* 20.3 (1999), pp. 171–183. DOI: [10.1016/S1146-609X\(99\)80030-7](https://doi.org/10.1016/S1146-609X(99)80030-7).
- [108] Lesschen, J., Cammeraat, L., Kooijman, A. and Wesemael, B. van: Development of spatial heterogeneity in vegetation and soil properties after land abandonment in a semi-arid ecosystem. *J. Arid. Environ.* 72.11 (2008), pp. 2082–2092. DOI: [10.1016/j.jaridenv.2008.06.006](https://doi.org/10.1016/j.jaridenv.2008.06.006).
- [109] Lewandrowski, W., Erickson, T. E., Dixon, K. W., Stevens, J. C. and Firn, J.: Increasing the germination envelope under water stress improves seedling emergence in two dominant grass species across different pulse rainfall events. *J. Appl. Ecol.* 54.3 (2017), pp. 997–1007. DOI: [10.1111/1365-2664.12816](https://doi.org/10.1111/1365-2664.12816).
- [110] Lewis, M. and Li, B.: Spreading speed, traveling waves, and minimal domain size in impulsive reaction–diffusion models. *Bull. Math. Biol.* 74.10 (2012), pp. 2383–2402. DOI: [10.1007/s11538-012-9757-6](https://doi.org/10.1007/s11538-012-9757-6).
- [111] Liu, B., Zhao, W. Z. and Wen, Z. J.: Photosynthetic response of two shrubs to rainfall pulses in desert regions of northwestern China. *Photosynthetica* 50.1 (2012), pp. 109–119. DOI: [10.1007/s11099-012-0015-9](https://doi.org/10.1007/s11099-012-0015-9).
- [112] Lowery, N. V. and Ursell, T.: Structured environments fundamentally alter dynamics and stability of ecological communities. *Proceedings of the National Academy of Sciences* 116.2 (2019), pp. 379–388. DOI: [10.1073/pnas.1811887116](https://doi.org/10.1073/pnas.1811887116).
- [113] Lundholm, J. T. and Larson, D. W.: Experimental separation of resource quantity from temporal variability: seedling responses to water pulses. *Oecologia* 141.2 (2004), pp. 346–352. DOI: [10.1007/s00442-003-1454-6](https://doi.org/10.1007/s00442-003-1454-6).
- [114] Lutscher, F., Pachepsky, E. and Lewis, M. A.: The effect of dispersal patterns on stream populations. *SIAM J. Appl. Math.* 47.4 (2005), pp. 749–772. DOI: [10.1137/s0036139904440400](https://doi.org/10.1137/s0036139904440400).
- [115] MacArthur, R.: Species packing and competitive equilibrium for many species. *Theor. Popul. Biol.* 1.1 (1970), pp. 1–11. DOI: [10.1016/0040-5809\(70\)90039-0](https://doi.org/10.1016/0040-5809(70)90039-0).
- [116] Macfadyen, W. A.: Vegetation patterns in the semi-desert plains of British Somaliland. *The Geographical Journal* 116.4/6 (1950), pp. 199–211. DOI: [10.2307/1789384](https://doi.org/10.2307/1789384).
- [117] Maestre, F. T., Bautista, S. and Cortina, J.: Positive, negative, and net effects in grass-shrub interactions in Mediterranean semiarid grasslands. *Ecology* 84.12 (2003), pp. 3186–3197. DOI: [10.1890/02-0635](https://doi.org/10.1890/02-0635).

## BIBLIOGRAPHY

- [118] Maidment, R. I., Grimes, D., Black, E., Tarnavsky, E., Young, M., Greatrex, H., Allan, R. P., Stein, T., Nkonde, E., Senkunda, S. and Alcántara, E. M. U.: A new, long-term daily satellite-based rainfall dataset for operational monitoring in africa. *Sci. Data* 4.1 (2017). DOI: [10.1038/sdata.2017.63](https://doi.org/10.1038/sdata.2017.63).
- [119] Marasco, A., Giannino, F. and Iuorio, A.: Modelling competitive interactions and plant–soil feedback in vegetation dynamics. *Ricerche di Matematica* (2020). DOI: [10.1007/s11587-020-00497-6](https://doi.org/10.1007/s11587-020-00497-6).
- [120] Marasco, A., Iuorio, A., Carteni, F., Bonanomi, G., Tartakovsky, D. M., Mazzoleni, S. and Giannino, F.: Vegetation pattern formation due to interactions between water availability and toxicity in plant–soil feedback. *Bull. Math. Biol.* 76.11 (2014), pp. 2866–2883. DOI: [10.1007/s11538-014-0036-6](https://doi.org/10.1007/s11538-014-0036-6).
- [121] Martinez-Garcia, R., Calabrese, J. M., Hernandez-Garcia, E. and Lopez, C.: Vegetation pattern formation in semiarid systems without facilitative mechanisms. *Geophys. Res. Lett.* 40.23 (2013), pp. 6143–6147. DOI: [10.1002/2013gl058797](https://doi.org/10.1002/2013gl058797).
- [122] Martinez-Garcia, R., Calabrese, J. M., Hernandez-Garcia, E. and Lopez, C.: Minimal mechanisms for vegetation patterns in semiarid regions. *Philos. Trans. R. Soc. A* 372.2027 (2014), p. 20140068. DOI: [10.1098/rsta.2014.0068](https://doi.org/10.1098/rsta.2014.0068).
- [123] Martinez-Garcia, R., Calabrese, J. M. and Lopez, C.: Spatial patterns in mesic savannas: the local facilitation limit and the role of demographic stochasticity. *J. Theor. Biol.* 333 (2013), pp. 156–165. DOI: [10.1016/j.jtbi.2013.05.024](https://doi.org/10.1016/j.jtbi.2013.05.024).
- [124] Martinez-Garcia, R. and Lopez, C.: From scale-dependent feedbacks to long-range competition alone: a short review on pattern-forming mechanisms in arid ecosystems (2018). arXiv: [1801.01399v1 \[q-bio.PE\]](https://arxiv.org/abs/1801.01399v1).
- [125] Mauchamp, A., Rambal, S. and Lepart, J.: Simulating the dynamics of a vegetation mosaic: a spatialized functional model. *Ecol. Model.* 71.1-3 (1994), pp. 107–130. DOI: [10.1016/0304-3800\(94\)90078-7](https://doi.org/10.1016/0304-3800(94)90078-7).
- [126] Mazzoleni, S., Bonanomi, G., Incerti, G., Chiusano, M. L., Termolino, P., Mingo, A., Senatore, M., Giannino, F., Carteni, F., Rietkerk, M. and Lanzotti, V.: Inhibitory and toxic effects of extracellular self-DNA in litter: a mechanism for negative plant-soil feedbacks? *New Phytol.* 205.3 (2015), pp. 1195–1210. DOI: [10.1111/nph.13121](https://doi.org/10.1111/nph.13121).
- [127] McPeek, M. A.: Intraspecific density dependence and a guild of consumers coexisting on one resource. *Ecology* 93.12 (2012), pp. 2728–2735. DOI: [10.1890/12-0797.1](https://doi.org/10.1890/12-0797.1).

## BIBLIOGRAPHY

- [128] Merchant, S. M. and Nagata, W.: Selection and stability of wave trains behind predator invasions in a model with non-local prey competition. *IMA J. Appl. Math.* 80.4 (2015), pp. 1155–1177. DOI: [10.1093/imamat/hxu048](https://doi.org/10.1093/imamat/hxu048).
- [129] Meron, E.: Pattern-formation approach to modelling spatially extended ecosystems. *Ecol. Model.* 234 (2012), pp. 70–82. DOI: [10.1016/j.ecolmodel.2011.05.035](https://doi.org/10.1016/j.ecolmodel.2011.05.035).
- [130] Meron, E.: Pattern formation - a missing link in the study of ecosystem response to environmental changes. *Math. Biosci.* 271 (2016), pp. 1–18. DOI: [10.1016/j.mbs.2015.10.015](https://doi.org/10.1016/j.mbs.2015.10.015).
- [131] Meron, E.: From patterns to function in living systems: dryland ecosystems as a case study. *Annu. Rev. Condens. Matter Phys.* 9.1 (2018), pp. 79–103. DOI: [10.1146/annurev-conmatphys-033117-053959](https://doi.org/10.1146/annurev-conmatphys-033117-053959).
- [132] Meron, E., Bennett, J. J. R., Fernandez-Oto, C., Tzuk, O., Zelnik, Y. R. and Grafi, G.: Continuum modeling of discrete plant communities: why does it work and why is it advantageous? *Mathematics* 7.10 (2019), p. 987. DOI: [10.3390/math7100987](https://doi.org/10.3390/math7100987).
- [133] Meron, E., Yizhaq, H. and Gilad, E.: Localized structures in dryland vegetation: forms and functions. *Chaos: An Interdisciplinary Journal of Nonlinear Science* 17.3 (2007), p. 037109. DOI: [10.1063/1.2767246](https://doi.org/10.1063/1.2767246).
- [134] Miller, P.: *Applied Asymptotic Analysis*. Graduate studies in mathematics. American Mathematical Society, 2006. DOI: [10.1090/gsm/075](https://doi.org/10.1090/gsm/075).
- [135] Mistro, D. C., Rodrigues, L. A. D. and Schmid, A. B.: A mathematical model for dispersal of an annual plant population with a seed bank. *Ecol. Model.* 188.1 (2005), pp. 52–61. DOI: [10.1016/j.ecolmodel.2005.05.010](https://doi.org/10.1016/j.ecolmodel.2005.05.010).
- [136] Montaña, C., Lopez-Portillo, J. and Mauchamp, A.: The response of two woody species to the conditions created by a shifting ecotone in an arid ecosystem. *J. Ecol.* 78.3 (1990), pp. 789–798. DOI: [10.2307/2260899](https://doi.org/10.2307/2260899).
- [137] Montaña, C.: The colonization of bare areas in two-phase mosaics of an arid ecosystem. *J. Ecol.* 80.2 (1992), pp. 315–327. DOI: [10.2307/2261014](https://doi.org/10.2307/2261014).
- [138] Montaña, C., Seghieri, J. and Cornet, A.: Vegetation dynamics: recruitment and regeneration in two-phase mosaics. *Banded vegetation patterning in arid and semiarid environments: ecological processes and consequences for management*. Ed. by Tongway, D. J., Valentin, C. and Seghieri, J. Springer, New York, 2001, pp. 132–145. DOI: [10.1007/978-1-4613-0207-0\\_7](https://doi.org/10.1007/978-1-4613-0207-0_7).

## BIBLIOGRAPHY

- [139] Mordelet, P., Menaut, J.-C. and Mariotti, A.: Tree and grass rooting patterns in an african humid savanna. *J. Veg. Sci.* 8.1 (1997), pp. 65–70. DOI: 10.2307/3237243.
- [140] Moro, M. J., Pugnaire, F. I., Haase, P. and Puigdefabregas, J.: Effect of the canopy of retama sphaerocarpa on its understorey in a semiarid environment. *Funct. Ecol.* 11.4 (1997), pp. 425–431. DOI: 10.1046/j.1365-2435.1997.00106.x.
- [141] Müller, J.: Floristic and structural pattern and current distribution of tiger bush vegetation in Burkina Faso (West Africa), assessed by means of belt transects and spatial analysis. *Appl. Ecol. Environ. Res.* 11 (2013), pp. 153–171. DOI: 10.15666/aeer/1102\_153171.
- [142] Murray, J.: *Mathematical Biology*. Biomathematics (Berlin). Springer-Verlag, 1989. DOI: 10.2307/2348289.
- [143] Musgrave, J. and Lutscher, F.: Integrodifference equations in patchy landscapes I: dispersal kernels. *J. Math. Biol.* 69.3 (2014), pp. 583–615. DOI: 10.1007/s00285-013-0714-2.
- [144] Musgrave, J. and Lutscher, F.: Integrodifference equations in patchy landscapes II: population level consequences. *J. Math. Biol.* 69.3 (2014), pp. 617–658. DOI: 10.1007/s00285-013-0715-1.
- [145] Nathan, J., von Hardenberg, J. and Meron, E.: Spatial instabilities untie the exclusion-principle constraint on species coexistence. *J. Theor. Biol.* 335 (2013), pp. 198–204. DOI: 10.1016/j.jtbi.2013.06.026.
- [146] Navarro, T., Pascual, V., Alados, C. and Cabezudo, B.: Growth forms, dispersal strategies and taxonomic spectrum in a semi-arid shrubland in SE Spain. *J. Arid. Environ.* 73.1 (2009), pp. 103–112. DOI: 10.1016/j.jariden.2008.09.009.
- [147] Neubert, M., Kot, M. and Lewis, M.: Dispersal and pattern formation in a discrete-time predator-prey model. *Theor. Popul. Biol.* 48.1 (1995), pp. 7–43. DOI: 10.1006/tpbi.1995.1020.
- [148] Noy-Meir, I.: Desert ecosystems: environment and producers. *Annu. Rev. Ecol. Syst.* 4 (1973), pp. 25–51. DOI: 10.1146/annurev.es.04.110173.000325.
- [149] Pachepsky, E., Nisbet, R. M. and Murdoch, W. W.: Between discrete and continuous: consumer–resource dynamics with synchronised reproduction. *Ecolology* 89.1 (2008), pp. 280–288. DOI: 10.1890/07-0641.1.

## BIBLIOGRAPHY

- [150] Parolin, P.: Ombrohydrochory: rain-operated seed dispersal in plants – with special regard to jet-action dispersal in Aizoaceae. *Flora* 201.7 (2006), pp. 511–518. DOI: [10.1016/j.flora.2005.11.003](https://doi.org/10.1016/j.flora.2005.11.003).
- [151] Peel, M. C., Finlayson, B. L. and McMahon, T. A.: Updated world map of the Köppen-Geiger climate classification. *Hydrol. Earth Syst. Sci.* 11.5 (2007), pp. 1633–1644. DOI: [10.5194/hess-11-1633-2007](https://doi.org/10.5194/hess-11-1633-2007).
- [152] Pelletier, J. D., DeLong, S. B., Orem, C. A., Becerra, P., Compton, K., Grestrett, K., Lyons-Baral, J., McGuire, L. A., Molaro, J. L. and Spinler, J. C.: How do vegetation bands form in dry lands? Insights from numerical modeling and field studies in southern Nevada, USA. *J. Geophys. Res., F: Earth Surface* 117:F04026 (2012). DOI: [10.1029/2012JF002465](https://doi.org/10.1029/2012JF002465).
- [153] Penny, G. G., Daniels, K. E. and Thompson, S. E.: Local properties of patterned vegetation: quantifying endogenous and exogenous effects. *Philos. Trans. R. Soc. London, Ser. A* 371:20120359 (2013). DOI: [10.1098/rsta.2012.0359](https://doi.org/10.1098/rsta.2012.0359).
- [154] Potapov, A. B. and Hillen, T.: Metastability in chemotaxis models. *Journal of Dynamics and Differential Equations* 17.2 (2005), pp. 293–330. DOI: [10.1007/s10884-005-2938-3](https://doi.org/10.1007/s10884-005-2938-3).
- [155] Powell, J. A. and Zimmermann, N. E.: Multiscale analysis of active seed dispersal contributes to resolving Reid's Paradox. *Ecology* 85.2 (2004), pp. 490–506. DOI: [10.1890/02-0535](https://doi.org/10.1890/02-0535).
- [156] Pueyo, Y., Kéfi, S., Alados, C. L. and Rietkerk, M.: Dispersal strategies and spatial organization of vegetation in arid ecosystems. *Oikos* 117.10 (2008), pp. 1522–1532. DOI: [10.1111/j.0030-1299.2008.16735.x](https://doi.org/10.1111/j.0030-1299.2008.16735.x).
- [157] Pueyo, Y., Kéfi, S., Díaz-Sierra, R., Alados, C. and Rietkerk, M.: The role of reproductive plant traits and biotic interactions in the dynamics of semi-arid plant communities. *Theor. Popul. Biol.* 78.4 (2010), pp. 289–297. DOI: [10.1016/j\(tpb\).2010.09.001](https://doi.org/10.1016/j(tpb).2010.09.001).
- [158] Pugnaire, F. I. and Luque, M. T.: Changes in plant interactions along a gradient of environmental stress. *Oikos* 93.1 (2001), pp. 42–49. DOI: [10.1034/j.1600-0706.2001.930104.x](https://doi.org/10.1034/j.1600-0706.2001.930104.x).
- [159] Rademacher, J. D. M. and Scheel, A.: Instabilities of wave trains and Turing patterns in large domains. *Int. J. Bifurcation Chaos* 17.08 (2007), pp. 2679–2691. DOI: [10.1142/s0218127407018683](https://doi.org/10.1142/s0218127407018683).
- [160] Rademacher, J. D., Sandstede, B. and Scheel, A.: Computing absolute and essential spectra using continuation. *Physica D* 229.2 (2007), pp. 166–183. DOI: [10.1016/j.physd.2007.03.016](https://doi.org/10.1016/j.physd.2007.03.016).

## BIBLIOGRAPHY

- [161] Reichenbach, T., Mobilia, M. and Frey, E.: Mobility promotes and jeopardizes biodiversity in rock–paper–scissors games. *Nature* 448.7157 (2007), pp. 1046–1049. DOI: [10.1038/nature06095](https://doi.org/10.1038/nature06095).
- [162] Reynolds, J. F., Smith, D. M. S., Lambin, E. F., Turner, B. L., Mortimore, M., Batterbury, S. P. J., Downing, T. E., Dowlatabadi, H., Fernandez, R. J., Herrick, J. E., Huber-Sannwald, E., Jiang, H., Leemans, R., Lynam, T., Maestre, F. T., Ayarza, M. and Walker, B.: Global desertification: building a science for dryland development. *Science* 316.5826 (2007), pp. 847–851. DOI: [10.1126/science.1131634](https://doi.org/10.1126/science.1131634).
- [163] Rietkerk, M., Boerlijst, M., van Langevelde, F., HilleRisLambers, R., Johan van de Koppel, Kumar, L., Prins, H. T. and de Roos, A.: Self-organization of vegetation in arid ecosystems. *Am. Nat.* 160.4 (2002), pp. 524–530. DOI: [10.1086/342078](https://doi.org/10.1086/342078).
- [164] Rietkerk, M., Dekker, S. C., de Ruiter, P. C. and van de Koppel, J.: Self-organized patchiness and catastrophic shifts in ecosystems. *Science* 305.5692 (2004), pp. 1926–1929. DOI: [10.1126/science.1101867](https://doi.org/10.1126/science.1101867).
- [165] Rietkerk, M., Ketner, P., Burger, J., Hoorens, B. and Olff, H.: Multiscale soil and vegetation patchiness along a gradient of herbivore impact in a semi-arid grazing system in West Africa. *Plant Ecol.* 148.2 (2000), pp. 207–224. DOI: [10.1023/A:1009828432690](https://doi.org/10.1023/A:1009828432690).
- [166] Rietkerk, M. and van de Koppel, J.: Regular pattern formation in real ecosystems. *Trends Ecol. Evol.* 23.3 (2008), pp. 169–175. DOI: [10.1016/j.tree.2007.10.013](https://doi.org/10.1016/j.tree.2007.10.013).
- [167] Rodriguez-Iturbe, I., Porporato, A., Ridolfi, L., Isham, V. and Coxi, D. R.: Probabilistic modelling of water balance at a point: the role of climate, soil and vegetation. *Proc. R. Soc. Lond. A* 455.1990 (1999), pp. 3789–3805. DOI: [10.1098/rspa.1999.0477](https://doi.org/10.1098/rspa.1999.0477).
- [168] Rossi, M. J. and Ares, J. O.: Water fluxes between inter-patches and vegetated mounds in flat semiarid landscapes. *J. Hydrol.* 546 (2017), pp. 219–229. DOI: [10.1016/j.jhydrol.2017.01.016](https://doi.org/10.1016/j.jhydrol.2017.01.016).
- [169] Saco, P. M., Willgoose, G. R. and Hancock, G. R.: Eco-geomorphology of banded vegetation patterns in arid and semi-arid regions. *Hydrol. Earth Syst. Sci.* 11.6 (2007), pp. 1717–1730. DOI: [10.5194/hess-11-1717-2007](https://doi.org/10.5194/hess-11-1717-2007).
- [170] Saco, P. M., Moreno-de las Heras, M., Keesstra, S., Baartman, J., Yetemen, O. and Rodriguez, J. F.: Vegetation and soil degradation in drylands: non linear feedbacks and early warning signals. *Curr. Opin. Environ. Sci. Health* 5 (2018), pp. 67–72. DOI: [10.1016/j.coesh.2018.06.001](https://doi.org/10.1016/j.coesh.2018.06.001).

## BIBLIOGRAPHY

- [171] Salvucci, G. D.: Estimating the moisture dependence of root zone water loss using conditionally averaged precipitation. *Water Resour. Res.* 37.5 (2001), pp. 1357–1365. DOI: 10.1029/2000WR900336.
- [172] Sandstede, B.: Stability of traveling waves. In: *handbook of dynamical systems ii (edited by b fiedler)*, elsevier. 2002, pp. 983–1055.
- [173] Sankaran, M., Hanan, N. P., Scholes, R. J., Ratnam, J., Augustine, D. J., Cade, B. S., Gignoux, J., Higgins, S. I., Roux, X. L., Ludwig, F., Ardo, J., Banyikwa, F., Bronn, A., Bucini, G., Caylor, K. K., Coughenour, M. B., Diouf, A., Ekaya, W., Feral, C. J., February, E. C., Frost, P. G. H., Hiernaux, P., Hrabar, H., Metzger, K. L., Prins, H. H. T., Ringrose, S., Sea, W., Tews, J., Worden, J. and Zambatis, N.: Determinants of woody cover in African savannas. *Nature* 438.7069 (2005), pp. 846–849. DOI: 10.1038/nature04070.
- [174] Sankaran, M., Ratnam, J. and Hanan, N. P.: Tree-grass coexistence in savannas revisited - insights from an examination of assumptions and mechanisms invoked in existing models. *Ecol. Lett.* 7.6 (2004), pp. 480–490. DOI: 10.1111/j.1461-0248.2004.00596.x.
- [175] Scheiter, S., Higgins, S. I., Weissing, A. E. F. J. and Geber, E. M. A.: Partitioning of root and shoot competition and the stability of savannas. *Am. Nat.* 170.4 (2007), pp. 587–601. DOI: 10.1086/521317.
- [176] Scholes, R. J. and Walker, B. H.: *An African Savanna*. Cambridge University Press, 1993. DOI: 10.1017/cbo9780511565472.
- [177] Scholes, R.: Convex relationships in ecosystems containing mixtures of trees and grass. *Environ. Resour. Econ.* 26.4 (2003), pp. 559–574. DOI: 10.1023/b:earc.0000007349.67564.b3.
- [178] Seghieri, J.: The rooting patterns of woody and herbaceous plants in a savanna; are they complementary or in competition? *African Journal of Ecology* 33.4 (1995), pp. 358–365. DOI: 10.1111/j.1365-2028.1995.tb01045.x.
- [179] Seghieri, J., Galle, S., Rajot, J. and Ehrmann, M.: Relationships between soil moisture and growth of herbaceous plants in a natural vegetation mosaic in Niger. *J. Arid. Environ.* 36.1 (1997), pp. 87–102. DOI: 10.1006/jare.1996.0195.
- [180] Serra-Diaz, J. M., Maxwell, C., Lucash, M. S., Scheller, R. M., Laflower, D. M., Miller, A. D., Tepley, A. J., Epstein, H. E., Anderson-Teixeira, K. J. and Thompson, J. R.: Disequilibrium of fire-prone forests sets the stage for a rapid decline in conifer dominance during the 21st century. *Sci. Rep.* 8:6749 (2018). DOI: 10.1038/s41598-018-24642-2.

## BIBLIOGRAPHY

- [181] Shabana, H. A., Navarro, T. and El-Keblawy, A.: Dispersal traits in the hyper-arid hot desert of the United Arab Emirates. *Plant Ecology and Evolution* 151.2 (2018), pp. 194–208. DOI: [10.5091/plecevo.2018.1359](https://doi.org/10.5091/plecevo.2018.1359).
- [182] Sheffer, E., Hardenberg, J., Yizhaq, H., Shachak, M., Meron, E. and Blasius, B.: Emerged or imposed: a theory on the role of physical templates and self-organisation for vegetation patchiness. *Ecol. Lett.* 16.2 (2013), pp. 127–139. DOI: [10.1111/ele.12027](https://doi.org/10.1111/ele.12027).
- [183] Sher, A. A., Goldberg, D. E. and Novoplansky, A.: The effect of mean and variance in resource supply on survival of annuals from mediterranean and desert environments. *Oecologia* 141.2 (2004), pp. 353–362. DOI: [10.1007/s00442-003-1435-9](https://doi.org/10.1007/s00442-003-1435-9).
- [184] Sherratt, J. A.: Pattern solutions of the Klausmeier model for banded vegetation in semi-arid environments I. *Nonlinearity* 23.10 (2010), pp. 2657–2675. DOI: [10.1088/0951-7715/23/10/016](https://doi.org/10.1088/0951-7715/23/10/016).
- [185] Sherratt, J. A.: An analysis of vegetation stripe formation in semi-arid landscapes. *J. Math. Biol.* 51.2 (2005), pp. 183–197. DOI: [10.1007/s00285-005-0319-5](https://doi.org/10.1007/s00285-005-0319-5).
- [186] Sherratt, J. A.: Pattern solutions of the Klausmeier model for banded vegetation in semi-arid environments II: patterns with the largest possible propagation speeds. *Proc. R. Soc. Lond. A* 467.2135 (2011), pp. 3272–3294. DOI: [10.1098/rspa.2011.0194](https://doi.org/10.1098/rspa.2011.0194).
- [187] Sherratt, J. A.: Numerical continuation methods for studying periodic travelling wave (wavetrain) solutions of partial differential equations. *Appl. Math. Comput.* 218.9 (2012), pp. 4684–4694. DOI: [10.1016/j.amc.2011.11.005](https://doi.org/10.1016/j.amc.2011.11.005).
- [188] Sherratt, J. A.: History-dependent patterns of whole ecosystems. *Ecol. Complexity* 14 (2013), pp. 8–20. DOI: [10.1016/j.ecocom.2012.12.002](https://doi.org/10.1016/j.ecocom.2012.12.002).
- [189] Sherratt, J. A.: Numerical continuation of boundaries in parameter space between stable and unstable periodic travelling wave (wavetrain) solutions of partial differential equations. *Adv. Comput. Math.* 39.1 (2013), pp. 175–192. DOI: [10.1007/s10444-012-9273-0](https://doi.org/10.1007/s10444-012-9273-0).
- [190] Sherratt, J. A.: Pattern solutions of the Klausmeier model for banded vegetation in semi-arid environments III: the transition between homoclinic solutions. *Physica D* 242.1 (2013), pp. 30–41. DOI: [10.1016/j.physd.2012.08.014](https://doi.org/10.1016/j.physd.2012.08.014).
- [191] Sherratt, J. A.: Pattern solutions of the Klausmeier model for banded vegetation in semiarid environments IV: slowly moving patterns and their stability. *SIAM J. Appl. Math.* 73.1 (2013), pp. 330–350. DOI: [10.1137/120862648](https://doi.org/10.1137/120862648).

## BIBLIOGRAPHY

- [192] Sherratt, J. A.: Pattern solutions of the Klausmeier model for banded vegetation in semiarid environments V: the transition from patterns to desert. *SIAM J. Appl. Math.* 73.4 (2013), pp. 1347–1367. DOI: [10.1137/120899510](https://doi.org/10.1137/120899510).
- [193] Sherratt, J. A.: Using wavelength and slope to infer the historical origin of semiarid vegetation bands. *Proceedings of the National Academy of Sciences* 112.14 (2015), pp. 4202–4207. DOI: [10.1073/pnas.1420171112](https://doi.org/10.1073/pnas.1420171112).
- [194] Sherratt, J. A. and Lord, G. J.: Nonlinear dynamics and pattern bifurcations in a model for vegetation stripes in semi-arid environments. *Theor. Popul. Biol.* 71.1 (2007), pp. 1–11. DOI: [10.1016/j.tpb.2006.07.009](https://doi.org/10.1016/j.tpb.2006.07.009).
- [195] Siero, E.: Nonlocal grazing in patterned ecosystems. *J. Theor. Biol.* 436 (2018), pp. 64–71. DOI: [10.1016/j.jtbi.2017.10.001](https://doi.org/10.1016/j.jtbi.2017.10.001).
- [196] Siero, E., Doelman, A., Eppinga, M. B., Rademacher, J. D. M., Rietkerk, M. and Siteur, K.: Striped pattern selection by advective reaction-diffusion systems: resilience of banded vegetation on slopes. *Chaos: An Interdisciplinary Journal of Nonlinear Science* 25.3 (2015), p. 036411. DOI: [10.1063/1.4914450](https://doi.org/10.1063/1.4914450).
- [197] Siero, E., Siteur, K., Doelman, A., van de Koppel, J., Rietkerk, M. and Eppinga, M. B.: Grazing away the resilience of patterned ecosystems. *Am. Nat.* 193.3 (2019), pp. 472–480. DOI: [10.1086/701669](https://doi.org/10.1086/701669).
- [198] Siteur, K., Eppinga, M. B., Karssenberg, D., Baudena, M., Bierkens, M. F. and Rietkerk, M.: How will increases in rainfall intensity affect semiarid ecosystems? *Water Resour. Res.* 50.7 (2014), pp. 5980–6001. DOI: [10.1002/2013wr014955](https://doi.org/10.1002/2013wr014955).
- [199] Siteur, K., Siero, E., Eppinga, M. B., Rademacher, J. D., Doelman, A. and Rietkerk, M.: Beyond Turing: the response of patterned ecosystems to environmental change. *Ecol. Complexity* 20 (2014), pp. 81–96. DOI: [10.1016/j.ecocom.2014.09.002](https://doi.org/10.1016/j.ecocom.2014.09.002).
- [200] Sprugel, D. G.: Disturbance, equilibrium, and environmental variability: what is ‘natural’ vegetation in a changing environment? *Biol. Conserv.* 58.1 (1991), pp. 1–18. DOI: [10.1016/0006-3207\(91\)90041-7](https://doi.org/10.1016/0006-3207(91)90041-7).
- [201] Staver, A. C., Archibald, S. and Levin, S.: Tree cover in sub-Saharan Africa: rainfall and fire constrain forest and savanna as alternative stable states. *Ecology* 92.5 (2011), pp. 1063–1072. DOI: [10.1890/10-1684.1](https://doi.org/10.1890/10-1684.1).
- [202] Sugerbaker, L. J., Constance, E. W., Heidemann, H. K., Jason, A. L., Lukas, V., Saghy, D. L. and Stoker, J. M.: *The 3D Elevation Program initiative: a call for action*. 2014. DOI: [10.3133/cir1399](https://doi.org/10.3133/cir1399).

## BIBLIOGRAPHY

- [203] Svenning, J.-C. and Sandel, B.: Disequilibrium vegetation dynamics under future climate change. *Am. J. Bot.* 100.7 (2013), pp. 1266–1286. DOI: 10.3732/ajb.1200469.
- [204] Synodinos, A. D., Tietjen, B. and Jeltsch, F.: Facilitation in drylands: modeling a neglected driver of savanna dynamics. *Ecol. Modell.* 304 (2015), pp. 11–21. DOI: 10.1016/j.ecolmodel.2015.02.015.
- [205] Taft, J. B.: Savanna and open-woodland communities. *Conservation in highly fragmented landscapes*. Springer New York, 1997, pp. 24–54. DOI: 10.1007/978-1-4757-0656-7\_2.
- [206] Tchuinté Tamen, A., Dumont, Y., Tewa, J., Bowong, S. and Couteron, P.: Tree–grass interaction dynamics and pulsed fires: mathematical and numerical studies. *Appl. Math. Modell.* 40.11-12 (2016), pp. 6165–6197. DOI: 10.1016/j.apm.2016.01.019.
- [207] Tchuinté Tamen, A., Dumont, Y., Tewa, J., Bowong, S. and Couteron, P.: A minimalistic model of tree–grass interactions using impulsive differential equations and non-linear feedback functions of grass biomass onto fire-induced tree mortality. *Math. Comput. Simul.* 133 (2017), pp. 265–297. DOI: 10.1016/j.matcom.2016.03.008.
- [208] Thiery, J. M., D’Herbès, J.-M. and Valentin, C.: A model simulating the genesis of banded vegetation patterns in Niger. *J. Ecol.* 83.3 (1995), pp. 497–507. DOI: 10.2307/2261602.
- [209] Thompson, S. E., Harman, C. J., Heine, P. and Katul, G. G.: Vegetation-infiltration relationships across climatic and soil type gradients. *J. Geophys. Res., G: Biogeosci.* 115:G02023 (2010). DOI: 10.1029/2009JG001134.
- [210] Thompson, S. and Katul, G.: Secondary seed dispersal and its role in landscape organization. *Geophys. Res. Lett.* 36.2 (2009). DOI: 10.1029/2008GL036044.
- [211] Thompson, S., Katul, G., Konings, A. and Ridolfi, L.: Unsteady overland flow on flat surfaces induced by spatial permeability contrasts. *Adv. Water Resour.* 34.8 (2011), pp. 1049–1058. DOI: 10.1016/j.advwatres.2011.05.012.
- [212] Tilman, D.: *Resource Competition and Community Structure*. Princeton University Press, 1982. 296 pp.
- [213] Tilman, D.: Competition and biodiversity in spatially structured habitats. *Ecology* 75.1 (1994), pp. 2–16. DOI: 10.2307/1939377.

## BIBLIOGRAPHY

- [214] Tongway, D. J. and Ludwig, J. A.: Vegetation and soil patterning in semi-arid mulga lands of Eastern Australia. *Aust. J. Ecol.* 15.1 (1990), pp. 23–34. DOI: [10.1111/j.1442-9993.1990.tb01017.x](https://doi.org/10.1111/j.1442-9993.1990.tb01017.x).
- [215] Touboul, J. D., Staver, A. C. and Levin, S. A.: On the complex dynamics of savanna landscapes. *Proceedings of the National Academy of Sciences* 115.7 (2018), E1336–E1345. DOI: [10.1073/pnas.1712356115](https://doi.org/10.1073/pnas.1712356115).
- [216] Trichon, V., Hiernaux, P., Walcker, R. and Mougin, E.: The persistent decline of patterned woody vegetation: the tiger bush in the context of the regional sahel greening trend. *Glob. Chang. Biol.* 24.6 (2018), pp. 2633–2648. DOI: [10.1111/gcb.14059](https://doi.org/10.1111/gcb.14059).
- [217] Tzuk, O., Ujjwal, S. R., Fernandez-Oto, C., Seifan, M. and Meron, E.: Interplay between exogenous and endogenous factors in seasonal vegetation oscillations. *Sci. Rep.* 9:354 (2019). DOI: [10.1038/s41598-018-36898-9](https://doi.org/10.1038/s41598-018-36898-9).
- [218] United Nations Convention to Combat Desertification: *The Global Land Outlook*. Version first edition. Bonn, Germany, 2017.
- [219] United Nations Food and Agriculture Organization: *Livestock sector briefs*. 2005.
- [220] Ursino, N. and Callegaro, C.: Diversity without complementarity threatens vegetation patterns in arid lands. *Ecohydrology* 9.7 (2016), pp. 1187–1195. DOI: [10.1002/eco.1717](https://doi.org/10.1002/eco.1717).
- [221] Ursino, N. and Contarini, S.: Stability of banded vegetation patterns under seasonal rainfall and limited soil moisture storage capacity. *Adv. Water Resour.* 29.10 (2006), pp. 1556–1564. DOI: [10.1016/j.advwatres.2005.11.006](https://doi.org/10.1016/j.advwatres.2005.11.006).
- [222] Valentin, C., d'Herbès, J. and Poesen, J.: Soil and water components of banded vegetation patterns. *CATENA* 37.1–2 (1999), pp. 1–24. DOI: [10.1016/S0341-8162\(99\)00053-3](https://doi.org/10.1016/S0341-8162(99)00053-3).
- [223] van de Koppel, J., Altieri, A. H., Silliman, B. R., Bruno, J. F. and Bertness, M. D.: Scale-dependent interactions and community structure on cobble beaches. *Ecol. Lett.* 0.0 (2006), p. 051109031307001. DOI: [10.1111/j.1461-0248.2005.00843.x](https://doi.org/10.1111/j.1461-0248.2005.00843.x).
- [224] van de Koppel, J., Rietkerk, M., van Langevelde, F., Kumar, L., Klausmeier, C., Fryxell, J., Hearne, J., van Andel, J., de Ridder, N., Skidmore, A., Stroosnijder, L. and Prins, H. T.: Spatial heterogeneity and irreversible vegetation change in semiarid grazing systems. *Am. Nat.* 159.2 (2002), pp. 209–218. DOI: [10.1086/324791](https://doi.org/10.1086/324791).

## BIBLIOGRAPHY

- [225] van der Stelt, S., Doelman, A., Hek, G. and Rademacher, J. D. M.: Rise and fall of periodic patterns for a generalized Klausmeier–Gray–Scott model. *J. Nonlinear. Sci.* 23.1 (2013), pp. 39–95. DOI: 10.1007/s00332-012-9139-0.
- [226] Van Langevelde, F., Van De Vijver, C. A. D. M., Kumar, L., Van De Koppel, J., De Ridder, N., Van Andel, J., Skidmore, A. K., Hearne, J. W., Stroosnijder, L., Bond, W. J., Prins, H. H. T. and Rietkerk, M.: Effects of fire and herbivory on the stability of savanna ecosystems. *Ecology* 84.2 (2003), pp. 337–350. DOI: 10.1890/0012-9658(2003)084[0337:eofaho]2.0.co;2.
- [227] van Rheede van Oudtshoorn, K. and van Rooyen, M. W.: *Dispersal Biology of Desert Plants*. Adaptations of Desert Organisms. Springer, Berlin Heidelberg, 2013.
- [228] van Wijngaarden, W.: Elephants, trees, grass, grazers : relationships between climate, soils, vegetation, and large herbivores in a semi-arid savanna ecosystem (Tsavo, Kenya). PhD thesis. International Institute for Aerospace Survey and Earth Sciences, Enschede, Netherlands, 1985.
- [229] Vasilyeva, O., Lutscher, F. and Lewis, M.: Analysis of spread and persistence for stream insects with winged adult stages. *J. Math. Biol.* 72.4 (2016), pp. 851–875. DOI: 10.1007/s00285-015-0932-x.
- [230] Volis, S.: Correlated patterns of variation in phenology and seed production in populations of two annual grasses along an aridity gradient. *Evol. Ecol.* 21.3 (2007), pp. 381–393. DOI: 10.1007/s10682-006-9108-x.
- [231] Volterra, V.: Variations and fluctuations of the number of individuals in animal species living together. *ICES Journal of Marine Science* 3.1 (1928), pp. 3–51. DOI: 10.1093/icesjms/3.1.3.
- [232] Walker, B. H., Ludwig, D., Holling, C. S. and Peterman, R. M.: Stability of semi-arid savanna grazing systems. *The Journal of Ecology* 69.2 (1981), p. 473. DOI: 10.2307/2259679.
- [233] Walker, B. H. and Noy-Meir, I.: Aspects of the stability and resilience of savanna ecosystems. *Ecology of tropical savannas*. Ed. by Huntley, B. J. and Walker, B. H. Berlin, Heidelberg: Springer Berlin Heidelberg, 1982, pp. 556–590.
- [234] Walter, H.: *Ecology of tropical and subtropical vegetation*; Oliver and Boyd, 1971.
- [235] Wang, W.-J., Huai, W.-X., Thompson, S. and Katul, G. G.: Steady nonuniform shallow flow within emergent vegetation. *Water Resour. Res.* 51.12 (2015), pp. 10047–10064. DOI: 10.1002/2015wr017658.

## BIBLIOGRAPHY

- [236] Wang, X. and Zhang, G.: Vegetation pattern formation in seminal systems due to internal competition reaction between plants. *J. Theor. Biol.* 458 (2018), pp. 10–14. DOI: [10.1016/j.jtbi.2018.08.043](https://doi.org/10.1016/j.jtbi.2018.08.043).
- [237] Wang, X. and Zhang, G.: The influence of infiltration feedback on the characteristic of banded vegetation pattern on hillsides of semiarid area. *PLOS ONE* 14.1 (2019), e0205715. DOI: [10.1371/journal.pone.0205715](https://doi.org/10.1371/journal.pone.0205715).
- [238] Wang, X. and Lutscher, F.: Turing patterns in a predator–prey model with seasonality. *J. Math. Biol.* 78.3 (2018), pp. 711–737. DOI: [10.1007/s00285-018-1289-8](https://doi.org/10.1007/s00285-018-1289-8).
- [239] White, L. P.: Vegetation stripes on sheet wash surfaces. *J. Ecol.* 59.2 (1971), pp. 615–622. DOI: [10.2307/2258335](https://doi.org/10.2307/2258335).
- [240] Whittaker, R. H., Levin, S. A. and Root, R. B.: Niche, habitat, and ecotope. *Am. Nat.* 107.955 (1973), pp. 321–338. DOI: [10.1086/282837](https://doi.org/10.1086/282837).
- [241] Worrall, G. A.: The Butana grass patterns. *J. Soil Sci.* 10.1 (1959), pp. 34–53. DOI: [10.1111/j.1365-2389.1959.tb00664.x](https://doi.org/10.1111/j.1365-2389.1959.tb00664.x).
- [242] Yatat, V., Couteron, P. and Dumont, Y.: Spatially explicit modelling of tree–grass interactions in fire-prone savannas: a partial differential equations framework. *Ecol. Complexity* 36 (2018), pp. 290–313. DOI: [10.1016/j.ecocom.2017.06.004](https://doi.org/10.1016/j.ecocom.2017.06.004).
- [243] Yatat, V., Couteron, P., Tewa, J. J., Bowong, S. and Dumont, Y.: An impulsive modelling framework of fire occurrence in a size-structured model of tree–grass interactions for savanna ecosystems. *J. Math. Biol.* 74.6 (2017), pp. 1425–1482. DOI: [10.1007/s00285-016-1060-y](https://doi.org/10.1007/s00285-016-1060-y).
- [244] Yatat, V. D., Tchuinté, A., Dumont, Y. and Couteron, P.: A tribute to the use of minimalistic spatially-implicit models of savanna vegetation dynamics to address broad spatial scales in spite of scarce data. *Biomath* 7.2 (2018), p. 1812167. DOI: [10.11145/j.biomath.2018.12.167](https://doi.org/10.11145/j.biomath.2018.12.167).
- [245] Yu, K. and D’Odorico, P.: An ecohydrological framework for grass displacement by woody plants in savannas. *Journal of Geophysical Research: Biogeosciences* 119.3 (2014), pp. 192–206. DOI: [10.1002/2013jg002577](https://doi.org/10.1002/2013jg002577).
- [246] Zelnik, Y. R., Gandhi, P., Knobloch, E. and Meron, E.: Implications of tristability in pattern-forming ecosystems. *Chaos: An Interdisciplinary Journal of Nonlinear Science* 28.3 (2018), p. 033609. DOI: [10.1063/1.5018925](https://doi.org/10.1063/1.5018925).
- [247] Zelnik, Y. R., Kinast, S., Yizhaq, H., Bel, G. and Meron, E.: Regime shifts in models of dryland vegetation. *Philos. Trans. R. Soc. London, Ser. A* 371.2004 (2013), p. 20120358. DOI: [10.1098/rsta.2012.0358](https://doi.org/10.1098/rsta.2012.0358).

## BIBLIOGRAPHY

- [248] Zimmerman, J. K., Comita, L. S., Thompson, J., Uriarte, M. and Brokaw, N.: Patch dynamics and community metastability of a subtropical forest: compound effects of natural disturbance and human land use. *Landscape Ecol.* 25.7 (2010), pp. 1099–1111. DOI: 10.1007/s10980-010-9486-x.